TECHNICAL UNIVERSITY OF KOŠICE, FACULTY OF MATERIALS, METALLURGY AND RECYCLING,
INSTITUTE OF METALLURGY
VŠB – TECHNICAL UNIVERSITY OF OSTRAVA, FACULTY OF MATERIALS SCIENCE AND TECHNOLOGY,
DEPARTMENT OF METALLURGY AND FOUNDRY

SILESIAN UNIVERSITY OF TECHNOLOGY, DEPARTMENT OF EXTRACTIVE METALLURGY AND
ENVIRONMENTAL PROTECTION

IRON AND STEELMAKING 2019

MODERN METALLURGY

The XXVIII INTERNATIONAL SCIENTIFIC CONFERENCE

Conference proceedings

WELLNESS HOTEL CHOPOK, DEMÄNOVSKÁ DOLINA, LIPTOVSKÝ MIKULÁŠ, SLOVAKIA

23rd to 25th October 2019

Partners

U. S. Steel Košice

INTOCAST

VEOLIA

ŽELEZIARNE PODBREZOVÁ

OFZ, a.s., ISTEBNÉ

ŽP Výskumno-vývojové centrum s.r.o.

SLOVALCO

eskada

PYROMETAL
Your partner for industry

BASF
We create chemistry

Silbitz Group

WELLNESS HOTEL CHOPOK

Nadácia U. S. Steel Košice

Disclaimer

This conference proceedings contains papers approved by the Conference Review Commitee. All articles have been reviewed. Authors are responsible for the content and accuracy.

ISBN: 978-80-553-3606-0

IRON AND STEELMAKING 2019, MODERN METALLURGY

Published by Technical University of Košice, Faculty of Materials, Metallurgy and Recycling, Institute of Metallurgy and Academy of metallurgy, o.z.

Email: academyofmetallurgy@gmail.com

Url: https://ohaz.umet.fmmr.tuke.sk/iasm2019/index_en.html

IRON AND STEELMAKING 2019

MODERN METALLURGY

The XXVIII INTERNATIONAL SCIENTIFIC CONFERENCE

GUARANTEE OF THE CONFERENCE

doc. Ing. Branislav Buľko, PhD., Technical University of Košice

HONORARY BOARD

doc. Ing. Iveta Vasková, PhD. - Dean of Faculty of Materials, Metallurgy and Recycling Technical University of Košice

prof. Ing. Jana Dobrovská, CSc. - Dean of Faculty of Materials Science and Technology VŠB - Technical University of Ostrava

dr hab. inż. Jerzy Łabaj, prof. nadzw. PŚ - dziekan Wydziału Inżynierii Materiałowej i Metalurgii

Politechnika Śląska

dr hab. inż. Marcin Knapiński, prof. PCz - dziekan Wydziału Inżynierii Produkcji i Technologii Materiałów Politechnika Częstochowska

prof. dr hab. inż. Mirosław Karbowniczek - prorektor ds. Ogólnych Akademia Górniczo-Hutnicza im. Stanisława Staszica w Krakowie

James E. Bruno - President U.S.Steel Košice, s.r.o.

Dr. h. c. Ing. Vladimír Soták - Chairman of the Board of Directors and CEO Železiarne Podbrezová, a.s.

Ing. Adrián Jakubek - Managing Director of Eurocast Košice, s.r.o.

Ing. Branislav Klocok - Executive Director OFZ, a.s.

SCIENTIFIC COMMITTEE

prof. Ing. Mária Fröhlichová, CSc., Technical University of Košice

prof. Ing. Alena Pribulová, CSc., Technical University of Košice

prof. Ing. Augustín Varga, CSc., Technical University of Košice

doc. Ing. Branislav Buľko, PhD., Technical University of Košice

doc. Ing. Jaroslav Legemza, PhD., Technical University of Košice

Ing. Marcel Novosad, U. S. Steel Košice, s.r.o.

Ing. Viera Kohúteková, PhD., U. S. Steel Košice, s.r.o.

prof. Ing. Ľudovít Parilák, CSc., - ŽP Výskumno - vývojové centrum s.r.o.

Ing. Pavol Beraxa, PhD. - ŽP Výskumno - vývojové centrum s.r.o.

dr hab. inż. Rafał Dańko, prof. nadzw. AGH, Akademia Górniczo - Hutnicza im. Stanisława Staszica w Krakowie

prof. dr hab. inż. Leszek Blacha, Silesian University of Technology

dr hab. inż. Mariola Saternus, prof. nzw. w Pol. Śl., Silesian University of Technology

dr hab. inż. Marek Warzecha, prof. PCz., Czestochowa University of Technology

prof. Ing. Karel Michalek, CSc., VŠB - Technical University of Ostrava

prof. Ing. Jiří Bažan, CSc., VŠB - Technical University of Ostrava

doc. Ing. Markéta Tkadlečková, Ph.D., VŠB - Technical University of Ostrava

doc. Ing. Pavlína Pustějovská Ph.D., VŠB - Technical University of Ostrava

doc. Ing. Petr Lichý, PhD., VŠB - Technical University of Ostrava

ORGANIZING COMMITTEE

doc. Ing. Dana Baricová, PhD., Technical University of Košice

doc. Ing. Branislav Buľko, PhD., Technical University of Košice

Ing. Martina Džupková, PhD., Technical University of Košice

Ing. Peter Demeter, PhD., Technical University of Košice

Ing. Marianna Bartošová, PhD., Technical University of Košice

Ing. Gustáv Jablonský, PhD., Technical University of Košice

doc. Ing. Ján Kizek, PhD., Technical University of Košice

Ing. Róbert Dzurňák, PhD., Technical University of Košice

Anna Buľková, Technical University of Košice

CONTENTS

SESSION - IRON AND STEELMAKING

THE BY PRODUCTS CREATED DURING THE OXYGEN STEELMAKING PROCESSES

Dana Baricová[1*], Alena Pribulová[1], Branislav Buľko[1], Peter Demeter[1], Martina Hrubovčáková[1]
[1]Technical University of Košice, Faculty of Materials, Metallurgy and Recycling, Institute of Metallurgy, 04200 Košice, Slovakia
*Correspondence: dana.baricova@tuke.sk

Abstract
In the technological process of the oxygen steelmaking plant, secondary products originate in parallel with the production of the main product, which have the character of secondary by products or industrial waste. The major secondary products of steelmaking production include waste gases, process fluids, flue dust, sludge, slags and mill scales. The major waste products of metallurgical production are slags. The amount of oxygen steelmaking slag is about 120-150 kg per tonne of crude steel, and it is approximately 80% of all by-products arising from the production of steel. Next on as an inevitable by-product of steelmaking in oxygen converters is flue dust. Flue dusts, by-products of oxygen converter process, are together with mill scales the most valuable secondary raw materials produced in steelmaking. The amount of by-products is primarily dependent on the type of technology, the ratio of scrap to pig iron in the batch, the grades of the steel being produced, the initial chemical composition of the pig iron and the amount of slag additives added. The paper presents the results of research project directed to the characterization of oxygen converter slag and oxygen converter flue dust created in oxygen converter, therefore chemical and mineralogical composition of the by-products have a main influence on their next utilization.

Keywords: oxygen converter; oxygen converter slag; oxygen converter flue dust; metallurgical waste

1. Introduction

Secondary products are produced in parallel with the production of the main product, in the technological process of the steelmaking in the oxygen converter. They have the character of secondary by products or industrial waste. According to the Waste Catalog issued by the Ministry of the Environment of the Slovak Republic, the Collection of Laws 365/2015, the slags from the steel production processes are included in the group of general wastes. This group of waste does not pose a major risk to the environment for its chemical composition but is particularly problematic due to its large volume. The flue dusts from the steelmaking production processes are included in the group of general wastes or hazardous wastes, it depending on its chemical composition, see Table 1 [1].
Under the laws applicable to waste management, the waste producer is required to ensure their disposal without negative environmental impacts.

Table 1 Categorization of the wastes from the ironmaking and steelmaking industry [1].

Group ID, subgroups, type and subspecies of waste	Name of group, sub-group, type and subspecies of waste	Waste category
10	**WASTES FROM THERMAL PROCESSES**	
10 02	**WASTES FROM THE IRONMAKING AND STEELMAKING INDUSTRY**	
10 02 01	wastes from slag processing	general
10 02 02	untreated slag	general
10 02 07	solid wastes from gas treatment containing dangerous substances	hazardous
10 02 08	solid wastes from gas treatment other than mentioned in 10 02 07	general
10 02 13	sludges and filter cakes from gas treatment containing dangerous substances	hazardous
10 02 14	sludges and filter cakes from gas treatment other than mentioned in 10 02 13	general

Ironmaking and steelmaking are always associated with waste production that presents for the entire metallurgical process either reversible and/or reusable material or lost waste not applicable in further production. At present the wastes from iron-and steelmaking find hardly applicability as secondary raw

material [2]. In case of increasing requirements for cleanliness of products in metallurgy it is necessary to take into account all sources accompanying elements from the entire course of the process [3].

1.1. Oxygen converter slag

Oxygen converter slag plays an important role in the processes of steel production and treatment [4]. The importance of converter slag as dephosphorization and desulphuration media has decreased with implementation of special pre-converter treatments and post-converter treatments [5, 6]. Despite all efforts, the amount of generated slag represents about 13% of the total batch. The process of steel production in oxygen converter is characterized by a high rate of individual operations [7]. For example, for a 180-ton converter, steel production from charging to tapping takes approximately 40 minutes, the blowing itself takes about 15-20 minutes. The rate of slag formation must also be adjusted to this time.

The main factors that determine the rate of slag formation are the contents of oxides of iron and manganese in the slag, the temperature of the steel, and the conditions under which the lime is added [8]. Other factor is the required final content of phosphorus.

The generated compositions and amounts of slag will depend on the process in which the slag is formed and on the raw materials used in the process, e.g. iron input and fluxing ingredients such as burnt lime, governed by the proportions of materials required for an effective process [9].

Slag in BOF (basic oxygen furnace) is heterogeneous and always contains some entrained gas bubbles and solid material (either un-dissolved or precipitated) [10].

Knowledge of the chemical, mineralogical, and morphological properties of steel slags is essential because their cementitious and mechanical properties, which play a key role in their utilization, are closely linked to these properties [11].

The authors of paper [12], [13], [14] reported that, the mineral phases of converter steel slag mainly include dicalciumsilicate ($2CaO.SiO_2$), tricalciumsilicate ($3CaO.SiO_2$), RO phase (free oxide phase) and calciumferrite ($2CaO{\cdot}Fe_2O_3$) and so on, where the proportion of silicate phase is about 50%.

1.2. Oxygen converter flue dust

Fly dusts from steel and cast iron production contain some part of FeO that is reducible in a cupola and blast furnace. It is a very fine material and it has to be pelletized or briquetted before its next use [15].
Oxygen converter steelmaking process produces a large amount of dust that is emitted with the evolved converter gases. This dust is a major pollutant in steel plants using the oxygen converter. Elaborate dust abatement systems are required to separate the dust from the flue gases before the gas is allowed to escape into the atmosphere. The oxygen converter dust thus separated and collected, which otherwise has very little use, is normally recycled into the processing stream at sintering plants.
Flue dusts, by-products of oxygen converter process, are together with mill scales the most valuable secondary raw materials produced in steelmaking [16, 17].
The amount of generated dust is dependent on the blowing practice, the bath chemistry, and the composition and granulometry of the input materials. Nevertheless, a fairly good estimation can be made for a given set of operating parameters. When the melts are cooled with ore, dust generation varies between 13 and 25 kg per ton of steel, but when melts are cooled with scrap, the amount is between 21 and 32 kg per ton of steel. Some works has been done toward characterization of the oxygen converter dust regarding its chemical composition, particle size distribution, and morphology. Most of studies were undertaken with an aim to control the generated dust and fumes. The main emphasis of the present tests has been to determine the nature and the morphology of the major iron-bearing phases, as well as the minor gangue constituents present in the dust samples.
This information will be useful in finding some better utilization of the dust, rather than recycling it back to the sintering plant. The chemical composition of the dust can vary widely depending on whether or not the gas evolved, which contains 70-95% carbon monoxide (CO), is subsequently burnt to carbon dioxide (CO_2) by adding secondary air. The former process is known as total combustion, while the latter is termed suppressed combustion [18].

2. Experimental Materials and Methods

Experimental part of paper presents the results of the investigation of the final composition of converter slag, and converter flue dust in a top-blown, 190-tonne oxygen converter. The total melting time was 46 minutes while the blowing time was 27 minutes in all the melting processes.

In the case of converter slag, this process was monitored using the slag samples that were collected after the oxygen blowing. For this purpose, the sampling was carried out during five consecutive melting processes (S1, S2, S3, S4, S5). The charge used in the oxygen converter consisted of raw iron and steel scrap, in approximately identical quantities in all melting processes. The slag-forming additives were lime and dolomitic lime. They were added into the oxygen converter gradually. The first dose was always added in the beginning of oxygen blowing and the second dose before minute 2 of oxygen blowing.

Flue dust from oxygen converters, as an inevitable by-product of steelmaking in oxygen converters, may be used for the production of briquettes to be reused in the oxygen converter charge. This part deals with the chemical composition briquettes. As to the chemical composition, the key monitored parameters which may be affected by adding the briquettes are the contents of phosphorus and sulphur.

The chemical analysis of the samples was carried out in the accredited laboratory by X-ray quantometer RIGKU and was supplemented with the identification of the slag basicity ($B=CaO/SiO_2$), as well as the analysis of free lime in the case of slags. The content of free lime was determined applying the method of chemical phase-analysis. This method uses the selective dissolution of free lime in the mixture of sugar and alcohol, and the subsequent determination through the titration with hydrochloric acid.

The performed analyses also included the EDX microscopy analysis that was aimed at qualitative as well as quantitative confirmation of the percentages of individual structural phases present in the slag. This EDX analysis was carried out using the Joel JSM-7000F scanning electron microscope.

2.1. Characterization of oxygen converter slag

The basic constituents of oxygen converter slags are CaO, originating from slag-forming additives, SiO2 and FeO from the metal bath oxidation reactions. These three major components represent from 77.89% to 84.97% of the total. The minor components represent from 15.05% to 22.11% of Femetal, Fe2O3, MnO, MgO (see Table 2). Figure 1 presents part of the CaO-SiO2-FeO ternary scheme [19], where is described final chemical composition of the oxygen converter slag for all analysed melting processes, as well as the evolution of the chemical composition of slag during the steelmaking processes.

Table 2 The final chemical composition of steelmaking slags from oxygen converters.

sample	Fe total [%]	FeO [%]	SiO_2 [%]	CaO [%]	MgO [%]	MnO [%]	P_2O_5 [%]	S [%]	B [-]	CaO free [%]
S1	15.00	22.13	12.24	50.20	5.89	5.62	1.21	0.09	4.10	0.95
S2	19.06	23.15	10.06	51.76	5.08	4.24	1.04	0.13	5.15	1.77
S3	15.01	15.09	11.82	50.98	5.87	4.66	1.36	0.10	4.31	0.89
S4	19.84	21.13	10.83	48.62	6.75	4.21	1.28	0.12	4.49	0.58
S5	21.44	22.13	10.24	46.55	4.34	5.79	1.28	0.12	4.55	0.72
average	**18.07**	**20.73**	**11.04**	**49.62**	**5.59**	**4.90**	**1.23**	**0.11**	**4.52**	**0.98**

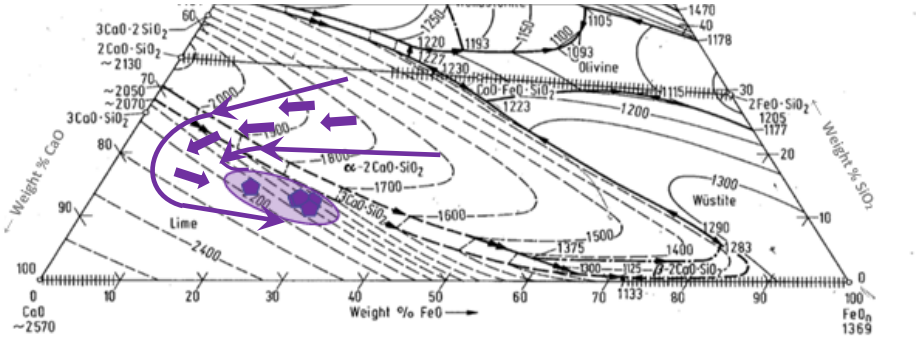

Figure 1 Final chemical composition of slag in the oxygen converter, and the evolution of the chemical composition of slag during the steelmaking processes for all analysed melting processes [19].

Another minor component is free CaO. The concentration of free CaO is between 0.58 to 1.77% in all analysed slag samples. The presence of free lime in the slag within the melting process S2 is visible even to the naked eye, as shown in Figure 2. The presence of free lime was also confirmed by EDX analysis. Figure 3 describes structure of the slag in melting processes S4 and EDX analysis proving the presence of the free CaO. The content of free lime in steel slag is the key factor that hinders potential applications of metallurgical slag in the building industry. If the free lime is not stabilised, it is hydrated at sites where it comes into contact with the surrounding atmosphere and its volume increases, thus causing the volumetric instability and the consequent decomposition of the slag.

Figure 2 Free lime in the slag at the end of oxygen blowing. Melting process S2.

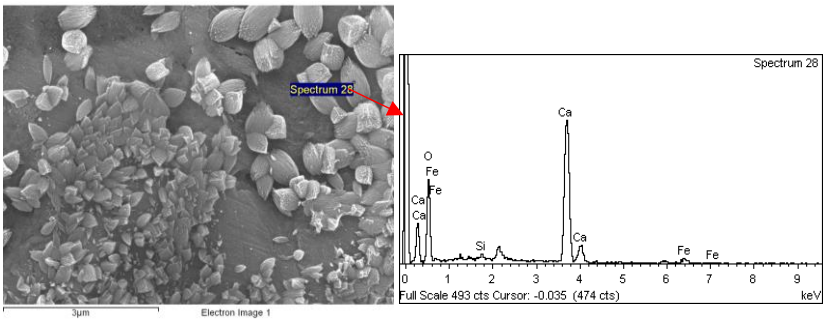

Element	Weight%	Atomic%
O	48.88	71.01
Si	0.67	0.56
Ca	45.40	26.33
Fe	5.04	2.10
Totals	100.00	

Figure 3 Structure of the slag in melting processes S4 and EDX analysis proving the presence of free CaO.

The structure of oxygen converter slag is very heterogenous. EDX microscopy analysis that was aimed at qualitative as well as quantitative confirmation of the percentages of individual structural phases present in the slag. From the mineralogical point of view, the structure of the oxygen converter slags consists of four main phases: tricalcium silicate $3CaO.SiO_2$, dicalcium silicate $2CaO.SiO_2$, stabilized tricalcium phosphate $3CaO.P_2O_5$, a solution of bivalent metals oxides, e.g. Ca, Fe, Mn, Mg, (RO-phase) and solid solutions of calcium and aluminium ferrites $2CaO.Fe_2O_3 – 2CaO.2Al_2O_3.Fe_2O_3$. Oxygen converter slag contain also large number of pores and drops of metal. Final structure of slag from oxygen converter melting process S1 is show on Figure 4.

Figure 4 Needles of tricalcium silicate and globular particles of dicalcium silicate, RO-phase and calcium ferrites in the slag sample melting process S1, 100-fold magnification.

2.1. Characterization of oxygen converter flue dust

A predominant mechanism of the flue dust production is the ejection of slag and metal particles from the bath. This is also confirmed by the fact that the majority of dust particles are spherical. The insertion of charging materials in the beginning of the blow results in the production of the majority of the flue dust. Slag-forming materials are typically charged in the first minute of the blow when the bath surface is not covered with the emulsion. If lime and dolomite lime are insufficiently sorted, a large amount of particles are too small and hence easily drawn into the exhaust burnt gases. Bigger particles get onto the bath surface where they dissolve; nevertheless, they can still get into the burnt gases before the slag-metal emulsion is formed. The flue dust produced in the first stages of the blow contains partially melted particles of lime and dolomite lime; this indicates that these particles were in contact with the bath surface.

The total contribution of the ejected particles to the flue dust production is as much as 67%. Ejection of metal is more intensive in the beginning of the blow and its intensity decreases in the final stage when evaporation occurs. Ejection of slag contributes to the production of flue dust especially in the second stage of the blow; this is explained by the fact that the slag-metal emulsion reaches its peak after six or seven minutes [20].

Liquid droplets are formed as beads, regardless of whether they originate from the impact of the oxygen jet onto the bath surface or from the bursting bubbles. The splashing and bursting of bubbles probably result in forming two types of beads – compact and porous. The beads, consisting of iron oxide edges and a solid iron core, develop as a result of the impact of the oxygen jet onto the bath surface. Zinc is only present on the surface; this indicates that the particles are formed from the bath as droplets of liquid iron. The high potential of oxygen near the nozzle oxidises the surface into iron oxide. Porous metal and slag beads are formed as a result of bubbles bursting on the bath surface and contain zinc inside, as well as on the surface; this indicates their origin in the slag-metal foam.

Fast evaporating elements, such as Zn, Pb and Cl, occur mostly in the flue dust in the beginning of the blow, and slower evaporating elements, such as Mn and Cu, were observed in the flue dust at the end of the blow, as shown in Figure 5.

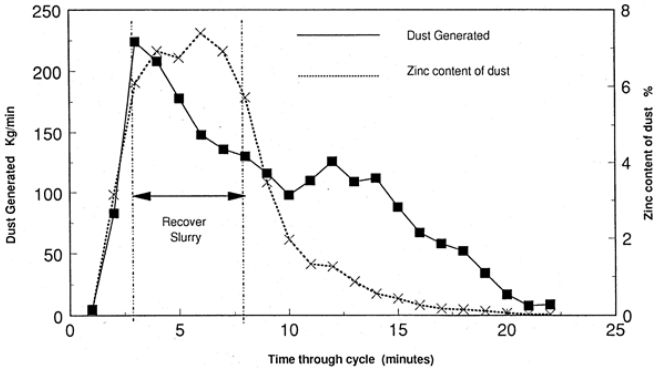

Figure 5 Typical development of converter flue dust in the BOF process including the regeneration of zinc-rich sludge [21].

Zinc is dissolved in the steelmaking slag but its extraction capacity is low and has no practical purpose. The convertor process efficiently removes zinc and leaves only a small amount thereof in the steel. The zinc evaporation rate is controlled by the diffusion in the liquid to a phase interface which is supported by fast stirring of the metal bath. An excessive amount of zinc compounds on the edges of the ejected metal droplets

indicates either fast oxidation of zinc into zinc oxide, accompanied with the production of a solid solution, or a surface reaction between iron oxides and gaseous zinc. When the zinc concentration reached 20% or more, the whole amount of the flue dust is removed from the process and utilized in the non-ferrous metals industry. The experiments were carried out analysis of the chemical composition of the briquettes made from the flue dust from an oxygen converter, Table 3. The used briquettes were of an elliptical shape, with the following dimensions: the length of 74 - 75 mm, the width of 43 - 45 mm, and the thickness of 25 - 27 mm.

Table 3 Chemical composition of the briquettes made from oxygen converter flue dust [%].

Fe met.	Fe tot.	FeO	Fe_2O_3	SiO_2	Al_2O_3	Mn	P	S	C
36.75	68.75	30.32	12.15	1.42	0.14	0.53	0.064	0.047	2.35
Na	**K**	**Cu**	**Ni**	**Cr**	**MgO**	**Zn**	**Cd**	**Pb**	**CaO**
0.500	0.364	0.026	0.001	0.028	2.50	0.585	0.001	0.131	7.75

3. Conclusion

The first part of the present article described the final chemical and mineralogical compositions of the slag that occur in an oxygen converter after the process of oxygen blowing. The chemical and mineralogical composition of oxygen converter slags is variable and depends on a large extent on the production aggregate, chemical composition and amount of input materials, technology of steel making, as well as on the grades of steel. The basic constituents of oxygen converter slags are CaO, originating from slag-forming additives, SiO2 and FeO from the metal bath oxidation reactions. These three major components represent about 80% of the total. Minor components represent less than 20% are Femetal, Fe2O3, MnO, MgO and free CaO. The mineralogical composition of oxygen converter slag consists of four main phases: dicalcium silicate 2CaO.SiO2, tricalcium silicate 3CaO.SiO2, stabilized tricalcium phosphate 3CaO.P2O5, a solution of bivalent metals oxides, e.g. Ca, Fe, Mn, Mg, (RO-phase) and solid solutions of calcium and aluminium ferrites 2CaO. Fe2O3 – 2CaO.2Al2O3.Fe2O3. The chemical and mineralogical composition of the oxygen converter slag is the most significant factor affecting its further potential use. The final properties of solidified oxygen converter slag are given by: chemical composition, mineralogical composition, crystal size, ratio of crystalline and glassy phase and porosity.

The second part of the present article was to describe flue dust from oxygen converter. Flue dust from oxygen converters, as an inevitable by-product of steelmaking in oxygen converters, may be used for the production of briquettes to be reused in the oxygen converter charge. The percentage of ejected particles is higher in the first stage of the blow. In the beginning of the blow the additives dissolve and within a short period of time the bath becomes uncovered. In an oxygen converter, gas falls onto liquid at a high speed and a large amount of droplets are formed; they are separated from the liquid phase, dispersed in the gaseous phase, and increase the speed of decarburisation. The chemical composition of the flue dust is the key monitored parameters which has a main influence on briquettes quality. With regard to the fact that converter flue dust contains also significant amounts of elements that are not beneficial for the steel properties, such as S, P, Zn, Pb, and Sn. The use of oxygen converter slag, and convertor flue dust is still limited by their chemical and mineralogical composition.

Acknowledgement

This research was funded by [VEGA MŠ SR a SAV] grant number [1/0868/17].

References

[1] Waste Catalog issued by the Ministry of the Environment of the Slovak Republic. The Collection of Laws 365/2015. Avaliable online: https://www.epi.sk/zz/2015-365 (accessed on 1 october 2019).

[2] Brožová, S.; Ingaldi, M.; Sperlin, I. Economical Aspects of High-Temperature Heating Utilization for Industrial Waste Treatment. 22nd International Conference on Metallurgy and Materials. *Metal 2013*. 15-17 May 2013. Brno, Czech Republic, Publisher: TANGER Ltd., 1735-1739.

[3] Pustějovská, P.; Brožová, S.; Jursková, S.; Kardas, E. Assessment of Technical-Economical Development Perspective of Selected Non-Ferrous Metal Potential in Metallurgy. 24nd International Conference on Metallurgy and Materials. *Metal 2015*. 03-05. Jun 2015. Brno, Czech Republic, Publisher: TANGER Ltd., 2040-2043.

[4] Baricová, D.; Pribulová, D.; Rosová, A. Steelmaking slag - waste or valuable secondary raw material. In: *SGEM 2013* : 13th International Multidisciplinary Scientific Geoconference, 16.-22. June 2013, Albena, Bulgaria. - Sofia : STEF92 Technology, 2013, 437-442, ISBN 978-619-7105-03-2.

[5] Socha, L.; Bažan, J.; Gryc K.; Morávka. P.; Styrnal, P.; Pilka, V.; Piegza, Z.; Michálek, K.; Tkadlečková, M. Evaluation of Steel Desulphurization in the Ladle During the Utilization of Briquetting Fluxing Agents for Slags. *Materiali in Tehnologije*, 2012, 6, 677-682.

[6] Socha, L.;, Bažan, J.; Styrnal, P.; Pilka, V.; Piegza, Z.; Melecký, J.; Michálek, K.; Tkadlečková, M. Evaluation of Influence of Fluxing Agents for Slags and Way of Desoxidation on Efficiency of Steel Desulphurization. In: *21st International Conference on Metallurgy and Materials*, Metal 2012. 23-25 May 2012. Brno, Czech Republic, Publisher: TANGER Ltd., 95-102.

[7] Kardas E., Brožová S., Pustějovská P. The Evaluation of Efficiency of the Use of Machine Working Time in the Industrial Company - case study, *Management systems in production engineering*, 2017, 4, 241-245.

[8] Yugov, I. P. Mechanism and Kinetics of Optimized Slag Formation in an Oxygen Converter. *Metallurgist*, July 2005, 307–310, ISSN 0026-0894.

[9] Lundkvist, K.; Brämming, M.; Larsson, M.; Samuelsson, C. Analysis of Metallurgical Processes and Slag Utilisation in an Integrated Steel Plant Producing Advanced High Strength Steels. Avaliable online: https://www.diva-portal.org/smash/get/diva2:1013704/FULLTEXT01.pdf (accessed on 3 october 2019).

[10] Deo, B.; Overbosch, A.; Snoeijer, B.; Das, D.; Srinivas, K. Control of Slag Formation, Foaming, Slopping, and Chaos in BOF. *Transactions of the Indian Institute of Metals*, 5-6, December 2013, Publisher: Springer India, 543–554, ISSN 0972-2815.

[11] Yildirim, I.Z.; Prezzi, M. Chemical, Mineralogical, and Morphological Properties of Steel Slag. *Advances in Civil Engineering*, 2011, Article ID 463638, 13.

[12] Zhao, J.; Yan, P.; Wang. D. Research on mineral characteristics of converter steel slag and its comprehensive utilization of internal and external recycle. *Journal of Cleaner Production*, 2017, 6, 50-61, ISSN 0959-6526.

[13] Sinelnikov, V., O.; Kalisz, D.; Kuzemko, R. D. Study of the Phase and Mineralogical Properties of Converter Slag During Splashing to Improve Lining Resistance, *Refractories and Industrial Ceramics*, 2018, 4, 403-409, ISSN 1083-4877.

[14] Sinelnikov, V., O.; Kalisz, D. Influence the FeO Content on Slag Viscosity at his Spraying. Increase the Life of the Refractory Lining. *Glass and Ceramics*, 2016, 3-4, 144-148, ISSN 0361-7610.

[15] Pribulová, A.; Baricová, D.; Gengeľ, P. Possibilietes of pelletizing and briquetting of fly dusts from steel and cast iron production, In: *SGEM 2010* : 10th international multidisciplinary scientific geoconference, 20-26 June, 2010, Bulgaria, Sofia, 2010, 901-907, ISBN 978-954-91818-1-4.

[16] Nedar, L.; Lindblom, B.; Björkman, A. Mechanism of dust formation in LD-converter, *Steelmaking conference proceedings*, Pittsburg, 24–27 March 1996, 173– 175.

[17] Gritzan, A.; Neuschütz, D. Rates and mechanizmus of dust generation in oxygen steelmaking, *Steel Research*, 2001, 9, 324–330.

[18] Santanu, K. R.; Gautam, Ch.; Asim, K. R. Evaluation of Dust Generated from Basic Oxygen Furnace Steel Making. Avaliable online: https://www.tandfonline.com/doi/pdf/10.1080/10473289.1997.10463929?needAccess=true (accessed on 7 october 2019).

[19] Allibert, M. Slag Atlas, 2nd ed.; Verein Deutscher Eisenhuttenleute: Dusseldorf, Germany, 1995, 126. ISBN 3-514-00457-9.

[20] Pribulová, A.; Baricová, D.; Futáš, P. The effect of adding briquettes made of converter flue dust on the quality of steel from oxygen converters. In: *Wybrane aspekty innowacyjne i ekologiczne technologii produkcijnych*, Publisher : Wydawnictwo Wydziału Inżynierii Produkcji i technologii Materiałów Politechniky Częstochowskiej, Częestochowa, Poľsko, 2018, 24-44. ISBN 978-83-63989-65-1.

[21] Mihok, L. Processing of secondary raw materials in black metallurgy. Technical university of Kosice. Faculty of Metallurgy. April 1994. Kosice.

INFLUENCE OF BATCH CHARACTERISTICS ON PRODUCTS OUTPUT IN IMPERIAL SMELTING PROCESS

Mikolaj Bernasowski[1*], Arkadiusz Klimczyk[1], Ryszard Stachura[1]
[1]Faculty of Metals Engineering and Insustrial Computer Science, AGH University of Science and Technology, 30-059 Krakow, Poland; mbernaso@metal.agh.edu.pl (M.B.); arkadiusz.klimczyk@agh.edu.pl (A.K.); stachura@metal.agh.edu.pl (R.S.)
*Correspondence: mbernaso@metal.agh.edu.pl; Tel.: +48-12-617-31-87

Abstract
The article presents research on modelling and calculating of product masses in the process of simultaneous smelting of zinc and lead, commonly known as Imperial Smelting Process. The aim of the study was to determine the output depending on miscellaneous raw materials using as a batch.

Keywords: zinc and lead production; Imperial Smelting Furnace (ISF); Imperial Smelting Process (ISP)

1. Introduction

The Imperial Smelting Process (ISP) was developed mid last century in the UK to create a pyrometallurgical continuous zinc winning process. HCM in Miasteczko Śląskie (Poland) is the only zinc smelter in Europe which uses Imperial Smelting Furnace (ISF). Despite the fact that the ISP technology disappears in the world, it is still very effective thanks to the parallel production of zinc and lead. Thus, in the furnace are not produced lead containing residues like in other zinc-making processes. Beside traditional raw materials as lead and zinc sulphides, it is also necessary to process oxides of these metals deriving from increasing amounts of post-processing waste [1,2].

The present paper shows what was found during three stages of ongoing project and details that need to be considered while process modelling, output calculation and especially coke consumption.

2. Sinter crusher gap size test

Generally, in a shaft furnace, the sinter is evaluated in terms of strength and reducibility. Strength is influenced by the chemical composition of the material and the manner in which the agglomeration process is carried out. Reducibility is a more complex indicator. It depends on the chemical composition, the type of compounds that make up the metals, but also on other factors, the most important of which is the graininess of material charged to the furnace. It follows that the total value of this indicator can be influenced by the selection of the reacting phase's surface. If the contact surface is more extensive, the reduction process is more intensive intensify, including indirect reduction. In the case of the furnace for the production of zinc and lead, the system of temperature zones is selected so as to counteract reoxidation carried with zinc gases. For this reason, the temperature of the flue gas should exceed 900 °C. Thus, almost the entire column of materials in the reactor working space is in the Boudouard reaction zone. It is therefore possible to assume a large advantage of endothermic direct reduction over indirect reduction. Zinc almost entirely will give oxygen with the participation of Boudouard reaction. In the case of lead, which is reduced at lower temperatures, a certain share of indirect reduction is possible. The greater its share, the better the utilization of the gas reduction potential and the lower fuel consumption in the furnace. Intensification of indirect lead reduction, with a stable chemical composition of the sinter is possible by selecting the optimum granularity of the batch. This feature of the charge, apart from the impact on the intensity of reduction processes, including indirect ones, also affects other elements of the shaft furnace operation. In the case of too small granules of batch, one can expect an excessive increase in resistance to gases flowing to the top of furnace, with constant values of pressure loss, a decrease in production resulting from the counter-current nature of the process. In the opposite situation, the charge of excessive chunkiness, the negative effect is the descent of unreacted feed material into the lower regions of the furnace. As part of the project supporting the presented work, at the blast furnace in HCM Miasteczko Śląskie was carried out an industrial test to investigate the impact of sinter size on the reducing ability of the gas phase and fuel consumption[3]. Changes in the sinter grain size were made by the gap size adjusting of the crushing unit, located between the sinter plant and the blast furnace. The normally used gap size is 140 mm. Table 1 shows sinter grain distribution.

Table 1 Sinter grain size distribution and ISF operation data in dependence of crusher gap size during industrial test.

Crusher gap size (mm)	Share of sinter grain size (wt%)				Top gas (vol%)		Coke consumption (kg/Mg Zn)
	0-20 (mm)	20-100 (mm)	100-150 (mm)	>150 (mm)	CO	CO_2	
140 (referenced)	1.64	28.39	33.76	36.21	31.80	6.62	1060
130	3.99	33.23	31.86	30.91	29.03	7.47	1047
110	6.25	38.14	29.41	26.34	28.40	7.17	970

3. Output calculation model

Complexity of winning process, where substances moves through several phases, does not allow to determine precisely the main product stream mass at the short period [4]. The accuracy of determining the mass of main products in an ISP is the more accurate the longer the time of overhead they are evaluated: shift, day, month. However, for the proper conduct of the process and especially for the control of the heat supply in dependence on its demand, it is necessary to determine the masses in a shorter period such as an hour, even half-hour.

Figure 1 shows material streams of ISP on which it is based charging model [5]. From the furnace top are charged sinter, coke and sometime gathered in smelter zinc scrap. These materials are precisely weighted. By-products as scale gathered from condenser well and black sludge from the off-gas filter are estimated daily in kg per tonne of raw zinc (tRZn). Also lead in condenser – sprinkled lead (SPb) - must be supplemented with about 70-80 kg/tRZn. So the unknown parameters in this system are the masses of raw zinc (RZn), raw lead (RPb) and slag. These unknowns can be found by solution of a system of three linear equations describing the material balance for Zn, Pb and SiO_2.

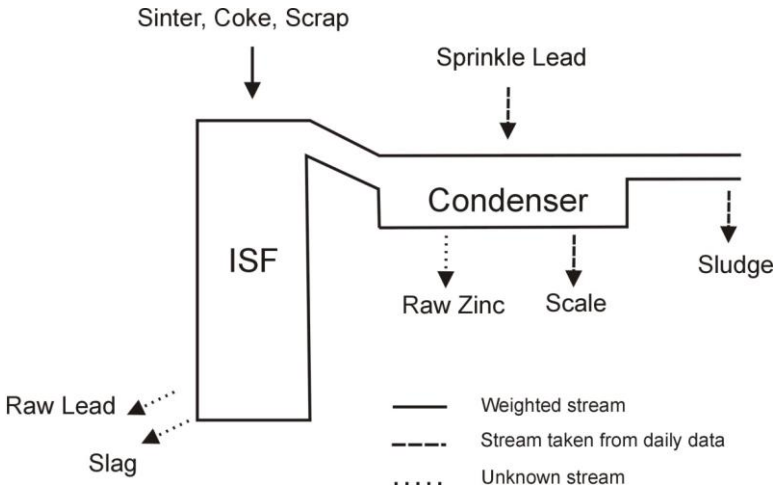

Figure 1 Materials streams in ISP [5].

Zinc balance:

$$\%Zn_{sinter} \cdot M_{sinter} + \%Zn_{scrap} \cdot M_{scrap} =$$
$$= \%Zn_{slag} \cdot \boldsymbol{M_{slag}} + \%Zn_{RZn} \cdot \boldsymbol{M_{RZn}} + \%Zn_{RPb} \cdot \boldsymbol{M_{RPb}} + \%Zn_{scale} \cdot M_{scale} + \%Zn_{sludge} \cdot M_{sludge} \quad (1)$$

Lead balance:

$$\%Pb_{sinter} \cdot M_{sinter} + \%Pb_{scrap} \cdot M_{scrap} + 100 \cdot M_{SPb} =$$
$$= \%Pb_{slag} \cdot \boldsymbol{M_{slag}} + \%Pb_{RZn} \cdot \boldsymbol{M_{RZn}} + \%Pb_{RPb} \cdot \boldsymbol{M_{RPb}} + \%Pb_{scale} \cdot M_{scale} + \%Pb_{sludge} \cdot M_{sludge} \quad (2)$$

SiO_2 balance:

$$\%SiO2_{sinter} \cdot M_{sinter} + \%SiO2_{scrap} \cdot M_{scrap} + \%SiO2_{coke} \cdot M_{coke} =$$
$$= \%SiO2_{slag} \cdot \boldsymbol{M_{slag}} + \%SiO2_{scale} \cdot M_{scale} + \%SiO2_{sludge} \cdot M_{sludge} \quad (3)$$

where: %Zn, %Pb, %SiO_2 – weigh percent of element or substance (wt%)

M – mass of stream per charge (kg)

Bold parameters in equations (1-3) are unknown.

Another parameter, calculated by application is C/Zn which reflects heat input to the furnace and can be adjusted:

$$C/Zn = \frac{M_{coke}}{(\%Zn_{sinter}+0.1\cdot\%Pb_{sinter})\cdot 0.01\cdot M_{sinter}+(\%Zn_{scrap}+0.1\cdot\%Pb_{scrap})\cdot 0.01\cdot M_{scrap}} \quad (4)$$

From equation (4) the mass of sinter necessary can be derived to adjust demanded C/Zn parameter:

$$M_{sinter} = \frac{\frac{M_{coke}\cdot 100}{C/Zn}-M_{scrap}\cdot(\%Zn_{scrap}+0.1\cdot\%Pb_{scrap})}{\%Zn_{scrap}+0.1\cdot\%Pb_{scrap}} \quad (5)$$

Figure 2 shows comparison of real sinter masses and proposed by model. Average standard deviation was 2% while max deviation about 8%.

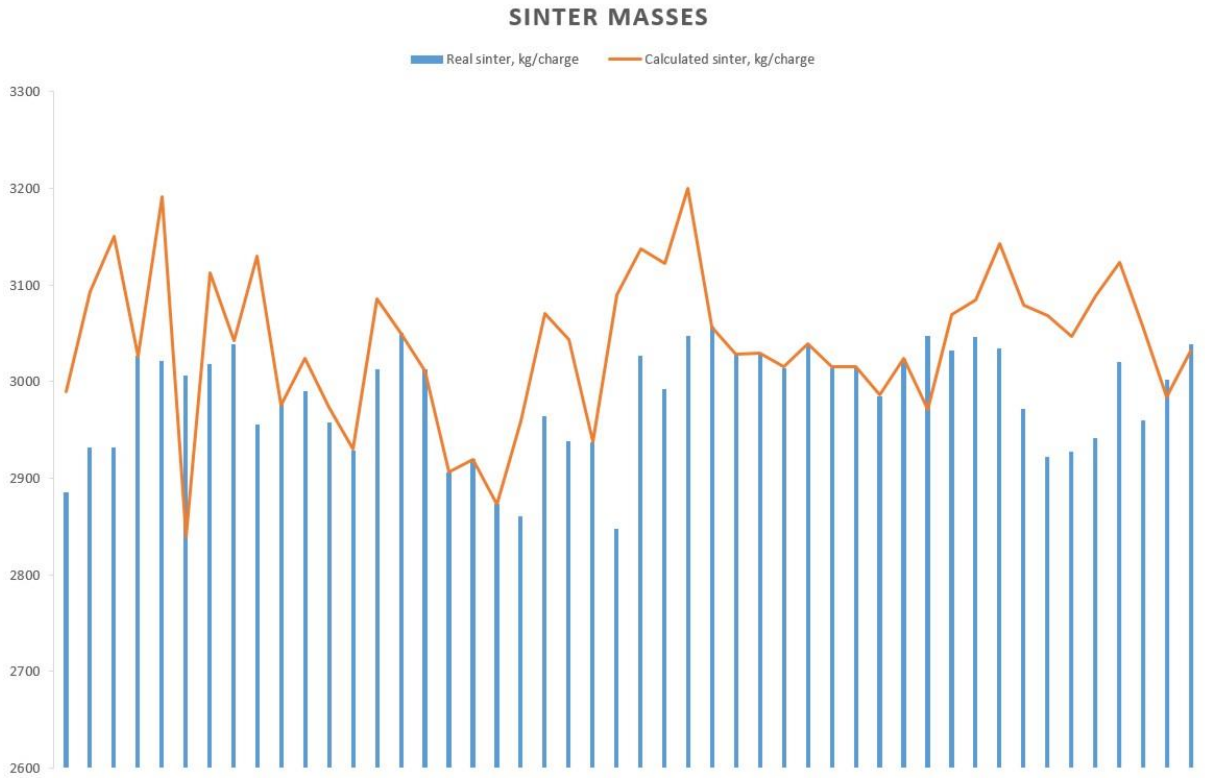

Figure 2 Real and calculated sinter masses during industrial test.

4. Equilibrium zone determining

The aim of this stage was to determine the effect of reductivity of various sinters produced from sulphide raw materials and from waste oxides on the operation of a shaft furnace. Real sinter samples from the sinter plant operating at the ISF furnace were collected for the experiment (Table 2). The experiment was carried out in a resistance furnace with a horizontal pipe at the temperatures below 900 °C to exclude zinc reduction. A mixture of nitrogen and carbon monoxide was used as a reducer. Reduction kinetics were determined based on the analysis of flue gas. Research has shown that at lower temperatures there are no significant differences in the reduction of sinters, while in higher temperatures the reduction of waste oxides sinter was faster. Moreover, from the comparison of the reduction characteristics at lower and higher temperatures, it was found that the use of too large pieces of sinter may delay the reduction of zinc and even cause endothermic direct reduction of lead.

Table 2 Chemical composition of sinter made from sulphide and oxide raw materials.

Sinter made of:	Mass %							
	Zn	Pb	FeO	CaO	SiO_2	MgO	Al_2O_3	S
Sulphide materials	42.82	13.64	11.59	3.28	4.26	0.87	1.09	2.10
Oxide materials	41.12	12.77	8.87	3.06	6.09	1.43	2.99	0.61

Therefore, it is very important to keep the grain size of sinter at an optimum level and avoid excessive chunkiness. This is delayed the reduction of lead and thus the beginning of reduction of ZnO in the shaft furnace. In addition, such a delay also causes the reduction of lead at Boudouard reaction temperature (II) and therefore the reduction of PbO in the two-step direct reduction mode:

$PbO+CO=Pb+CO_2$ (I)

$CO_2+C=2CO$ (II)

$PbO+C=Pb+CO$ (III)

It means that real ISP should be modelled as showed in Figure 3 or at least idealized schema should be used for preliminary calculation [6, 7].

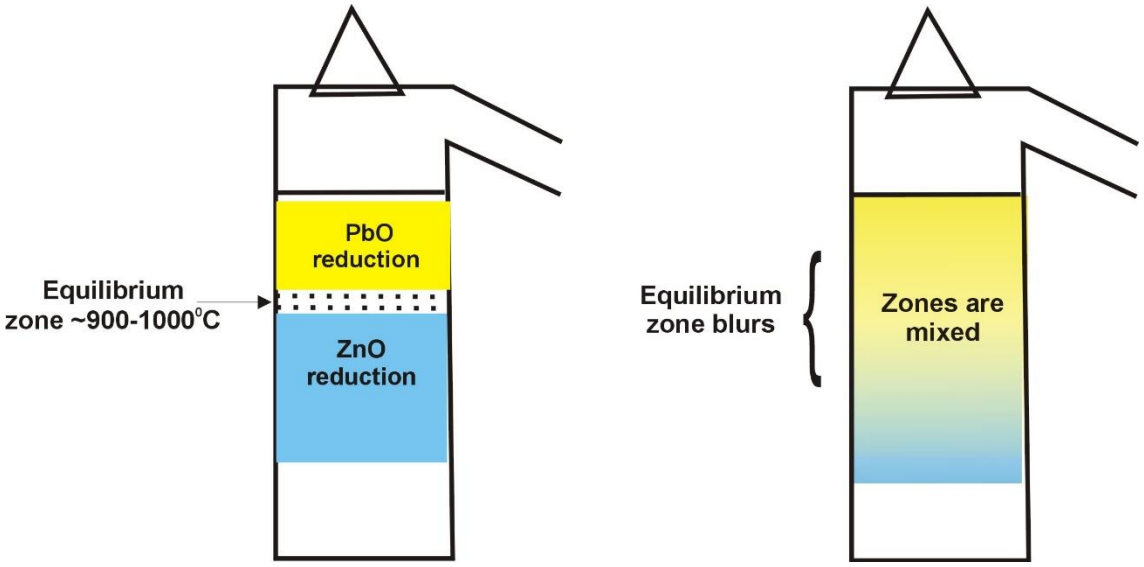

a) Idealized ISP b) Real ISP

Figure 3 Differences between idealized and real run of ISP [8].

5. Conclusion

The product output in ISP situated in Miasteczko Śląskie mainly depends on technological situation of sinter plant and character of using batch materials.

Industrial grain size test of sinter used as batch in ISF showed a favourable direction in changing the flue gas composition (CO, CO_2) and reducing the consumption of coke.

Output calculation model allows to calculate demanded masses of batch materials depending on heat state of ISF. There is also possibility of the main products masses calculation obtained after actual charging.

The main objective of reduction test was to determine the occurrence of metallic phases in sinters made from sulphide and oxide raw materials after medium temperature reduction and comparing of the reduction kinetics. Test shown that kinetic of sulphides and oxides sinters are similar, however oxides sinter seems to reduce a bit faster. This can be explained by lower sulphur content in the batch. Presence of PbO shows that at temperatures below 900 °C the Pb reduction is not finished, what entails that in ISP blast furnace the PbO reduction zone is not clearly separated from ZnO reduction zone. PbO reduction zone penetrates to the high

temperature area in ISP and equilibrium zone fades. The range of this penetration can affect on the degree of increased consumption of coke in the process because PbO will be reduced directly.

Acknowledgement

This work has been financed by European Funds, Operational Programme Smart Growth 2014-2020, Sectoral Programme INNOSTAL, project no. POIR.01.02.00-00-0174/16.

References

[1] Ingaldi, M.; Jursova, S. Economy and possibilities of waste utilization in Poland. METAL 2013: 22nd International Conference on Metallurgy and Materials, Czech Republic, **2013**, 1779-1784.

[2] Pustejovska, P.; Brozova, S.; Jursova, S.; Lyzbicka, N. The environmental aspect of production of sinter, SGEM 2015 15th International Multidisciplinary Scientific Geoconference , Bulgaria, **2015**, 855-861

[3] Stachura, R.; Klimczyk, A.; Bernasowski, M. Influence of selected batch properties on the operation of imperial smelting furnace. METAL 2018: 27th International Conference on Metallurgy and Materials, Czech Republic, **2018,** 1729–1733

[4] Zhou, P.; Liu, C.; Jiang, A.; Chen W.; Mei, C. Numerical simulation of transfer process in imperial smelting furnace. ASME International Mechanical Engineering Congress and Exposition, USA, **2008**, vol. 3., 585-589

[5] Bernasowski, M.; Klimczyk, A.; Stachura, R. Imperial smelting furnace charging model. METAL 2018: 27th International Conference on Metallurgy and Materials, Czech Republic, **2018,** 1478–1482

[6] Banerjee, A.; Sen, P.K.; Roy, S.K. Novel approach to modelling of imperial smelting furnace behaviour, *Min. Proc. Ext. Met. Rev.*, **2006**, 28, 159-176.

[7] Creese R.C.; Healy G.W. A chemical equilibrium model of the imperial smelting blast furnace, *Can. Metall. Quart.*, **1975**, 14, 175-181.

[8] Bernasowski, M.; Stachura, R.; Klimczyk, A.; Kargul, T.; Kopia A. Studies of Zn-Pb sinter reduction used as a batch in imperial smelting process, SGEM 2019 19th International Multidisciplinary Scientific Geoconference , Bulgaria, **2019**, 925-930.

EFFECT OF LADLE SHROUD MISALIGNMENT IN THREE STRAND T SHAPED TUNDISH

Adrián Bitto[1*], Slavomír Hubatka[1]

[1]Technical University of Košice, Faculty of Materials, Metallurgy and Recycling, Košice, Slovakia Department of Metallurgy, Faculty of Materials, Metallurgy and Recycling, Technical University of Košice, Letná 9, 042 00 Košice, Slovakia

*Correspondence:adrianian.btt@tuke.sk; Tel.: +421 44 130 497

Abstract

The present work involves the use of physical modelling in order to study the effect of slight misalignments of the ladle shroud on wearing of refractory lining of a T shaped three strand continuous casting tundish. For a physical modelling a 1:2 scale water model was used to observe the effect of ladle shroud alignment on residence time distribution of each strand resulting in different wearing of the refractory lining. Those observing should give us better understanding of the importance of accurate ladle shroud placing leading to savings in maintenance of working lining.

Keywords: Physical modelling; residence time distribution; refractory lining

1. Introduction

Constantly raising demand for higher production rates of higher quality steel is creating pressure on production process of steel slabs. Continuous casting is most common method of producing these slabs [1]. The molten steel flow patterns inside the components of the caster play an important role in the quality of these products. A simple yet effective design method that yields optimum designs is required to design the systems influencing the flow patterns in the caster. The tundish is one of these systems. Characteristics of steel flow in the tundish can be affected by means of shape, size and dimensions changing of the tundish or using the steel flow modifiers. Traditionally, experimental methods were used in the design of these tundishes, making use of plant trials or water modelling [2].

At the present time, increasing demands are placed on the tundish, as it provides several metallurgical operations. In addition it's providing many possibilities of steel treatment, in particular chemical and thermal homogenization, deoxidation, type and flow control, reduction of ferrostatic pressure and others [3]. One of its main tasks is to transport the liquid metal into one or more molds uniformly, at the selected flow rate and temperature without the inclusions contamination.

Well optimised and regulated flow also plays important role in affecting working lining of the tundish. Various factors may affect perfect flow balance which one of them is misalignment of ladle shroud. After examination of the problem, these main factors were summarized:

1. Technological limitations of operator capability to precisely fit ladle shroud. Operator can only count on his own judgement and guess correct position, which doesn't only affect the impact point but also impact angle.
2. The ladle turret does not have automatic shut off. It is done manually by operator.
3. Wrong selection of impact pad.

2. Experimental Materials and Methods

Experimental measurements were performed on water model of three strand T shaped tundish(Figure 1), that was built in collaboration with steel plant Podbrezová and it is located at the Technical University of Košice, Faculty of Materials, Metallurgy and Recycling, Department of Ferrous Metallurgy and Foundry. The model, taking into account theory of similarity, is built at scale 1:2. Water flow automation is secured through a top flowmeter, an electromagnetic valve for reservoir filling, automatic valves at the outlet nodes, and reservoir and tundish water level sensors.

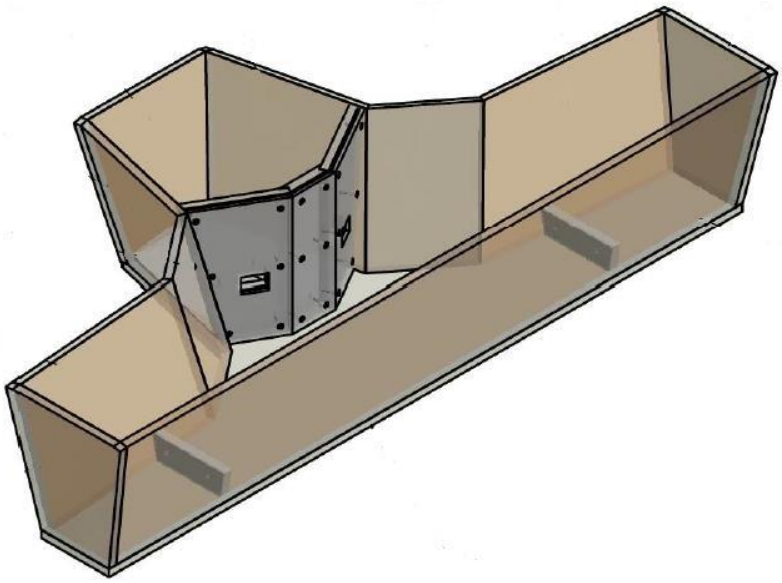

Figure 1 Configuration of the three-stand tundish [7].

System Simatic is used for measurements of ongoing processes. The system interface is based on the same one used on the real device. Such control allows simulation of all tundish operating states as well. To clarify various effects that occur in the tundish and affect the properties of produced steel, it is necessary to know the time spent by a particular element in the tundish. The period is called residence time distribution [4].

Two RTD values are known:

- Minimum residence time τmin which is the minimum time at which the impulse of the marker injected into the ladle shroud (τ0= 0s) appears on the outlet from the tundish.
- Maximum residence time τmax is duration between τ0 and the maximum measured concentration of the marker on the outlet of the tundish [5].

The minimum residence time and τmin and the maximum residence time τmax is determined from the C-curve. Values for C-curve computation are most commonly obtained under laboratory conditions on water models, where measured values of the change in conductivity of the trace substance between the inlet to the tundish and the outlet at the individual outlet nodes are obtained.

From the measured values a graph is created, resulting in the C-curve presented in Fig.2 [6]. The value of the minimum residence time has a decisive effect on the time that non-metallic inclusions discharge from steel to slag. This time should be as long as possible.

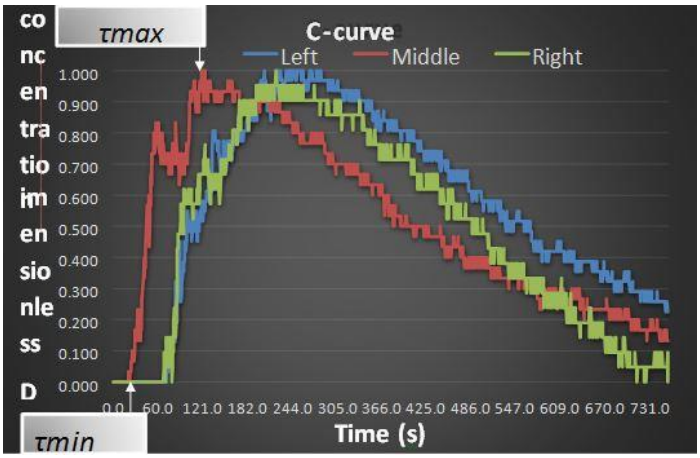

Figure 2 C-curve.

For measurement, the ladle shroud was deliberately misalign from its optimal position. The deflection of the outlet opening from the center was 5cm and the position of ladle shroud was shifted by 45° after each

measurement as is shown in Fig. 3. There were conducted three measurements for each configuration under the same conditions, from which average values for minimum and maximum residence time distribution were evaluated. For visual comparison, solution of potassium permanganate was used and observations were captured at three time intervals depending on the greatest difference observed.

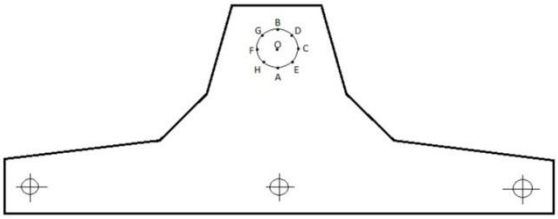

Figure 3 Ladle shroud configurations.

3. Results and Discussion

Demonstrated graphs and visual cuts from the measurements allow us to compare mutual flow differences for each configuration. Fig.4 and Fig.5 represents minimal and maximal residence time distributions for each configuration in comparison with optimal configurations (Lmin – Left strand, Cmin – Center strand, Rmin - Right strand).

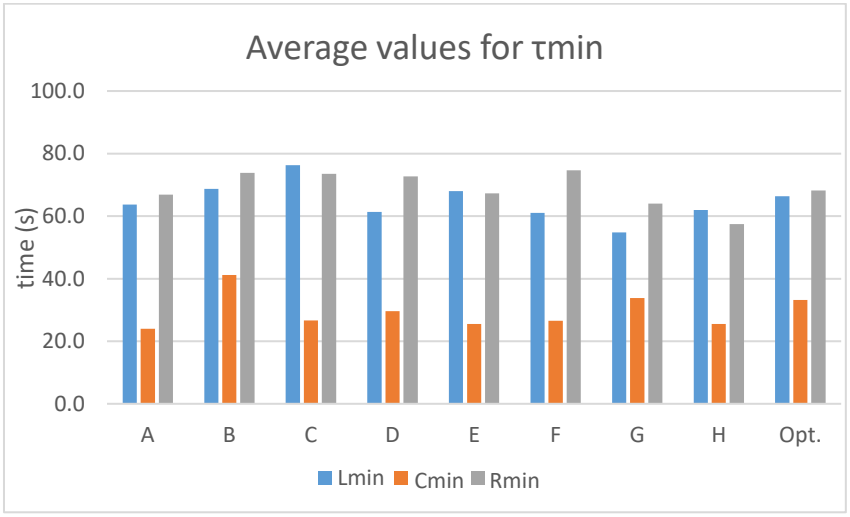

Figure 4 Average values for τmin.

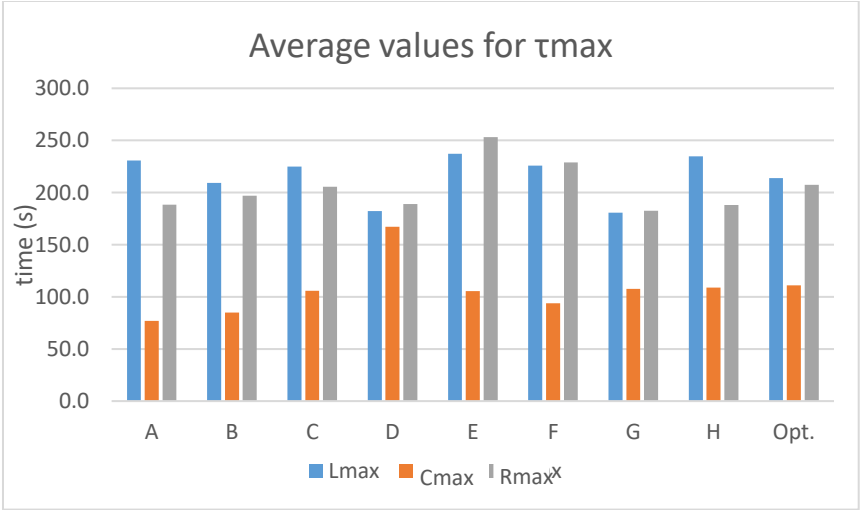

Figure 5 Average values for τmax.

The verify measurements reliability, mirror configurations were compared as is shown in Fig. 6 Representative configuration F-C was chosen. Relatively high match was found between graphs and mirror configuration. Some inaccuracies may be result of turbulent flow and deviations while adjusting position of ladle shroud. The pictures were taken in 15, 30 and 45 seconds intervals.

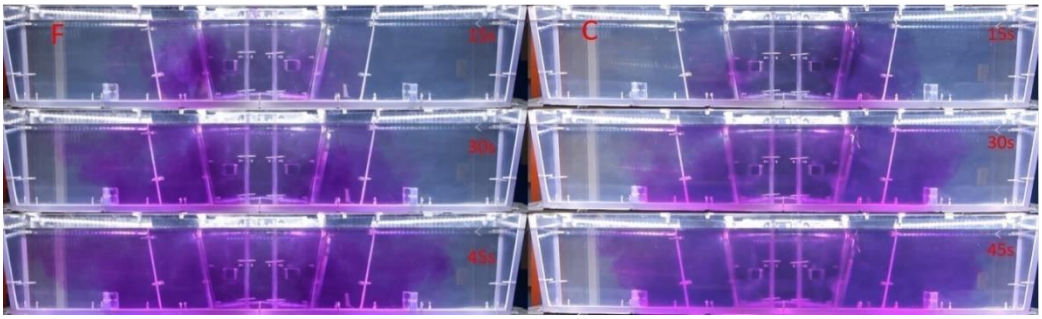

Figure 6 F-C mirror configurations.

Mirror configuration shown in Fig. 7 represents top view and is aimed to highlight a marker delay between each configuration. The pictures were taken in 5, 10 and 15 seconds intervals.

Figure 7 A-B mirror configurations**.**

4. Conclusions

When comparing the configurations A, B, there is a considerable difference in the length of the total time for which the liquid remains in the volume of the tundish. Even though change in steel quality is negligible, such prolonging has significant effect on degree of lining wearing. Configuration C, F showed tilting of steel flow to one outlet node, causing uneven wearing of lining on both sides of tundish.

Ladle shroud isn't the only tundish furniture which affects deflection of casting flows. Currently used reverse V shaped impact pad even more amplifies the flow deflection effect. It is recommended to switch this impact pad for one which will reduce that effect.

References

[1] Steel Statistical Yearbook. [online]. Available at: https://www.worldsteel.org/en/dam/jcr:e5a8eda5-4b46-4892-856b-00908b5ab492/SSY_2018.pdf

[2] T.R.Vijayaram, Metallurgy of continuous casting technology.

[online].Available at: https://www.researchgate.net/publication/286457723_TRVijayaram_Metallurgy_of_continuous_casting_technology_International_conference_on_advances_in_civil_structural_and_mechanical_engineering_Proceedings_CSM_2013_03-04_August_2013_Organised_by_IRED_Ins

[3] T. BÖHM: Continuous steel casting, 1.publisment, STNL Praha 1992

[4] MICHÁLEK, K.: Use of physical and numerical modelling for optimization of metallurgical processes, 2001, ISBN 80-7078-861-5.

[5] THOMAS, B. G., ZHANG, L.: Mathematical Modelling of Fluid Flow in Continuous Casting, ISIJ International, Vol. 41, 2001, No. 10, p. 1181–1193

[6] TASSOT, P., REICHERT,N.: *Ways of improving steel quality in the tundish.* In: Metallurgical research and technology, Publication 107, number 5, 179 – 185 s. 2010.

[7] Continuous casting steel flow optimization control – OPTICON, final work for year 2018

THE COMPARISON OF THE TWO TYPES OF IMPACT PADS IN TUNDISH OF ŽP A.S.

Branislav Bul'ko[1], Peter Demeter[1,*], Vladimír Chomič[2], Pavol Buček[2], Matej Brenkus[3]

[1]Technická univerzita v Košiciach, Fakulta materiálov, metalurgie a recyklácie, Ústav metalurgie, Oddelenie hutníctva a zlievarenstva, Letná 9, 04200 Košice

[2]ŽP Výskumno-vývojové centrum s.r.o., Kolkáreň 35, 97681 Podbrezová

[3]Železiarne Podbrezová a.s., Kolkáreň 35, 97681 Podbrezová

[*]Correspondence: peter.demeter@tuke.sk; Tel.: +421 55 602 3169

Abstract

The task of the physical simulation of steel flow in a tundish equipped with the KLT 4 impact pad resulted from the requirement of the Steelworks ŽP a.s. to prevent the negative impact of the ladle shroud deflection on the steel flow assessment criteria in the tundish. If the results of experiments using physical model were successful, the KLT 4 impact pad would replace the standard impact pad 4/B. The internal configuration of the tundish would remain the same as that normally used for casting on continuous casting machine in Železiarne Podbrezová, a.s. In addition to the new design of the impact pad, the influence of the ladle shroud deviation on the residence times of the individual strands was analysed. Experiments with KLT 4 impact pad were performed using a physical model in SimConT laboratory "Physical model of tundish of ŽP, a.s." in cooperation with the ŽP VVC s.r.o. and the Institute of Metallurgy of the Faculty of Materials, Metallurgy and Recycling of Technical University of Košice.

Keywords: impact pad; tundish; steel cleanliness; continuous casting

1. Introduction

The basis of a properly functioning tundish is in particular suitably selected covering and refining powders and the associated slag regime of a tundish. A prerequisite for the proper functioning of the slag system is an appropriate steel flow in a tundish so that the inclusions from steel are transferred into the slag and refining reactions occur at the steel-slag phase interface. From this point of view, the primary and most important is the geometric adjustment of the impact point of the steel in tundish. The vortex flow at the point of impact is due to the high kinetic energy of the inflowing steel.

One of the main indicators of the flow adjustment quality in tundish is the residence time, which is defined as the residence time of the steel particle in tundish. The longer residence time enables the more time of the inclusions in the steel have to float into the slag [1, 2, 3, 4].

The aim of the research was to compare the character of the steel flow in the tundish using the KLT 4 impact pad with the standard impact pad used in ŽP a.s. Another aim was to analyse and avoid the effect of ladle shroud deflection on the assessment criteria of steel flow in tundish using KLT 4 impact pad and the standard impact pad.

2. Methodology

The SimConT laboratory is a part of the Laboratory for Simulation of Flow Processes (LSPP) (**Figure 1**) at the Faculty of Materials, Metallurgy and Recycling, TU of Košice [5, 6]. The SimConT laboratory has been designed to utilize the long-term experience of faculty members and scientists according to the following requirements:

- Simatic®-based, fully-automatic regulation of the water level and all volumetric flow rates in the tundish;
- Easy access to the tundish equipment to facilitate service and maintenance, and future upgrades;
- Flow measurement in steady state (C-curves);
- Flow measurement in transient conditions (F-curves);
- Flow measurement in non-standard, limiting states (e.g. one- or two-strand casting, low steel level with vortex formation, shroud deviation and others);
- Evaluation of flow patterns using colorimetric and conductivity methods.

C-curves measurement method was selected to compare two tested impact pads. A C-curve is one of the most important tundish parameters in terms of steel flow quality. It describes the residence time for any given tundish configuration. The residence time is the overall time a steel particle “spends” in the tundish or, more technically, the time between entering the tundish via the ladle shroud and leaving it via one of the exit ports (submerged entry nozzles), Figure 4. C-curves are measured in steady state, i.e. with constant water level in the tundish (input flow rate = output flow rate) [7, 8, 9].

During the verification measurements it was empirically found that the optimal quantity of tracer in terms of the working range of conductivity probes is 150 ml. In general, three measurements are performed for each set of tundish configurations and casting conditions.

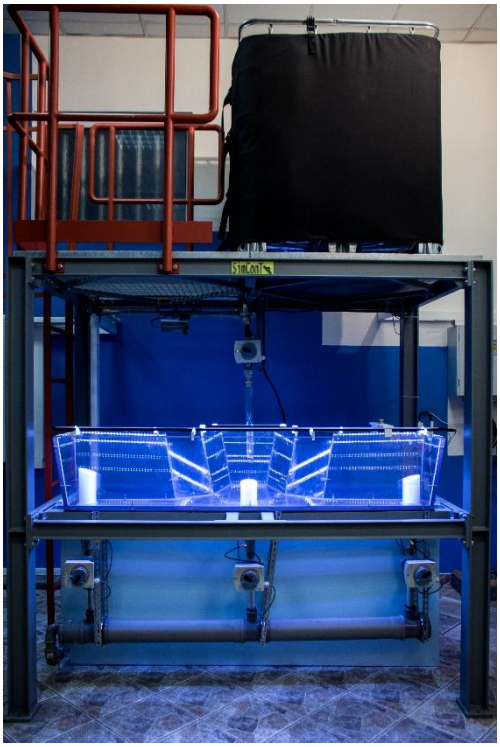

Figure 1 The water model of tundish of ŽP a.s.in scale 1:2, laboratory SimConT.

On Figure 2 is impact pad KLT4, which was compared to standard impact pad Figure 3.

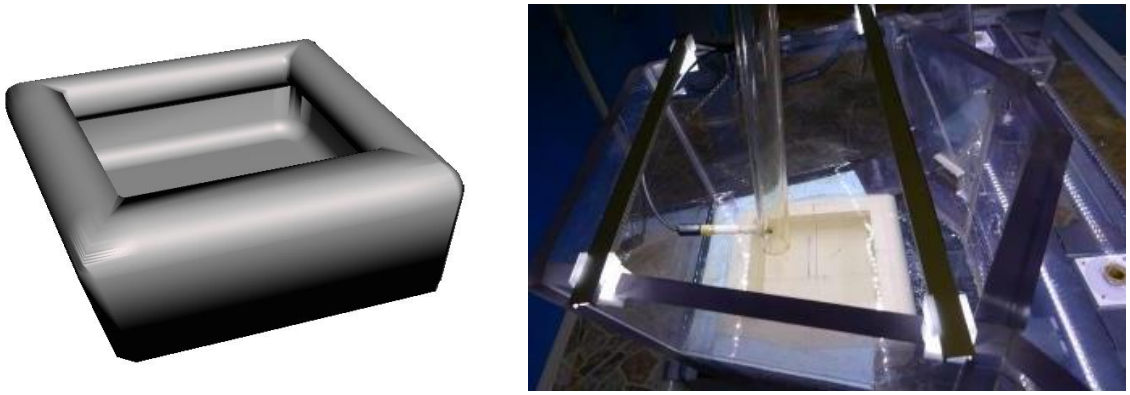

Figure 2 Impact pad KLT4.

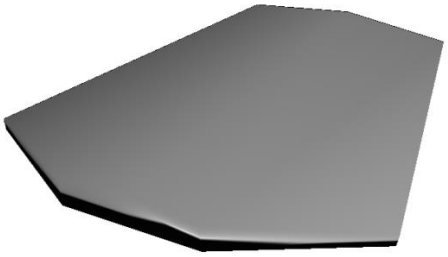

Figure 3 Standard impact pad 4/B.

To approximate the quantification of the deflection effect of the ladle shroud, a large number of experiments were performed for the outlet of the tube deflected by 50 mm relative to the vertical axis along the circle at 8 points. This deflection corresponds to a deflection of 100 mm of the real tube. Individual configurations are marked with letters A - H (Figure 4). The "O" configuration represents a correctly set ladle shroud. The parameters of casting simulation are in Table 1.

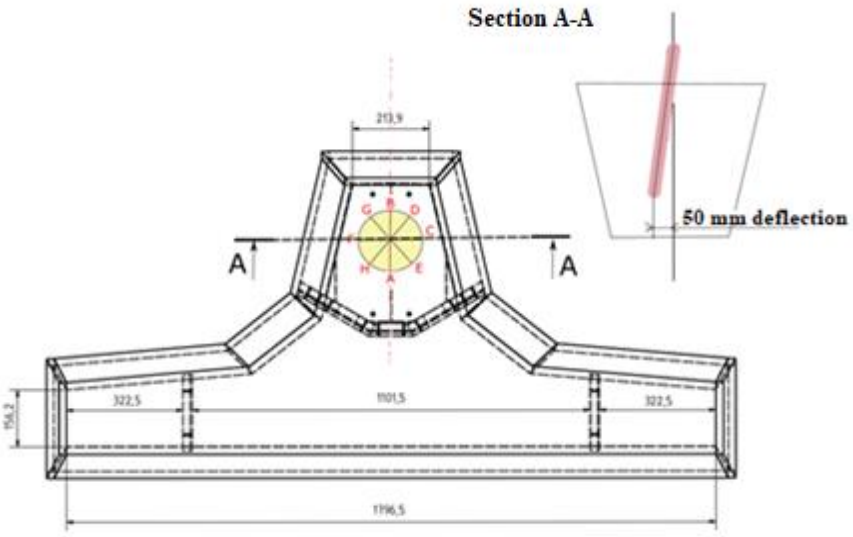

Figure 4 The measured points of deflection of ladle shroud.

Table 1 Parameters of simulation.

State	**Steady State**
Level of water in the tundish	300 mm
Volumetric flow in each strand	8 $l.min^{-1}$
Inlet flow into the tundish	24 $l.min^{-1}$
Number of repeating each measurement	3
Volume of injected tracer	150 ml

Since it is a physical model, it is not possible to achieve 100% agreement and reproducibility of measurements. However, this does not reduce the quality and informative value of the presented results. In order to increase the cleanliness of the steel in tundish, the required residence time must be as long as possible.

3. Results

The results of measurement of C-curves represented by residence time for each configuration is in Figure 5 for each strand (L – Left, C – centre, R – Right). Every configuration was tested three times and all presented measured times are calculated as an average of three measurements.

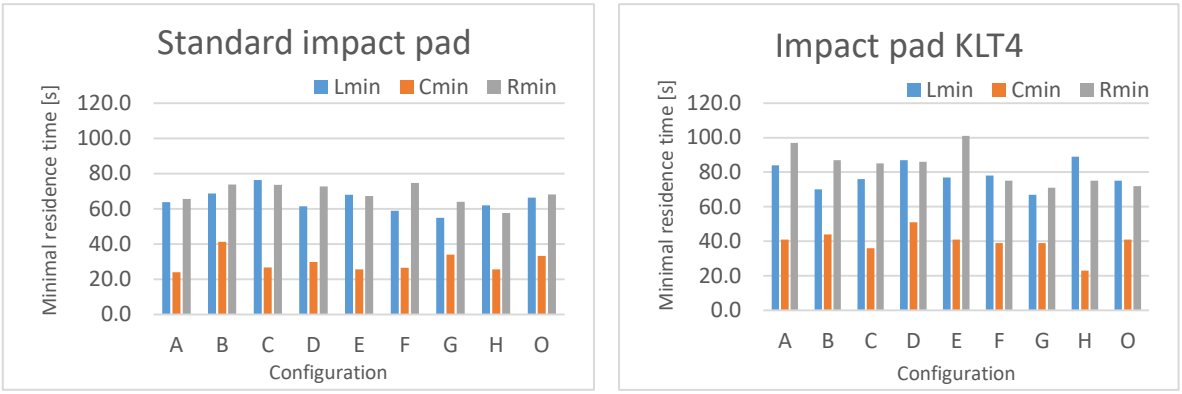

Figure 5 Minimal residence time for each configuration for both tested impact pads (in seconds).

It was found, that minimal residence time for all tested configurations is longer using impact pad KLT4. This impact pad is not so sensitive correct position of ladle shroud. Despite of high difference in residence times of centre and side strands, the real plant test were performed.

4. The results of plant trials at ŽP a.s. using impact pad KLT 4

Here is an overview of the individual testing of steel casting in ŽP a.s. using the KLT 4 impact pad.

Plant trial No. 1: casted 3 heats, sequence A

Plant trial No. 2: casted 6 heats

Plant trial No. 3: casted 6 heats

Plant trial No. 1

The test was not taken into account because more slag escaped from the main ladle during steel casting. This probably caused considerable chemical stress on ladle shroud, which was already melted after the second heat (thinner type of ladle shroud was used).

Plant trial No. 2

It was realized with a thicker type of ladle shroud. There was no splashing of steel during casting, ladle shroud handling and casting was smooth. After casting, approximately 1600 kg of steel remained in the tundish, which is a normal amount. In the area of ladle shroud was not observed formation of the so-called red eye. Excessive wear of the working liner was found in the slag area in the tundish inflow part.

Plant trial No. 3

This testing confirmed results from Plant trial No. 2.

The KLT 4 impact pad has higher minimum residence time values at all ladle shroud deflection positions, which is a basic parameter of the tundish steel flow with a direct impact on the tundish refining ability. The difference in residence times between the middle strand and the side strands should have a direct effect on the different micro-cleanliness of the steel casted on individual strands. For this purpose, the micro-cleanness according to DIN 50602 for casting with a KLT 4 impact pad was evaluated. There were no differences in the micro-cleanliness of the mid-region of all casted blocks, except 4th blocks. When assessing the micro-cleanliness of the samples, the contamination was evaluated by the K4 method. In the cross-section, mostly fine globular oxides were observed. The measured values are shown in Table 2.

The standard DIN 50602 describes the determination of the content of non-metallic inclusions in the form of sulphides and oxides in steel. The standard specifies the procedure for microscopic inspection, which uses a systematically compiled table of image standards and a description according to the type of inclusions, size of the inlay (length, width and diameter) and allowed frequency. The characteristic value (degree), which is proportional to the content of the inclusions of the specified limit size, can be calculated separately according to the oxide and sulphide fractions or as a total value. In general, the degree of cleanliness is tested on at least 6 samples. Sections are observed on a microscope at a magnification of 100 : 1. This magnification is equal to the scale display of the standard table. Each sample is inspected for the entire area of the cut to be evaluated, and the standard series of the standard table is determined. In this case, the samples were evaluated on a Neophot 21 microscope.

Table 2 The comparison of steel cleanliness using standard impact pad 4/B and impact pad KLT4.

Batch	Impact pad	Value K4	Surface area (mm^2)
A	KLT4	0	1160
A	KLT4	0	1280
A	KLT4	0	1160
A	KLT4	0	1140
A	KLT4	2.5	1180
A	KLT4	0	1200
B	4/B	6	1060
C	4/B	3	1020
D	4/B	3	1000
E	4/B	4	1040
F	4/B	5	1040

The results from laboratory SimConT, where the higher values of residence time were measured, were confirmed in plant trials. The low values of parameter K4 for impact pad KLT is in relation with longer residence times. [10-12]

5. Conclusions

Regardless of the ladle shroud position, using both the standard impact pad and the KLT4 impact pad, the minimum tundish residence time is the shortest for the 2nd (centre) strand. In the case of the reference (ideal) position of the ladle shroud, the residence times according to the results of the SimConT laboratory on the KLT 4 shaped impact pad are increased by an average of 20% for all casting strands compared to the standard pad. In general, the deflection of ladle shroud has a negative effect on the steel flow in the tundish, which may have a negative effect on the cleanliness of the cast steel. In all cases of deflected ladle shroud, the minimum residence times when using the KLT 4 impact pad are longer compared to the standard impact pad. Extensive measurements in the SimConT laboratory have also revealed that the KLT4 impact pad is less sensitive to ladle shroud deflection and the differences in residence times for the ladle shroud deflection relative to the reference position are smaller for the KLT 4 impact pad than for the standard impact pad used in ŽP a.s. These results are also confirmed by real plant tests where higher steel cleanliness was observed using the KLT4 impact pad. However, the tested impact pad KLT4 is characterized by a more intense piston flow which causes more dynamic slag movement in the tundish inflow area, resulting in increased wear of the refractory material at the slag line level. Therefore, it is necessary to adjust the shape of the tested impact pad with regard to extending the lifetime of refractory lining in the tundish.

ACKNOWLEDGEMENTS

This paper was prepared under grant project No.1/0868/17 with financial support of VEGA MŠ SR and SAV.

References

[1] Michalek, K.; Gryc, K.; Socha, L.; Tkadlečková, M.; Saternus, M.; Pieprzyca, J.; Merder, T.; Pindor, L.: Physical modelling of tundish slag entrainment under various technological conditions, Archives of Metallurgy and Materials, 2017, 62, 1467-1471, DOI: 10.1515/amm-2017-0227.

[2] Warzecha, M.: Numerical Modelling of Non-metallic Inclusion Separation in a Continuous Casting Tundish, Available online: https://www.researchgate.net/publication/221913237, DOI: 10.5772/22693.

[3] Kalisz, D.; Kuglin, K.: The influence of adsorbed Al_2O_3 inclusions on the viscosity behavior of mould slag, Archives of Foundry Engineering, 19(2), 67-74.

[4] Kalisz, D.; Zak, P.L.; Kuglin, K.: Analysis of Agglomeration of Al_2O_3 Particles in Liquid Steel, Archives of Metallurgy and Materials, 61(4), 2091-2096, DOI: 10.1515/amm-2016-0336

[5] Bul'ko, B.; Priesol, I., Demeter, P., Vrábľová, N., Baricová, D., Atyafiová, I., Chomič, V.: Optimization of the impact area in tundishes. Iron and steelmaking 4. – 6. 10. 2017, Horní Bečva, ČR, 191–200.

[6] Buľko, B.; Kijac, J.: Optimization of Tundish Equipment, Acta Metallurgica Slovaca, Vol. 16, 2010, No. 2, pp 76-83, [online], [viewed 2018-11-22]. Available from: <http://www.ams.tuke.sk/data/ams_online/2010/number2/mag01/mag01.pdf.

[7] Braun, A.; Warzecha, M.; Pfeifer, H.: Numerical and Physical Modeling of Steel Flow in a Two-Strand Tundish for Different Casting Conditions. Metal. and Mater. Trans. B, Vol. 41, No. 3, (June 2010), 549-559, ISSN 1073-5615.

[8] Chattopadhyay, K.; Isac, M.; Guthrie, R.I.L.: Physical and mathematical modelling of steelmaking tundish operations: A review of the last decade (1999–2009). ISIJ International, 2010, 50, 331-348, ISSN 0915-1559.

[9] Kowitwarangkul, P.; Harnsihacacha, A.: Tracer injection simulations and RTD analysis for the flow in a 3-strand steelmaking tundish In: Key Engineering Materials: ICEI 2016: 1st International Conference on Engineering Innovation: Bangkok, 6-7 June, 2016, 728, 72-77, ISSN: 1013-9826, ISBN: 978-303835691-2.

[10] Chatterjee, S.; Chattopadhyay K.: Formation of Slag 'eye' in an Inert Gas Shrouded Tundish, ISIJ International, 2015, 55, 1416–1424, DOI:10.2355/isijinternational.55.1416.

[11] Gerasin, S.; Kalisz, D.: Modeling of the Mn and S microsegregation during continuous casting of rail steel, Archives of Foundry Engineering, 2015, 15, 35-38.

[12] Michalek, K.: Využití fyzikálního a numerického modelování pro optimalizaci metalurgických procesů, Vysoká škola báňská - technická univerzita Ostrava, 2001, ISBN 80-7078-861-5.

THE COAL QUALITY FOR METALLURGICAL COKE PRODUCTION FROM THE COAL SURFACE MORPHOLOGY POINT OF VIEW

Martina Džupková [1,*], Mária Fröhlichová [1], Jaroslav Legemza [1], Róbert Findorák [1]

[1]Faculty of Metallurgy, Technical University of Košice, 04200 Košice, Slovakia; martina.dzupkova@tuke.sk (M.D); maria.frohlichova@tuke.sk (M.F.); jaroslav.legemza@tuke.sk (J.L.), robert.findorak@tuke.sk (R.F.)

[*]Correspondence: martina.dzupkova@tuke.sk; Tel.: +421 55 602 2755

Abstract

The paper deals with comparison of the morphology of the coal grains surface of coals, suitable for the metallurgical coke production. For metallurgical coke production are used various kind of coal, from different regions origin. Quality of metallurgical coke influence the quality, ecology and economy of pig iron production. For this purpose were selected coal mined from different locations. The selected sites were from America and Europe, while the European coals came from Poland and the Czech Republic. Besides comparing their chemical and petrographic composition, the microscopic views of the various coals after their mechanical agitation were also compared. The aim of the microscopic analysis was to study the surface texture of milled coal. Theoretical knowledge present coal as a structurally very complex substance, which is a mixture of many very complicated organic compounds and minerals. It was found that coals, belonging to the group with approximately the same level of coalification exhibited the same character of surfaces, irrespective of the shape of the grains. Conversely, varying degrees of coalification in coals of the same composition manifested different surface characteristics.

Keywords: metallurgical coal; morphology of coal; fracture surface; EDX; EDS analysis

1. Introduction

Coal as a rock is still strategic fossil raw material used by different manufacturing sectors. Major hard coal deposits formed about 300-200 million years ago in the Paleozoic era, when North America, Europe and Asia formed a proto-continent - Laurasia. In the later period began mutual separation of parts of this proto-continent, when Africa, Antarctica, Australia and India formed one proto-continent Gondwana [1]. There is an assumption that coal formed under the same conditions in proto-continent Laurasia, at the same level of coalification, could have similar properties. In metallurgical industry, in the blast furnace method of iron production, hard coal is used for coke production, which requires maintaining specific conditions during its processing.

Supplies of coking coal continue to shrink, therefore coke manufacturers, due to high coal prices at the world market, try using coal from different world deposits. This leads to the question whether the characteristics of coal from different continents influence the preparation of charge and coke formation without affecting its quality and quantity on existing plant equipment. In addition to evaluating the coking properties of the coal, particle size and morphology of the grains is equally important, as these parameters affect not only productivity of coke batteries, but also the production of refined fuels (liquid and gaseous) as well as the use of coal in other industries [2]. The composition of the coal vary depending on the location of their formation and extraction, while differences are observed in such properties as: degree of coalification, sulfur and ash content, moisture content, chemical composition, maceral composition, crude ash etc. [3, 4, 5]. By [6] for coke quality is to be able to determine coke properties before the coke is produced. This is determining for the technical as well as financial value of coke. Coal quality also affects coke quality parameters such as CSR and CRI. For example, the composition and amount of ash in coal significantly affects the quality and reactivity of coke [1].

From the petrographic perspective, coal grains are non-homogeneous - made up of macerals, which in their spatial arrangement form microlithotypes of different chemical and physical properties. These microlithotype grains react as a whole, rather than individual macerals. Accurately discriminating and quantifying macerals in coal is important as the proportion of reactive macerals is used to predict combustion behaviour [7]. All these parameters of coal are used in the international trade according to the International coal classification system (ECE), from which the price of traded coal is derived. However, this system does not provide its physical properties. One of the important properties of coal is cleavability, which is linked to the formation of coal and its gradual coalification. The cracks generated by reduction of the volume of coal-forming materials during coalification are oriented mainly horizontally, vertically and transversely in a deposit along x, y, z axes [8].

Cracking is also affected by the forces due to the pressure exerted by the adjacent rock layers typically at 45° to the plane of the coal deposit. Their number is associated with a dynamic rock pressure. Cracking is affected by petrographic composition of coal and crude ash content in the coal.

The issue of granularity of the charge for the coke production have been addressed in research works and studies by many authors [9]. Little attention, however, was given to morphology, namely the shape and surface of coal grains, which affects the use of coal in coke production as well as in other sectors. Present work, therefore, deals with grain morphology of three kinds of coal according to the degree of coalification R_0 and the comparison of differences according to origin in different deposits. In foreign studies, more attention have recently been devoted to this issue in terms of monitoring cracks and pores in the coal for the purpose of the possibility of obtaining methane from coal deposits [10-13]. In addition, various mineralogical and chemical composition of coal should also be taken into account. Increased amount of some elements in coal causes problems in the entire process in cokemaking process, blast furnace and steelproduction, as well as the negative impact on environment [14] [15] [16]. By authors [17] in the steel industry, bituminous coals are carbonized into coke in coke ovens and coke is charged into blast furnaces with sintered iron ore to produce pig iron. In this process chlorine in coke is released as HCl and could cause corrosion problems in blast furnace facilities, then it is important to know the chlorine content in coke and the behavior of coal chlorine in the cokemaking process.

2. Experimental Materials and Methods

For evaluation of coal grains morphology, as well as the mineral compositions of coal and coal ash, eight kinds of coal A-H from three different mining locations were used, with light reflectance of vitrinite ranging from 0.8 to 1.44%. Subjected to the evaluation were coals from:

America: location Buchanan, Ranger

Czech Republic: Ostrava-Karvina coal basin (part of the Upper Silesian Basin)

The Republic of Poland: Upper Silesian Basin

Coal was crushed on a jaw crusher, then subjected to sieve analysis, and for the purpose of experimental analysis was selected coal with a grain size 0.5 - 3 mm.

The determination of the shape of coal grains and subsequent evaluation of their surface was done by microscopic examination of the samples. Electron microscope TESCAN MIRA 3SE was used and the samples were observed at 98, 600 and 4000 fold magnification (EDX analysis). Similar procedure was reported by other authors [18] [19] [20]. By observation of the coal fracture planes were compared coals with respect to the degree coalification and mining location. For purposes of the coal surface morphology comparison, the samples were divided into three categories according to R_0: 0.64 -0.95% (i.e. gas coal) R_0: 1.12 to 1.14% (i.e. fat coal), R_0: 1.38 to 1.44% (coking coal).

3. Results and discussions

3.1. Comparison of coal grain shape and surface

The shape and size of grains are influenced by mechanical stress during the extraction of coal, followed by milling to the desired particle size. The process depends on the chemical and petrographic composition of coal, degree of coalification, physical characteristics, and other factors. The shape and size of coal grains, unevenness of the surface together with moisture affect the charge. density, the number of contacts between coal grains and consequently carbonization process. All this affects productivity of battery and coke quality.

Evaluation of grains of coal at about 100x magnification showed that the grinding of coal produced the grains of mainly cubic, even spherical, in less amounts of polygonal shape. There have been the grains, wherein the cubic grain shape was not maintained at 1:1 ratio, but there took place an elongation in one direction up to the ratio of 1:1.4. Sporadically, there were occurring grains of atypical form, mostly in coking coals.

Coal belongs to the materials with brittle fracture. According to [8] for bituminous coal is characteristic cleavable, brittle fracture, while grains are of cubic or spherical shape. During coal crushing smooth fracture surfaces can form, which indicate cleavage by layers of coal deposit in the seam. There is also conchoidal fracture, which occurs when vitrinite components of coal are breached.

3.1.1 Comparison of coals surfaces from the location Europe - America, R_0 (1.38% -1.44%)

At a magnification of 300x the observed surface of samples changed. There were smooth and also wrinkled surfaces. At 600x magnification of samples were observed different surfaces (Fig. 1) in coal A with cleavage fracture and coal B, which shows signs of conchoidal fracture surface. The surface of coal A is evenly wrinkled, without the presence of smooth surfaces, in contrast to the surface of the coal B, in which smooth surfaces alternate with wrinkled surface areas with conchoidal fracture elements. The differences between the observed surfaces can be explained by the fact that coals are characterized by different degrees of coalification, which affects the structure of the coal. This is also confirmed by higher magnification (4,000 times) where porous texture coal is visible. Carbonaceous matter has very diverse surface interwoven with pores and cracks, however, in coal A is observable more pronounced segmentation of fracture surface. Such a structured surface may indicate more effective reactions of decomposition products arising at thermal load. In both observed samples are visible crude ash-mineral materials.

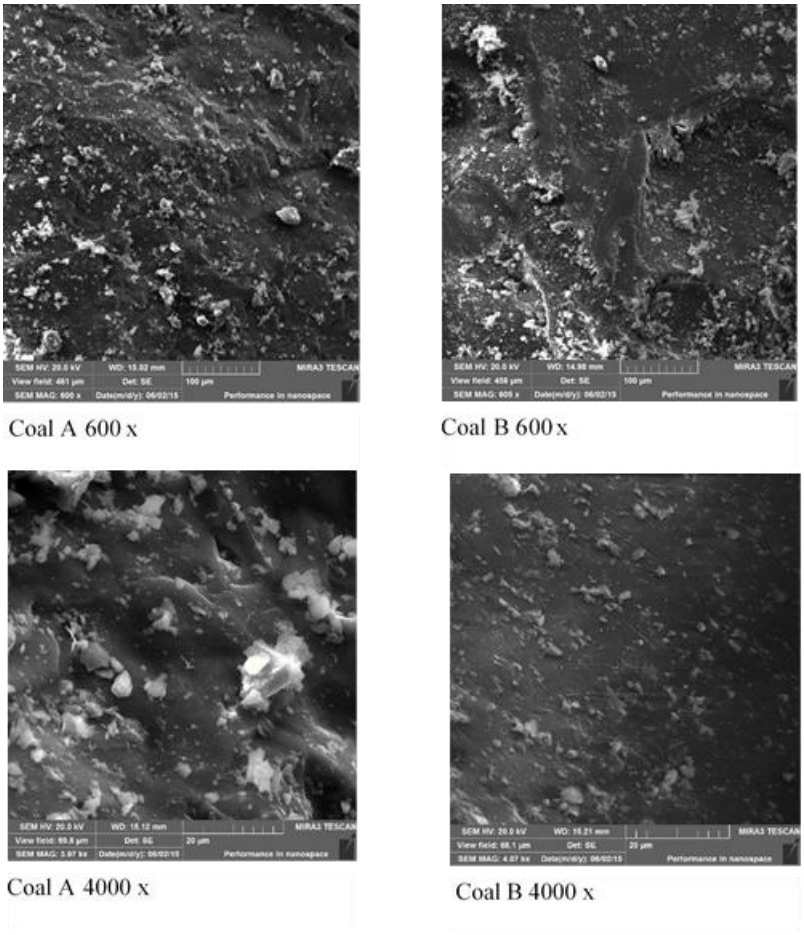

Figure 1 Surface morphology of coals A, B.

3.1.2 Comparison of coal surfaces from location Europe - America, R_0 (1.12 to 1.14)

There were observed coals C, D, E, where coals of the C, E group come from coal deposits in Europe and coal D from deposit in America. Microscopic analysis of studied coals showed that coal obtained from the same locations - C, E had very similar, almost identical surface shape with more pronounced segmentation. As shown in Fig. 2, different shape of surface may be observed in coal D, with surface after mechanical disruption formed by smoother, less wrinkled fracture surfaces as well as a significant porosity in the lower right portion of the sample. Besides of that the carbon D differs from European coals also by the highest percentage of vitrinite (77.8%), whereas coals C, E have the vitrinite content at almost the same percentage level.

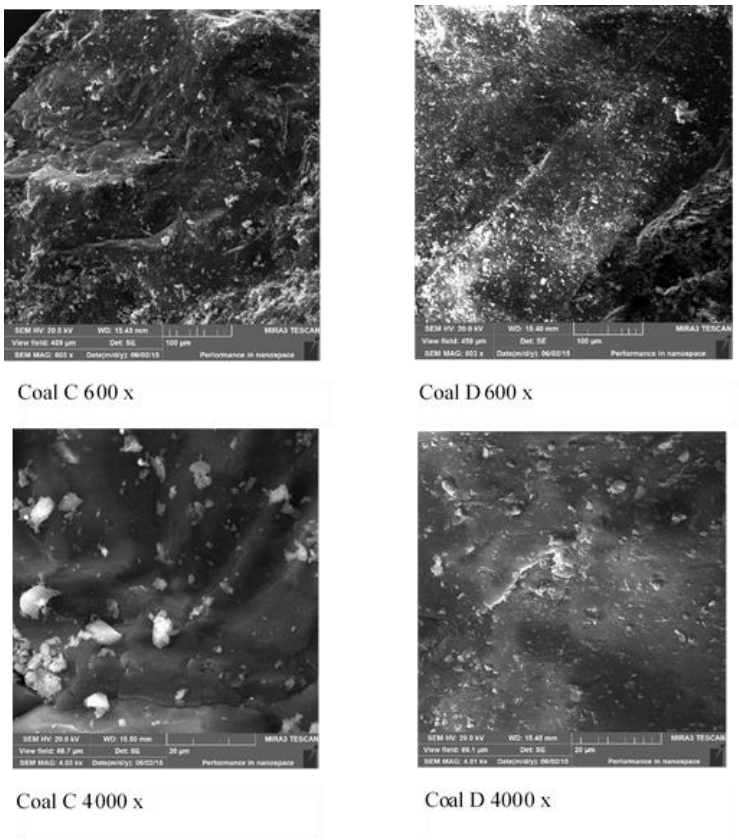

Figure 2 The surface morphology of coals C, D.

3.1.3 Comparison of coal surfaces from the location Europe, R_0 (0.64 to 0.95)

Observation of coal surfaces from one location, samples F, G, H, brought interesting results. Although the type composition of coals was almost identical, coal surfaces were markedly different at 600x magnification of samples, see Fig. 3. In coal G (600x) are well observable terrace-like fracture surfaces.

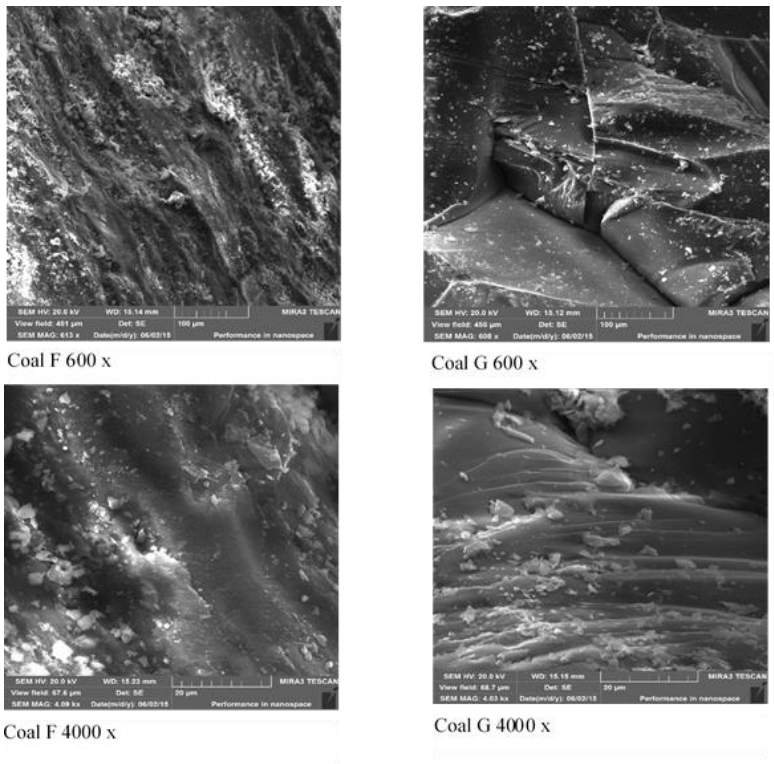

Figure 3 The surface morphology of coals F,G.

At 4000x magnification Fig. 3 was found that the samples have the same wrinkled surface shape which did not confirm presumptions about different surfaces of coal samples. Coals labelled F, G, H, coming from the European continent had also well wrinkled and wavy surface. It can be concluded that the samples with lower degree of coalification had more wavy, uneven surface, while the mining area did not play a role. The variable surface may, as in the previous analysis, influence the connection of grains during heating of coal matter, while there may occur more rapid escape of volatiles, which in turn will not provide extrusion of partially melted carbonaceous matter into the intergranular spaces. The above mentioned subsequently influences the strength of the walls of emerging product

4. Conclusion

The results of evaluations are based on specific observed samples. During the analysis and evaluation of results, it is important to also take into account the uniqueness of coal grains of coal as a natural material. Based on the above-mentioned research and analyses, it is possible to predict the properties of coals mined from various locations for various use in coal processing. The paper was intended to bring forth the diversity of individual coal seams on different continents from the perspective of their surface morphology and mineralogical composition.

There were detected:

- Differences in surfaces of coals after crushing; there were shown the smoother and wrinkled surfaces
- Coal mined in the American continent had smoother surfaces at the same value of luminous reflectance of vitrinite, in some cases, more porous structure than European coals.
- There also have been observed various representation of elements between American and European coals.

It was found that coals, belonging to the group with approximately the same level of coalification exhibited the same character of surfaces, irrespective of the shape of the grains. Conversely, varying degrees of coalification in coals of the same composition manifested different surface characteristics. This proves that the geological origin of coals does not affect the morphology of coal grains. Coalification level, however, has an important role. The surface texture is also significantly influenced by maceral and type compositions. The study showed

that observation of the surfaces of the coals can find its justification in terms of the further processing of coal.

Acknowledgement

This work was supported by Slovak Research and Development Agency (APVV), Slovak Republic, No. APVV – 16-0513.

References

[1] Roubíček V., Buchtele J., 2002. Uhlí – zdroje, procesy, užití. Praha 10-14.

[2] Kucková A., Čižmárová M., Džupková M., Fröhlichová M., 2015.Výroba ušľachtilých palív. TUKE, Košice, 20-23.

[3] Smith Lee,K., Smooth L.D., Fletcher Th.H., Pugmire R. J., 1994. *The structure and reaction processes of coal*. New York 230-235.

[4] Rajabzaki M.,Ghorbani Z., Keshavarzi B., 2016. Chemistry, mineralogy and distribution selected trace – elements in the parvadeh coals, tabas. Fuel, Vol.174, 216-224

[5] Crelling J.C., Hippo E.J., Woerner B.A.,. West D.P. Combustion characteristics of selected whole coals and macerals, Fuel, 71 (2) (1992), 151-158

[6] North L., Blackmore K., Nesbitt K., Mahoney M., Methods of coke quality prediction: A review, Fuel 219, 2018, 426-445

[7] Su A, Pohl J.J., Holcombe D., Hart J.A., 2001. A proposed maceral index to predict combustion behaviour of coal. Fuel, Vol. 80 (5), 699-706

[8] Píša M., 1978. Výroba koksu. STNL, Praha, 43-44.

[9] Burat F., Kuymcu. H. Z., Sander S., 2015.Effect of particle-size distribution and degree of saturation on coal-compacting processes within a coke-making operation. International journal for coal preparation and utilization, Vol 35 (4), 216-231.

[10] Gamson P.D., Beamish B.B., Johnson D. P., 1993. Coal microstructure and micropermeability and their

effects on natural gas recovery. Fuel, Vol. 72, 87-99.

[11] Ting F.T.C., 1977. Origin and spacing of cleats in coalbeds. Journal of pressure vessel technical transactions, Vol.99, 624-626.

[12] North L, Blackmmore K, Nesbitt K, Mahoney R. Methods of coke quality prediction: A review.Fuel 2018, 219: 426-445

[13] Crelling, J.C., Hippo, E.J. Woerner, B.A., West D.P. Combustion characteristics of selected whole coals and macerals, Fuel, 71 (2) (1992), 151-158

[14] Chakravarty, S. Mohanty, A. Banerjee, A. Tripathy, R. Mandal, G..K. Basariya, M.R et al. Composition, mineral matter characteristics and ash fusion behaviour of some Indian coals,Fuel, 150 (2015), 96-101

[15] Vassilev, S.V. Vassileva, C.G., A new approach for the combined chemical and mineral classification of the inorganic matter in coal. 1. Chemical and mineral classification systems,Fuel, 88 (2009), 235-240

[16] Milligan J.B., Thomas, K.M., Crelling J.C., Temperature-programmed combustion studies of coal and maceral group concentrates, Fuel, 76 (13) (1997), 1249-1255

[17] Nomura S., Behavior of chlorine during co – carbonization of coal and chloride compounds in cokemaking process, International journal of coal geology, vol.130, 2014, 27-32

[18] Guangqing H, Guijian L, Dun V, Biao F. Geochemical behavior of hazardous volatile elements in coals with differentgeological origin during combustion. Fuel 2018, 233, 361-376.

[19] Saikia B.K, Ward C.R, Oliveira M.L.S, et al. Geochemistry and nano-mineralogy of two medium-sulfur northeast Indian coals, Int J Coal Geol, 121, 2014, 26-34.

[20] Ruoyu S., Guijian L., Liugen Z., Chen – Lin. Ch, Geochemistry of trace elements in coals from the Zhuji Mine, Huainan coalfield, Anhu, China, International journal of coal geology, 81,2010, 81-96.

TESTING OF BLACK PELLETS IN IRON ORE SINTERING CONDITIONS

Róbert Findorák[1*], Mária Fröhlichová[1], Jaroslav Legemza[1], Martina Džupková[1]
[1]Faculty of Materials, Metallurgy and Recycling, Technical University of Košice, 04200 Košice, Slovakia;
robert.findorak@tuke.sk (R.F); maria.frohlichova@tuke.sk (M.F.); jaroslav.legemza@tuke.sk (J.L.);
martina.dzupkova@tuke.sk (M.D.).
*Correspondence: robert.findorak@tuke.sk; Tel.: +421-55-602-3155

Abstract
This paper provides a primary testing records of industrial wood pellets for application in iron ore sintering process conditions. The aim of this research was to analyze burning process of tested biomass and define optimal granularity for application in the sintering mixture. The laboratory sintering pan (LSP) was customized and used for purposes of experimental tests. The obtained results showed important differences in vertical burning speed in regard of testing conditions and parameters. Based on the experiments carried out within of industrial black pellets burning in sintering layer conditions it can be stated that the substitution of coke breeze by the grain size customized pellets is real and expected results should be better or same than sintering results with sawdust and walnuts shells respectively.

Keywords: pellets; burning; sintering; biomass; iron ore

1. Introduction

The popularity of biomass pellets is getting higher and become the most popular fuel due to coal burning prohibition in most areas and high cost of natural gas. More and more countries start to use biomass extensively and a large utility companies and power plants, using industrial pellets as fuel for heat and power production [1,2]. We know that steelmaking sector is mainly based on energy consumption and utilization of fossil-based fuels. Moreover the global energy politics in conjunction with reduction of carbon dioxide emissions is immediately concerned with iron and steel industry which belong to the biggest industrial carbon dioxide emitters with portion of 4–7% from the global emissions [3, 4, 5, 6] On the other side the properties of the fossil-based fuels and biomass are inherently different for different biomass sources. Even though it has been highlighted that, from the metallurgical process point of view, the most suitable raw materials are wood-based biomasses [7]. The sintering process is an important pre-treatment step in the production of iron by the most important route for steel production (Blast Furnace (BF) – Basic Oxygen Furnace route (BOF)) which represents about 70% of world steel production. Approximately 2/3 source of iron for BFs consist of sinter and 1/3 of pellets. BF-BOF route is mainly based on coke and coal whereby sintering process use the coke breeze as a standard fuel.

Considering this facts coke has been substituted with different type of biomass and many papers was reported about [8-12]. It was found that some biomass-based fuels have potential to substitute coke breeze even though that higher volatile matter and reactivity biofuels increases vertical sintering speed and decreases the peak temperature [13].

The aim of this research was to analyse burning process of tested biomass and define optimal granularity for application in the sintering mixture.

2. Experimental Methods and Materials

The combustion experiments of selected biomass, in terms of sucking layer, were carried out at the Laboratory sintering pan (LSP) [14], which was modified for testing smaller volumes of the mixtures. For this purpose was installed the reduced pot element with a circular cross section of d=100 mm and the possibility of monitoring temperature profile in three horizon levels of 400 mm mass height. Parallel installed SiO2 tube connected to the common suction of LSP was used for visual monitoring of the combustion zone (Figure 1).

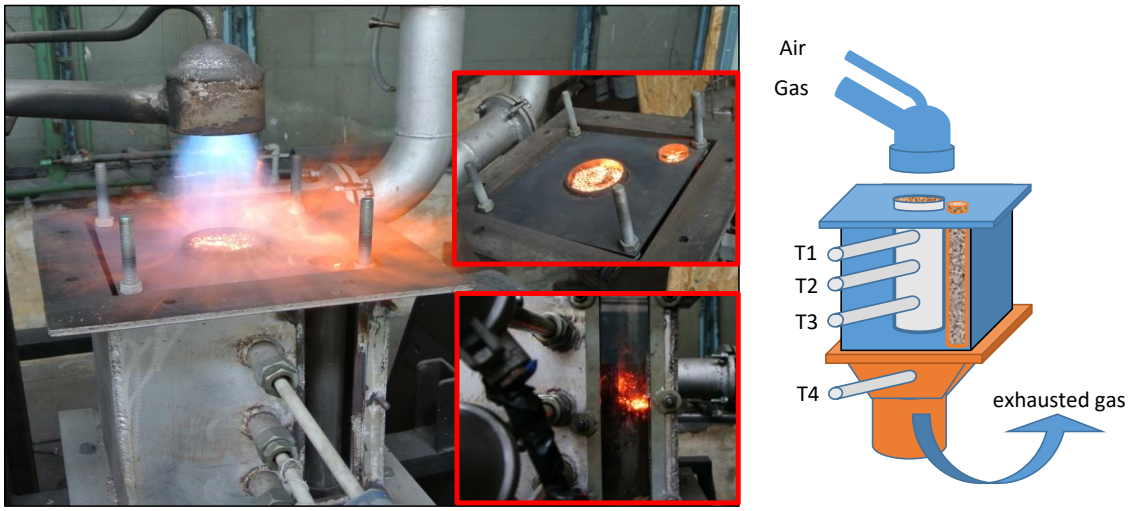

Figure 1 Laboratory sintering pan modification for experimental works.

A defined quantity of the test fuel [15, 16] was mixed with the inert heat-resistant material which (Figure 2) has been adjusted to the grain size in the range of real pre-pelletization sintering mixture. Disintegration of inert heat-resistant material (firebrick on the base MgO) has been realized gradually in two subsequent steps by the jaw crusher and swing-hammer mill. The black pellets on the base of lignin (LIG) was disintegrated using a hammer crusher. Sieve analyse of disintegrated materials has been done by vibrating sieve machine and the weight fractions of individual grain size classes were assessed. Subsequently the distribution and cumulative grading curves were calculated and constructed as well.

Figure 2 Black pellets (left - as received, middle-fraction after disintegration) and final MgO inert material (right).

3. Results and discussions

The grain distribution and the cumulative curves after the grinding and milling of the inert material are shown in Figure 3. Due to formation of a relatively high percentage of fine-grained fractions and the other side the requirement for ensuring sufficient permeability of the mixture, fractions below 1mm has been omitted and the mean grain size of the inert material increased from 1.98mm to 2.85mm. The permeability of the separated refractory material was determined for a column of 400 mm batch at 0.25 m3/hour, which falls within the permeability interval of the pre-pelletized batch for our permeability machine conditions.

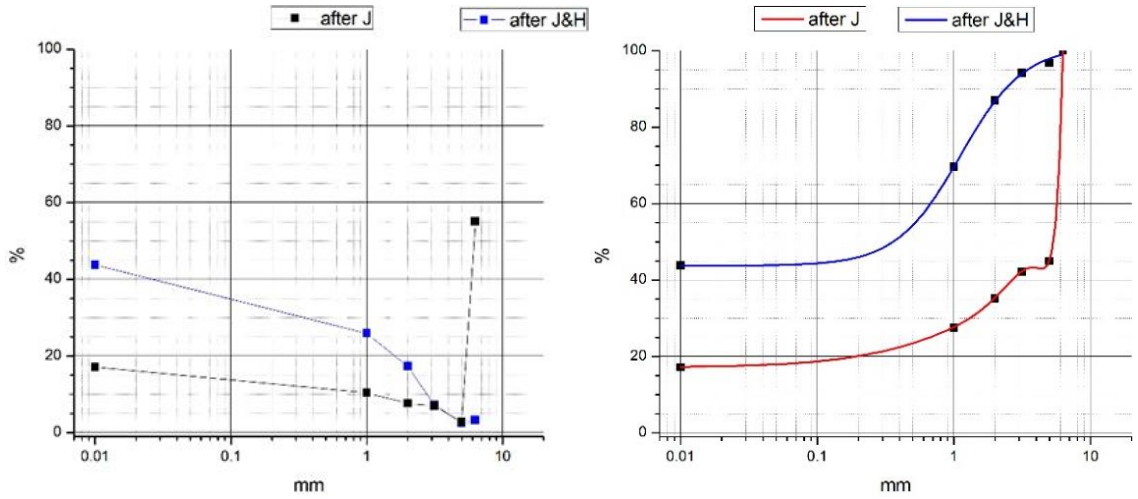

a) b)

Figure 3 Distribution (*a*) and cumulative curves (*b*) after disintegration process (J-jaw crusher, H-hammer mill).

Individual model situations were used for black pellet burning experiments in comparison with standard coke breeze (Table 1). As we can see the LIG burns faster as coke breeze in all tested grain size range. Burning speed was calculated from 26 to 30 mmmin-1 for 5kPa underpressure sucking. Reducing the underpressure to 3kPa result in decrease the burning rate, with a more pronounced effect on the reduction being measured at LD1. Although the increased reaction surface of the fuel promotes the combustion kinetics, in this case the parameter of the reduced air permeability and the air flow rate prevailed.

Table 1 Chosen parameters of testing.

Experiment	fuel	D_{avg} / mm	ΔP /kPa	speed /mm.min^{-1}	time /min:sec
K2	coke	1.55	5	11.80	33:50
LA3	LIG	1.93	5	28.90	13:50
LB1	LIG	4.08	5	29.70	13:27
LC1	LIG	6.50	5	26.14	15:18
LC2	LIG	6.50	3	21.66	18:28
LD2	LIG	1.05	5	23.30	17:08
LD1	LIG	1.05	3	15.80	25:16

4. Conclusion

The following knowledges can be deduced from pilot tests of LIG burning under conditions of sinter layer simulation:

- the simulation of combustion under agglomeration layer conditions showed differences in kinetic parameters of oxidation for individual types of fuels,
- a treatment of the tested LIG biomass in a hammer mill and selecting a suitable mesh size will ensure a suitable grain size for use in the sintering process,
- the LIG burning rate increases with increasing underpressure while maintaining the batch permeability,
- a fuel grain size affects the overall permeability of the mixture and the conditions of oxidant supply to the reaction surface of the fuel,
- the black pellets burns more intensively over the whole range of usable grain size compared to sinter coke
- the optimum grain size of black pellets for sintering process application was determined in a narrower interval 2-4mm

Based on the experiments carried out within of industrial black pellets burning in sintering layer conditions it can be stated that the substitution of coke breeze by the grain size customized pellets is real and expected results should be better or same than sintering results with sawdust and walnuts shells respectively [13, 14, 17, 18].

Acknowledgement.
This work was supported by Slovak Research and Development Agency (APVV), Slovak Republic, No. APVV-16-0513.

References

[1] Thrän, D., Peetz, D., Schaubach, K., Backéus, S., Benedetti, L. and Bruce, L., 2017. Global wood pellet industry and trade study 2017. IEA Bioenergy Task 40.

[2] Proskurina, S., Junginger, M., Heinimö, J., Tekinel, B. and Vakkilainen, E., 2019. Global biomass trade for energy—Part 2: Production and trade streams of wood pellets, liquid biofuels, charcoal, industrial roundwood and emerging energy biomass. Biofuels, Bioproducts and Biorefining, 13(2), pp.371-387.

[3] European Commission. 2050 Low-carbon Economy. <https://ec.europa.eu/clima/policies/strategies/2050_en>[accessed on 2 June 2017].

[4] Jursová, S., Burchart-Korol, D., Pustějovská, P., Korol, J. and Blaut, A., 2018. Greenhouse gas emission assessment from electricity production in the Czech Republic. Environments, 5(1), p.17.

[5] Worldsteel Association. Steel Statistical Yearbook 2016. Available online: https://www.worldsteel.org/publications/bookshop/product-details.~Steel-Statistical-Yearbook-2016~PRODUCT~SSY2016~.html (accessed on 9 November 2018).

[6] Arens M. Energy efficiency and CO2 emissions reduction in the steel industry, EFONET Workshop 4.3: increasing energy efficiency in industrial processes. Berlin; 2010.

[7] Suopajärvi, H., Pongrácz, E. and Fabritius, T., 2013. The potential of using biomass-based reducing agents in the blast furnace: A review of thermochemical conversion technologies and assessments related to sustainability. Renewable and Sustainable Energy Reviews, 25, pp.511-528.

[8] Ooi TC, Aries E, Ewan BC, Thompson D, Anderson DR, Fisher R, et al. The study of sunflower seed husks as a fuel in the iron ore sintering process. Miner Eng 2008;21:167–77.

[9] Gan M, Fan X, Ji Z, Jiang T, Chen X, Yu Z, Li G, Yin L. Application of biomass fuel in iron ore sintering: influencing mechanism and emission reduction. Ironmaking Steelmaking 2015;42:27–33.

[10] Zheng Z, Wang J, Wei S, Guo Z, Yang J, Wang Q. Optimization of gaseous fuel injection for saving energy consumption and improving imbalance of heat distribution in iron ore sintering. Appl Energy 2017;207:230–42.

[11] Lovel RR, Vining KR, Dell'Amico M. The influence of fuel reactivity on iron ore sintering. ISIJ Int 2009;49:195–202.

[12] Fröhlichová, M., J. Legemza, R. Findorák, and A. Mašlejová. "Biomass as a source of energy in iron ore agglomerate production process." Archives of metallurgy and materials 59, no. 2 (2014): 815-820.

[13] Legemza, J. Fröhlichová, M. Findorák, R. Traditional and alternative fuels in metallurgy, TU Kosice, 2015, 286 p., ISBN 978-80-553-2154-7

[14] Findorák, R., Fröhlichová, M. and Legemza, J., 2014, March. The study of saw-dust addition on iron-ore sintering performance. In Acta Metallurgica Slovaca-Conference (Vol. 4, pp. 23-30).

[15] Fröhlichová, M., Findorák, R., Legemza, J. and Džupková, M., 2018. The Fusion Characteristics of Ashes from Lignin and the Coke Breeze. Archives of Metallurgy and Materials, 63.

[16] Findorak, R., Frohlichova, M., Legemza, J. and Dzupkova, M., 2018. UTILIZATION OF INFRARED THERMOMETRY FOR ANALYSE OF BIOMASS BURNING PROCESS. International Multidisciplinary Scientific GeoConference: SGEM: Surveying Geology & mining Ecology Management, 18, pp.1017-1022.

[17] Hudák, J., Fröhlichová, M., Legemza, J., Findorák, R. and Lesko, J., 2015. QUALITY AND TECHNOLOGICAL PARAMETERS OF AGGLOMERATES WITH OAK AND PINE SAWDUST AS A REPLACEMENT FUEL. International Multidisciplinary Scientific GeoConference: SGEM: Surveying Geology & mining Ecology Management, 1, p.667.

[18] Findorák, R., Fröhlichová, M. and Legemza, J., 2014. The effect of saw-dust addition from pine and oak wood on iron-ore sintering performance. International Multidisciplinary Scientific GeoConference: SGEM: Surveying Geology & mining Ecology Management, 3, p.973.

RELATED ASPECTS OF CO_2 RECYCLING FROM METALLURGICAL PROCESSES

Jan Haščin[1*], Bohumil Horák[2], Bohumil Horák ml.[3]

[1]Faculty of Materials Science and Technology , Technical University of Ostrava, 70833 Ostrava, Czech republic; jan.hascin@vsb.cz

[2]Faculty of Electrical Engeniring and Computer Science, Technical University of Ostrava, 70833 Ostrava, Czech republic; bohumil.horak@vsb.cz

[3]Faculty of Materials Science and Technology , Technical University of Ostrava, 70833 Ostrava, Czech republic; horak.bohumil@gmail.cz

*Correspondence: jan.hascin@vsb.cz; Tel.: +420-59-732-1585

Abstract

Carbon is a chemical element that makes up all living organisms on this planet. It belongs to biogenic elements and its cycle on the planet is a natural process. Carbon compounds are very important fuels and their extraction takes place in different ways. The most important extracted materials are oil and coal. These energy sources serve as highly concentrated energies for the development of industry and technology used by man. In metallurgy, carbon is an integral part of pig iron production. In the blast furnace, coke is burned to produce CO_2 [1]. The carbon dioxide produced in this way has no other major uses. Therefore, it is considered waste. Carbon dioxide as a "greenhouse gas" contributes to the climate change occurring on Earth. Modern metallurgy aims to search for alternatives limiting waste production and its environmental impact. An alternative is the possibility of recycling waste to produce products with higher added value and long-term usability, for example, using carbon dioxide as waste from metallurgical production with hydrogen - a product realized by electrolysis from "waste" electricity.

The VŠB-TU Ostrava team has long been involved in the issue of renewable and alternative energy sources and waste utilization, also from metallurgical production in the region. Renewable and alternative energy sources are increasingly being used for electricity generation. These do not in principle have a continuous character of electric power production. The quality parameters of the supplied electricity fluctuate; there is an excess of electricity in the grid, which may be problematic to use. In the moment, electricity is “waste”. The regional concept of using CO_2 as waste from metallurgical production and hydrogen generated from electricity surplus in the electricity grid gives the activities of VŠB-TUO laboratories and the team another dimension of the application of knowledge and experience in industry [2], [3], [4].

Keywords: metallurgy; energy; resources; renewable and alternative sources; low carbon economy

1. Introduction

Carbon is a biogenic element and can be considered as the cornerstone of all organic compounds on Earth and its cycling in nature as a natural biogeochemical cycle of its exchange between the biosphere, lithosphere, hydrosphere and atmosphere. However, this cycle has been disturbed by human activity in recent millennia. Especially in the last centuries, called the period of "technical revolution" and "scientific-technical revolution". The solution should be to treat the masses so that the CO_2 escapes into the atmosphere. Only in this way can the environmental impact be reduced.

The carbon footprint is an indirect indicator of the consumption of energy, products and services. It measures the amount of greenhouse gases that correspond to the company's activities or products. The sum of emissions for a certain period of time, most often a calendar year, is referred to as the carbon footprint. This is currently monitored and reported by thousands of companies abroad, dozens of companies in the Czech Republic. Their reporting becomes a corporate standard, much like environmental management systems (EMS) or corporate social responsibility (CSR). Procedures for determining GHG emissions are codified in ISO 14064 - Greenhouse gases, ISO 14067 - Carbon footprint of a product, service and society, and the international standard is the GHG Protocol.

In general, the use of the carbon footprint is related to international (Kyoto Protocol) and national and corporate greenhouse gas reduction (GHG) commitments derived therefrom. Reducing the company's carbon footprint contributes to protecting the climate and reducing the greenhouse effect on the planet. Companies use the carbon footprint as one of the key indicators of social responsibility and environmental

sustainability. Reporting of GHG emissions is obligatory for entities involved in the European Emissions Trading Scheme and voluntary for other firms. Companies most often determine carbon footprint in accordance with the GHG Protocol procedure. It divides emissions into 3 categories according to origin:

- Scope1 - activities that are under the control of a given enterprise and which release emissions directly into the air. These are direct emissions. They include, for example, emissions from boilers in the company, cars owned by the company or emissions from industrial processes.
- Scope2 - indirect emissions from the purchased energy (electricity, heat, steam or cooling) that do not arise directly in the enterprise but are the result of the enterprise's activities. These are indirect emissions from sources that are not directly controlled by the company.
- Scope3 (other indirect emissions) - emissions that result from the enterprise's activities and that arise from sources outside the control or ownership of the enterprise but are not classified as emissions under point 2. Examples are business trips by means of transportation that are not landfilling or the purchase of materials and fuels.

Reporting of emissions under Scope1 and Scope2 is mandatory, Scope3 is optional. The resulting carbon footprint is most often built in tons of carbon dioxide equivalent (CO_2 eq).

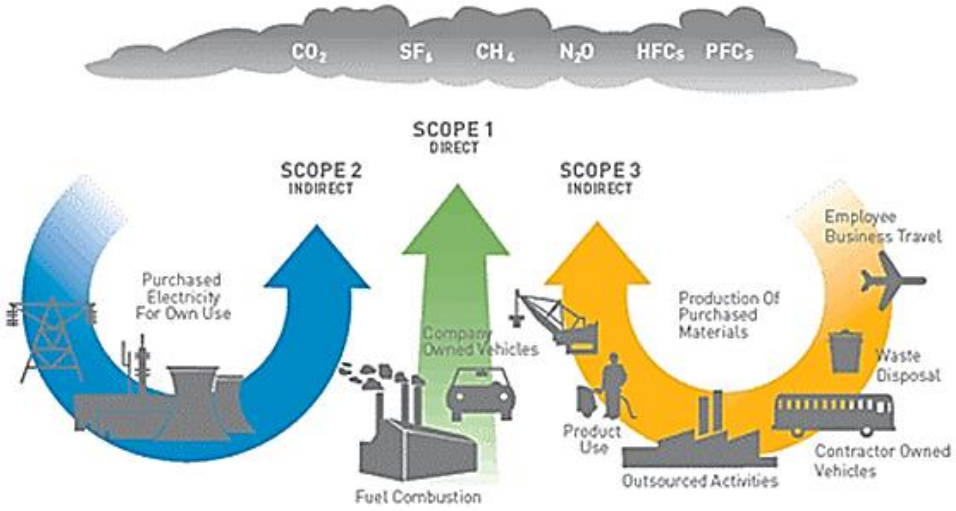

Figure 1 Graphical representation of cumulation for reporting generated CO_2 within Scope 1-3 [6].

2. Metallurgical process

Steel is on the ground, in front of cement, a mass-produced commodity. Every year 750 mill. t of steel is produced with an energy intensity of about 20-100MJ / kg. In iron metallurgy, carbon is an integral part in the production of pig iron in blast furnaces and steel furnaces by coke combustion, direct and indirect reduction of iron oxides by coke or carbon monoxide (Fig. 2).

Reaction in a blast furnace

burning coke

$C + O_2 \rightarrow \mathbf{CO_2}$ (1)

$CO_2 + C \rightarrow 2\ CO$ (2)

Direct reduction of iron	Indirect reduction of iron	
$Fe_2O_3 + 3\ C \rightarrow 2\ Fe + 3\ CO$	$3\ Fe_2O_3 + CO \rightarrow 2\ Fe_3O_4 + \mathbf{CO_2}$	(3)
$Fe_3O_4 + 4\ C \rightarrow 3\ Fe + 4\ CO$	$Fe_3O_4 + 4CO \rightarrow 3\ Fe + \mathbf{4\ CO_2}$	(4)
$FeO + C \rightarrow Fe + CO$	$FeO + CO \rightarrow Fe + \mathbf{CO_2}$	(5)

Figure 2 Graphical representation of the metallurgical process of iron and steel production [4]

Identified flue gas sources in metallurgical and related processes:

- Steel plant - converter (tandem) gas, flue gas from preheating, flue gas mini-fuel
- Blast furnaces - blast furnace gas, flue gases from wind heaters
- Agglomeration - flue gases from sinter agglomeration (sintering coke + ore + limestone)

3. Waste raw material

Waste is precisely defined by law from the legal point of view. It is considered to be a movable thing that one discards or intends or is obliged to discard. Existing waste is often a valuable raw material for other processors. The past decades could be called a period of searching for alternatives leading to the trend of further future sustainable development of society. Modern metallurgy cannot do without the development and implementation of alternative technologies, nor can it do without technologies that limit its impact on the environment.

The CO_2 sequestration / recycling project from industrial metallurgical processes is motivated by several aspects. Coke carbon in the blast furnace charge has several irreplaceable properties for iron production. This generates waste CO_2, which would be one of the feedstocks of the recycling process. At the same time hydrogen H_2 enters this process. Hydrogen becomes a strategic raw material. It is a carrier of energy. However, it does not occur freely on Earth. Only bound in compounds. As an element, it has many specific physical and chemical properties that significantly reduce the technology of its use by technicians. Especially in relation to explosion safety.

Hydrogen must be produced for the intended process. In the Czech Republic, hydrogen is produced in several places. However, 96% of hydrogen is produced from non-renewable energy sources. The European Union's futuristic idea of a hydrogen society has not yet been fully realistic. However, the change has occurred in recent years in connection with the mass launch of renewable and alternative energy sources (mainly in Germany and Denmark in previous years).

Thus, both the locally and globally the state of its supersaturation can occur in the electricity grid. The electricity grid, unlike the gas grid, does not have the property of a certain energy storage and so the excess electricity in the electricity grid reduces its immediate quality. Capturing these states and controlled loads will allow for future regulation of the quality of electricity and the use of surplus electricity to produce eg hydrogen.

The quality of electric energy is ensured by the standard ČSN EN 50160 and by the ERO Decree No. 306/2006. It states that each electricity customer has the right to purchase electricity of clearly defined quality. The guaranteed parameters of electricity in the Czech Republic network include, for example, defined voltage amplitude, frequency, sinusoidal waveform, and symmetry between individual phases in a three-phase system. Electricity producers and distributors must therefore endeavor to maintain these parameters at the required level.

4. Theoretical bases of hydrogen methanization [7], [8], [9], [10]

Since 1900, French chemist Paul Sabatier has studied the reaction of hydrogen with carbon dioxide or carbon monoxide using various catalysts [7]. In the first experimental experiments, carbon dioxide in the presence of hydrogen was successfully converted to methane using a nickel catalyst. The reaction proceeds according to equation:

$$\mathrm{CO_2} + 4\mathrm{H_2} \rightarrow \mathrm{CH_4} + 2\mathrm{H_2O} \qquad \Delta \mathrm{H}^0_{296} = -165\mathrm{kJ/mol} \tag{6}$$

The reaction is exothermic. However, an initial activation energy is required to initiate it. Components entering the reaction should have a stoichiometric ratio of CO_2 to H_2 of 1: 4 [8].

Methanization is a highly exothermic reaction associated with volume reduction, indicating that the greatest yields are obtained at lower temperatures and high pressures. To achieve a methane, yield above 98%, the reaction must be carried out at a pressure of at least 2MPa and a temperature below 300 °C [9, 10].

4.1 Experiment preparation [11], [12], [13]

For testing of methanization of hydrogen and carbon dioxide as an introductory work for the intention of using hydrogen technologies for metallurgical processes, an experimental apparatus is prepared at VŠB-TUO to monitor and control the reaction of hydrogen and carbon dioxide under various experimental conditions (input gas ratio, temperature, pressure, catalyst, residence time of the mixture in the reactor) [12], [13].

The apparatus is designed as a modular element for demonstration and teaching purposes for temperatures up to 500 °C and pressures up to 10MPa.

The mixture of H_2 and CO_2 with the required pressure, concentration and flow can be realized in the Fuel Cell Laboratory by an already existing set of valves and flow meters connected to the reaction gas tanks in the integrated technical gas storage.

Individual control and measuring elements of the device are controlled by a digital programmable and power supply unit, which is connected via RS 232 interface to a computer. The apparatus is shown schematically in Fig. 3.

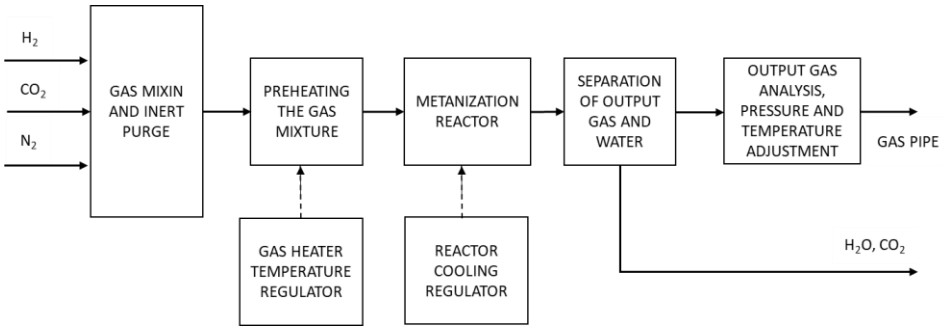

Figure 3 Block diagram of experimental apparatus for methanization of hydrogen and carbon dioxide.

4.2. Measurement procedure design

A nickel-based catalyst was selected for the initial methanization tests. The catalyst and basic control system settings will be used similarly as described in [9] (model stoichiometric gas mixture flow rate up to 10 l/min with overpressure up to 2MPa and temperature 270 °C).

The reactor is designed to be air cooled. At the start of the reaction, it is expected that the output gas flow will be reduced to about 1.0 l/min due to the methanization reaction with the necessity of water separation. The course of the methanization reaction will be monitored by the analyzer with the expectation of the output gas ratio at the level see Fig. 4.

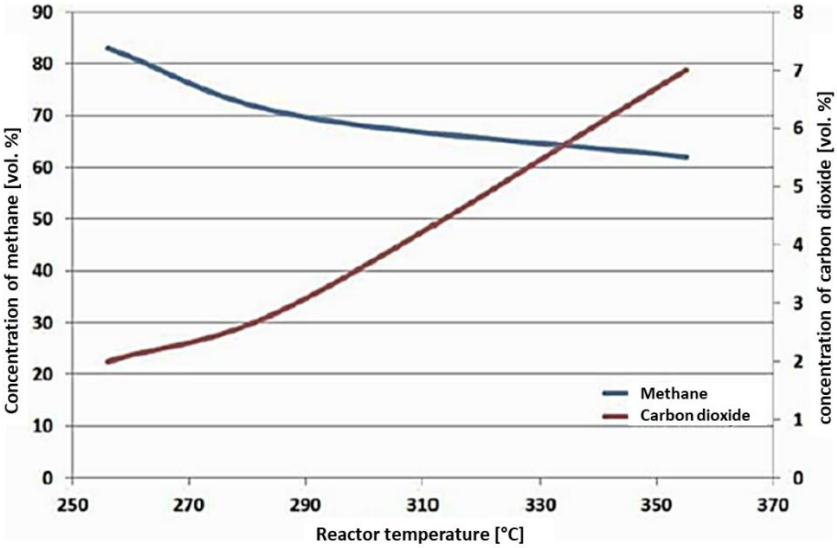

Figure 4 Expected results - graphical representation of the course of the methanization reaction as a function of the reactor operating temperature [9].

5. Carbon recycling international [5]

Carbon Recycling International (CRI) is a world leader in methanol technology. It produces renewable methanol from carbon dioxide (geothermal), hydrogen and electricity (wind, hydro) for use in fuels and chemicals (Figure 5). Involved in the development of recycling technologies and energy. It works with partners (Iceland, China, Sweden and the Netherlands) in the manufacturing and energy industries on transformation projects that increase production efficiency and create waste-added products with significant added value. CRI solutions are environmentally friendly and have no impact on the food chain or land use.

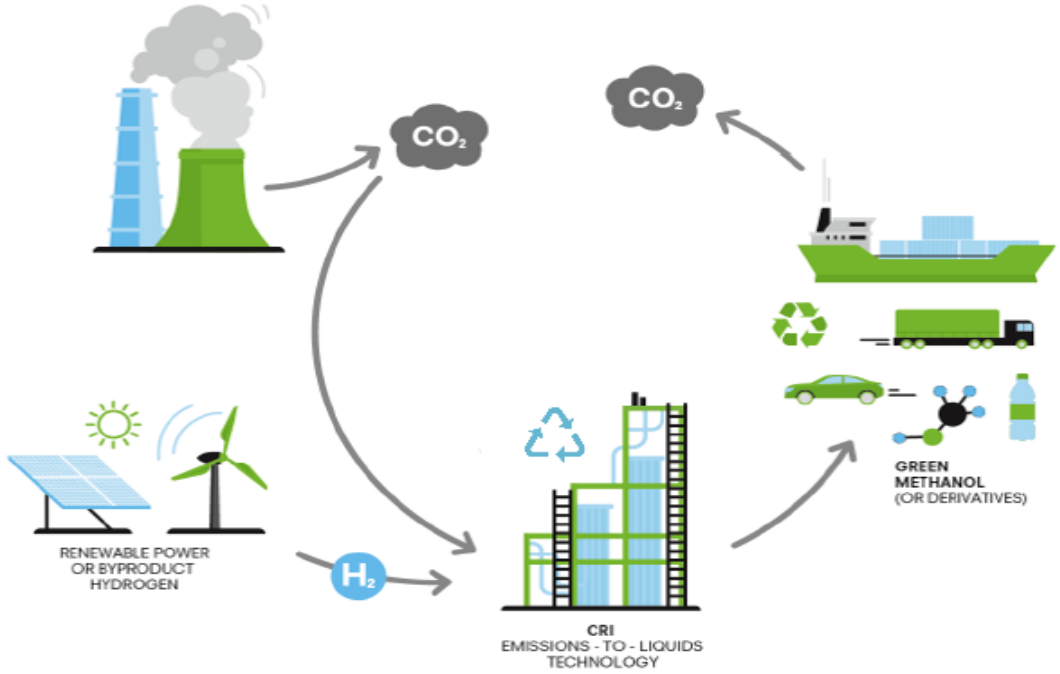

Figure 5 Ideological diagram of the CO2 recycling process implemented by CRI in the form of pilot technology as a follow-up element of the Svartsengi geothermal power plant / heating plant in Iceland [5]

In 2016, during a meeting at KIT (Keilir Institute of Technology) in Keflavik, the team became acquainted with the issues addressed by CRI in Iceland. Ideas of similar use of waste from metallurgical processes in the Moravian-Silesian region were postulated. In 2018, the VSB-TU research team established targeted cooperation with CRI on the project of recycling CO_2 from metallurgical processes [15], [16]. A long-term plan was presented and a pilot visit using pilot inputs using the geothermal power plant / heating plant Svartsengi (near the Blue Lagoon) in Reykjannes was realized.

Svartsengi technology mainly produces heat and electricity for Reykjavik, Iceland's capital. The water is pumped into the subsoil by a system of boreholes and is heated to a temperature of about 300 °C at a depth of about 3000m. Along with the steam, the CO_2 is also released from the magmatic process. This is captured and, together with hydrogen, synthesized to form methanol and higher hydrocarbons. In doing so, hydrogen is produced from the surplus electric power of the plant. An important attribute of the presented pilot technology is its modularity and direct usability for existing metallurgical plants.

6. Conclusion

The article summarizes the preparatory, research and consulting work of the team in the last period. The visit of the cooperating universities in Iceland in 2018 motivated the shift of activities and change of the original privileged orientation of the team from the field of measurement and management of renewable and alternative energy sources to waste management and utilization of the global characteristic of renewable and alternative energy function for the region. The aim of CO_2 recycling from metallurgical processes associates some currently proclaimed directions:

- Recovery of waste from the metallurgical process.
- Use of excess energy in the electricity grid.

- Improving the synthesis gas energy content for the metallurgical process.
- Electrical energy storage with hydrogen production.
- Creation of closely related value-added by-products (high purity technical gases, chemically pure hydrocarbon derivatives, refueling of CNG, LNG, H_2 vehicles).
- Motivation of other workplaces of the University for cooperation and further research in the field of waste processing from the metallurgical process.
- Employment increase
- Active involvement in European projects to reduce emissions in transport, smart cities, hydrogen society, low carbon economy and others.

Acknowledgement

Implementation and presentation of preparatory activities of the project of CO2 recycling from metallurgical processes was supported by the INTERREG CZ-PL project "Practical and research-oriented program of education of professional staff developing low-carbon economy on the Polish-Czech border" and the FEI VŠB-TUO OAZE 2018 SP2018/183.

References

[1] Lecture Horák, B.: Sequestrace CO2. 4th International Scientific Conference New Trends in Management and Production Engineering - Regional, Cross-Border and Global Perspectives. Cieszyn, 2016

[2] Balajka, J.: Vodík a iné nosiče energie. Alfa, Bratislava 1982 ISBN 68-128-82

[3] Horák, B., Kurowska-Pysz, J. a kol.: Nízkouhlíková ekonomika. Vysokoškolská příručka. VŠB-TUO, Ostrava 2017 ISBN 978-80-248-4134-2

[4] Brož, L., Bilík, J., Kret, J.: Vysokopecní výroba železa. Učební texty vysokých škol. VŠB-TUO, Ostrava, 1985

[5] Carbon recycling international [online]. 2018 [Cit.23.10.2019]. Available from: http://www.carbonrecycling.is

[6] Merseyside Enviromental Trust [online]. University of Liverpool 2019 [Cit.23.10.2019]. Available from: http://www.met-net.org.uk/greenhouse-gas-reporting.html

[7] Sabatier, P.S., J. B., New synthesis of methane. Comptes Rendus Hebdomadaires des Seances de l'Academie des Sciences, 1902. 134: p. 514-516.

[8] Brooks, K.P., et al., Methanation of carbon dioxide by hydrogen reduction using the Sabatier process in microchannel reactors. Chemical Engineering Science, 2007. 62(4): p. 1161-1170.

[9] Hoekman, S.K., et al., CO2 recycling by reaction with renewably-generated hydrogen. International Journal of Greenhouse Gas Control, 2010. 4(1): p. 44-50.

[10] Centi, G. and S. Perathoner, Opportunities and prospects in the chemical recycling of carbon dioxide to fuels. Catalysis Today, 2009. 148(3–4): p. 191-205.

[11] Andersson, M.P., et al., Structure sensitivity of the methanation reaction: H2-induced CO dissociation on nickel surfaces. Journal of Catalysis, 2008. 255(1): p. 6-19.

[12] Schlereth, D. and O. Hinrichsen, A fixed-bed reactor modeling study on the methanation of CO2. Chemical Engineering Research and Design, 2014. 92(4): p. 702-712.

[13] Pennline, H.W., R.R. Schehl, and W.P. Haynes, Operation of a Tube Wall Methanation Reactor. Industrial & Engineering Chemistry Process Design and Development, 1979. 18(1): p. 156-162.

[14] Mills, G.A. and F.W. Steffgen, Catalytic Methanation. Catalysis Reviews, 2006. 8(1): p. 159-210.

[15] Hlincik, T., Ciahotny, K. a col.: The conversion of hydrogen and carbon dioxide to methane. Journal Fuels 2015, p.7-12

[16] Green Car Congress [online]. BioAge Group © 2004-2020 [Posted 25.06.2013]. [Cit. 23.10.2019] Available from: http://www.greencarcongress.com/2013/06/audi-20130625.html

[17] Bechník, B.: Možnosti akumulace elektřiny z širšího pohledu [on-line]. Topinfo © 2001-2020 [Posted 05.01.2015]. [Cit.13.09.2019]. Available from: https://oze.tzb-info.cz/akumulace-elektriny/12195-moznosti-akumulace-elektriny-z-sirsiho-pohledu

ASPECTS OF EXTENDING THE LIFE OF A BLAST FURNACE SLAG RUNNER

Jan Haščin[1*], Bohumil Horák[2], Jan Růžička[3]

[1]Faculty of Materials Science and Technology , Technical University of Ostrava, 70833 Ostrava, Czech republic; jan.hascin@vsb.cz

[2]Faculty of Electrical Engeniring and Computer Science, Technical University of Ostrava, 70833 Ostrava, Czech republic; bohumil.horak@vsb.cz

[3]Faculty of Materials Science and Technology , Technical University of Ostrava, 70833 Ostrava, Czech republic; jan.ruzicka1@gmail.cz

*Correspondence: jan.hascin@vsb.cz; Tel.: +420-59-732-1585

Abstract

The metallurgical industry is a material base for engineering, construction and other industries, and is therefore a core industry not only in the Czech Republic but also in the world. From this point of view, the main task is to intensify the metallurgical production, which can be achieved by improving technological processes. The quality of technological processes can be improved by treatment of feedstock, oxygen enrichment of blast furnace wind, equipment modernization, etc. Unfortunately, these efforts are currently complicated by the slowing development of Czech metallurgy, which translates into reduced transport capacity, fuel and energy provision. charges etc.

The metallurgical industry is connected with other equally important sectors without which it would not be possible to develop metallurgy. The industrial refractory industry is proof of this. Versatility and a wide range of ceramic materials have helped in the development of metallurgy. In the metallurgy, refractory materials are used primarily for protection, construction, load-bearing skeleton in the form of working lining, permanent lining or insulation in various high-temperature aggregates.

Blast furnaces are a typical example of the use of refractory materials. These are used for the transport and distribution of pig iron and slag. The gutters consist of multiple layers of refractory materials and must withstand temperatures around 1450 ° C. There are high demands on materials:

- Corrosion resistance
- Abrasion resistance
- Minimum volume changes
- Heat resistance
- Chemical resistance, etc.

Keywords: blast furnace; slag runner; metallurgy; slag; pig iron

1. Introduction

The purpose of the blast furnance (BF) chute system is to control the flow of pig iron and slag from the tap hole BF. Furthermore, separating pig iron from slag, removing pig iron to mobile mixers or ladles and removing slag to ladles for further processing. [2]

The BF gutter system consists of the main gutter that is connected to a tap hole, a baffle to separate the slag from liquid pig iron, an iron gutter, and a slag gutter.

Refractory materials for blast furnace troughs have to meet high-quality requirements because the length of the furnace operation and the safety of operation depend on it. The surface of the working lining is more stressed, where it is exposed to high temperatures, the chemical action of slag, pig iron and gases. [3]

1.1. Material testing

The test specimens were manufactured according to the standard ČSN EN 1402-1 [4]. After weighing the dry refractory mixture, it was first homogenized without the liquid component, then the mixing water was added in an amount of 6 % wt.preparation of mixture for production of test specimens.

Further, the refractory mixture was formed and vibrated into metal molds (Fig. 1). Nine beams of approx. 160x40x40 mm were produced from each type of mixture.

In the next step, the filled molds were placed in a hydration box for 24 hours. After the required time in the hydration box, the resulting test specimens were dried in an oven (Fig. 1) to 110 °C. Drying was carried out for 24 hours and then to constant weight. After drying, the test specimens were measured and weighed.

Figure 3 Test specimen in drying oven.

After drying, some of the samples were placed in a desiccator before the properties were determined so that the samples did not absorb air humidity. The remaining samples were fired to temperatures of 1000, 1400 ° C in an electric furnace, according to the standard ČSN EN 1402-5 [5], determining the course of heat treatment during the preparation of test specimens. The test specimens were also weighed and measured after firing. The testing of materials took place at VŠB-TU Ostrava within 3 months, at the workplace of Department 635, Department of Thermal Engineering and Industrial Ceramics. Static tests performed:

- Compressive strength
- Flexural strength
- Water absorption
- Real porosity
- Apparent porosity
- Volume density
- Density

1.2. Abrasion resistance

Abrasion resistance is a measure of the resistance of a refractory material when particles with high velocity abrade the surface refractory. It measures the bond strength and refractory particles and its resistance to the flow of high-speed particles through its surface. The need for good abrasion resistance of refractory materials is most evident in petrochemical industries where fine particles impact the refractory surface at high speeds at slightly elevated temperatures. A direct correlation between abrasion resistance and cold compressive strength have recently been established. Thus, the cold compressive strength can provide and have a direct indication of the predictability of the refractory material in terms of its abrasion resistance. [8]

1.3. Changing the surface of refractory ceramics

Coating materials are widely used in the refractory lining to avoid various detrimental effects such as reactions on the contact surface of the mold, abrasions of liquid metal or alloys, gases, slags and other materials in contact with the coating. An example is the research of Serbian researchers. Cordierite samples sintered at 1200 and 1400 °C were used for the tests. Weight loss, the level of surface degradation obtained by image analysis and thermal imaging analysis were used to evaluate cavitation erosion. The results showed that cordierite samples can be used successfully in conditions where cavitation resistance is required. [7]

1.4. Other aspects of lifetime extension

Other aspects of extending the life of a blast furnace slag trough include direct changes:

- Changing the shape of the tray
- Change geometry or structure
- Changing the tray material

And also indirect changes:

- Change slag flow rate
- Change in slag viscosity
- Change the chemical composition of the slag
- Changing the slag temperature [1]

2. Results of laboratory tests

Preparation and testing of given mixtures of refractory concrete took place in the laboratories of VŠB-TUO. The results in this chapter are on average, for faster orientation and clarity. The following were determined:

- flexural and compressive strength
- density criteria
- density

Refractory concrete blend A can be used up to 1600 °C, with hydraulic coupling. Refractory concrete B can be used up to 1700 °C, with hydraulic coupling. Refractory concrete C is usable up to 1600 °C, with hydraulic bonding. Chemical composition of every refractory concrete blend is contained in Tab. 1.

Table 1 Chemical composition of blends [6].

	Al_2O_3	SiO_2	Fe_2O_3	CaO	SiC, C	C	SiC	TiO_2
	[%]							
Blend A	55	-	1	1.6	30	-	-	-
Blend B	69.1	7.2	0.7	0.7	-	2.7	17.2	2.4
Blend C	77	6	0.5	2	-	-	0.6	2.1

2.1. Compressive strength

Compressive strength was determined on cube halves of approx. 160x40x40 mm Tab. 2. The test halves of every block were obtained by the flexural strength test at the temperature of 110 °C. For the other temperatures, the samples were cut in half with a saw and then heated to the desired temperatures.

Table 2 Compressive strength results.

Oxidizing atmosphere						**Inert atmosphere**					
Blend A		**Blend B**		**Blend C**		**Blend A**		**Blend B**		**Blend C**	
[°C]	[MPa]	[°C]	[MPa]	[°C]	[MPa]	[°C]	[MPa]	[°C]	[MPa]	[°C]	[MPa]
110	7.00	**110**	7.04	**110**	4.37	**110**	24.89	**110**	5.97	**110**	5.58
1000	19.63	**1000**	15.70	**1000**	11.10	**1000**	19.15	**1000**	16.07	**1000**	10.02
1400	17.49	**1400**	20.78	**1400**	33.40	**1400**	26.55	**1400**	19.88	**1400**	30.06

2.2. Flexural strength

Flexural strength was determined on the rectangles of approx 160x40x40 mm which were used for the test crushing strength test results are in Table 3.

Table 3 Flexural strength results.

Oxidizing atmosphere						**Inert atmosphere**					
Blend A		**Blend B**		**Blend C**		**Blend A**		**Blend B**		**Blend C**	
[°C]	[MPa]	[°C]	[MPa]	[°C]	[MPa]	[°C]	[MPa]	[°C]	[MPa]	[°C]	[MPa]
110	0.33	**110**	0.31	**110**	0.69	**110**	0.80	**110**	0.71	**110**	0.70
1000	1.10	**1000**	2.08	**1000**	1.22	**1000**	1.91	**1000**	0.91	**1000**	1.01
1400	1.66	**1400**	2.19	**1400**	3.37	**1400**	2.06	**1400**	1.55	**1400**	1.89

2.3. Density criteria

Density criteria include apparent porosity AP, real porosity RP, water absorption WA, volume density VD. Properties were determined on samples after drying and firing. The resulting values are the average of two measured values, Tab. 4.

Table 4 Density criteria results.

Oxidizing atmosphere					**Inert atmosphere**				
	AP	**RP**	**WA**	**VD**		**AP**	**RP**	**WA**	**VD**
110 °C	[%]	[%]	[%]	[g.cm^{-3}]	**110 °C**	[%]	[%]	[%]	[g.cm^{-3}]
Blend A	28.00	24.37	12.23	2.29	**Blend A**	15.41	20.55	5.47	2.81
Blend B	16.66	25.24	6.16	2.70	**Blend B**	16.81	21.73	6.23	2.69
Blend C	15.57	16.92	5.51	2.82	**Blend C**	14.53	21.04	5.11	2.84
1000 °C					**1000 °C**				
Blend A	25.75	26.02	10.09	2.36	**Blend A**	15.32	20.58	5.44	2.81
Blend B	20.21	27.01	7.65	2.63	**Blend B**	18.84	22.33	7.03	2.67
Blend C	19.17	18.92	6.95	2.75	**Blend C**	17.59	22.10	6.28	2.80
1400 °C					**1400 °C**				
Blend A	20.95	25.67	8.83	2.37	**Blend A**	16.13	21.84	5.82	2.77
Blend B	14.78	25.50	5.48	2.69	**Blend B**	17.49	21.67	6.47	2.70
Blend C	15.20	17.05	5.39	2.74	**Blend C**	17.10	22.60	6.14	2.78

2.4. Density

The density was measured for all three Blends, from ground samples with a fraction below 0.063 mm tab. 5. On the Pycnomatic ATC.

Table 5 Measured density results.

Oxidizing atmosphere			**Inert atmosphere**		
Blend A	**Blend B**	**Blend C**	**Blend A**	**Blend B**	**Blend C**
[g·cm^{-3}]			[g·cm^{-3}]		
3.19	3.61	3.39	3.54	3.44	3.59

3. Conclusion

Blend A (ULTRABET PK-B) from Industrial Ceramics s.r.o. after the materials were submitted for testing, the first material inspection was performed visually and by granulometry. The largest grain in the material was found to be 5 cm. Then, it was compared with the material sheets.

Excess water required for sample production (declared 120 ml, needed 240 ml) Need for granulometry adjustment to create test specimens

Test specimens were also made from blend and proved in an oxidizing and inert atmosphere. The results of static tests of materials for 1400 °C shows:

Oxidation firing

- − Worsens the parameters of this blend

Inert firing

- + Mechanical properties (compressive and flexural strength)
- + Density criteria (apparent porosity AP, real porosity RP, water absorption WA, volume density VH)

Blend B (HYDRA-MAX VX-281M) from the Vesuvius Czech Republic, a.s. was studied already in 2016 and now 2018. The chemical composition of this particular blend remained the same. After checking the supplied material, the granulometry and the water required to manufacture the test specimen fit with the manufacturer's declaration.

Test specimens were also made from mixture and proved in an oxidizing and inert atmosphere. The results of static tests of materials for 1400 °C show:

Oxidation firing

- + Mechanical properties (compressive and flexural strength)
- + Apparent porosity AP, water absorption WA, volume density VH
- − Real porosity RP

Inert firing¨

- − Apparent porosity AP, water absorption WA
- − Mechanical properties (compressive and flexural strength)
- − Density criteria (apparent porosity AP, real porosity RP, water absorption WA, volume density VD)

Blend C (TRB ECOCAST 54N13) from TRB is a newly investigated material in 2018. After checking the supplied material, the granulometry and the water required to manufacture the test specimen fit with the manufacturer's declaration. This material was best processed and vibrated into molds.

Test specimens were also made from mixture and fired in an oxidizing and inert atmosphere. The results of static tests of materials for 1400 °C show:

Oxidation firing

- + Mechanical properties (compressive and flexural strength)
- + Density criteria (apparent porosity AP, real porosity RP, water absorption WA, volume density VD)

Inert firing

- + Mechanical properties (compressive and flexural strength)
- + Water absorption WA, volume density VD
- − Apparent porosity AP, real porosity RP

The Blend C (TRB ECOKAST 54N13) seems to be the best. If the blend of refractory concrete is installed correctly, the service life of the blast furnace chute should be extended. However, this is not the only solution for this effect can also be achieved by changing the surface of the working lining, the inclination, and shape of the trough or replacing it with a prefabricated element.

Recommendations for subscribers:

- Blend change for chute of blast furnace
- Change of the supplier
- Solving problematic blends with the manufacturer
- Check feedstock before use

- Modification of blast furnace chute technology
- Granulometry adjustment before blast furnace trough preparation
- Change of blast furnace trough equipment
- Surface change, blast furnace trough geometry

Acknowledgement

This article was elaborated under the grant program "Support for Science and Research in the Moravian-Silesian Region 2017" (RRC / 10/2017) and financed from the budget of the Moravian-Silesian Region.

References

[1] HORÁK, Bohumil, HAŠČIN, Jan a kol. Úprava a prodloužení životnosti žlabu VP. HS4501807. VŠB-TU Ostrava, Ostrava 2018

[2] GEERDES, Maarten, Hisko TOXOPEUS a Cor van der VLIET. Modern blast furnace ironmaking: an introduction. Amsterdam: IOS Press, 2009, xii, 176 p. ISBN 978-1-60750-040-7.

[3] BABICH, Alexander. Ironmaking: textbook. Aachen: RWTH Aachen University, Department of Ferrous Metallurgy, 2008, 402 s. ISBN 978-3-86130-997-1.

[4] ČSN EN 1402-1. Žárovzdorné výrobky netvarové. Část 1: Úvodní ustanovení a klasifikace. Plzeň: Český normalizační institut, 1996.

[5] ČSN EN 1402-5. Žárovzdorné výrobky netvarové. Část 5: Příprava a zpracování zkušebních těles. Praha: Český normalizační institut, 2004.

[6] ArcelorMittal Ostrava firemní zdroje. [disk]. [cit 10. 2. 2019]

[7] PAVLOVIĆA, Marko, Sanja MARTINOVIĆB, Milica VLAHOVIĆB, Zoran STEVIĆC a Tatjana VOLKOV HUSOVIĆA. Non destructive monitoring of cavitation erosion of cordierite based coatings. *Composites: Part B: Engineering* [online]. 2016, 15. July 2016, (Volume 97), 84-91 [cit. 2019-09-14]. ISSN 1359-8368. Dostupné z: https://www.sciencedirect.com/science/article/pii/S135983681630525X

[8] SCHACHT, Charles A. *Refractories Handbook*. 1. Boca Raton: Taylor & Francis Group, 2004, s. 6. ISBN 9780824756543.

CFD SIMULATION OF FLOW IN THE CONTINUOUS CASTING TUNDISH

Slavomír Hubatka [1,*] Adrian Bitto [1], Peter Demeter [1], Branislav Buľko [1]
[1]Faculty of Materials, Metallurgy and Recycling,, Technical University of Košice, 04200 Košice, Slovakia;
*Correspondence: slavomir.hubatka@gmail.com

Abstract
Mathematical modeling became a worldwide trend in 21. century. Top-notch programs in which a mathematical model is being realized are applied in great deal of industries in complex solution of most diverse tasks. This type of programming product is labeled as „Computational Fluid Dynamics (CFD) ". Usage of CFD can in some cases replace labor and financial costly experimentation. It is therefore an indispensable tool for developmental tasks. In the field of steel metallurgy, CFD programs are most often used to solve melt flow problems in metallurgical vessels and to solve heat transfer problems. One of the key factors to improve steel quality is the steel cleanliness. In the continuous casting process, the tundish serves not only as a reservoir and a distributor of molten steel, but also as a metallurgical reactor to diminish the inclusion content in the final product. This research is aimed to study the flow behaviour inside 3-strand tundish. The commercial computational fluid dynamics software, ANSYS FLUENT (student version), was used for simulation. The data of geometry and operating parameters were collected from tundish-model at Faculty of Metallurgy, Technical University of Košice, Slovakia. The simulations were performed under isothermal conditions.

Keywords: mathematical modeling; CFD system; Ansys; clean steel; tundish flow

1. Introduction

Mathematical modeling is a very important tool for modern society to find out as much information about its surroundings as possible without the need for physical contact with a real object. It is used in various economic, natural, social and especially technical sciences. In modern steelmaking, steel cleanliness (or freedom from non-metallic inclusions) is a key factor in order to achieve a high-quality steel product. Today more than 95% of the world steel production is cast via tundish and continuous casting process [1]. Tundish plays an important role to minimize non-metallic inclusions in order to improve the steel cleanliness. Although the tundish serves as a reservoir and a distributor of molten steel, its function is also a metallurgical reactor. Non-metallic inclusion, such as Al_2O_3 and SiO_2, can be floated and captured by the slag in the top layer of molten steel if there is enough residence time for the flow from inlet to outlet in tundish. [2]

As the metallurgical performance of tundish depends on fluid flow, the flow behaviour in tundish can be improved by incorporating suitable flow control mechanisms (i.e., Turbostop or impact pad) and placing them at strategic locations. With the use of CFD (computational fluid dynamics) simulations, the flow behaviour can be visualized in several ways – the velocity flow, the temperature field, the residence time of each streamline from inlet to outlet and the RTD (Residence Time Distribution) These Data are useful for the design of tundish in order to diminish the inclusion content. [3]

2. Experimental Materials and Methods

In this study the numerical model of tundish flow is simulated by using the commercial software ANSYS FLUENT 19.0 (student version). Initial equations that describe the flow of real liquids are an expression of the basic laws of mass, momentum, and energy. The flow of actual fluids is affected by internal friction, which causes the cross-flow velocity to vary [4].

The Reynolds number (referred to as Re) flows from the indicated inertia and frictional forces ratio. The Re criterion is of decisive importance for determining the basic flow types in a pipeline. We recognize laminar flow and turbulent flow. In the case of one-way flow in a pipeline, the critical Reynolds number ReCrit, which is defined by:

$$\mathbf{Re} = \frac{\mathbf{v_s d}}{\mathbf{v}} \quad (1)$$

Where: vs (flow speed) [$\mathbf{m.s^{-1}}$]

d (diameter) [m]

v (kinematic viscosity) [$\frac{\mathbf{m^2}}{\mathbf{s}}$]

The critical ReCrit value for a circular diameter pipe is 2320. Re ≤ ReKrit - laminar flow is arranged in the pipeline, movement takes place in layers and fluid particles do not move across the cross section. Re ≥ ReKrit flowing transit into turbulent. At higher Re values, the fluid particles perform an erratic movement in all possible directions. This movement is irregular, random, and resembles the movement of gas molecules, but may disintegrate and lose identity as compared to molecules and fluid particles. The flows in the current study are considered as turbulent flow, since the Reynolds numbers (Re) are equal to or greater than 5000. The numerical simulations of turbulent flow are carried out on the basis of the Reynolds-Averaged Navier-Stokes (RANS) modelling [5,6]

An important requirement when using CFD methods is to verify the achieved results under actual operating conditions. This verification is desirable for further refinement of the calculation e.g. by selecting a more suitable flow pattern and ultimately in terms of ensuring the validation of the result for each subsequent case. A combination of mathematical and physical modeling is considered to be a very effective and optimal variant of model research. Physical modeling serves to verify the validity of mathematical modeling results and to solve and simulate particularly complicated cases for which numerical modeling would be problematic [7].

Verifying of achieved results were performed at Department of Ferrous Metallurgy and Foundry, Faculty of Materials, Metallurgy and Recycling, Technical University Košice, Slovakia water-model. Water model is assembled at scale 1:2 to original [8].

The CFD simulation of a two-strand tundish with water flow inside is performed using boundary conditions - gravity in Y direction = -9.81 $\mathrm{m.s^{-2}}$, tundish material - liquid water and pre-defined IN-LET conditions. The tundish geometry is shown in Figure 1.

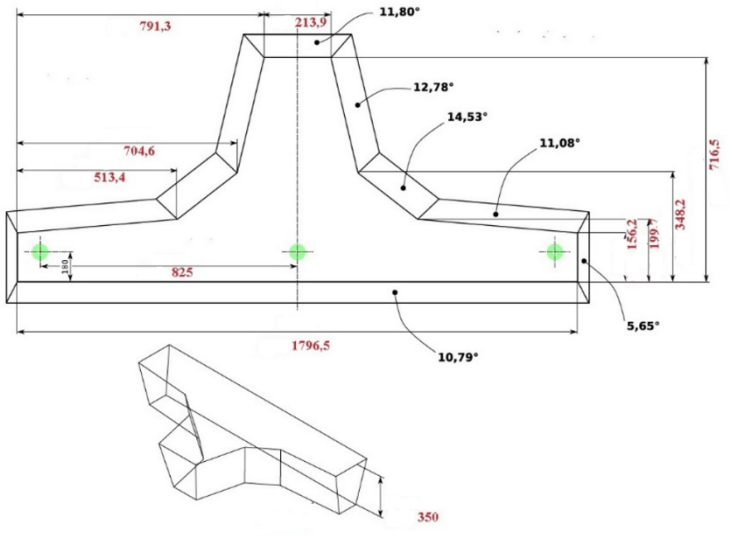

Figure 1 Geometry of the 3-strand tundish model.

An unstructured computational mesh of 500 thousand cells is used (low number of cells is determined by using only free student version of ANSYS FLUENT). Mathematical mesh for 3-strand tundish model is shown in Figure 2. The simulations of tundish flow are performed by using ANSYS FLUENT 19.0. (student version). The k-epsilon standard model is used to simulate the turbulent flow. The SIMPLEC algorithm is used in the numerical simulation. The calculation convergence is influenced by the number of cells and the overall quality of the computational mesh. Acceleration of convergence can be achieved by appropriate initial estimation of variables that are relevant to the simulated plot. The number of iterations specified was set to 2000. Boundary conditions are sumarized in Table 1 [9].

For discovering residence times of tundish water model was used. The basic parameter which is often used for tundish flow description is minimal and maximal residence time. Minimal residence time is defined as shortest time when particle injected to the ladle shroud can be observed on the tundish output. One of aims of steel flow optimization is to reach maximum value of minimal residence time. Maximum residence time have definitive influence on time which inclusions have to rise from steel into slag. Cross section plane in which flow is observed is shown in Figure 3 [3].

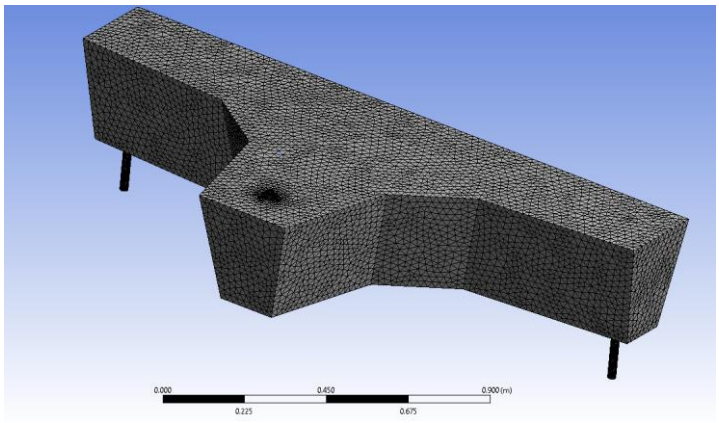

Figure 2 Mesh for the 3-strand tundish model.

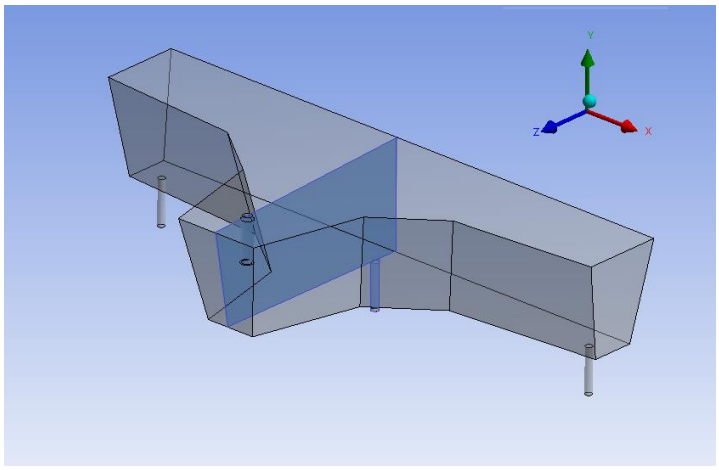

Figure 3 2-D Cross Section plane at interested position.

Table 1 Boundary conditions.

Boundary Conditions	
Temperature	Izotermic
Operating pressure	101 325 (Pa)
Effect of gravity	X=0 / Y= -9.81 / Z=0 ($m.s^{-2}$)
H_2O (l)	
Density	998.2 ($kg.m^{-3}$)
Viscosity	0.001003 $(kg.(m.s)^{-1})$
In-let	
Flow speed	0,16 $m.s^{-1}$
Turbulence intensity	4.8%
Turbulent viscosity ratio	0,5
Out-let	
Pressure	101 325 (Pa)
Turbulence intensity	4.4%
Wall	
Friction	undefined

3. Results and discussions

The velocity flow field of tundish flow is illustrated in a 2-D cross section plane at interested position as shown in Figure 4. The flow structure can be captured from the 2-D CFD simulation during time period t1-t9.

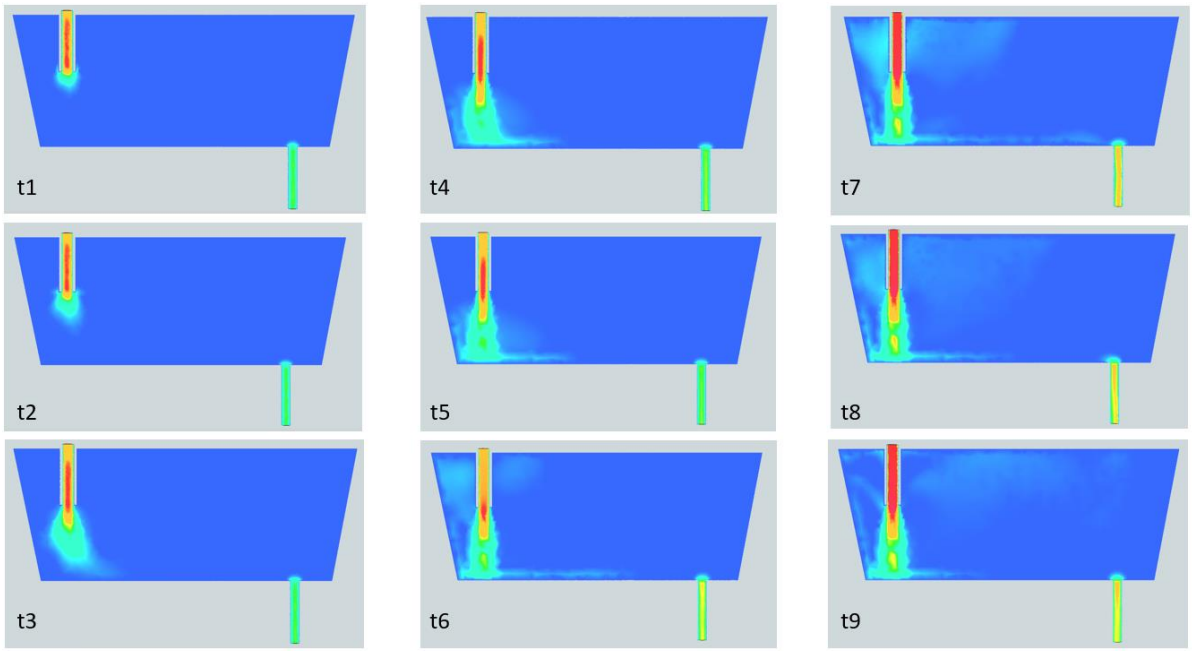

Figure 4 Velocity flow field in 2-D cross plane section.

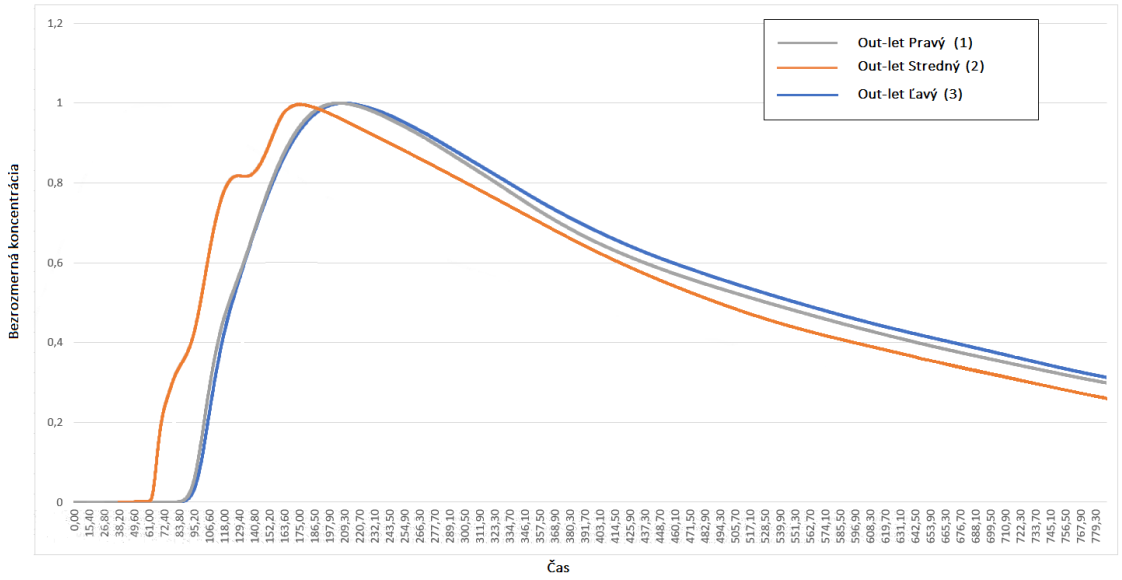

Figure 5 C-curve of RTD characteristics obtained from water model and CFD for bare tundish [10].

The comparison of the flow pattern between the CFD simulation and the experiment results shows good agreement with minor difference. Residence times from water-model can be seen in Figure 5, 6 [9]. The residence time of each outflow particle in tundish model is calculated from the inlet-to-outlet flow time. C-Curve of RTD characteristics obtained from CFD model as shown in Figure 6. is created of data that are only an approximation of real object because of limited potential of student version of Ansys Fluent. Data were obtained from iterations (2000) during each 10 steps.

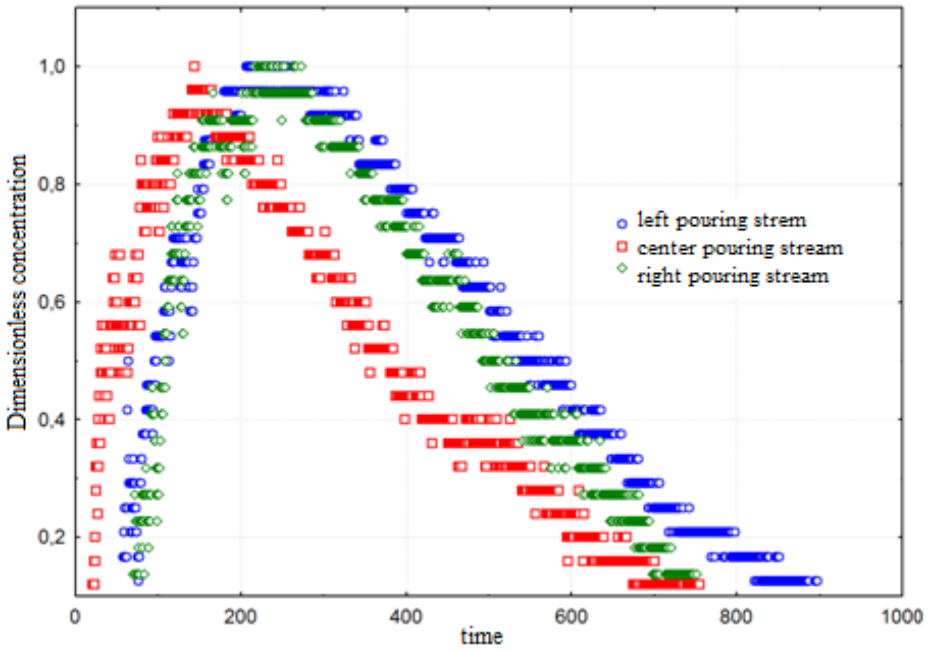

Figure 6 Approximate C-Curve of RTD charateristics obtained from CFD model.

4. Conclusion

From the current study, the 3-strand tundish model have been simulated using CFD program, ANSYS Fluent. The calculated results of the flow in 3-strand tundish model such as velocity, flow field and minimum/maximum residence time distribution show good agreement with the experimental results from water-model.

Therefore, it is confirmed that numerical simulations are satisfactorily accurate. The 3-strand tundish model is created based on the geometry of water model at Faculty of Metallurgy, Technical University of Košice, Slovakia. The results from the current study will support and enhance the potential for next study of steel-flow in tundish to produce high quality steel in the future. Full version of Ansys Fluent is necessary for more in-depth simulations of steel flow processes, further research in this area is essential.

References

[1] Steel Statistical Yearbook 2018, World Steel Association, https://www.worldsteel.org/en/dam/jcr:e5a8eda5-4b46-4892-856b-00908b5ab492/SSY_2018.pdf

[2] N. Grundy, Continuous Casting: Optimizing Both Machine and Process with Simulation. [Online]. Available: http://www.comsol.com/story/ continuous-casting-optimizing-both-machine-and-process-with-simulation-19247

[3] B. Buľko and J. Kijac. "Optimization of Tundish Equipment," Acta Metallurgica Slovaca, Vol. 16, 2010, No. 2, p. 76-83

[4] J. Huelstrung, "Development and Use of an Optimized SEN for the Thin Slab Casting Using Computational Fluid Dynamics," Ph.D. thesis, RWTH Aachen University, Germany 2006

[5] M. Warzecha. (2011). "Numerical Modelling of Non-metallic Inclusion Separation in a Continuous Casting Tundish," in Computational Fluid Dynamics Technologies and Applications, Prof Igor Minin. [Online]. Available from: http:// www.intechopen.com/books/computational-fluid-dynamicstechnologies-and-applications/ numerical-modelling-of-non-metallic-inclusion-separation-in-a-continuouscasting-tundish

[6] Michalek, K., Gryc, K., Tkadlečková, M., Morávka, J., MODELOVÁNÍ A VIZUALIZACE METALURGICKÝCH PROCESŮ, 2013, ISBN 978-80-248-3352-1

[7] Čarnogurská, M.: Základy matematického a fyzikálního modelovania v mechanike tekutin a termodynamike. SF TU Košice, 2000, 176 s.

[8] https://ohaz.umet.fmmr.tuke.sk/lspp/#druhy

[9] Michalek, K.: Využití fyzikálního a numerického modelování pro optimalizaci metalurgických procesů. VŠB-TU Ostrava, 2001, 125 s.

[10] T. MERDER : INFLUENCE OF DESIGN PARAMETERS OF TUNDISH AND TECHNOLOGICAL PARAMETERS OF STEEL CONTINUOUS CASTING ON THE HYDRODYNAMICS OF THE LIQUID STEEL FLOW, 2014

LADLE SLAG FORMING WITH OPTIMAL PHYSICOCHEMICAL PROPERTIES FOR MINIMIZATION OF NONMETALLIC INCLUSIONSS

Mirosław Karbowniczek[1*], Piotr Migas[1], Artur Dobosz[2], Wojciech Ślęzak[1*], Marta Ślęzak[1]

[1]AGH-University of Science and Technology, Faculty of Metals Engineering and Industrial Computer Science, 30 A. Mickiewicza Av., Krakow, Poland; pmigas@agh.edu.pl; mslezak@agh.edu.pl

[2]ArcelorMittal Warszawa, Kasprowicza 132, Warszawa, Poland; Artur.Dobosz@arcelormittal.com,

*Correspondence: mkarbow@agh.edu.pl, wslezak@agh.edu.pl

Abstract

The production of steel with high metallurgical purity is associated with the formation of ladle slag with appropriate physicochemical properties. Such slag must be characterized by a low degree of oxidation and good ability to absorb non-metallic inclusions. The results of industrial research with the use of new slag forming materials to create good quality of a ladle slag will be presented. Chemical compositions of slags obtained after the use of new slag forming materials as well as obtained oxygen contents and types of non-metallic inclusions will be also presented.

The obtained results indicate that due to the appropriate selection of the type and amount of slagging materials, it is possible to obtain steel with high metallurgical purity, meaning low content of oxygen and non-metallic inclusions.

Keywords: ladle slag formation; non-metallic inclusions; dephosphorization; desulphurization

1. Introduction

Both in the BOF and the EAF the melting process takes place with the presence of the furnace slag. The following oxides are primary constituents of the furnace slag: CaO, SiO_2, MgO, MnO, FeO, Fe_2O_3, and Al_2O_3. The furnace slag has oxidising properties and has high contents of sulphur and phosphorus. Because of these characteristics it is not suitable for carrying out the steel refining process in its presence. In previous years, when steel was refined in a steelmaking furnace, the chemical constitution of the furnace slag would be modified in order to ensure its proper refining properties. Now, when steel is refined in other devices, the metal bath is tapped to a ladle without the furnace slag. Refining takes place under specifically made ladle slag. Ladle slag properties are decisive to the quality of steels obtained, and the process of its formation determines the process economics [1, 2].

The content, type, size and distribution of non-metallic inclusions are a relevant indicator of steel purity. Non-metallic inclusions in steel result from incomplete floating of casting products, and sulphates and nitrides, erosion of refractory lining, slag particles penetrating into the liquid steel. During steel refining in secondary steelmaking installations one aims at forming slag, which can assimilate oxide inclusions. The above condition is met by refining slags based on the $CaO\text{-}Al_2O_3\text{-}SiO_2$ system, where the content of individual constituents corresponds to the Mannesmann Index.

During ladle steel refining, a calcium-aluminium slag should be created at the steel surface. Its chemical constitution complies with the optimum value of the Mannesmann Index. It is important that the melt is sufficiently long and intensively stirred with an inert gas. This slag can be formed by:

- adding a synthetic slag to the ladle,
- creating a refining slag on the basis of mixtures from the $CaO\text{-}Al_2O_3\text{-}SiO_2$ system,
- adding lime, and the appropriate constitution of the refining slag will be formed by dissolution of CaO in Al_2O_3 forming from aluminium steel deoxidation.

The most preferable constitution corresponds to the eutectic $12CaO{\cdot}7Al_2O_3$. In addition, slag usually contains some MgO in order to protect basic ladle refractory. The presence of a few percent magnesium oxide in the slag also intensifies the metal bath desulphurization process. Often basic synthetic slags also contain some amounts of additions improving their physico-chemical properties, i.e.: reduction of the melting temperature, improvement of fluidity, positive changes in surface properties. The best known addition of this type is fluorite (CaF_2) [3-6].

2. Analysis of refining slags at the ladle furnace station

To compare conditions for refining slag formation in the ladle furnace, test heats were made in the industrial conditions. Three variants of slag formation were compared: 1) on the basis of steelmaking lime (Mixture 1) only; using a material containing CaF_2 (Mixture 2); using a material with a commercial name AF-3-F (Mixture 3). 16 test heats were made with mixture 1, 24 heats with mixture 2 and 14 heats with mixture 3. Slag samples would always be taken at the final stage of the refining process. The chemical analysis was performed with an x-ray fluorescence spectrometry Twin-X from Oxford-Instruments. Average, minimum and maximum values for all analysed test series are presented in Table 1.

Table 1 Average, minimum and maximum content of refining slag constituents from the set of heats tested for individual slag forming mixtures.

	Average chemical composition [wt. %]									Basacity [-]	Mannesmann index [-]
		CaO	SiO_2	Al_2O_3	MgO	P_2O_5	S	MnO	FeO		
Mixture 1	Av.	48.78	10.3	26.28	10.6	0.073	1.33	0.17	0.86	4.931	0.189
	Min.	43.50	7.9	21.30	8.5	0.050	0.56	0.03	0.21	3.240	0.118
	Max.	54.00	14.9	30.00	13.8	0.100	2.35	0.72	1.94	6.430	0.260
Mixture 2	Av.	45.53	10.0	23.73	11.9	0.063	1.01	0.25	0.97	4.582	0.194
	Min.	42.20	8.3	20.00	9.2	0.020	0.57	0.06	0.35	3.760	0.164
	Max.	47.40	12.3	26.80	15.9	0.080	1.43	0.52	2.70	5.510	0.241
Mixture 3	Av.	45.23	9.4	24.19	11.3	0.065	0.89	0.25	0.91	4.866	0.201
	Min.	44.00	7.7	23.10	8.6	0.050	0.49	0.03	0.49	4.080	0.168
	Max.	46.60	10.9	25.80	17.3	0.070	1.24	0.66	1.21	5.870	0.230

Average, minimum and maximum values of desulphurization and dephosphorization degree and phosphorus and sulphur distribution coefficients [7] at the subsequent stages of the refining process (LF, VD), for individual slag-forming mixtures for all analysed test series are presented in Table 2.

Table 2 Average values of desulphurisation and dephosphorisation degree and phosphorus and sulphur distribution coefficients at the subsequent stages of the refining process (LF, VD) for individual slag-forming mixtures.

	Average values [%]								
		$\eta_{P\ LF}$	$\eta_{P\ VD}$	η_P	$\eta_{S\ LF}$	$\eta_{S\ VD}$	η_S	L_P	L_S
Mixture 1	Av.	-115.5	11.31	-0.9	12.9	-85.4	-53.562	6.57	196.3
	Min.	-1011.1	0.0	-11.1	-25.0	-340.0	-214.286	0.80	14.0
	Max.	0.0	90.9	16.7	71.4	40.0	47.059	12.86	1175.0
Mixture 2	Av.	4.8	12.0	16.5	8.1	-12.3	-4.136	5.05	79.9
	Min.	-6.7	-7.1	-7.1	0.0	-115.8	-105.000	0.78	39.5
	Max.	90.0	90.0	90.7	25.9	87.8	88.421	7.78	188.0
Mixture 3	Av.	0.6	-0.1	0.6	15.4	-46.7	-24.989	5.75	63.3
	Min.	-12.5	-10.0	-12.5	4.2	-140.0	-91.667	3.18	28.8
	Max.	10.0	8.3	10.0	41.7	40.0	60.000	8.75	123.0

Changes in the desulphurisation and dephosphorisation degree and the phosphorus and sulphur distribution coefficients in the subsequent heats, for refining stages (LF, VD), for individual slag-forming mixtures are graphically presented in Figure 1 to Figure 8.

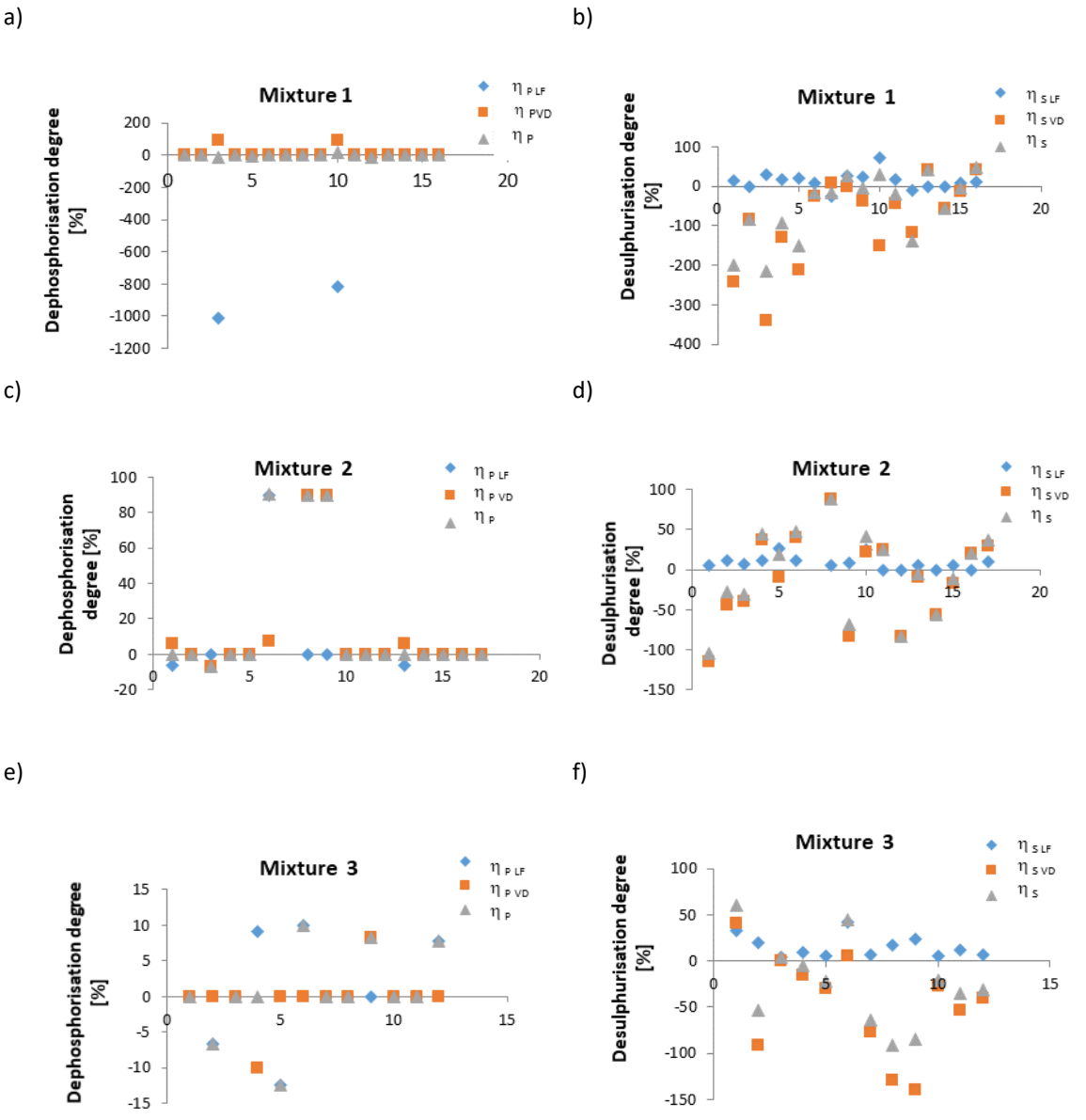

Figure 1 The dephosphorisation degree a), c), e), and the desulphurisation degree b), d), f), for the individual slag-forming mixtures.

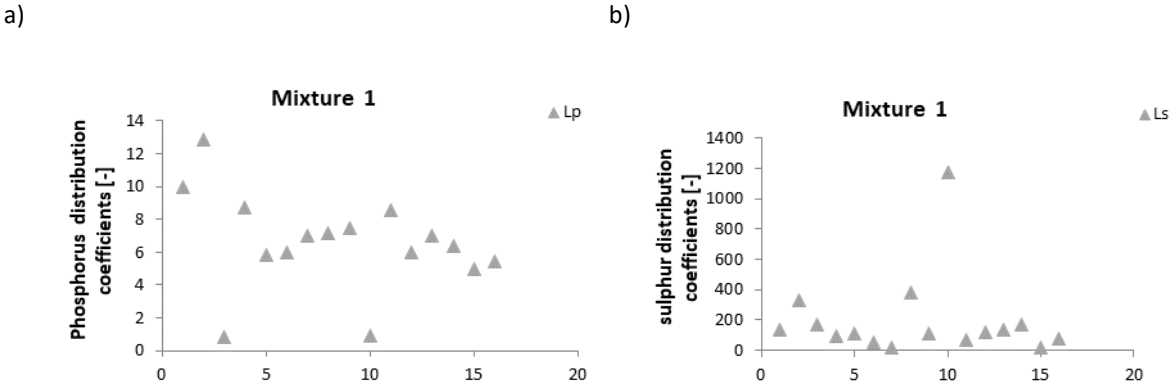

c)

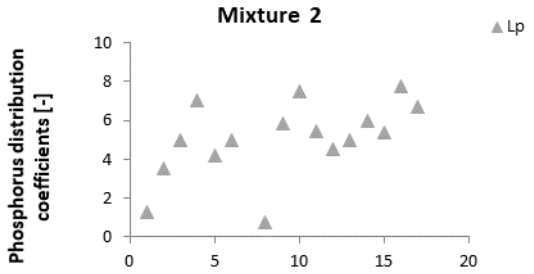

d)

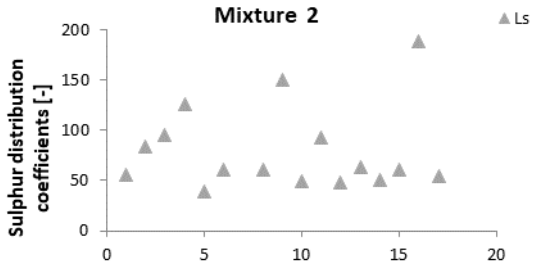

e)

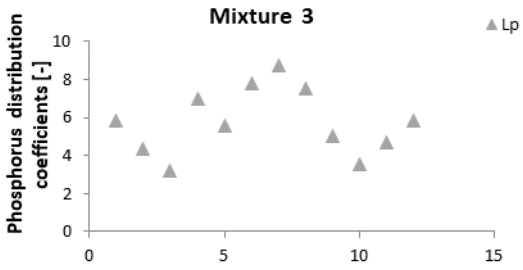

f)

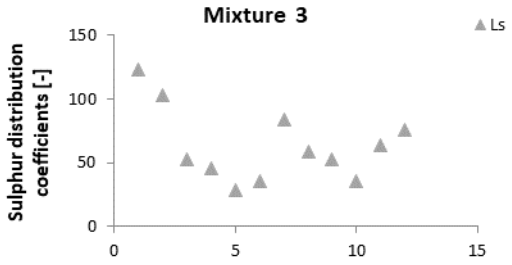

Figure 2 The distribution coefficient of phosphorus a), c), e), and sulphur b), d), f), for the individual slag-forming mixtures.

a)

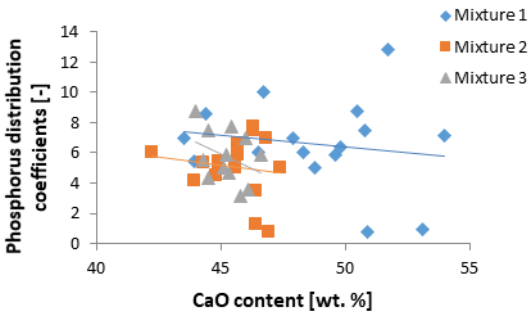

b)

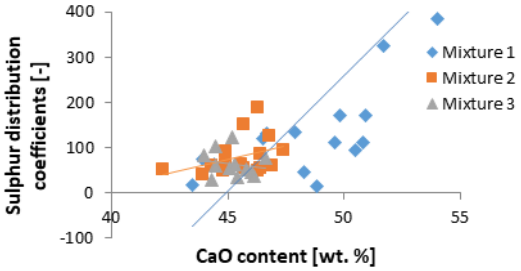

Figure 3 The distribution coefficient of phosphorus a), and sulphur b) depending on the CaO content.

a)

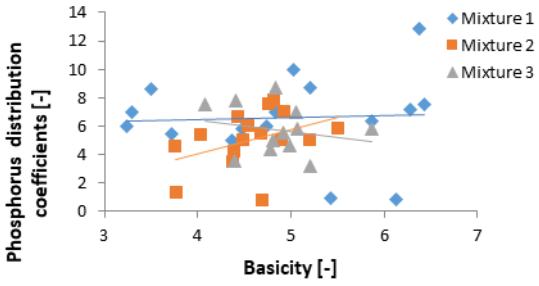

b)

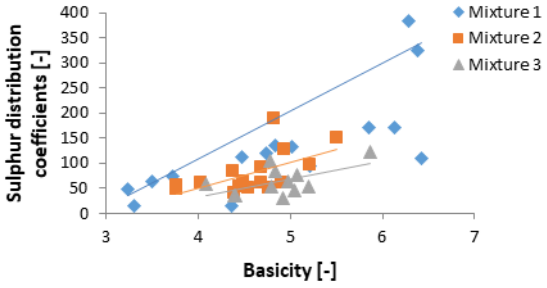

Figure 4 The distribution coefficient of phosphorus a), and sulphur b), depending on the slag basicity.

a) b)

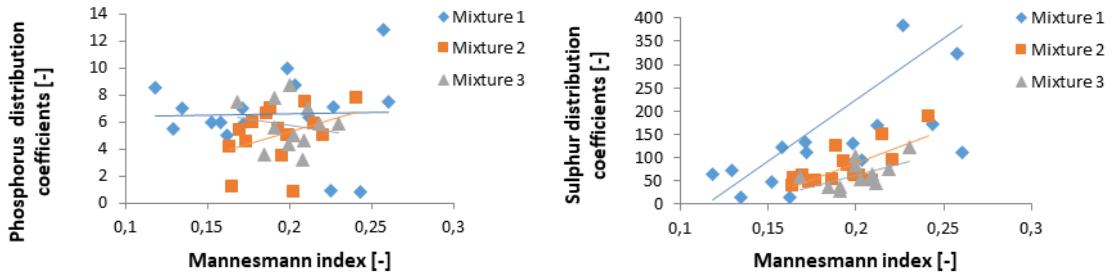

Figure 5 The distribution coefficient of phosphorus a), and sulphur b), depending on the Mannesmann index.

a) b)

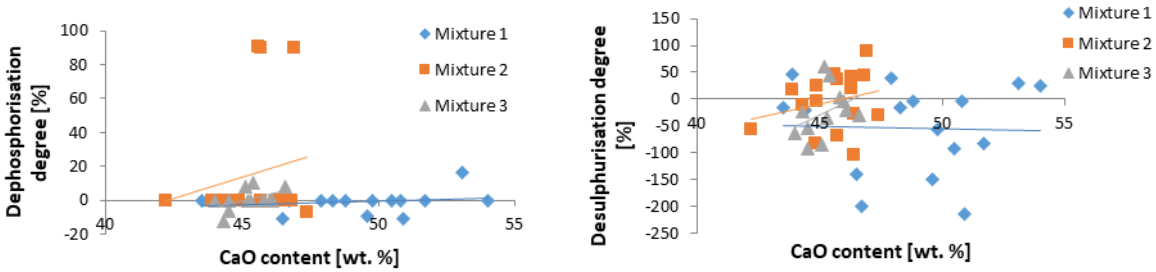

Figure 6 Dephosphorisation and desulphurisation degree depending on the CaO content.

a) b)

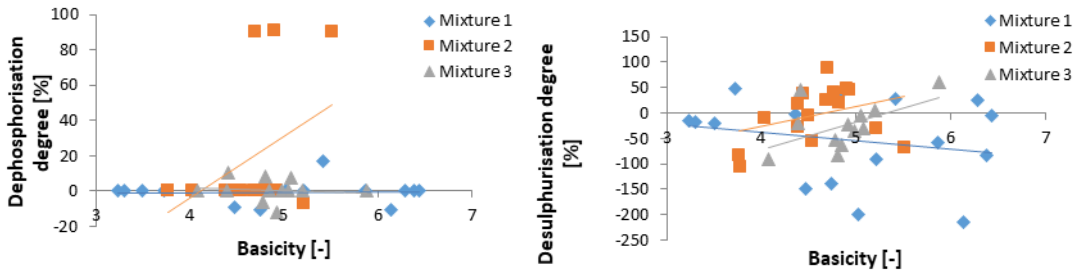

Figure 7 Dephosphorisation and desulphurisation degree depending on the slag basicity.

a) b)

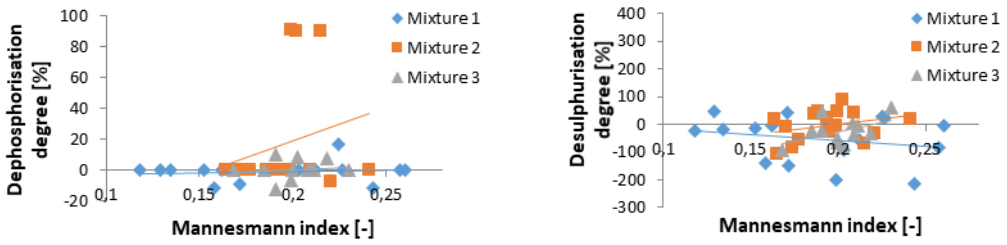

Figure 8 Dephosphorisation a) and desulphurisation degree b) depending on the Mannesmann index.

Figure 9 shows changes in the slag viscosity as a function of temperature for average slag constitutions computed with the FactSage software, for individual mixtures.

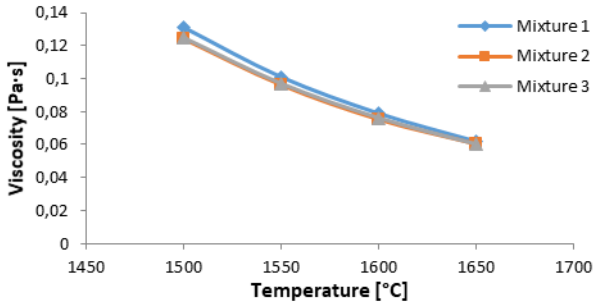

Figure 9 Change in viscosity as a function of temperature for average slag constitutions computed with the FactSage software.

3. Conclusions

As follows from the data, the average values for individual constituents, as well as basicities are similar for all series. The obtained differences are very low. It means that no differences were observed in the slag chemical constitutions, despite using various methods for ladle slag formation. One should accept that both tested mixtures have similar properties from the perspective of chemical constitution of the slag formed.

The performed industrial tests indicate that non -metallic inclusions based on aluminium oxides Al_2O_3 with the addition of calcium, magnesium and silicon prevail in steel. Inclusions of this kind can be eliminated by appropriate selection of the slag chemical constitution to enable appropriate physico-chemical properties to be obtained. In this connection the following recommendations concerning the chemical constitution have been developed:

- the CaO content in slag should be within the range 45-55 wt. %,
- the SiO_2 content in slag should be within the range 10-15 wt. %,
- the Al_2O_3 content in slag should be within the range 24-31 wt. %,
- the MgO content in slag should be within the range 6-14 wt. %,
- the sum of the FeO+MnO contents should be under 1 wt. %,
- basicity B1=CaO/SiO_2 should be 2.5-4.0,
- basicity B3=CaO/SiO_2/Al_2O_3 should be 1.2-1.8.

Acknowledgements

Research carried out as part of a project executed by ArcelorMittal Warszawa in the sectoral programme “INNOSTAL”, financed by Measure 1.2 “Sectoral R&D programmes” and the priority axis “Support for business R&D” of the Smart Growth Operational Programme, 2014-2020; agreement no. POIR.01.02.00-00-0161/16.

References

[1] Gavanescu, A.; Kiss, I. Treating the liquid steel with synthetic slag in the casting ladle, Hutnik – Wiadomości Hutnicze, nr 3, **2009**, s. 185 – 188.

[2] Wcisło, Z.; Michaliszyn, A. Zastosowanie żużli rafinacyjnych w metalurgii kadziowej, Prace Instytutu Metalurgii Żelaza, nr 4, **2006**.

[3] Kargul, T. Opracowanie hybrydowego modelu procesu pozapiecowej rafinacji stali do oceny wybranych technologii metalurgicznych, Rozprawa doktorska, Kraków **2009**.

[4] Lis, T. Metalurgia stali o wysokiej czystości, Wydawnictwo Politechniki Śląskiej, Gliwice **2009**.

[5] Riyahimalayeri, K.; Slag, Steel, Ladle and Non-metallic Inclusions Equilibria in an ASEA-SKF Ladle Furnace, Doctoral Thesis Department of Materials Science and Engineering School of Industrial Engineering and Management KTH Royal Institute of Technology Stockholm, Sweden, **2012**, pp. 1-76

[6] Sheshukov, O. Yu and others; Unit Ladle-Furnace: Slag Forming Conditions And Stabilization, KnE Materials Science / Technogen-2017, **2017**, pp. 70-75.

[7] Karbowniczek, M.; Kawecka-Cebula, E.; Reichel, J. Investigations of the dephosphorization of liquid iron solution containing chromium and nickel, Metallurgical and Materials Transactions. B, vol. 43 no. 3, **2012**, pp. 554–561.

NUMERICAL SIMULATION OF LIQUID STEEL FLOWING INTO THE INGOT MOULD FOR DIFFERENT TYPES OF FLOW CHANNELS

Vladislav Kurka[1*], Petr Jonšta[1], Jaroslav Pindor[1], David Bocek[2], Bohuslav Chmiel[2]
[1]MATERIÁLOVÝ A METALURGICKÝ VÝZKUM s.r.o., Pohraniční 693/31, 703 00 Ostrava, Czech Republic;;
petr.jonsta@mmvyzkum.cz (P.J.); jaroslav.pindor@mmvyzkum.cz (J.P.)
[2]ITŘINECKÉ ŽELEZÁRNY, a. s., Průmyslová 1000, Staré Město, 739 61 Třinec, Czech Republic;
David.Bocek2@trz.cz (D.B.); Bohuslav.Chmiel@trz.cz (B.Ch.)
*Correspondence: vladislav.kurka@mmvyzkum.cz

Abstract
During the casting of the steel into the ingot mould, one of the key parts is the initial input and the subsequent flow of the steel into the ingot mould. Especially in terms of the possibility of spraying steel on the mould walls or mixing the liquid steel with the casting powder. If we focus on the shape of the outflow runners, its small design change affects the flow and shape of the melt flow in the ingot mould both at the beginning and during the casting of the ingot body. The initial casting phase has the greatest influence on the possibility of exogenous inclusions input into the body of the ingot, in particular from the casting powder lying on the surface of the cast melt. Using the numerical simulation in the MAGMA 5 software, three different types of outflow runners were compared in terms of flow. The present work deals with the influence of shapes of outflow runners on the possibility of clogging exogenous inclusions into the body of cast 5 t of ingot, in the first half of the steel melt casting with 1 % C and 1.5 % Cr.

Keywords: numerical simulation; steel melt; steel flow; outflow runners; ingot mould

1. Introduction

When casting several ingots in parallel on a casting plate, defects of their inner structure arise, particularly during the solidification process. The defects may be caused by the setup of the input metallurgical conditions, which largely include, in particular, the temperature and speed of the molten metal casting procedure. Inner defects also occur due to improper selection of the design and material composition of the structure in which the melt cools down. These concerns, in particular, the shape and material composition of the ingot moulds, head adapter, including the materials inside [1-3]. The shape, location and material composition of the mould inlet and the complete gating are also important. And last but not least, the inner quality may also be influenced by the casting ladle, i.e. the amount, temperature and method of casting the melt from the ladle into the ingot mould set [4-6]. Deeper details such as the chemical composition of the melt and the melt production method play a role too, of course, but these lie beyond the scope of this treatment. Numerical simulations have been used recently to simulate the molten metal casting and solidification processes, with a view to eliminating the formation of defects inside the solidified ingot through proper setting of the input metallurgical conditions and a suitable design of the casting system, see e.g. [7-11].

2. Experiment Description

The experiments were focused on the areas where the molten metal enters the mould, with a view to avoiding contamination of the solidifying melt by exogenous inclusions, particularly the casting powder. The mould set was filled with the molten metal always to 50%. The objective was to use numerical simulations in Magma 5.4, year 2019, software to compare three types of outflow runners with respect to their effect on the melt flow into the mould and on the melt solidification process during the casting procedure. The melt, the chemical composition of which is listed in 0, was cast at the same metallurgical parameters into the same mould sets composed of 8 moulds handled on a mould plate (the geometrical shape of the casting set is shown in 0). All the 8 moulds in a casting set were fitted with a single runner type. Three runner types were used, referred to as runner A, B and C. Accordingly, the simulations were marked A, B, C when using runner type: A, B or C, respectively. The runner designs are as follows:

- runner A has 2 straight outlet openings, see 0,
- runner B has 1 oval outlet opening, see 0,
- runner C has 2 conical and elevated outlet openings, see 0.

The runners also differ in the outlet opening cross-sections: they were 3 180 mm^2 for runners A and C and 2 285mm^2 for runner B (hence, lower than for runner A or C).

Table 1 Chemical composition of the melt marked as CrC (wt. %).

	C	P	S	Si	Mn	Cr	Ni
Contents	1.0	0.01	0.002	0.25	0.4	1.5	0.05

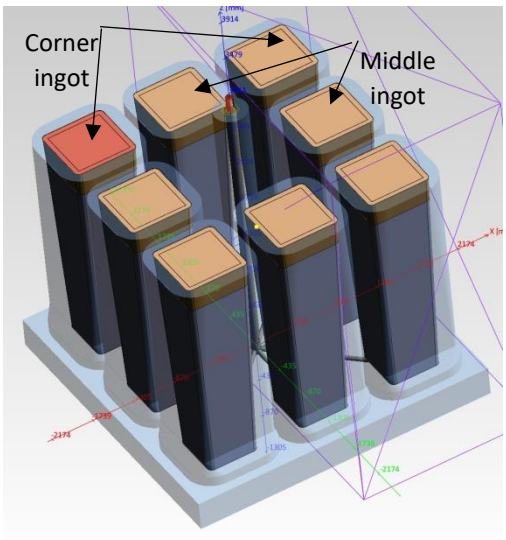

Figure 1 Mould set with 5 t moulds, including the casting system.

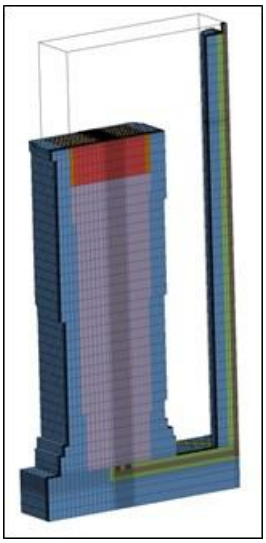

Figure 2 Meshed middle ingot and the casting assembly.

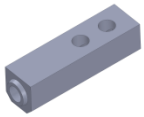

Figure 3 Runner type A.

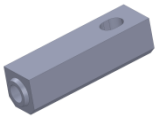

Figure 4 Runner type B.

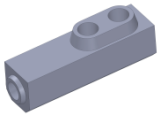

Figure 5 Runner type C.

The next important step after making a drawing of the mould set was to find the most suitable mesh with hexagonal cells dividing the mould set parts and the molten metal into elements. Example of a "meshed" ingot is shown in 0.

After the meshing, the input metallurgical parameters were defined for all the three types of numerical simulation. The defined temperatures of the melt and the casting set parts were are in the 0 and 0.

Table 2 Temperatures of the part of the ingot mould set.

Temperature	[°C]
ingots	50
runners	50
sink head lining	20
casting powder	20

Table 3 Temperature of the melt.

Temperature	[°C]
solidus	1326
liquidus	1453
casting	1485

3. Evaluation of the experiment

In the numerical simulations, the three runners were compared for both the middle and corner ingots of the mould set containing 8 ingots on a single casting plate. Hence, 8 numerical simulations are shown in total. Due to a higher complexity of meshing in the diagonal direction (corner ingots) compared to the transverse directions (middle ingots), the resulting numerical times of melt inlet into the runners of the corner ingots are shifted by approx. 2.6 s against the middle ingots. The view of the corner ingot is diagonally cut, and so it has proportionally different dimensions (height and width).

The cross sections of the runners A and C are identical 3 180 mm^2. This cross-section is 28 % larger than that of the runner B, which has only one oval outlet with a cross-section of 2 285 mm^2.

The pictures of the melt flow velocity in the inlet runner and the outlet runners in 0 at 2.120 s show that the melt entering the runner hits the end of the outlet runner wall in the same way for all the three runners. The melt in the runners A and B, however, has a higher spurt into the mould than in the runner C, which is probably related with the elevation of the outlets in the runner C. 0 also shows that with the runners A and B, the melt tends to tear, which indicates possible spattering on the mould walls. The higher spurt in the case of runner B may be caused by the smaller runner diameter. 0, depicting the situation at 407 s after start of the casting operation, shows that due to the higher discharge velocity from the runner B the newly entering melt gets closer to the melt level than with the runner C, which has the lowest discharge velocity towards the surface level, closely followed by the runner A.

As to the temperature field of the cast melt: the melt temperature was above the liquidus temperature till approximately the 40th second for all the three runners. At 80 s, from the start the casting procedure, the melt started to solidify at the bottom of the ingot at the mould stool, first with the runner C, see 0. Then after 200 s the melt started to solidify on the mould wall with the runner B and then, after 240 s, also on the mould stool with the runner A; the final mould temperature at 407 s is shown in 0.

The pressure induced in the melt during the casting procedure was also evaluated: the pressures were identical in all the three assemblies during the end runner filling procedure within 2.477 s after the start of casting. Once the runners had been completely filled, the pressure in the end runner B increased due to the smaller cross-section and remained higher than the other pressures until the time of 11.088 s, see 0. Although subsequently the pressures tended to equalize, the pressure remained higher in the runner B, followed by the runner A, the lowest pressure being in the runner C until the time of 110 s. During the period from 200 to 407 s, the ferrostatic pressure began to outweigh the resistance of the openings in the runners and the pressures in the runners were equal.

When looking at the summary thermal flux of the main parts from the melt in the corner and ingots towards the moulds, heat removal is seen to be fastest with the runner B, followed by the runner C, and the slowest heat removal is in the casting set A, see 0.

4. Discussion

The evaluation shows that the risk of mould body contamination with the casting powder due to the effect of the melt flow velocity, mainly at the beginning of the casting procedure, and to possible melt spurts of the melt, is lowest with the runner C, followed by the runner A, and is highest with the runner B.

The runner geometry also influences the solidification process and the development of pressures in the runners. It is also shown that filling is more uniform with the runner C compared to the runner A, and the worst situation is with the runner B.

In terms of the heat flux from the melt in the corner and middle ingots towards the moulds, the best heat dissipation was observed in the casting set with the runner B, followed by the runner C and then the runner A. This is also borne out by the development of the minimum and mean melt temperatures, which are in accordance with the development of heat transfer from the melt to the casting set components.

5. Conclusion

The present article described numerical simulations of ingot mould sets used for casting steel CrC into 8 moulds arranged into a pattern of 4 corner moulds and 4 middle moulds. The numerical simulations were performed for 3 end runner types both for the middle and corner moulds. The objective of the work was to identify the runner that exhibits the lowest tendency to contaminate the metal with the casting powder during the casting procedure, in particular in the initial phase.

The melt flow velocity, temperature field and pressure induced by the melt were evaluated, and the lowest tendency to contaminate the system with the casting powder during the casting procedure was found for the runner marked as C with two elevated conical outlets, followed by the runner A with two straight outlets and finally by the runner B with one oval outlet.

It should be emphasized that the work was focused on the assessment of the hazard of metal contamination with the casting powder for 50 % filling with the cast metal; hence, there were another 50 % of the molten metal missing in the mould, which may have influenced the results. Completion of the numerical simulations for 100 % mould filling with the molten metal, including solidification and evaluation of the effect of the end runner design on the inner quality of the ingot, is planned for the next stage of the experiments.

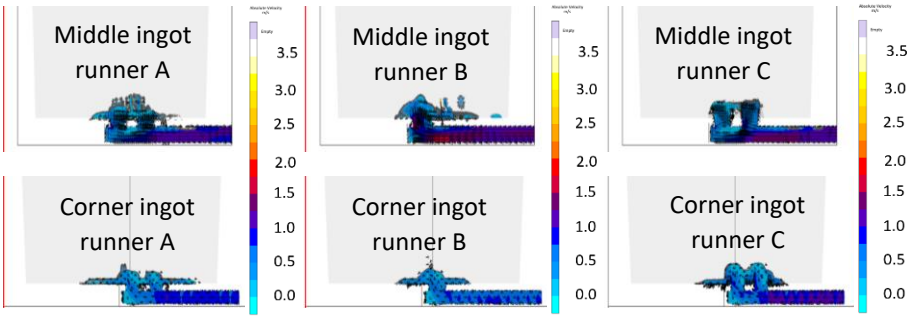

Figure 6 Melt flow velocity with the velocity vectors at 2.120 s, range 0-3.5 m.s^{-1}.

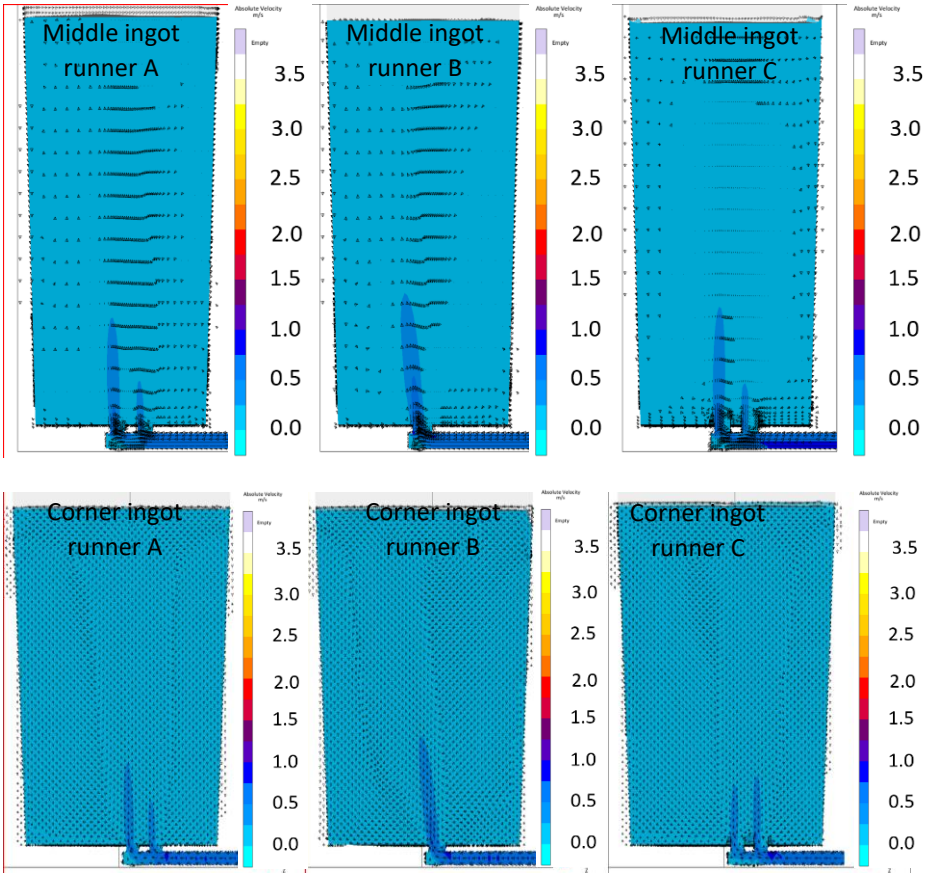

Figure 7 Melt flow velocity with the velocity vectors at 407 s, mould filled to 50 %, range 0-3.5 m.s^{-1}.

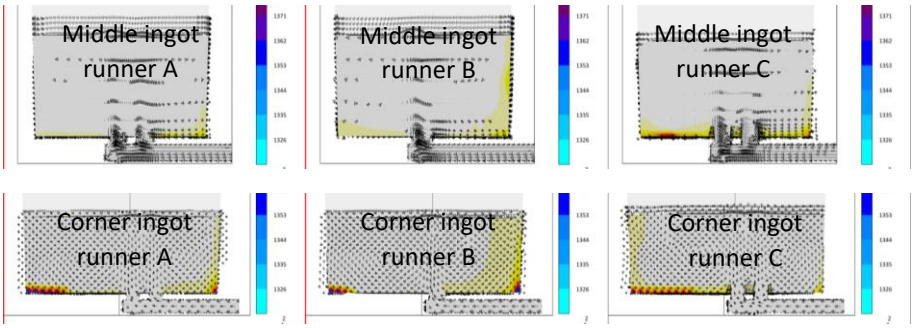

Figure 8 Melt temperature field with the melt flow vectors at 80.061 s, range 1326-1453 °C.

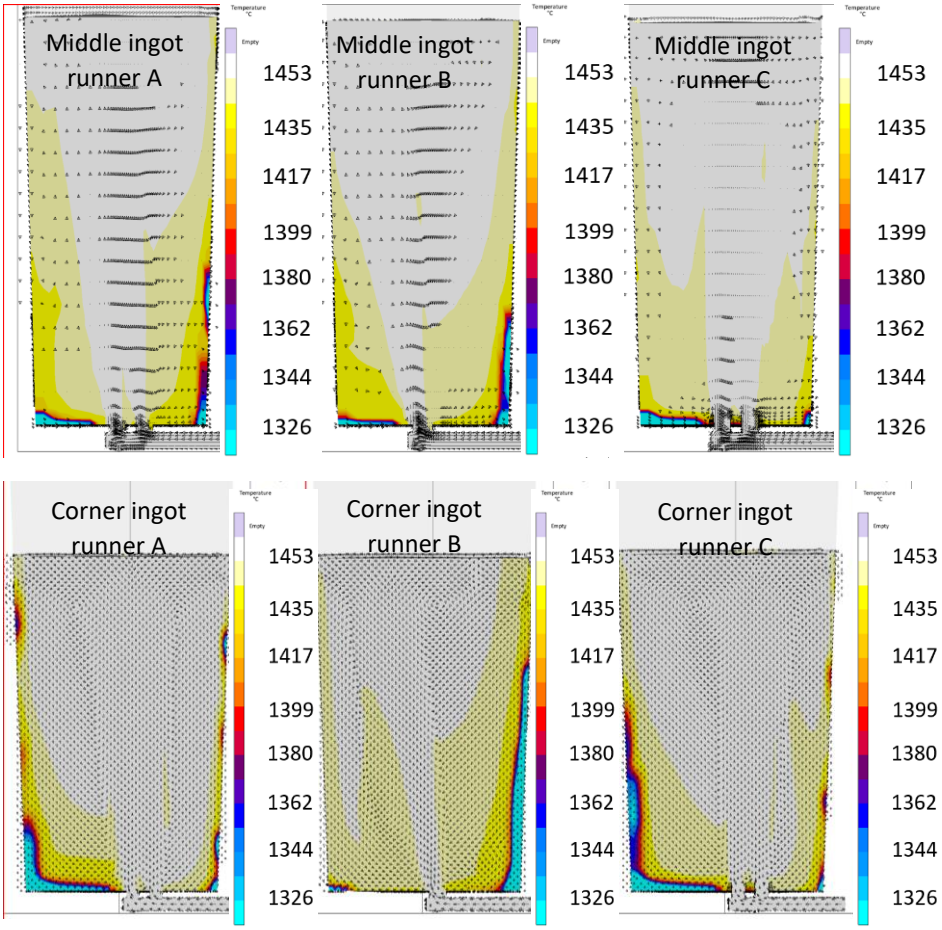

Figure 9 Melt temperature field with the melt flow vectors at 407 s, range 126-1453 °C.

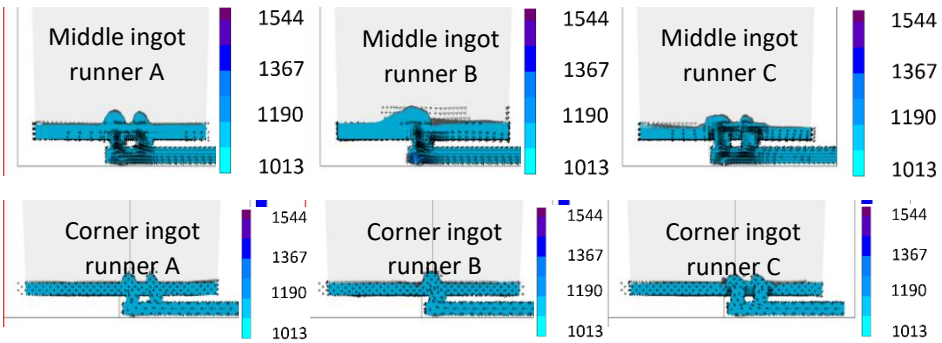

Figure 10 Pressure induced by the melt with the melt flow vectors at 11.088 s, range 1013-2500 mbar.

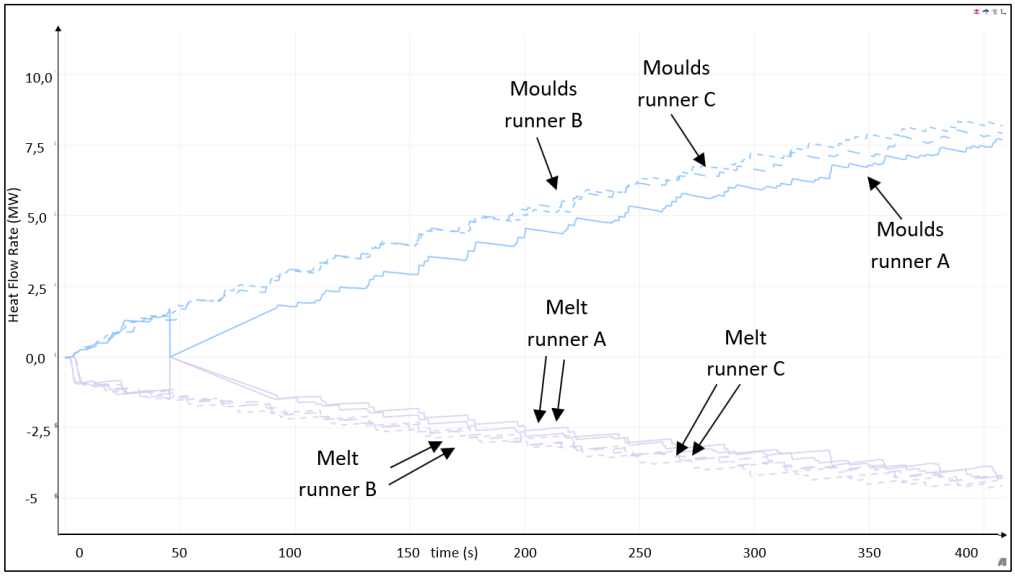

Figure 11 Heat flux from the melt to the mould set and its parts at 0-407 s, range from -5,0 MW to 10,0 MW.

Acknowledgments

The article was created thanks to the project No. CZ.02.1.01/0.0/0.0/17_049/0008399 " Development of inter-sector cooperation of RMSTC with the application sphere in the field of advanced research and innovations of classical metal materials and technologies using modelling methods " from the EU and CR financial funds provided by the Operational Programme Research, Development and Education, Call 02_17_049 Long-Term Intersectoral Cooperation for ITI, Managing Authority: Czech Republic-Ministry of Education, Youth and Sports.

References

[1] Heidarzadeh, M.; Keshmiri, H. Influence of mould and insulation design on soudness of tool steel ingot by numerical simulations. *Journal of iron and steel reseach, international* 2013, 20 (7), 78-83.

[2] Shengwen, Q.; Xiaoqiang, H.; Yanfei, C.; Xiuhong, K.; Dianzhong, L. Hot top design and its influence on feeder channel segregates in 100-ton steel ingots. Materials and design 87 (2015), 205-214.

[3] Marx, K.; Rödl; S., Schramhauser, S.; Seemann, M. Optimization of the filling and solidification of large ingots. *La Metallurgia Italiana.* 2014.

[4] Baoguang, s.; Xiuhong, K.; Dianzhong, L. A novel technique for reducing macrosegregation in heavy steel ingots. *Journal of Materials Processing Technology,* 210 (2010), 703-711.

[5] Lan, P.; Zhang, J., Q. Numerical analysis of macrosegregation and shrinkage porosity in large steel ingot *Ironmak. & Steelmak.* 2014, 41, 8, 598-606.

[6] Li, W.; Shen, H.; Zhang, X.; Liu, B. Modeling of species transport and macrosegregation in heavy steel ingots *Metall. and Mater. Trans. B.* 2014, 45B**,** 464-471.

[7] Tkadleckova, M.; Machovcak. P.; Gryc, K.; Klus, P.; Michalek, K.; Socha L.; Kovac, M. Setting a numerical simulation of filling and solidification of heavy steel ingots based on real casting conditions. *Materials and technology*. 2012, 46, 4, 399–402.

[8] Kermanpus, A.; Eskandaria, M.; Purmohamada, H.; Soltani, M. A.; Shateri, R. Influence of mould design on the solidification of heavy forging ingots of low alloy steels by numerical simulation. *Materials & Design*. March 2010, 31, 3, 1096-1104. doi:10.1016/j.matdes.2009.09.045.

[9] Kurka. V.; Vindyš, M.; Jonšta, P.; Pindor J. The use of numerical simulations to obtain the basic knowledge about casting process of heavy circular ingot. In Metal 2019, Brno, Czech republic, EU. Tanger. 2019, p. 168-174. ISBN 978-80-87294-84-0.

[10] Mazumdar, D., Ewans, J., W. *Modelling of Steelmaking Processes*. CRC Press, 1st Ed., 2009. ISBN 978-1-4200-6243-4.

[11] Couturier, G., Rappaz, M. Modelling and Simulation in Materials Science and Engineering, 2006, 14, 253.

MASS AND THERMAL BALANCE OF IRON SINTERING PROCESS WITH LIGNIN

Jaroslav Legemza[1*], Mária Fröhlichová[1], Róbert Findorák[1], Martina Džupková[1], Jozef Hudák[2]
[1]Faculty of Metallurgy, Technical University of Košice, 04200 Košice, Slovakia; jaroslav.legemza@tuke.sk (J.L.); maria.frohlichova@tuke.sk (M.F.); robert.findorak@tuke.sk (R.F.); martina.dzupkova@tuke.sk (M.D.)
[2]Arcelor Mittal, Vratimovska 689, 70702 Ostrava, Czech republik; jozef.hudak@arcelormittal.com (J.H.)
*Correspondence: jaroslav.legemza@tuke.sk; Tel.: +421-55-602-3155

Abstract
This paper specifies a mass and thermal balance of high-temperature sintering of an iron materials in laboratory conditions. These experiments were carried out by substituting coke with biomass (lignin). For realization of experimental sintering, a sintering apparatus – laboratory sintering pan (LSP) – was used, which is fully equipped with measuring devices and analysers. An important goal of the work was to specify mathematical modeling using thermodynamic software HSC Chemistry. Gibbs equilibrium diagrams, Kellog diagrams and mass and thermal balance were calculated. On the basis of the results, the correlation was obtained in the comparison of some values of sintering during modelling and experimental simulation. High correlations were found in the calculated fuel (substituting coke with lignin) for sintering, and determined produced amount of agglomerate. In the process of sintering with lignin, it was necessary to increase the amount of total fuel in the charge due to its lower calorific values. The maximum temperatures in the sintering process were lower (about 140–270 °C) with lignin than with coke.

Keywords: sintering; agglomerate; coke; biomass; lignin; modelling; mass-thermal balance

1. Introduction

The agglomerate is a basic input material for the production of pig iron and plays an important role in the integrated metallurgical cycle. It is produced by high-temperature sintering of fine iron ore, iron ore concentrates and other materials (e.g. secondary materials from iron and steel production, basic components, carbon fuels). In the agglomeration process, bituminous coal coke, grain size < 3 mm, is used as a fuel. In addition to traditional coke powder, biomass can be used as a substitute fuel. The creation of models, simulations, and predictions of the sintering process is very important today. For these models we can define physical chemical and thermal processes that alter the structure and composition of input sintering raw materials. The sintering process takes place in a heterogeneous system of the gas–liquid–solid phase, while the gas phase ensures the fuel combustion, heat transfer, and oxidation-reduction processes [1-2]. The creation of a computational model of agglomeration process is based on knowledge of the events taking place in the sintered layer, as well as the principles of conservation of mass and thermodynamic stability of compounds [3]. The agglomeration process has been modeled worldwide in several studies. Many authors show the predicted melting of grains and solidification heats of agglomerates [3-6]. These processes are very important for forming the final agglomerate structure and good reducibility of sinter [7]. Some authors developed a mathematical models with the heat and mass transfer processes in a sintering bed or discussed sinter properties produced on a pot apparatus experimental facility and presented a mathematical model based on the transport phenomena [3-6].

2. Experimental Methods and Materials

This paper shows an application of the mathematical model and a physical simulation of the sintering process in laboratory conditions. For mathematical modelling the basic chemical reactions with standard Gibbs energy and mass and thermal balance were calculated. Thermodynamic data were obtained from the software HSC Chemistry, Figure 1 [8]. Thermochemical calculations are based on enthalpy H, entropy S, heat capacity Cp or Gibbs energy G values for chemical species. They can all be mathematically derived from experimental observations [3]. Due to the modelling principles based on Gibbs free energy minimization, the applications range from high temperature systems to analysis and process simulation. The experiments were carried out in a laboratory sintering pan (LSP), which simulates the conditions on an agglomeration belt, as well as the quality of the agglomerate, Figure 1. For the simulation of Fe agglomerate production using biomass, close monitoring of the sintering process needs to be maintained. For the high temperature range in the sintered layer, three thermocouples of the PtRh10-Pt type were used. The flue gas temperature was read at two levels by the NiCr-

Ni type thermocouple. The chemical composition and temperature of the flue gas were analysed by the TESTO 350 device.

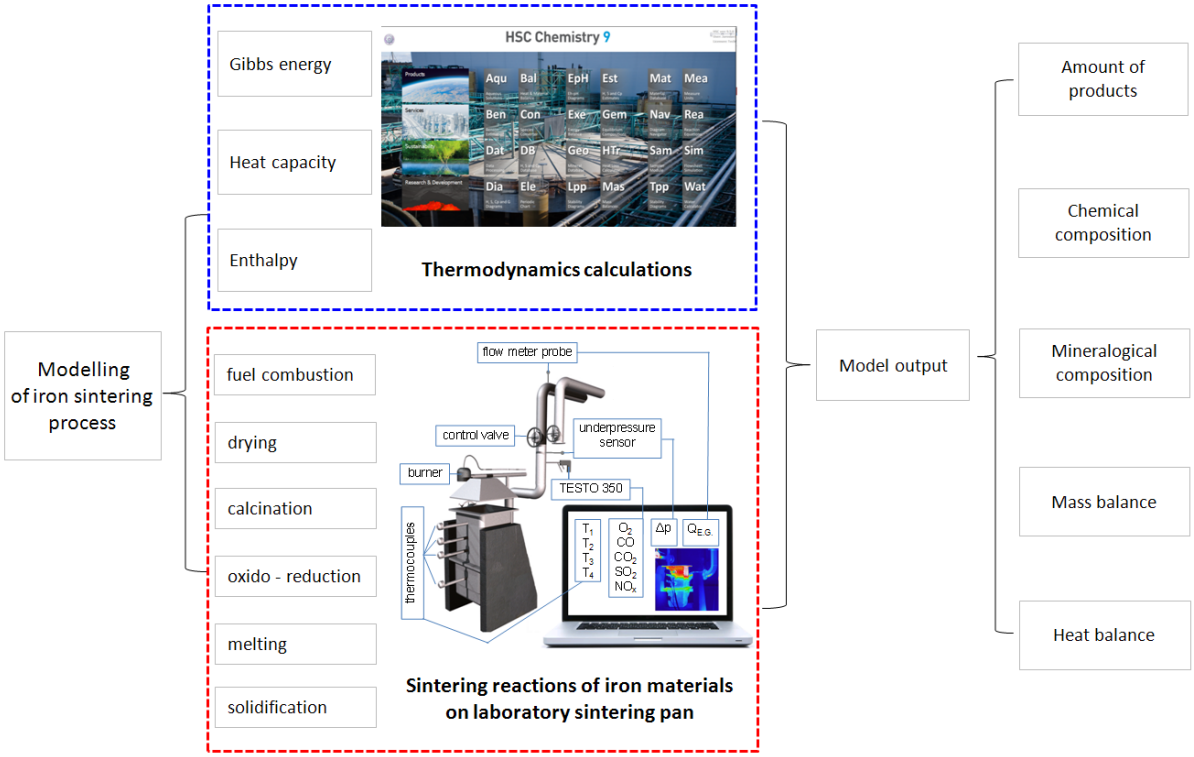

Figure 1 Scheme presenting the modelling of the iron sintering process.

Laboratory experiments were performed using iron raw materials-aggloore from the Ukraine (content of Fe_{TOT} = 60.39 wt%) and concentrate from the Ukraine (content of Fe_{TOT} = 67.95 wt%). In the agglomeration process, standard coke powder (C_{FIX} = 81%, ash = 12%, caloric value = 28 MJ/kg) was used as fuel. Biomass was a technical hydrolyzed lignin (C_{FIX} = 20%, ash = 3.4%, caloric value = 23 MJ/kg) [9]. The other mixture components (dolomite, calcite, and lime) had a commercial standard chemical composition. These inputs were included in prepared agglomeration mixtures with basicity within the interval of 1.5–1.9. The produced Fe agglomerates had Fe_{TOT} content within the interval of about 48–53 wt%. Chemical analysis of the samples was determined using XRF spectrometer ARL 9900S.

3. Results and discussions

The authors of this paper carried out a large number of experiments and studies focused on the use and application of biomass in the context of the production of Fe agglomerates in laboratory conditions. In addition to the chemical composition of the agglomerate, the results of balance calculations include also mass data of produced agglomerates, which are calculated based on the balance of the chemical composition. The calculations have implemented the above requirements and adjustments from the perspective of various losses and chemical processes during the process. The actual model consists of several basic parts. The first part of the calculation model includes analysis of different components. The second part of the model includes the actual calculation of consumptions of materials in the agglomixture to ensure the desired chemical composition of the agglomerate. The third part of the model provides a summary overview of the material balance of the process. The current mathematical model used in this study was extended with thermal balance determined on the basis of input and output enthalpies of individual components (including the types of biomass). Fuel burning and heat transfer are important for the sintering process. The best sintering results are achieved when the speed of the heat wave movement is the same as the speed of the solid fuel combustion zone movement. The difference in speed of these processes is causing the increase of the combustion zone width, the decrease of the maximum temperature in the combustion zone, and the deteriorated quality of agglomerate.

The speed of the thermal layer movement is given by equation (1):

$$V_{tv} = K\frac{C_g}{C_{vs}}\omega_0 \quad (1)$$

Where V_{tv} – speed of thermal layer movement (mm.min^{-1}),

K – factor of proportionality,

C_g – thermal capacity of gas (kJ.m^{-3}.K^{-1}),

C_{vs} – apparent volumetric thermal capacity of agglomeration charge (kJ.m^{-3}.K^{-1}),

ω_0 – rate of air suction through the layer (mm.min^{-1}).

A charge with coarser grain size and materials with reduced thermal conductivity remove the heat from the gas stream at a slower rate. In that case the thermal conductivity of gas and the speed of thermal layer movement increase. As a result of the heat transfer, the heat produced in the combustion of fuel and the heat supplied by the ignition of charge is utilised multiple times in the sintered layer. The value of regenerated heat is also calculated when the total thermal balance is determined. The share of regenerated heat in the sintering process is assessed using the mean temperature of the layer according to equation (2):

$$t_k = \frac{Q_{vs}}{m_{vs}.C_{vs}+V_g.C_g} \quad (2)$$

Where t_k – mean temperature of the layer provided the charge and the air were not preheated (°C),

Q_{vs} – amount of heat consumed to heat the layer to the temperature of t_k (kJ),

m_{vs} – amount of the elementary layer charge (kg),

C_{vs} – mean thermal capacity of agglomeration charge (kJ.kg^{-1}.K^{-1}),

V_g – volume of gas sucked from the layer (m^3),

C_g – mean thermal capacity of the sucked-off gas (kJ.m^{-3}.K^{-1}).

The maximum temperature in the sintered layer and the time for which this temperature is maintained in the charge depends both on the amount of heat released by the combustion of solid fuel and the amount of accumulated heat. The maximum temperature in the sintered layer is calculated according to equation (3):

$$t_{max} = \frac{Q}{m.C_{vs}} \quad (3)$$

Where t_{max} – maximum temperature in the sintered layer (°C),

Q – heat supplied to the elementary layer (kJ),

m – weight of the elementary layer charge (kg),

C_{vs} – specific thermal capacity of agglomeration charge (kJ.kg^{-1}.K^{-1})

When sintering using biomass (lignin), the effect of the amount of fixed carbon, the amount of volatile matter and moisture is also thermodynamically reflected in the final thermic effect and the composition of the gas phase. Table 1 shows the selected parameters of the mass and thermal balance of agglomerate production using coke and lignin, while these mathematical models were verified by laboratory experiments. It is apparent that in the event of sintering with certain shares of lignin, it will be necessary to increase the amount of lignin in the charge due to its lower calorific values.

Table 1 Selected parameters of mass and thermal balance of agglomerate production with lignin (calculation for 100 kg of charge).

Fuel	**Amount of Agglomerate** (kg)		**Amount of Added Fuel** (kg)		**Thermal Effect of Sintering*** (MJ/sintering)	**Maximum temperature in the sintered layer** (°C)
	LSP (real)	HSC (calculated)	LSP (real)	HSC (calculated)		
Coke	78.55	80.18	4.35	4.97	−1.15	1420
Coke + 20% lignin	-	77.92	-	5.00	32.45	-
Coke + 20% lignin	76.21	77.89	5.52	5.70	−1.84	1280
Coke + 50% lignin	76.08	76.12	7.77	7.83	−1.22	1210
Coke + 86% lignin	73.21	73.55	10.21	9.85	−1.65	1150

Legend: *—negative thermal effect means sufficiency or excess of heat on sintering

It is apparent that the model calculations of added fuel are highly correlated with the experimentally determined values (see Figure 2). An even higher correlation was found for the amount of produced agglomerate (simulated and real). The maximum temperatures in the agglomeration process were lower with lignin than with actual coke breeze, Table 1.

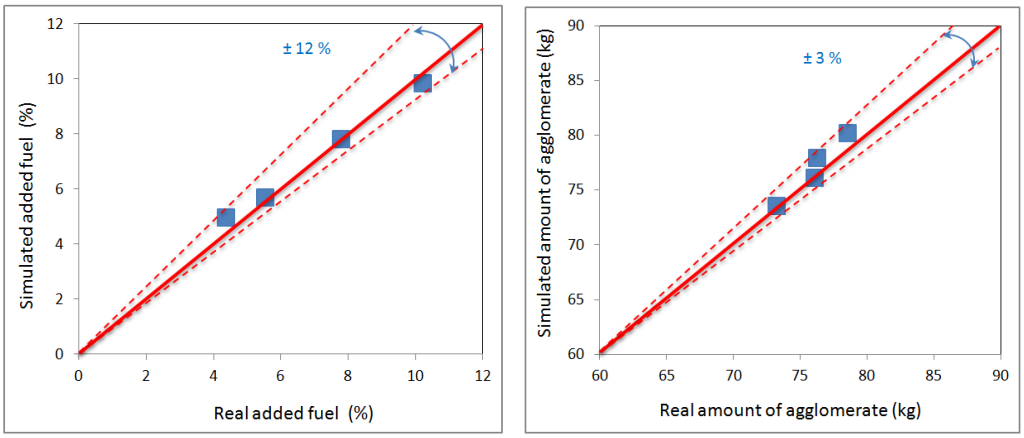

(a) (b)

Figure 2 Comparison between the real and simulated added fuel for sintering (**a**) and real and simulated amount of the agglomerate (**b**) in the iron sintering process with lignin.

Figure 3 gives characteristics of certain agglomerates produced with lignin substitution of coke powder. Worse quality parameters (lower production and strenght of agglomerates) were achieved even with the higher coke powder substitution (86%). The combustion zone is considerably wider for lignin replacement of coke and the lignin burns in the sintering zone faster than coke due to his high porosity and large interface area. Further detailed specifications of modelling and simulation of the sintering process using biomass are given in another article by the authors [3].

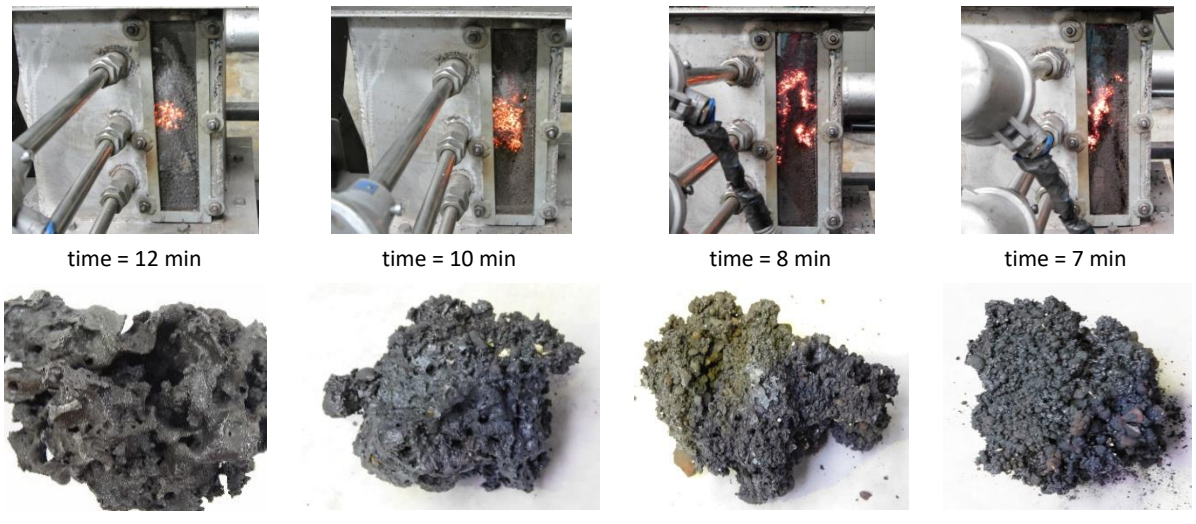

(**a**) (b) (c) (d)

Figure 3 Characteristics of sintering zone and agglomerates produced using coke + lignin (**a**) coke, (**b**) coke + 20% lignin, **(c)** coke + 50% lignin, **(d)** coke + 86% lignin.

4. Conclusion

The aim of this paper was to get the simplest approach (using software HSC Chemistry) to allow one to predict the output parameters based on the initial composition of entered materials. On the basis of the results, the correlation was achieved with the comparison of some values of combustion and sintering during modelling with HSC Chemistry software and experimental simulation. High correlations were found in added fuel (coke + lignin) for sintering, and determined amount of agglomerate. Some conclusions drawn from thermodynamics modelling were:

1. It is possible to substitute about 50% of coke by lignin in the agglomeration. Using lignin up to 50% coke substitution, agglomerates with minimal variations within the chemical, and mineralogical composition were produced. Lignin is one of the most suitable substitutes for coke in the agglomeration process.
2. In the process of sintering with biomass (lignin), it was necessary to increase the amount of total fuel in the charge due to its lower calorific values.
3. The maximum temperatures in the sintering process were lower (about 140–270 °C) with lignin than with coke.
4. Lignin fuels can burn more quickly than coke powder due to his high porosity and large interface area, while there is a significant increase in the vertical speed of sintering.
5. The computational model is currently being transformed into software and can be verified and also adjusted according to the actual outputs from laboratory sintering.

Acknowledgement

This work was supported by Slovak Research and Development Agency (APVV), Slovak Republic, No. APVV-16-0513.

References

[1] Legemza, J.; Frőhlichová, M.; Findorák, R. Tradičné a alternatívne palivá v metalurgii; Technical University of Košice: Košice, Slovakia, **2015**.

[2] Bazilevič, S.V.; Vegman, E.F. Aglomeracija Metalurgia; MISIS Moskva: Moskva, Russia, **1961**.

[3] Legemza, J.; Fröhlichová, M.; Findorák, R.; Džupková, M.;. Modelling of Mass and Thermal Balance and Simulation of Iron Sintering Process with Biomass. *Metals*, **2019**, 9, 1010.

[4] Yang, L.X.; Matthews, E. Sintering reactions of magnetite concentrates under various atmospheres. *ISIJ Int.* **1997**, 37, 1057–1065.

[5] Zhou, H.; Zhao, J.P.; Loo, Ch.E.; Ellis, B.G.; Cen, K.F. Numerical modeling of the iron ore sintering process. *ISIJ Int.* **2012**, 9, 1550–1558.

[6] Young, R.W. Dynamic mathematical model of (Iron-Ore) sintering process. Ironmaking Steelmaking, **1977**, 6, 321–328.

[7] Jursova, S.; Pustejovska, P.; Brozova, S. Study on reducibility and porosity of metallurgical sinter. *Alex. Eng. J.*, **2018**, 57, 1657–64.

[8] HSC Chemistry 9, version 9; Thermodynamic software for process simulation, Outokumpu Research Oy: Pori, Finland, **2018**.

[9] Frőhlichová, M.; Findorák, R.; Legemza, J.; Džupková, M. The fusion characteristics of ashes from lignin and the coke breeze. *Arch. Metall. Mater.*, **2018**, 3, 1523–1530.

MIXING OF LIQUID STEEL IN A STEEL LADLE BY A COMBINED METHOD

Tomasz Merder[1*], Jacek Pieprzyca[1], Michał Szymanowski[1]

[1]Faculty of Materials Engineering and Metallurgy, Silesian University of Technology, Katowice, Poland; jacek.pieprzyca@polsl.pl; michszy416@student.polsl.pl

*Correspondence: tomasz.merder@polsl.pl; Tel.: +48-32-603-4168

Abstract

Purging of liquid steel with inert gases belongs to the basic operations in secondary metallurgy treatment. Its main objectives are homogenization and refining of liquid steel. Basically, it consists of purging argon through a porous plug installed at the bottom of the steel ladle. In special cases, there is a need to support this process by using an additional blow through the lance from above. The article presents the results of model research on the application of a combined blow (porous plug + lance) in a steel ladle. The research has visualized character, also mixing curves were determined for different variants of purging. As a consequence, the obtained results were used to determine the optimal purging method.

Keywords: ladle; homogenization of liquid steel; porous plug; lance; physical modelling

1. Introduction

The modern steel smelting process is basically divided into three stages. In the first stage, the steel charge is melted in the primary metallurgical reactor, which is an oxygen converter or electric arc furnace. In the second stage, secondary metallurgy of liquid steel takes place at the ladle furnace stand and possibly in vacuum treatment equipment. This stage aims at regulating the required chemical composition, refining and homogenizing the temperature in the melt volume. The third stage is the process of casting steel for ingot molds or using a CC device. A very important thing in this system is the synchronization of individual stages of steel production in such a way as to avoid interruptions or stoppages between individual stages. As a rule, a buffer stage where some adjustment is possible is a ladle furnace. Factors determining the residence time of the melt at this site are mainly hydrodynamic phenomena occurring in liquid steel caused in the process of blowing it with inert gases. In order to reduce this time, it is often necessary to intensify the purging process by increasing the intensity of the inert gas supplied to the porous plug. However, this has a negative impact on the refining process. In extreme cases, it seems rational to increase the mixing intensity by means of an additional blast using a lance from above [1-4].

The article presents the results of model tests (water model of the ladle) of the application of a combined blast (porous plug + lance) in a steel ladle. The research was quantitative (visualization) and qualitative (mixing curves). Various variants of the combined blows were analyzed. The obtained results were used to determine the optimal purging method.

2. Research Methodology and Object of the Research Study

The tests were carried out using a test stand (Figure 1a) equipped with a steel ladle model (Figure 1b). This model was made of plexiglass on a linear scale S_L = 1: 5 = 0.2. The basic dimensions of the industrial ladle and its model are shown in Table 1. The model is built in accordance with the requirements of the theory of kinematic and dynamic similarity, and also meets the condition of geometric similarity [5]. The test stand is equipped with a precise gas flow regulation system and a device for precise tracer introduction. The research was divided into two stages: qualitative and quantitative. In qualitative (visualization) tests, the tracer was an aqueous solution of $KMnO_4$. However, in quantitative experiments, consisting in determining the mixing characteristics, the tracer was an aqueous NaCl solution. In both research, the method of pulse signal forcing (Dirac) [6] was used. A specified, equal amount of tracer was added to the steel ladle model. The tracer for each of the experiment variants was given in the axis of the porous plug. The flow image was recorded using a video camera. This enabled uninterrupted observation of the model liquid circulation. In quantitative research used to determine the mixing curves, the signals constituting the basis for their determination were generated by conductometers [7]. They are installed in selected points of the model workspace (Figure 2). Voltage generated in half-second intervals by conductometers is equivalent to changes in tracer concentration in water. The signals recorded from the measuring sensors (conductometers) registered using the recorder are subject to further processing in order to draw curves. This model is described in detail in [8].

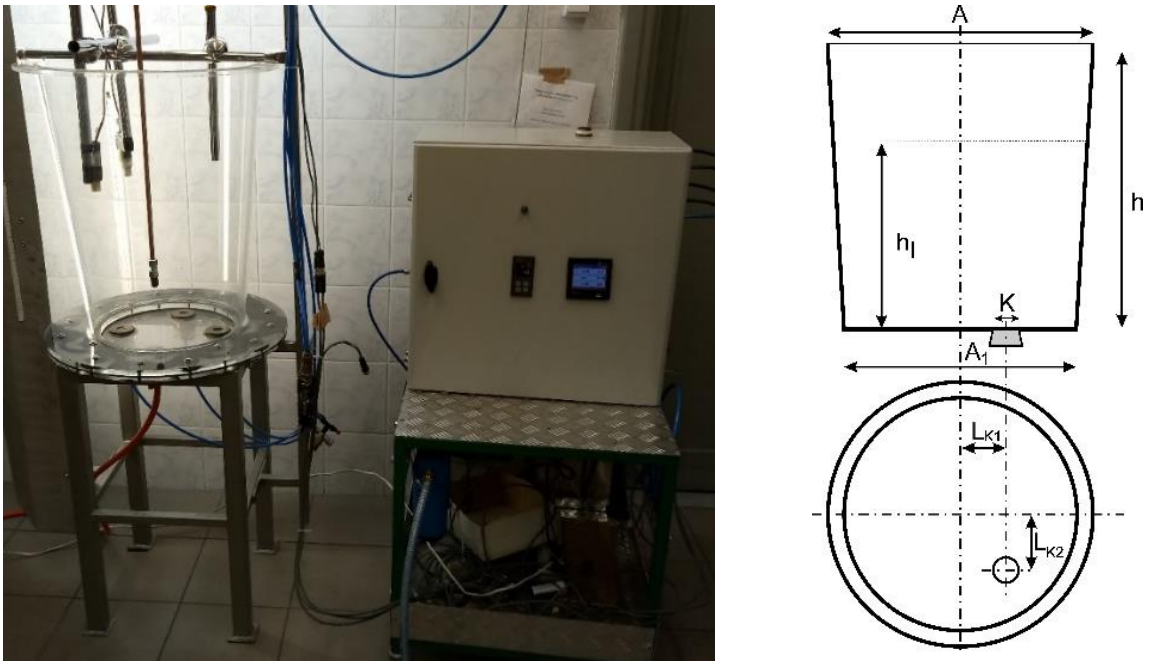

a) b)

Figure 1 View of the test model (a), scheme ladle (b).

Table 1 Design parameters of the model and the industrial ladle.

Parameter	Symbol	Unit	Industrial ladle	Model ladle
			Value	
Diameter	A	m	2.555	0.511
	A_1		1.930	0.386
Height	h		3.300	0.660
Height (to the liquid steel level)	h_l		2.200	0.440
Porous plug diameter	K		0.115	0.023
Porous plug position	L_{K1}		0.470	0.094
	L_{K2}		0.480	0.096

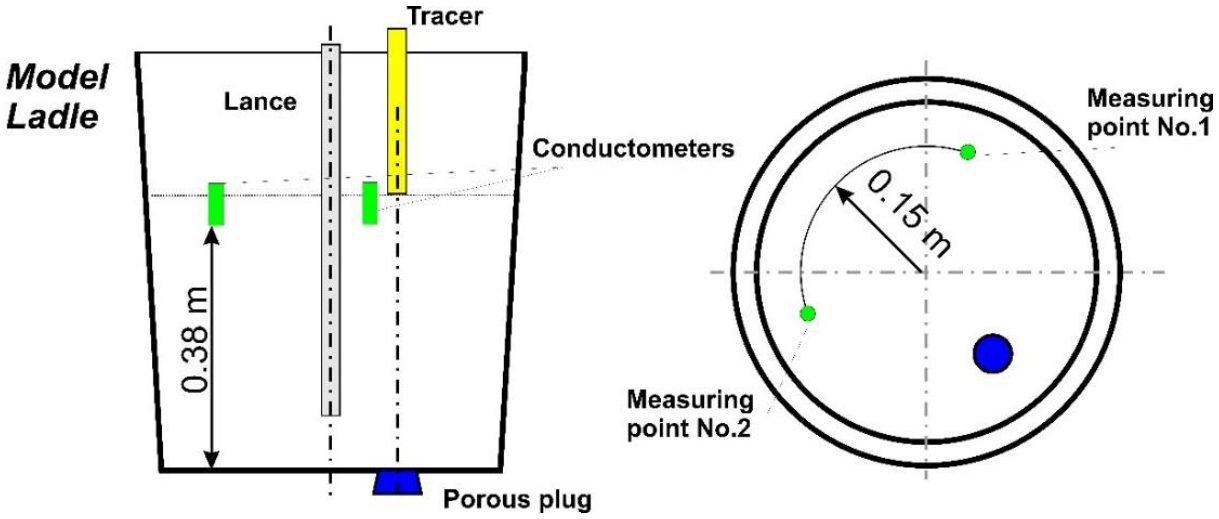

Figure 2 Marking of measuring points in the model.

Parameters for model tests (values of gas flows from real to model conditions) were calculated using the relationship resulting from the modified Froud`s criterion [8, 9]:

$$Q' = \left(\frac{c'}{c}\right)^{-\frac{1}{2}} \cdot S_L^{\frac{5}{2}} \cdot Q \quad (1)$$

where: Q' - is volumetric stream of gas flow for the water model, Q - is volumetric stream of gas flow for the industrial reactor, c' is constant for the water model, c is constant for the industrial reactor, S_L is linear scale.

Table 2 contains the designation of the experiments and the calculated quantities taking into account the linear scale of the model S_L 0.2.

Table 2 Gas flow in industrial and model conditions (ladle).

Experiment variant	Argon flow rate under real conditions		Air flow rate in the model	
	($m^3.h^{-1}$)		($dm^3.min^{-1}$)	
	porous plug	lance	porous plug	lance
A1	10.8	-	1.2	-
A2	9.72	1.08	1.08	0.12
A3	8.64	2.16	0.96	0.24
A4	7.56	3.24	0.84	0.36
A5	6.48	4.32	0.72	0.48
A6	5.40	5.40	0.6	0.6
A7	4.32	6.48	0.48	0.72
A8	3.24	7.56	0.36	0.84
A9	2.16	8.64	0.24	0.96
A10	1.08	9.72	0.12	1.08
A11	-	10.8	-	1.2

3. Results and discussions

3.1. Visualization

The tests were carried out in series, recording their course using a high resolution camera. Film sequences were created from the recorded footage. Then the sequences were divided into individual frames from which a series of frames with the same time parameters for individual variants of the experiment were selected. Figure 3 presents exemplary results of research on visualization of the tracer mixing (flow) process in the model's workspace.

3.2. Mixing curves

In order to determine mixing curves, changes in tracer concentration in modelling liquid (by measuring the electrical conductivity) were recorded at two measuring locations. To reliably compare the results of individual experiments, calculations were made of the measured values of the electrical conductivity recorded by the conductometers to dimensionless form. The following relationship was used for this purpose:

$$C_b = (C_t - C_0)/(C_\infty - C_0) \quad (2)$$

where: C_t, C_0, C_∞ – tracer concentration at time t, at the beginning and end of the process.

An example of characteristics (variant A8) illustrating changes in dimensionless concentration of the tracer during gas injection into the modelling liquid is shown in Figure 4.

The presented mixing curves describe the hydrodynamic conditions prevailing in the steel ladle model during the experiment. The obtained data was processed to determine the mixing time. That is the time necessary to achieve the desired chemical homogenization after the introduction of the alloying additive in the real ladle at the secondary steel furnace stand. In order to read the mixing time, the lines (red) are marked on the graphs informing about the degree of mixing at the level of 95%, which corresponds to C_b ⟨0.95; 1.05⟩. It was assumed that the mixing time is the value of time read from the x axis at the point where the mixing curves for both measuring points fall within the described range (red lines).

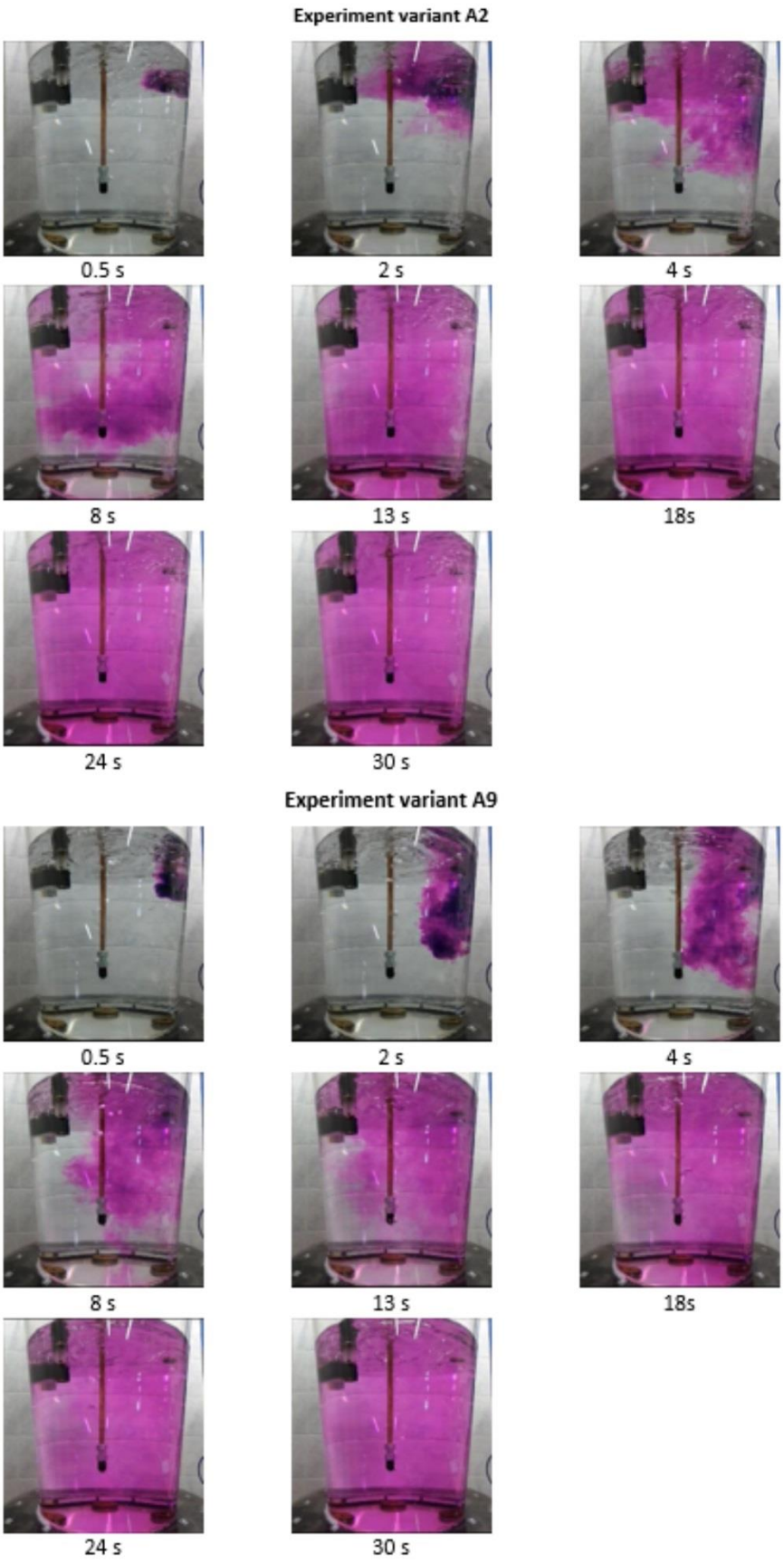

Figure 3 Exemplary results of visualization: a) variant A2, b) variant A10.

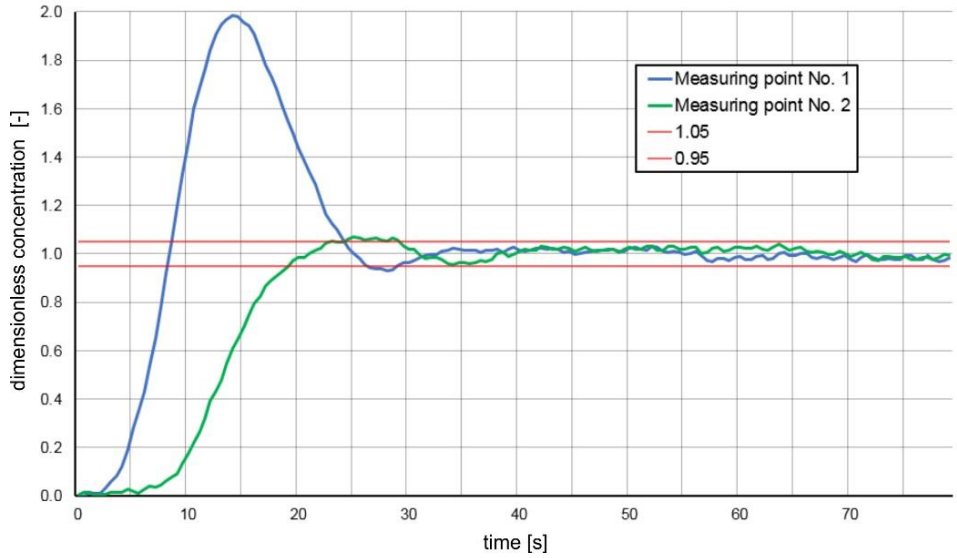

Figure 4 Exemplary changes of dimensionless concentration of the tracer – variant A8.

The read mixing times for individual monitoring points for each of the experiments are shown in Table 3.

Table 3 Mixing times for measuring points.

Experiment variant	Measuring point No. 1 (sec.)	Measuring point No. 2 (sec.)
A1	42.5	35.5
A2	53.5	41.5
A3	61.0	30.5
A4	56.5	68.5
A5	64.0	67.5
A6	42.5	58.0
A7	27.5	49.5
A8	29.0	29.5
A9	61.5	53.0
A10	66.0	73.5
A11	40.5	41.5

The obtained data show that the determined mixing time depends on the location of the measuring place, it was assumed that the longest of them is treated as the minimum mixing time. A summary of the minimum mixing time for each of the analyzed experiment variants is shown in Figure 5.

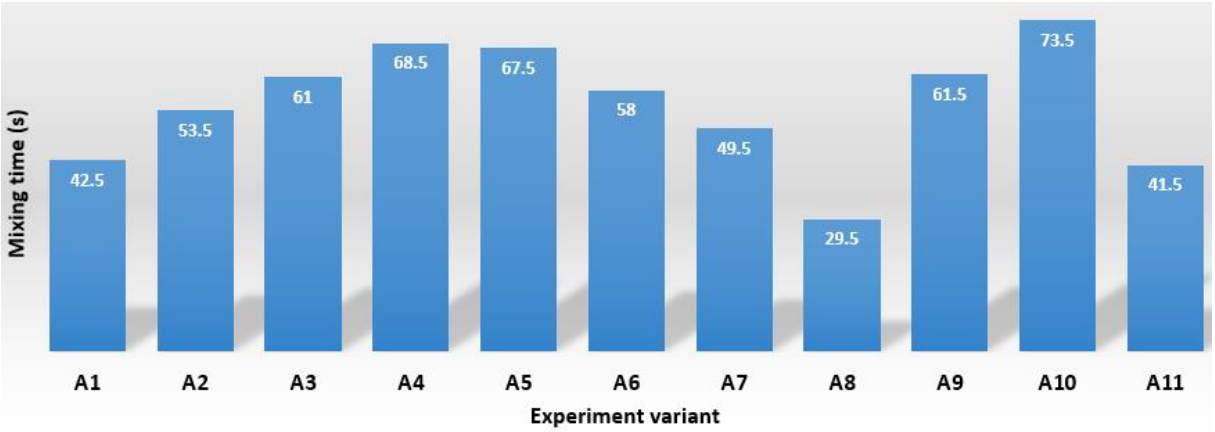

Figure 5 The tracer mixing time for the analyzed variants.

4. Conclusion

Analysis of the presented results of research concerning water model ladle and assuming that the determined mixing times constitute the criterion for assessing the degree of homogeneity of the model liquid, allows to state:

- in variants A1 and A11 of the experiment, mixing times determined in the experiments are similar. This is due to the fact that the required homogeneity of the bath at the gas flow rate (used in the experiment) occurs equally, both with the use of a porous plug and lance in advance,
- in the case of gas injection with the combined method, these times are longer. On the other hand, the longest mixing time was observed in variants A4 and A10,
- in one case only improvement of mixing conditions can be achieved, i.e. in variant A8 of the experiment, with a ratio of gas flow rate distribution in porous plag and lance 3:7.

It follows from the above conclusions that the shortening of the time of stay of a ladle at the ladle furnace stand can be obtained using only specific blowing conditions used in the variant A8 of the experiment.

The presented test results relate only to the impact of using a combined blast on mixing time and, as a consequence, to the effectiveness of the process of homogenizing bath in a steel ladle. However, another issue is the effectiveness of the process of refining liquid steel from non-metallic inclusions. These issues will be described in the next article.

Acknowledgement This work was also supported by Polish Ministry for Science and Higher Education under internal grant BK-205/RM0/2019 for Faculty of Materials Engineering and Metallurgy, Silesian University of Technology, Poland.

References

[1] Szekely, J.; Carlsson, G.; Helle, L. *Ladle metallurgy*; Springer-Verlag, New York, USA, 1989.

[2] Stolte, G. *Secondary metallurgy – fundamentals processes applications*; Woodhead Publishing, Dusseldorf, Germany, 2002.

[3] Ghosh, A. *Secondary steelmaking; principles and application*; CRC Press, USA, 2000.

[4] Sahai, Y.; Guthrie, R.I.L. The formation and role of bubbles in steelmaking operations, Proceedings of the International Symposium on Modern Developments in Steelmaking, Jamshedpur, India, 1981.

[5] Wen, C.; Fan, L.T. *Models for flow systems and chemical reactions*, Dekker, New York, USA, 1975.

[6] Michalek, K. *The use of physical modeling and numerical optimization for metallurgical processes* , Technical University of Ostrava , Ostrava, Czech Republic, 2001.

[7] Information materials G Instruments 2017. Available online: http://www.ginstruments.com/condtx.htm (accessed on 20 February 2017).

[8] Merder, T.; Pieprzyca, J.; Warzecha, M.; Warzecha, P. Application of high flow rate gas in the process of argon blowing through steel, *Arch. of Metall. and Mater.*, **2017**, *62*, 905-910. [DOI: 10.1515/amm-2017-0133]

[9] Merder, T.; Pieprzyca, J. The influence of porous plug type on argon blowing process. In METAL 2017: 26rd International Conference on Metallurgy and Materials. Ostrava, TANGER, **2017**, 188-193.

LABORATORY OF MODEL RESEARCH AT WIMIM SILESIAN UNIVERSITY OF TECHNOLOGY

Jacek Pieprzyca[1*], Tomasz Merder[1], Mariola Saternus[1]
[1]Faculty of Materials Engineering, Silesian University of Technology, Katowice, Poland;
tomasz.merder@polsl.pl; mariola.saternus@polsl.pl
*Correspondence: jacek.pieprzyca@polsl.pl

Abstract
The article presents information on the equipment and research capabilities of the Laboratory of Modeling Research at the Faculty of Materials Science of the Silesian University of Technology. The modernization carried out in it recently and the significant enrichment with new positions for model research meant that it has become an important research center in the country for conducting research in the field of modeling the metallurgical processes. This is evidenced by the implementation of many projects, both in cooperation with industrial entities and other scientific centers, both in the country and abroad. The information presented at the Iron and Steelmaking Conference is aimed at even wider dissemination of knowledge about the capabilities of this laboratory and is an invitation to constructive cooperation.

Keywords: physical modelling; iron; steel; aluminium refining

1. Introduction

In 2016, a wide range of modernization works were carried out at the Laboratory of Modelling Research. The plumbing and electrical installation has been replaced, and mobile power sources have been used to connect the necessary equipment to anywhere in the laboratory. At that time, the construction of the latest research stand for modeling phenomena occurring during the continuous steel casting process was also started. This installation meets the latest requirements of this type of station and is fully automated. As a result, a very modern modelling laboratory was created to conduct research in the full range of technologies conducted in metallurgical enterprises. This range includes: phenomena occurring during the smelting of pig iron in a blast furnace, phenomena occurring during the smelting of steel in an oxygen converter, phenomena occurring during the secondary treatment - both in furnace ladle and vacuum treatment on the RH device, and finally phenomena occurring during steel casting by traditional methods, and above all in the device for continuous steel casting. The view of the currently operating laboratory is shown in Figures 1 and 2.

Figure 1 Part of the Laboratory for Modelling Research concentrating on steel smelting and refining processes.

Figure 2 Part of the Laboratory for Modelling Research concentrating on the continuous steel casting process.

2. Selected examples of tests carried out in a modeling laboratory.

2.1. Model for testing solid and gas flow in a metallurgical shaft furnace

The works carried out with the use of the model mainly concern such issues as the analysis of gas flow resistance in a fixed packed bed or explanation of the phenomenon of its blocking and suspension. Therefore, several generations test installation of a two-phase gas-dust flow through moving packed bed were designed and constructed. This installation, after ongoing improvements and additions to modern control and measurement equipment as well as IT casing, is characterized by wide functional and research capabilities. The apparatus view and exemplary results of determining the moment of the blockade occur are shown in Figure 3

Figure 3 View of the third generation installation and the criterion determining the moment of blockage of two-phase flow (gas + dust) through the packed bed.

2.2. Oxygen converter model.

The physical model of the oxygen converter provides extensive research capabilities. An example is the PhD thesis implemented with its use, which was successfully defended at the WIMiM of the Silesian University of Technology. These studies concerned the determination of optimal conditions for adding lump fuel containing carbon to the oxygen converter from the point of view of optimizing its consumption. The use of a physical model of an oxygen converter allows the identification and description of hydrodynamic phenomena occurring when adding various portions of fuel during bath purging. The results of such tests, in turn, can be used as guidelines to develop a process control system so as to obtain an increase in fuel efficiency and quality of the produced steel while minimizing the costs of its production. The application of the results of model tests in industrial practice may also result in reducing the negative impact of the steel production process on the environment.

Obtained results of model tests, depending on the methodology used, can have different forms. The basic ones are mixing curves and dissolution rates of KPZW in liquid steel during refining of the melt - see Figure 4.

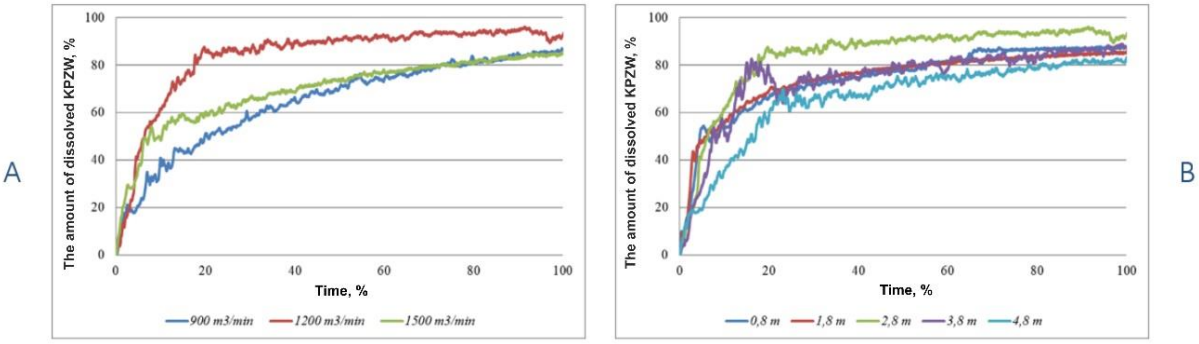

Figure 4. Exemplary mixing curves and KPZW dissolution rates in liquid steel during melting.

A different form of results is obtained during visualization studies – examples of such results are presented on Figure 5.

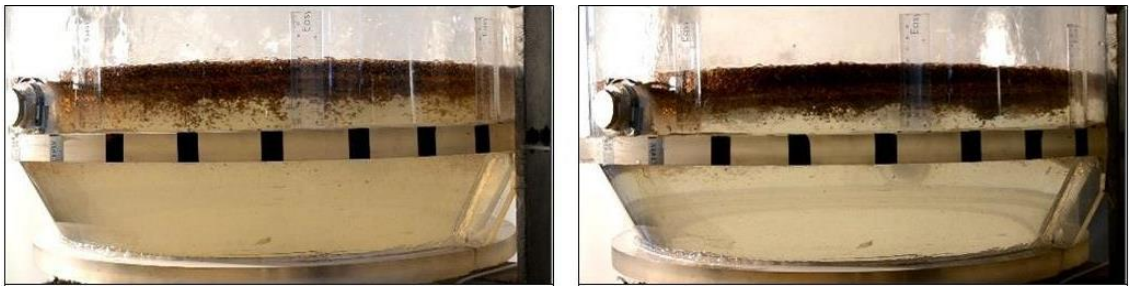

Figure 5 Exemplary images of piece fuel mixing visualization in an oxygen converter model.

2.3. Modelling research of secondary metallurgy

In one of the completed research projects, the problem of optimizing the work of stands for secondary steelmaking was taken up: stands for purging steel with inert gases and stands for vacuum treatment of RH steel, from the point of view of increasing their efficiency.

As a result of the research project, a new research technique was developed in the country to investigate the phenomena of hydrodynamic steel flows in secondary metallurgy processes, involving purging steel with inert gases in a steel ladle and vacuum treatment of steel in an RH device. This technique is based on experiments carried out on specially constructed, and made in accordance with the principles of the similarity theory, water physical models of the industrial devices tested, assisted at the same time by numerical modeling techniques. Built physical models allow to conduct visualization research. The measuring apparatus installed at the laboratory stands also enables the determination of the marker mixing characteristics (marker residence time) in the tested reactors, which uniquely determine the kinetics and effectiveness of the processes tested.

The main issue during the project was research that aimed to determine the optimal hydrodynamic conditions for purging steel with inert gases from the point of view of the effectiveness of gas-permeable plugs depending on their design and location at the bottom of the steel ladle. Exemplary results of these tests are shown in Figure 6.

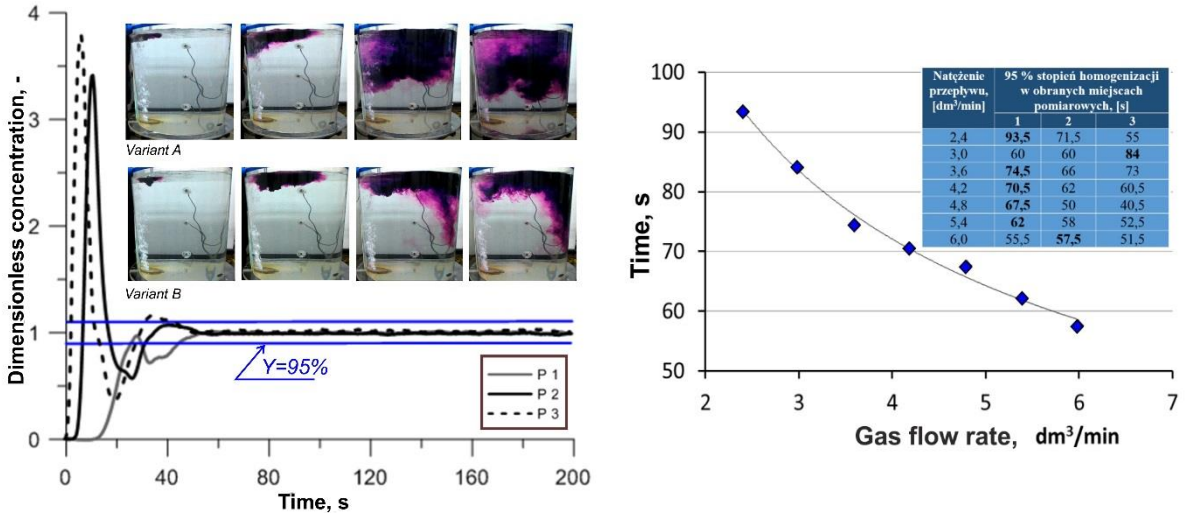

A B

Figure 6 Exemplary results of tests on the effectiveness of inert gas injection in the purging process:
A) changes in the dimensionless concentration of the marker; b) the dependence of the mixing time on the intensity of the gas introduced (for 95% homogenization).

The presented results of the analysis carried out on water models have been supplemented with numerical simulations, which exemplary results are shown in Figure 7.

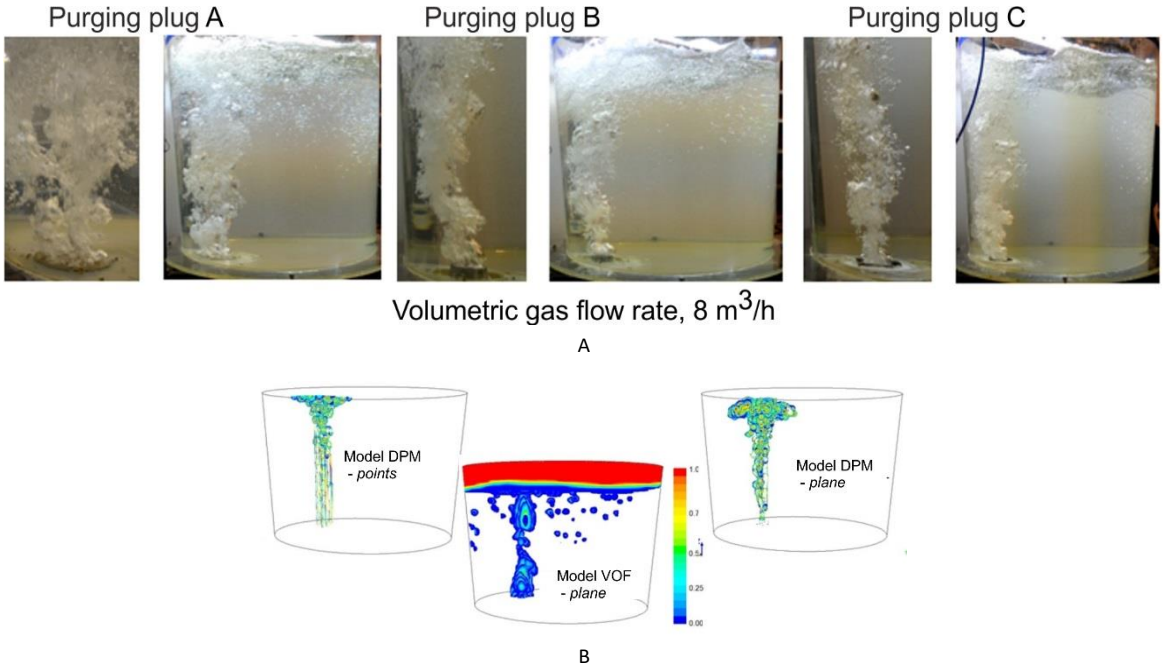

Figure 7 Gas bubble formation depending on the type of porous plug A) physical modeling, B) CFD modeling.

The research using the RH device model was aimed at determining the optimal processing parameters of the device. Exemplary test results are shown in Figure 8.

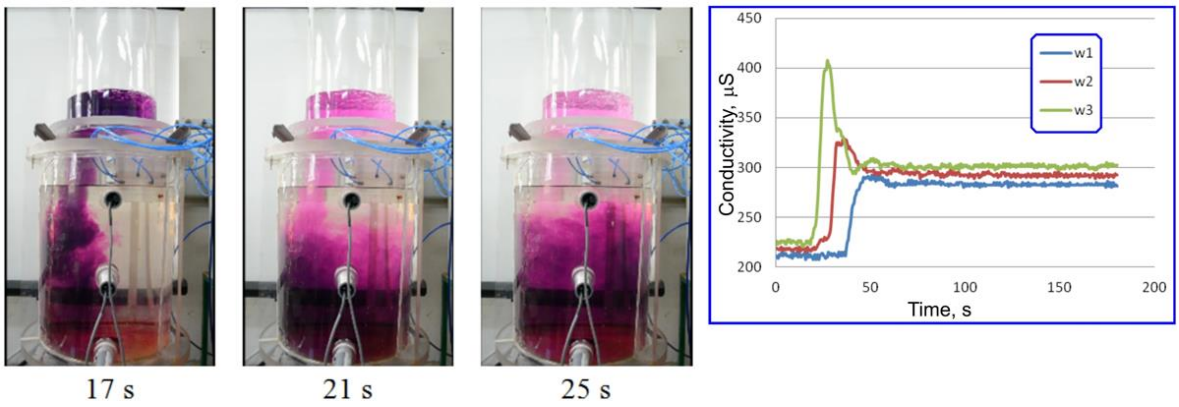

Figure 8 Exemplary visualization results of the RH process.

2.4. Modeling of the CC process

Physical modeling of hydrodynamic phenomena occurring during the continuous steel casting process has a history of several decades in the laboratory. Work in this area has already been started when this method is used in the domestic steel industry. During this period, several stands for this type of research were designed and built. Currently, the laboratory is equipped with an installation that meets the highest functional standards set for laboratory test stands designed to model phenomena occurring during the CC process. It is segmented. The main segment is a tundish or mould model that can be replaced. This means that the station's capabilities are in no way limited by specific parameters of the construction and types of industrial CC devices. A rich set of auxiliary segments, from hydraulic infrastructure to control and measuring equipment, gives the researcher wide possibilities of conducting the experiment. The scheme of the test stand is shown in Figure 9.

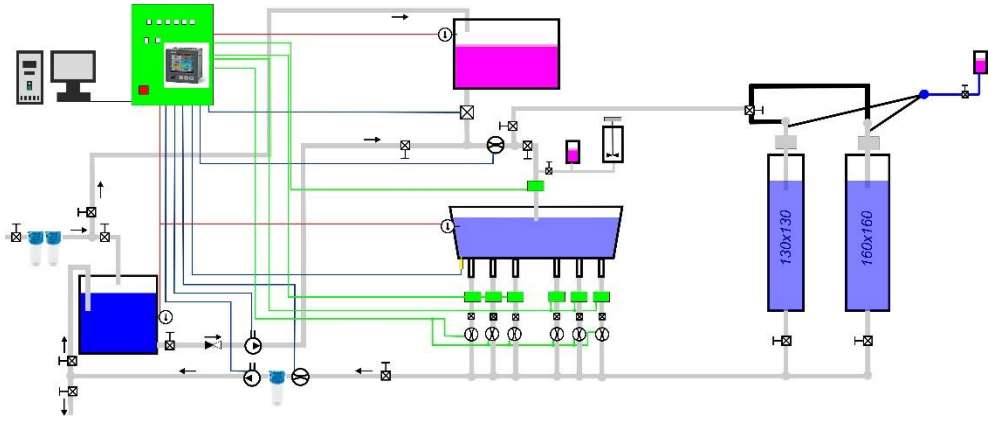

Figure 9 Scheme of the test stand for modelling continuous steel casting.

Figure 10, as an example, shows the results of model tests carried out to assess (qualitative and quantitative) the nature of the flow of liquid steel in a tundish used for various steel grades.

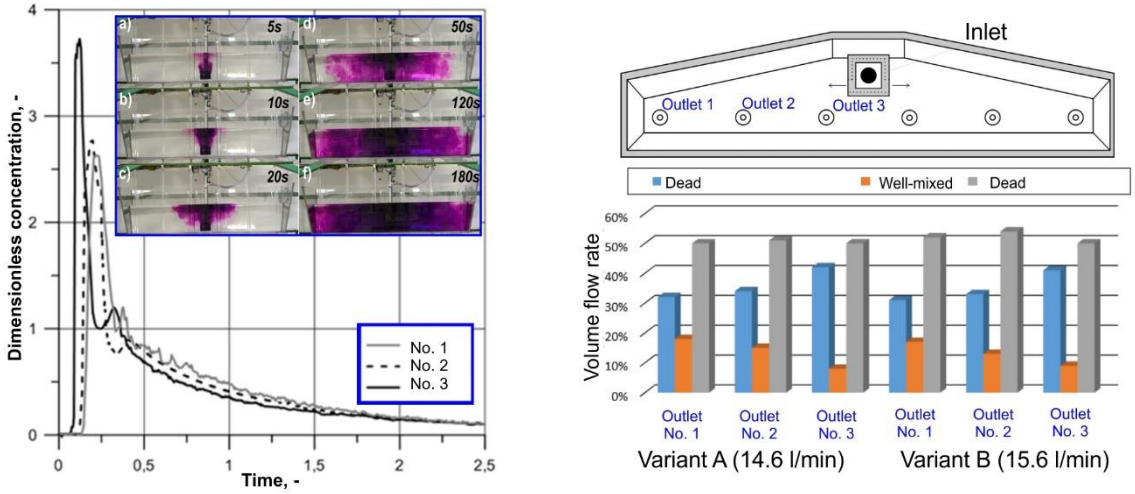

A B

Figure 10 Changes in marker concentration, B) Summary of the value of individual flow shares.

Another example of the use of the CC device model are laboratory tests using microparticles, which are a solid phase dispersed in water, which give the opportunity to determine the distribution of microparticles in a liquid depending on their size and duration of stay in the working space of the model. The research being carried out concerns the essence of the movement of these particles (their distribution in liquid), which has a significant impact on the final effect, which is the removal of non-metallic inclusions from liquid steel. These tests are possible thanks to the "laser knife" installation, which is presented in the Figure 11.

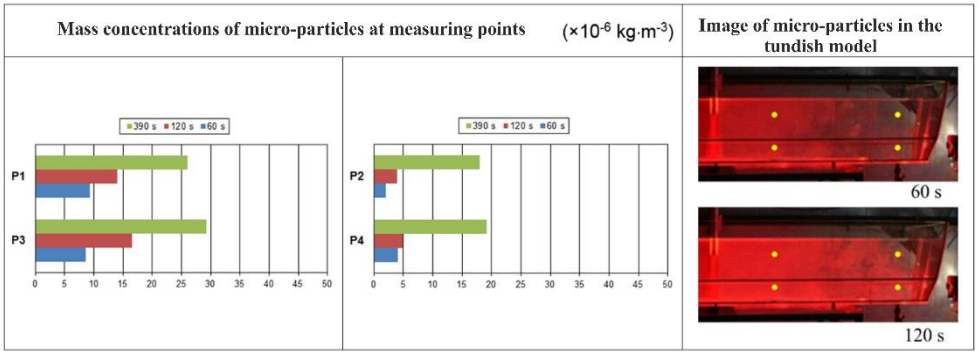

Figure 11 Determined microparticles concentrations for fractions (20 μm) at measuring points.

After installing the mould model of CC device as the main segment on the research stand, one can, among others, conduct experiments to determine the optimal position of the immersion nozzle in it for given casting speeds. Exemplary test results are shown in Figure 12.

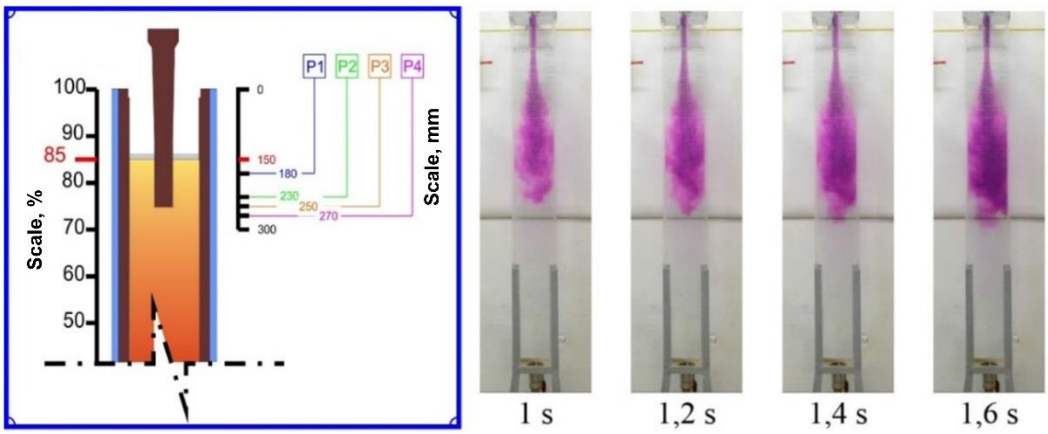

Figure 12 Exemplary results of tests on the immersion depth of the immersion nozzle in the mould.

2.5. Modeling of the aluminium refining process

The next research area regarding the scope of modeling implemented in the Laboratory of Modelling Research is the aluminum refining process. Currently, one of the most popular methods is purging liquid metal with inert gases, especially argon. In this process, refining inert gas is introduced into the liquid metal through lances, porous gas-permeable plugs and rotors. The refining process is effective when a uniform dispersion (mixing) of dispersed gas bubbles is observed in the entire volume of liquid metal. Figure 13 presents a view of the test stand and exemplary results of refining efficiency of liquid aluminum.

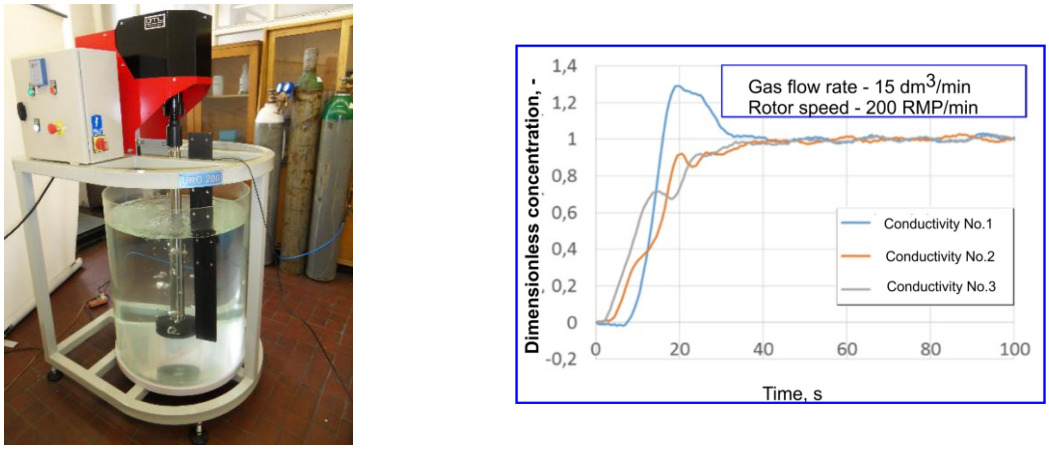

A B

Figure 13 A) View of the URO-200 reactor model, B) Exemplary RTD diagram for the URO-200 reactor.

3. Summary

In summary, it should be emphasized that, in addition to the extensive infrastructure for physical modeling research, the modeling laboratory is also equipped with a numerical modeling workshop. The software used in this studio, both commercial and proprietary, is based on the same mathematical principles and laws of fluid theory as the physical models described in the article. This allows using both modeling techniques together and solving complex metallurgical problems in the hybrid modeling system. The results obtained in this way are highly reliable and the verification process is much easier.

OPTIMIZATION OF SLAG FORMATION CONDITIONS IN THE STEELMAKING PROCESS IN ORDER TO INCREASE THEIR DEPHOSPHORIZATION AND DESULPHURIZATION CAPACITY

Marta Ślęzak[1*], Mirosław Karbowniczek[1], Michał Moskal[2*], Piotr Migas[1], Wojciech Ślęzak[1]
[1]AGH-University of Science and Technology, Faculty of Metals Engineering and Industrial Computer Science, 30 A. Mickiewicza Av., Krakow, Poland; mkarbow@agh.edu.pl, pmigas@agh.edu.pl; wslezak@agh.edu.pl
[2]COGNOR SA Branch HSJ in Stalowa Wola, Kwiatkowskiego 1, Stalowa Wola, Poland
*Correspondence: mslezak@agh.edu.pl, mmoskal@hsjsa.pl,

Abstract
Phosphorus and sulfur are undesirable elements in the steel and they should be controlled at every stage of production, especially in liquid state. One of the conditions for good dephosphorization and desulphurization of a metal bath is the formation of slag with appropriate properties in the furnace as well as during secondary metallurgy processes.

The principles of slag formation in the conditions of the steelmaking shop of COGNOR S.A. Branch HSJ in Stalowa Wola, which is equipped with an electric arc furnace, a ladle furnace and a vacuum chamber will be discusses in this paper. Based on results of chemical compositions of slags and metal baths obtained from industrial conditions, optimal processes parameters have been proposed. Parameters have been verified.

Verification studies showed that in the analyzed heats conditions for lowering the sulfur and phosphorus content in the metal were obtained, although their unstable parameters were observed. Nevertheless, despite the lack of stability of these conditions, at the end of refining both elements content are always lower than the norm permits.

Keywords: steelmaking slag formation; dephosphorization; desulphurization

1. Introduction

Scrap is processed in electric arc furnaces by its simultaneous melting and refining with gaseous oxygen, with the aid of gas burners. At the next stage, the obtained semi-product is refined in a ladle-furnace or another device for the so-called secondary steelmaking. So the process comprises two production stages. The first stage is carried out in a furnace, and its objective is to obtain a metal bath with the minimum contents of alloy elements in as fast and cost-effective manner as possible, using one slag. The second stage is usually carried out in a ladle furnace where refining operations are conducted, often using vacuum, most frequently using two slags. These operations include deoxidising, supplementing the chemical composition and heating to a temperature suitable for casting the obtained steel.

In steelmaking processes, slag already forms at the beginning of the melting in the furnace, and it exists until the end of tapping. Its chemical composition and properties and functions continuously change during the process. It is caused by oxidation of metal bath impurities, dissolution of slag-forming materials, erosion of the refractory lining and temperature changes. The following oxides are the primary components of the steelmaking slag: CaO, SiO_2, MgO, MnO, FeO, Fe_2O_3, Al_2O_3, P_2O_5. The share of individual slag components varies, and continuously changes during the production process. The steelmaking slag, regardless of the process stage and its chemical composition, always has oxidising properties and contains relatively high amounts of sulphur and phosphorus. However, the refining slag must feature a very low oxidising capability and a very good capability of assimilation of non-metallic inclusions [1]. Ladle slag properties are decisive to the quality of steels obtained, and the process of its formation determines the process economics.

2. Dephosphorization and desulphurization of steel

The charge melting process is accompanied by oxidation of the phosphorus contained in the charge, as per the reaction:

$$2\,[P]+5\,[O]+3\,\left(O^{2-}\right)=2\,(PO_4^{3-}) \quad (1)$$

The forming anion (PO_4^{3-}) has a strong affinity to the calcium cation Ca^{2+}, occurring in the forming slag. Then, calcium phosphates form (stable at high temperatures) in accordance with one of the molecular reactions:

$$2\,[P]+5\,(FeO)+3\,(CaO)=(3\,CaO\cdot P_2O_5)+5\,[Fe] \quad (2)$$

$$2\,[P]+5\,(FeO)+4\,(CaO)=(4\,CaO\cdot P_2O_5)+5\,[Fe] \quad (3)$$

It is assumed that reaction (2) occurs when cations Ca^{2+} (slag basicity under 2.5) are less accessible, while reaction (3) when they are more accessible (slag basicity above 2.5). At the initial melting stage, it is rather reaction (3) that occurs. The dephosphorising of the melt occurring at this time can be characterised by a coefficient of phosphorus distribution between metal and slag. To define this coefficient a simplified reaction of phosphorus oxidation is assumed:

$$2\,[P]+5\,[O]=(P_2O_5) \quad (4)$$

Then, the coefficient of phosphorus distribution is the quotient of the amount of the phosphorus contained in the slag, bounded in the pentoxide, and the phosphorus contained in the metal:

$$L_P=\frac{(P_2O_5)}{[P]} \quad (5)$$

In the industrial conditions, a parameter being the so-called dephosphorising degree η_p [%] is often used, which is defined as follows:

$$\eta_P=\frac{[P]_i-[P]_f}{[P]_i}\,100\% \quad (6)$$

where symbols $[P]_i$ and $[P]_f$ mean the initial and the final content of phosphorus in the melt.

The mechanism of sulphur oxidation in the steelmaking process is different than of other metal bath constituents. It is a reaction of anion exchange at the metal and slag interface in accordance with the following:

$$[S] + (O^{2-}) = (S^{2-}) + [O] \quad (7)$$

Sulphur does not form any oxide or a complex anion in the slag. To chemically bond the forming sulphur anions, slag should contain “free cations” of the relevant elements. The most advantageous is the calcium cation Ca^{2+}, hence lime is used in adequate amounts to form slag in the steelmaking process. Then the reaction is presented as follows:

$$[S] + (CaO) = (CaS) + [O] \quad (8)$$

In the industrial practice, the course of desulphurisation is often assessed using the value of sulphur distribution coefficient L_S [-], where (S) is a sulphur content in a slag, and [S] is an amount of sulphur in a liquid metal:

$$L_S=\frac{(S)}{[S]} \quad (9)$$

and the so-called desulphurisation degree η_S, [%] defined as follows, where $[S_i]$ is an initial value of sulphur, and $[S_f]$ is a final value of sulphur in metal bath:

$$\eta_S=\frac{[S]_i-[S]_f}{[S]_i}\,100\% \quad (10)$$

3. Analysis of slag forming conditions in the steelmaking process

Slag forming conditions in the steelmaking process were analysed in the operating conditions of the COGNOR S.A. Branch HSJ in Stalowa Wola steelmaking shop operating along the process line: EAF, ladle furnace, vacuum chamber and continuous steel casting. Steel grades with various carbon contents were considered: 15B34,

16MnCr5, 18CrNiMo7-6, 27MnCrNiB6, 30MnVS6, 33MnCrMoB5, 41CrS4, 42CrMo4. The technological process of melting in furnace is the same for all tested steel grades under the analysed conditions of steelmaking shop. But the steel refining technological process in the ladle was varied depending on carbon content in metal bath. Chemical compositions of slags taken from the furnace after charge melting and before tapping, and refining slags taken at the beginning and the end of the ladle process, and after the vacuum treatment, were included in the analysis. But chemical composition for only chosen, most important and most relevant components of slags, only for ladle refining stage are presented in the paper.

The first and very important activity of the refining process in the ladle is the rapid formation of slag covering the metal bath. This process begins before and during the tapping of meta bath from the furnace. Before setting the ladle, deoxidizing and slag forming materials are thrown into the ladle. The tapping with cutting off furnace slag is important. Deoxidizing materials are used to remove oxygen dissolved in a metal bath. Ferro-alloys: FeSi, FeSiMn or aluminum are used for this purpose. Types and amounts are selected according to the carbon content and oxygen level in metal bath before tapping.

Recommended optimal chemical composition of ladle slag at the beginning of refining is: 45÷50% CaO, 8÷12% SiO_2, 20÷30% Al_2O_3, at basicity 3÷4. The FeO content in the slag, which is an indicator of its oxidation potential should be monitored throughout the refining process in ladle. Expected level of FeO content is less 1%, and optimally the sum of FeO + MnO content is less 1%. For this purpose, throughout the entire refining process, depending on the needs, should be apply slag deoxidation by adding ground CaC_2, carbon or FeSi (approx. 10-15 kg/heat) or granulated aluminum. In order to create slag with proper basicity and fluidity, metallurgical lime and slag liquefier (synthetic slag, bauxite or other) are added.

In order to protect the refractory lining of ladle, the proper MgO (5-8%) content should be controled through the possible use of an MgO carrier. The proportion of metallurgical lime should not be less than 8 kg/t of steel. During the process, the bath is constantly mixed by argon, which increases the contact area between the slag and metal, which results in increased reaction kinesics and reducing the oxygen content in steel. During the refining phase, desulphurization processes, bath deoxidation and removal of non-metallic inclusions occur.

The desulphurization efficiency during refining process in ladle depends on:

- FeO content in slag - if less oxygen required the less FeO must be,
- slag basicity - it is assumed that the optimal CaO/SiO_2 value is 4÷5,
- the amount of slag - if the greater desulphurisation required, the greater amount of slag must be.

Recommended optimal chemical composition of ladle slag at the end of refining is: 45÷55% CaO, 10÷12% SiO_2, 25÷35% Al_2O_3, at basicity 4÷5.

The following slag components were considered as relevant for the process of refining in ladle: CaO, SiO_2, Al_2O_3 and FeO. The variability of contents of individual components of the ladle slags is presented graphically for a subsequent heats. A line showing the carbon content of 0.3% is marked on the graphs. The level of 0.3% carbon is the criterion determining the level of some technological indicators of the metal bath, which are the quality determinants of produced steel. At the same time, some technological elements of refining processes were different for steel below and above 0.3% C. Results of the analysis are presented in Fig. 1 - 6.

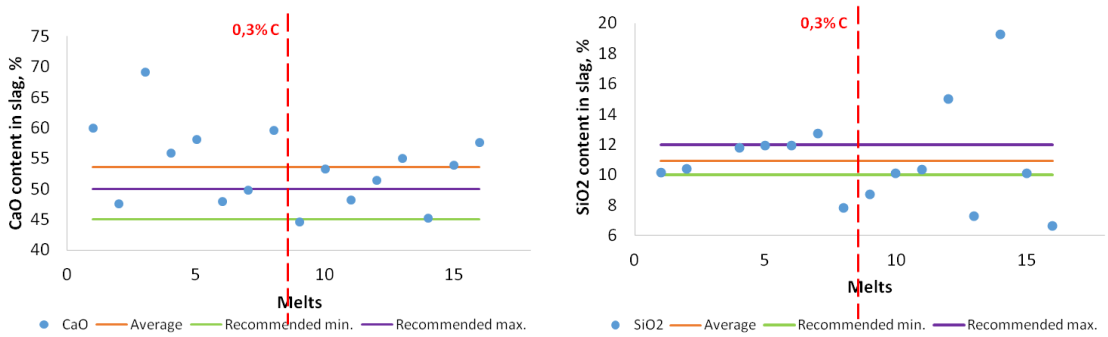

Figure 1 Contents of CaO and SiO_2 in the initial refining slag in the ladle furnace.

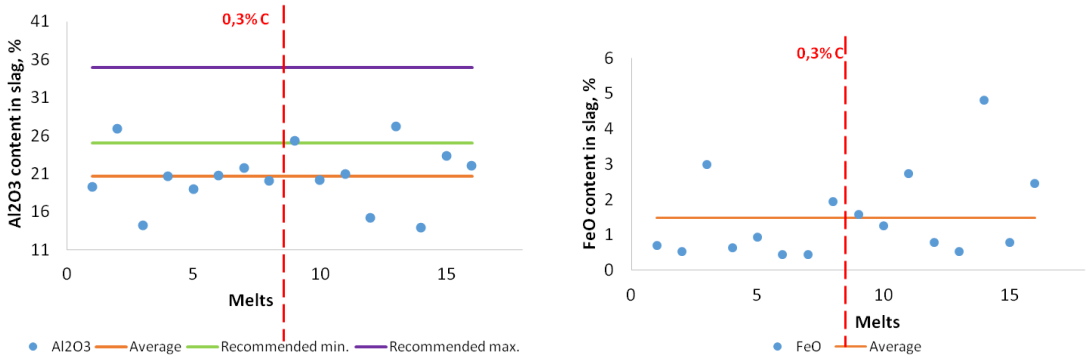

Figure 2 Contents of Al_2O_3 and FeO in the initial refining slag in the ladle furnace.

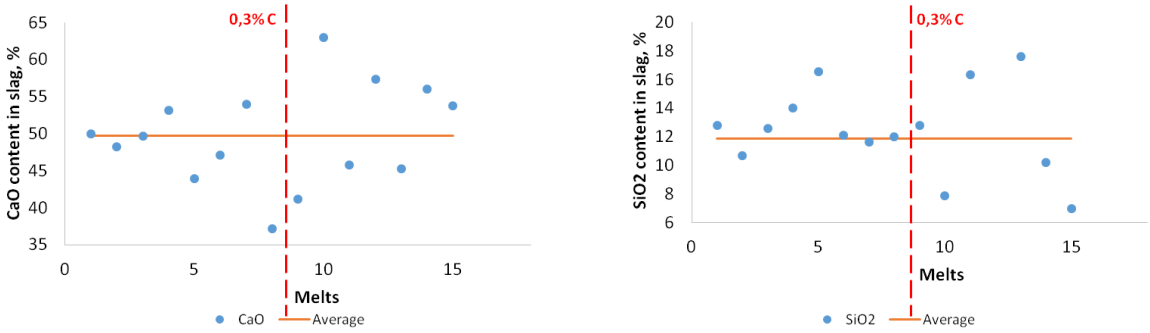

Figure 3 Contents of CaO and SiO_2 in the final refining slag in the ladle furnace.

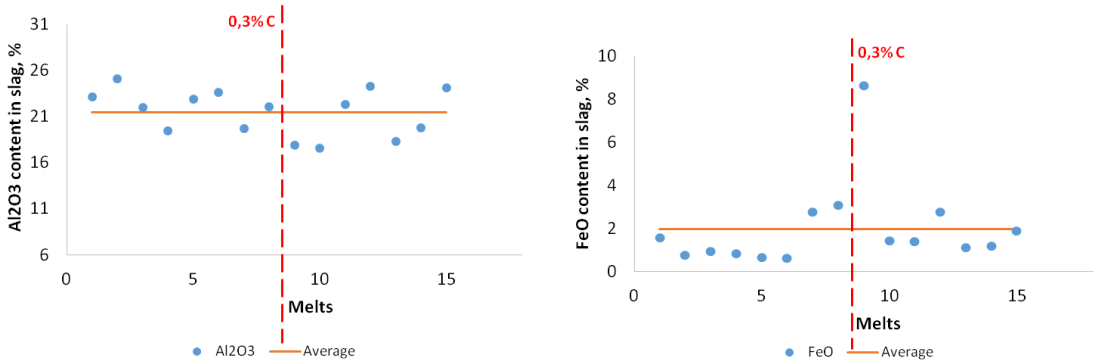

Figure 4 Contents of Al_2O_3 and FeO in the final refining slag in the ladle furnace.

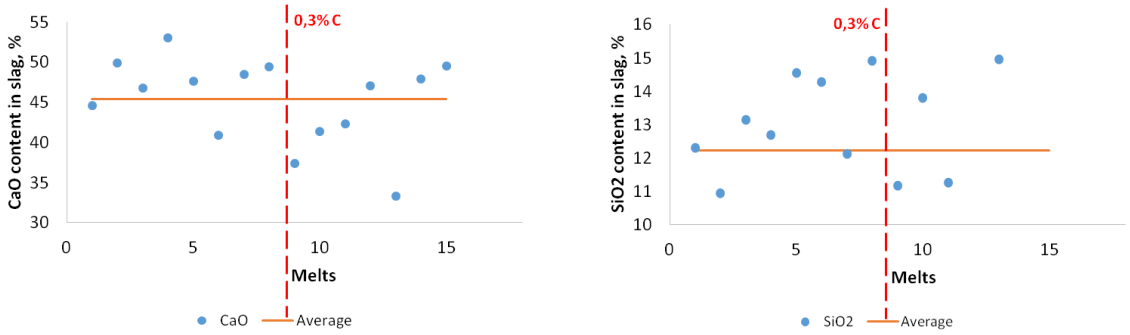

Figure 5 Contents of CaO and SiO_2 in the refining slag after VD.

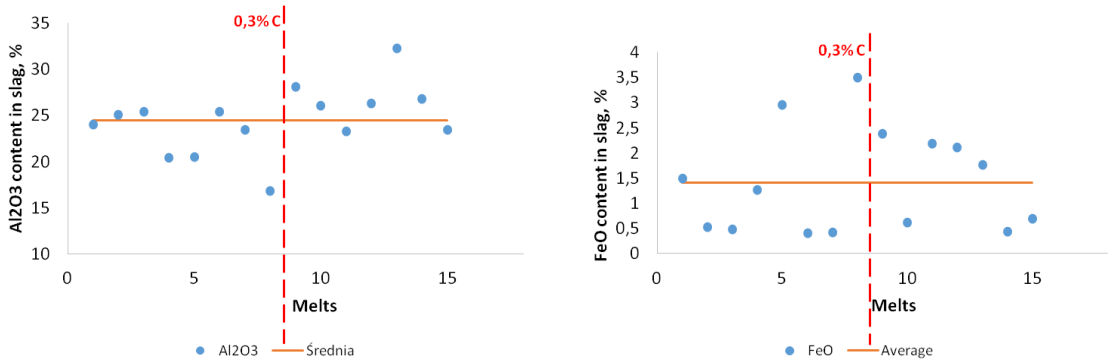

Figure 6 Contents of Al_2O_3 and FeO in the final refining slag after VD.

In the ladle process the refining slag, which substantially accounts for the quality of the steel manufactured, is not typical, it does not meet the classic standards for this sort of slags. However, it fulfils its role, by guaranteeing that the obtained steel meets the requirements assumed by the standards.

With reference to the recommended values, the CaO content in the initial refining slag in the ladle furnace is generally too high, the SiO_2 content is adequate, and the Al_2O_3 content is generally too low, while the FeO content is rather adequate, in exceptional cases too high. With reference to the recommended values, the CaO content in the final refining slag in the ladle furnace is generally too high, the SiO_2 content is adequate, the Al_2O_3 content is generally adequate, though sometimes too low, while the FeO content is rather adequate, in exceptional cases too high. With reference to the recommended values, the CaO, SiO_2 and Al_2O_3 contents in the refining slag after the vacuum process are generally adequate, while the FeO content is rather adequate, in exceptional cases too high.

About whether exist the optimal conditions of formation, both furnace or ladle slag is evidenced by its chemical composition. The obtained desired chemical composition of slags is to guarantee the production of appropriate steel quality.

The foregoing results should enable the ultra-clean steel quality parameters to be achieved, assumed as the objective to be accomplished in this presented research.

It was assumed that this objective will be satisfied with following requirements:

- the total oxygen content: max 12ppm for steels containing C ≤ 0.30%; max 10 ppm for steels containing C > 0,30%;
- the phosphorous content – max 0.015 %;
- the maximum size of D type inclusions according to ASTM E45-13 max 0.5/0.5;
- the complete elimination of the slag entrapment risk.

These requirements were met in all carried out heats. The required level of total oxygen, phosphorus level below the allowable value as well as size of D type inclusions according to ASTM E45-13 were obtained.

Dephosphorisation and desulphurisation ratio graphs calculated with reference to the difference in the phosphorus and sulphur contents, accordingly, in the metal bath in the furnace, and after the vacuum treatment, are presented in fig. 7

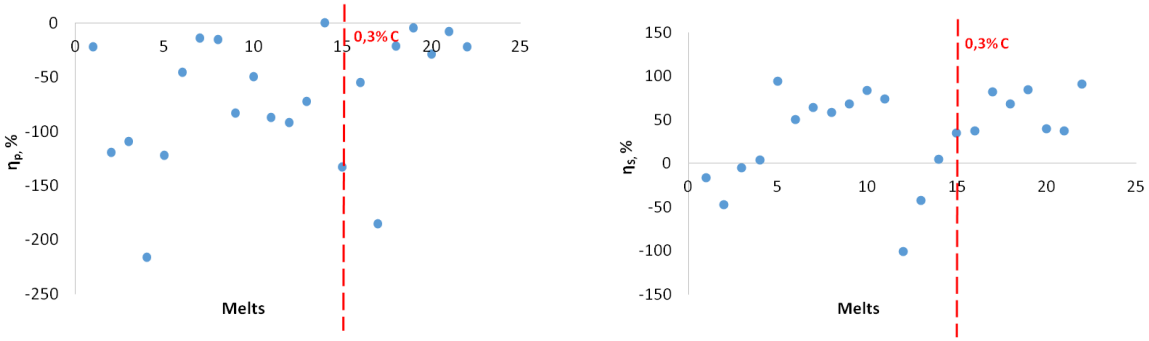

Figure 7 Dephosphorisation and desulphurisation ratio.

During steel refining in the ladle furnace a slight increase in the phosphorus content in the melt is observed. It is caused by a reverse reduction from the slag; however, a very low phosphorus level in the melt after tapping from the furnace contributes to obtaining substantially (on average more than twice) lower contents of phosphorus at the end of the process than required by the standard in finished steel. Therefore an engineering procedure like this should be considered correct.

In the heats analysed, conditions for reducing the phosphorus and sulphur content in the metal bath were obtained during ladle furnace refining, although instability of their parameters was observed. Thus, although these conditions are unstable, at the end of refining always the phosphorus and sulphur contents are obtained below the limits acceptable by the standard.

4. Summary

On the basis of the conducted analysis of the slag forming process in the context of conditions of dephosphorising and desulphurising of the metal bath in the steelmaking process, we can say that the steel produced in the conditions of the steelmaking shop of Cognor S.A. HSJ Branch in Stalowa Wola complies with standards for the content of primary constituents; namely carbon, manganese and silicon, and meets the requirements concerning other constituents. The phosphorus and sulphur contents in steel are low – as per the standard, which indicates that the refining process was correct.

Generally, the slag forming technique in the steelmaking process in the conditions of the steelmaking shop of COGNOR S.A. Branch HSJ in Stalowa Wola is correct. It ensures that the finished product is obtained at an adequate quality level. The only recommendation is to stabilize the engineering working conditions, potentially to implement slight modifications to the process, to increase confidence and consistency of manufacturing good quality steel.

Acknowledgement

The research was conducted with the financial support as part of the Project: No POIR.01.02.00-00-0207/17, title: „Innovative manufacturing process for a very high metallurgical purity steel for the most critical applications in the automotive industry“.

References

[1] Karbowniczek, M.; Wcislo, Z. Technologia wytapiania stali w elektrycznym piecu łukowym, *Hutnik-Wiadomości Hutnicze*, **1997**, 7, 284-287

[2] Karbowniczek, M. Stalowniczy piec lukowy, Wydawnictwo AGH, **2015**

[3] Dziarmagowski, M.; Karbowniczek, M. Optimization of the slag formation conditions in the ladle steel refining process, *Acta Metall. Slovaca*, **1999**, 5(3), 26-30

[4] Toulouevski, Y.; Zinurov, I. Innovation in electric arc furnaces, Springer, **2010**

APPROACHES TO COMPUTATIONAL MESH GENERATION AND MONITORING OF STEEL FLOW IN TUNDISH DURING NUMERICAL MODELLING

Markéta Tkadlečková[1*], Karel Michalek[1], Tomáš Huczala[2], Josef Walek[1], Jana Sviželová[1], Michaela Strouhalová[1], Dana Horáková[1], Monika Krejzková[1]

[1]Faculty of Materials Science and Technology, VŠB – Technical University of Ostrava, Ostrava, Czech Republic; karel.michalek@vsb.cz; josef.walek@vsb.cz; jana.svizelova@vsb.cz; michaela.strouhalova@vsb.cz; dana.horakova@vsb.cz; monika.krejzkova@vsb.cz

[2]TŘINECKÉ ŽELEZÁRNY a.s., Technology and Research; Průmyslová 1000, Staré Město, 739 61Třinec, Czech Republic; Tomas.Huczala@trz.cz

*Correspondence: marketa.tkadleckova@vsb.cz ; Phone: +420-59-732-4464

Abstract

Continuous casting technology is currently the primary method used for the production of steel billets, blooms or slabs. Flow in the tundish region during the continuous casting of steel can influence many important phenomena, especially the removal of inclusions or the range of transition zone. Flow in the tundish can be simulated using numerical modelling. The numerical modelling offers fast answer to many questions. The results of numerical modelling depend, however, on the accuracy of model setting. The stability of calculation convergence is influenced by the quality of the model computational mesh. Especially in the case of verification of difficult internal geometry arrangement on steel flow in tundish, the method of computational mesh generation and the form of results monitoring must be the same. Therefore, we validated the approaches of computational mesh generation and the types of results monitoring. We compared the numerical results using the tetrahedral and hexahedral mesh elements. We used the Multizone and Hexa dominant meshing. The Assembly method was considered as the most appropriate. The point and surface monitors enabled us to control the stability of calculation.

Keywords: steel, continuous casting; tundish; computational fluid dynamics (CFD), computational mesh

1. Introduction

At present, the world production of continuously cast steel makes 96 %. In the Czech Republic approx. 92 % of steel is cast by continuous casting [1]. During continuous casting of steel, the ladle with steel melt is placed on the rotating casting stand of a casting machine. From the ladle, the steel is cast through the shrouding tube into the tundish. Then the steel is taken through the submerged entry nozzle to the oscillating moulds (in the primary cooling zone), where the "controlled" solidification of steel is ensured. Under moulds, there is a system of guiding and supportive rollers (the secondary cooling zone) including refrigerating nozzles, which ensure the drawing, transforming and cooling of the casting strand of steel. The layout of ladles, the tundish and mould of five-strand machine for the continuous casting of steel is illustrated in Figure 1 [2].

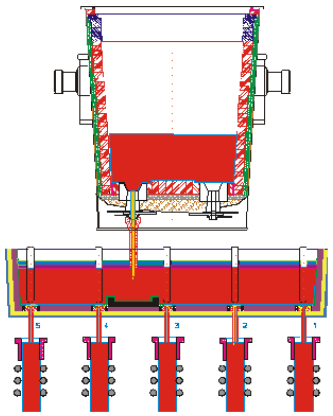

Figure1 Technology node of a machine for continuous casting of steel [2].

Tundish is one of the most important technology nodes of a continuous casting machine. It primarily serves as the melt reservoir in the sequential casting during the exchange of ladles and ensures the melt distribution into individual casting strands. Tundish also regulates the steel mass flow into moulds, reduces ferrostatic pressure of the liquid steel and homogenizes temperature of the melt. Flow in the tundish region during the continuous casting of steel can influence many important phenomena, especially separation of the non-metallic inclusions or the range of transition zone (intermixing zone) in cast strand [3, 4, 5, 6]. Therefore, with increasing demands on the final quality of continuously cast steel billets, the tundish plays a key role as the last reactor, in which it is possible to influence the final chemical composition of the steel before solidification.

The time available for all of the mentioned operations is very short, and therefore, it is necessary to have a good understanding of fluid flow behaviour in the tundish. One of the ways how to monitor and optimize the processing parameters of the steel flow in tundish is the application of numerical modelling where numerical methods are used for solving mathematical equations of the mass transfer, movement and energy. The advantage of the numerical modelling under metallurgical conditions of the steel production is the possibility of relatively simple change of the boundary conditions and verification of the influence of these changes of the process parameters on the final character of technology [7].

Nevertheless, the results of numerical modelling depend on the accuracy of the setting of the model. In published papers, the mathematical formulations of solving equations are obviously discussed [8-16]. In the case of generation of computational mesh, only the information about the number and the shape of mesh elements are given. But the stability of calculation convergence is influenced by the quality and by the independence of the model computational mesh. In this case, the [17] presented only short information about the study of grid independence. But if we want to analyse the steel flow phenomena comprehensively, the first precondition of using numerical simulations is high-quality, independent and fast preparation of the computational mesh. Therefore, in this paper, we validated the approaches of mesh generation in correlation with stability of calculation and expected results.

2. Expected results

The residence time distribution (RTD) curves are widely used for the optimization of steel flow depending on internal configuration of tundish with impact pads, dams, weirs and baffles. Also, the RTD curves can be used for analysis of extent of transition zone during the sequence casting [18]. Then, the concentration change at the time for each casting strand at the outlets of a tundish for the relevant variants can be processed into the transitional dimensionless characteristics (see Figure 2a) of the dependence of the dimensionless concentration of time, and the changes of the dimensionless concentration of the length of blanks, on the basis of which it is possible to predict the length of a mixed area (see Figure 2b). The typical required results of numerical modelling comprise the velocity vectors (Figure 2c), temperature (Figure 2d) and concentration fields, which offers occasion of visual control of flow. The option of animation of steel flow is also very user-friendly.

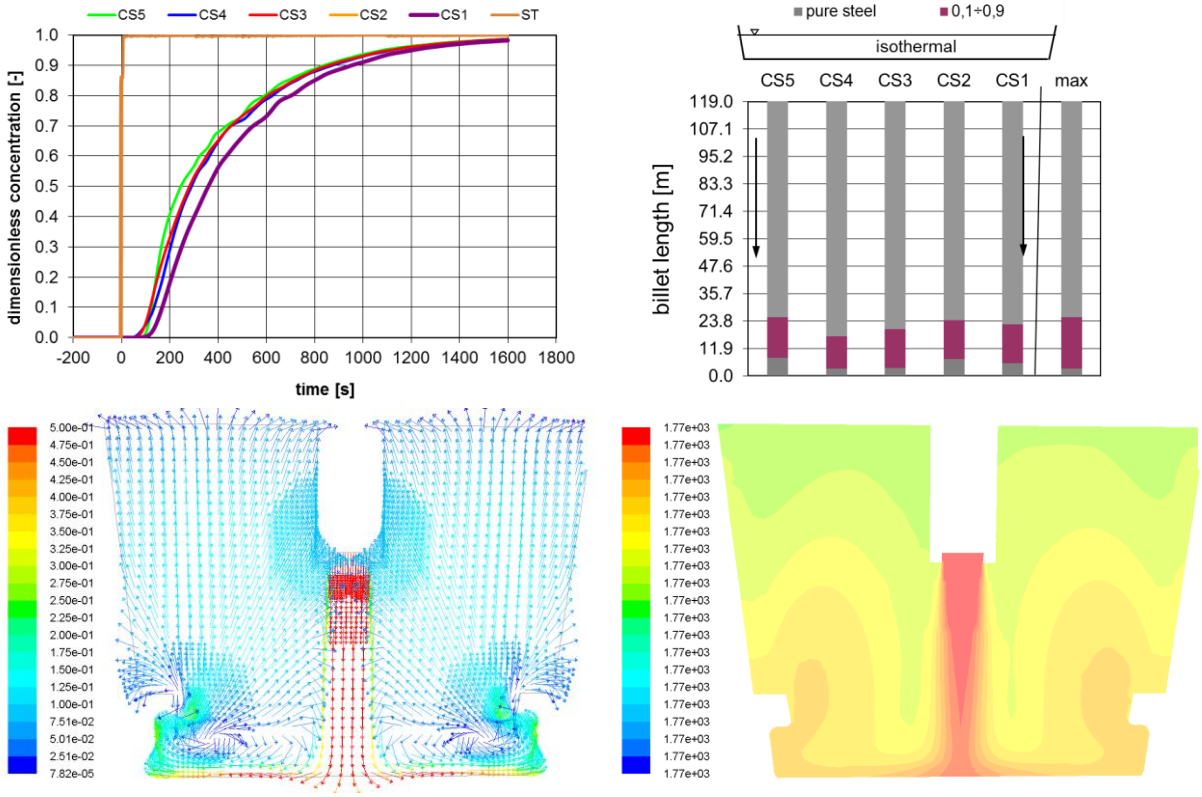

Figure 2 Examples of numerical modelling results **a)** transition characteristics of changes in the concentration for individual casting strands of a tundish **b)** Range and the location of the mixed area **c)** velocity vectors ($m.s^{-1}$) and **d)** temperature field in a cut section of tundish (in K).

If we try to control the flotation and separation of non-metallic inclusion, the results of numerical modelling (see **Figure 3**) are proceed to distribution curves. From the results of non-metallic inclusions it is possible to predict the percentage amount of inclusions captured by slag and amount of inclusions taken down into a casting strand.

Fate	Number	Elapsed Time (s)				Injection, Index	
		Min	Max	Avg	Std Dev	Min	Max
Escaped - Zone 5	**1511**	5.977e+00	3.532e+03	2.321e+02	3.420e+02	inclusion 1559	inclusion 1693
Escaped - Zone 7	**94**	1.474e+02	1.833e+03	4.153e+02	3.256e+02	inclusion 158	inclusion 55
Escaped - Zone 8	**90**	1.035e+02	2.492e+03	4.910e+02	3.886e+02	inclusion 1853	inclusion 903
Escaped - Zone 9	**170**	7.978e+01	2.127e+03	4.639e+02	3.291e+02	inclusion 871	inclusion 468
Escaped - Zone 10	**152**	9.688e+01	2.572e+03	4.295e+02	3.837e+02	inclusion 1467	inclusion 874
Escaped - Zone 11	**103**	7.199e+01	3.299e+03	3.806e+02	4.343e+02	inclusion 1482	inclusion 146

Figure 3 The calculated results from numerical modelling of inclusion separation depending on steel flow phenomena in the tundish, where the zones introduce the zone, from which the inclusions escaped the steel. Zone 5 = surface melt-slag, zone 7 to 11 = individual casting strands of five strands tundish.

3. Approaches to computational mesh generation

From the previous chapter it can be seen, that during the optimization of steel flow in the tundish, many types of results can be observed. And if we want to react to the technical problems connected with the final quality of steel billets influenced by the tundish metallurgy very quickly, we need the optimal, quickly prepared and universal method of numerical approach.

For this reason, we validated the approaches of computational mesh generation for the case of optimization of internal configuration of tundish construction, which affects the steel flow, or separation of non-metallic inclusions. Because most authors used the package CFD ANSYS Workbench with software ANSYS Fluent, we also realized our analysis using this software. For generation of mesh, the ANSYS Meshing was applied.

3.1 Purpose of Computational Mesh

The differential equations of flow and heat-transfer or substance redistribution, etc. are solved using the numerical methods. The numerical solution of equations describing the flow and solidification of liquids has developed over time. The oldest classical method is the finite differences method, for partial differential equations the finite volumes method can be used, or the finite element method.

The principle of differential equation solutions lies in the geometry coverage of the solved areas by computational mesh (dividing the whole area into partial successive 2D cells/elements in a two-dimensional area, or 3D cells/elements in a three-dimensional area) and the search of discrete solutions in these sufficiently small sub-areas of the basic geometry using the so-called differential (algebraic) equations. The difference between the differential and the difference equation is defined as discretization error e.

So, the computational mesh is necessary for the discretization of equations. On the other hand, we need the mesh to be as coarse as possible, but at the same time, it must be able to capture the potential of the task and all variables. Also, it is good to take into account the mesh requirements to the computing performance (CPU and memory requirements).

3.2 Geometry preparation before meshing

Before dealing with the studied system using numerical modelling and meshing, it is necessary to define the modelled area. When defining the geometry we shall take into account the desired objectives (What do I really want to find?), the shape of studied system (symmetrical or asymmetrical area, details), the complexity of a mathematical model (which partial differential equations will be addressed), set-up options in the solving software, the performance of a computational system.

The advantage of flow modelling in flow reactors using SW ANSYS Fluent is the ability to limit the geometry only to the internal study system volume. This means that there is no need to model the geometry of flow reactor walls and the conditions on the wall (heat transfer, roughness, the entry of blown internal gas, etc.) are defined by values or features. During modelling of the tundish geometry, it is good to neglect small closed edges and to check the sharp edges or gaps in the modelled domain, and to verify that all edges are perfectly

connected. Typical examples are the area of inlet, impact pad or nozzles (see Figure 4 – green lines). These parts of geometry may generate distorted mesh elements and decrease the mesh quality.

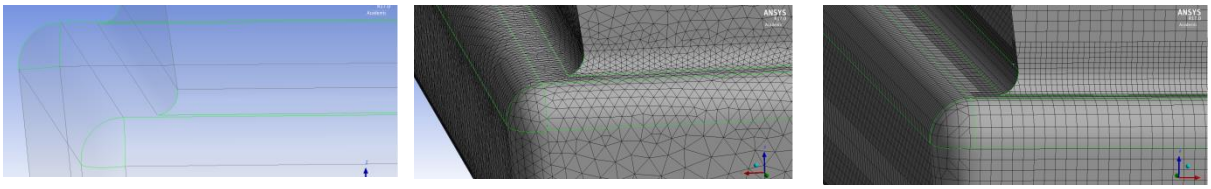

Figure 4 Example of edges in the impact pad area of tundish which influences the final quality of computational mesh.

3.3 Mesh Quality, Independence of Mesh, Convergence Stability

Bad quality of a computational mesh can cause convergence difficulties, bad physics description and diffuse solution. At first, the mesh quality can be controlled by mesh metric tools, such as Element quality, Aspect Ratio, Jabobean Ration, Warping Factor, Parallel Deviation, Maximum Corner Angle, Skewness and Orthogonal quality. Especially in the case of CFD simulation, it is good to control the skewness and orthogonal quality when the values are between 0 to 1. The value of metrics with evaluation of quality mesh is defined in Table 1 [19].

Table 1 Metrics spectrum for skewness and orthogonal quality of computational mesh [19].

Metric	Unacceptable	Bad	Acceptable	Good	Very Good	Excellent
Skewness	0.98-1.00	0.95-0.97	0.80-0.94	0.50-0.80	0.25-0.50	0-0.25
Orthogonality	0-0.001	0.001-0.14	0.15-0.20	0.20-0.69	0.70-0.95	0.95-1.00

After the tundish meshing, it is necessary to realize the primary simulations with control not only of the character of convergence solution by residuals but it is also necessary to monitor the velocity and temperature at the point or through the surface at the inlet and outlet area to achieve constant values of variables.

3.4 Discussion of Mesh Generation Methods

To prepare the computational mesh for asymmetric five strands tundish with impact pad and stopper rods, in our case during the mesh tuning we compared the solution using the mesh with tetrahedral and hexahedral elements. In all verified cases, at the inlet and outlets, we monitored the velocity and temperatures using the velocity surface monitor and temperature point monitor. For generation of mesh, we used at first the hexahedral method with Patch Conforming Algorithm of mesh generation, and then with Patch Independent Algorithm and Multizone Method.

The direct utilization of Hexa dominant method was not possible. To use the Multizone method, there was necessary to slice the geometry and to define in ANSYS Fluent the interfaces between the individual slice surfaces of geometry. This method was very time consuming and very difficult. Therefore, for the next validation of approaches, it was evaluated as not suitable.

In the case of Patch conforming Algorithm, the size of elements was not sufficiently small, which was manifested even during the unstable convergence of the calculation and also by the large distortion of the calculated velocity at the nozzle, or in the velocity differences between nozzles (Figure 5). Therefore, the Patch Independent method was used, which neglected some small edges. At the same time, to achieve good quality of the mesh, it was necessary to reduce the size of the elements, which led to an increase in the number of elements up to 5 million and an increase in computing time.

In the end, the Assembly Method with Cut Cell approach, which could be used only for CFD calculation, was tested. The size of 5.3 mm was achieved as an independent size of the element and at the same time a high-quality mesh was obtained. Just couple of cells achieved substandard metrics, such as skewness and orthogonality. At the same time, by using this method we achieved a very fast stabilization of the expected velocity (depending on the flow rate on the inlet) at the outputs that were equal and constant through of all outlets. The approach chosen was satisfactory even when the tundish geometry was changed. The statistics of individual meshes are given in Table 2.

Table 2 The statistics of used meshes during setting validation of the numerical model.

Method	Type of Elements	Nr. Of Elements	Element Size mm	CPU (6 processors) FL+TH Eq	Skewness Min./max.	Orthogonality Min. /Max.
Patch Conforming	Tetra	1,107,862	3.4	6 hours	0.22	0.85
Patch Independent	Tetra	5,739,912	1.7	10 hours	0.0006/0.61	0.43/0.99
Assembly method	Hexa	761,085	5.3	2 hours	$1.3 \cdot 10^{-10}$/0.55	0.55/1.00

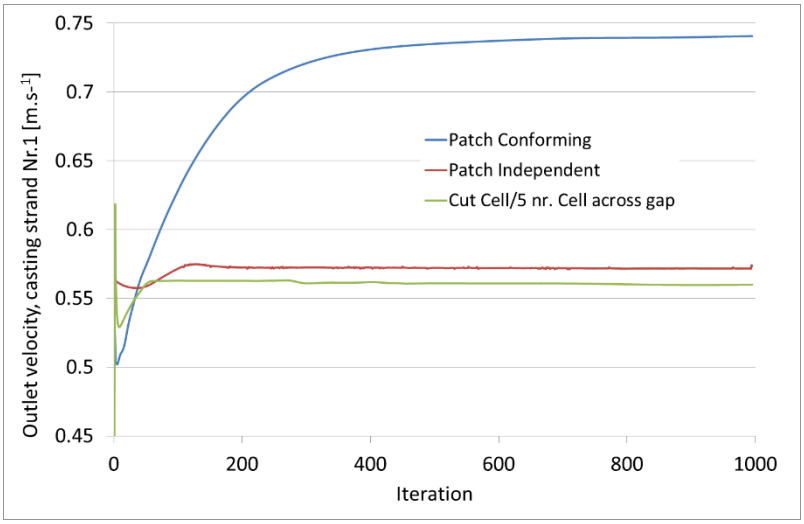

Figure 5 Graphical comparison of the evolution of calculation of steel flow speed through selected nozzle of 5-flow asymmetric tundish.

4. Conclusions

The paper deals with the control of a computational mesh designed for numerical modelling of steel flow in a five-strand asymmetric tundish of a continuous casting machine. The following findings were achieved from the research and development of the authors:

- Tundish is an important technological node of the machine for continuous casting of steel
- Apart from its function as a reservoir, tundish today also fulfils a refining function. Depending on the nature of steel flow in the tundish, it is possible to influence the separation of non-metallic inclusions or minimize the extent of the transition zone in the continuously cast billet during sequential casting.
- In order to ensure the refining capacity of the tundish, it is necessary to verify the character of the steel flow in the tundish.
- Numerical modelling is now widely used to verify the tundish steel flow.
- The prerequisite for use of numerical modelling is achieving stability of the calculation and convergence of the task, which is largely dependent on the quality of the computational mesh.
- Numerous approaches exist for preparation of the computational mesh. To make numerical modelling efficient, with as little consumption of time as possible, it is important to find a suitable way of forming a mesh.
- The authors of the paper verified several methods of creation of computational mesh - Patch Conforming, Patch Independent, MultiZone and Assembly Method. The Assembly Method with the prevalence of Hexa elements seemed to be the most suitable, which proved competent thanks to its speed, simplicity, accuracy, especially in the case of modification and geometry of the modelled area. On the other hand, it is necessary to take into account the assumed nature of the steel flow when using this technique. The use of hexaedric meshes in CFD analyses is useful when simulating the character of the steel flow. If the flow is directed perpendicularly to the cell wall, the mesh is characterized by low numerical diffusion. If the flow is not perpendicular to the cell walls, the numerical diffusion increases. Moreover, in the case of more complex geometries, the formation of a hexaedric mesh that would perfectly cover its shape is complicated.

Acknowledgements

The article was created thanks to the project No. CZ.02.1.01/0.0/0.0/17_049/0008399 from the EU and CR financial funds provided by the Operational Programme Research, Development and Education, Call 02_17_049 Long-Term Intersectoral Cooperation for ITI, Managing Authority: Czech Republic - Ministry of Education, Youth and Sports. Next, due to the financial support of Student Grant Competition No. SP2019/148 and SP2019/43. This work was supported also by The Ministry of Education, Youth and Sports from the Large Infrastructures for Research, Experimental Development and Innovations project „IT4Innovations National Supercomputing Center – LM2015070".

References

[1] Worldsteel Association. Steel Statistical Yearbook 2018. Available online: https://www.worldsteel.org/en/dam/jcr:e5a8eda5-4b46-4892-856b-00908b5ab492/SSY_2018.pdf (accessed on 9 September 2019).

[2] Michalek, K. Využití fyzikálního a numerického modelování pro optimalizaci metalurgických procesů. 1.vyd. Ostrava, VŠB-Technická univerzita Ostrava, **2001**. 34. ISBN 80-7078-861-5. (In Czech)

[3] Bul'ko, B., Molnar, M., Demeter, P., Baricova, D., Pribulova, A.;Futas, P. Study of the Influence of Intermix Conditions on Steel Cleanliness. *METALS,* **2018**, 8, 852, 1-9. DOI: 10.3390/met8100852

[4] Cwudziński, A. Numerical simulation of liquid steel flow and behaviour of non-metallic inclusions in one-strand slab tundish with subflux turbulence controller and gas permeable barrier. *Ironmaking & Steelmaking*, **2010**, 37 (3), 169-180, DOI: 10.1179/030192309X12549935902383.

[5] Cwudziński, A. Numerical, Physical, and Industrial Studies of Liquid Steel Chemical Homogenization in One Strand Tundish with Subflux Turbulence Controller. steel research int., **2015**, 86 (9), 972-983. DOI: 10.1002/srin.201400207

[6] Merder, T. Numerical simulation of liquid flow and mixing steel in multi-strands tundish. The Journal of Achievements in Materials and Manufacturing Engineering, **2012**, 55 (2), 561-566.

[7] Chattopadhyay, K., Isac, M., Guthrie, R.,I., L. Physical and Mathematical Modelling of Steelmaking Tundish Operations: A Review of the Last Decade (1999–2009). ISIJ International, **2010**, 50 (3), 331–348. DOI: 10.2355/isijinternational.50.331

[8] Bul'ko, B., Priesol, I., Demeter, P., Gasparovic, P., Baricova, D., Hrubovcakova, M. Geometric Modification of the Tundish Impact Point. *METALS*, **2018**, 8, 944, 1-11. DOI: 10.3390/met8110944

[9] He, Z., Zhou, K., Liu, S., Xiong, W. and Li, BK. Numerical Modeling of the Fluid Flow in Continuous Casting Tundish with Different Control Devices. *Abstract and Applied Analysis*, **2013,** Article ID 984894, 8. DOI: 10.1155/2013/984894.

[10] Warzecha, M. Numerical and Physical Modelling of Steel Flow in a One-Strand Continuous Casting Tundish. *METALURGIJA* , **2011**, 50, 147-150.

[11] Merder, T., Pieprzyca, J., Warzecha, M. Numerical Modeling of Steel Flow in the Six-Strand Tundish With Different Flow Control Devices. *METALURGIJA*, **2009**, 48 (3), 143-146.

[12] Warzecha, M. Numerical Modelling of Non-metallic Inclusion Separation in a Continuous Casting Tundish. Computational Fluid Dynamics Technologies and Applications, Prof. Igor Minin (Ed.), **2011**. ISBN: 978-953-307-169-5, InTech, Available from: http://www.intechopen.com/books/computational-fluid-dynamicstechnologies-and-applications/numerical-modelling-of-non-metallic-inclusion-separation-in-a-continuouscasting-tundish. DOI: 10.5772/22693

[13] Sowa, L. Numerical Modelling of Fluid Flow and Thermal Phenomena in the Tundish of CSC Machine. *ARCHIVES of FOUNDRY ENGINEERING*, **2014**, 14, 103 – 106. DOI: https://doi.org/10.2478/afe-2014-0023

[14] Alaeia, A. R., Edrisa,H., Shiranib, E. Upward Molten Flow for Optimization of Fluid Flow in Continuous Casting Tundish. Journal of Iron and Steel Research, International, **2010**, 17 (11): 29-33. DOI: 10.1016/S1006-706X(10)60166-5

[15] Khana, M., F., Hussaina, A., Usmanib, A., Y., Yadavc, R., Jafria, S.A.H.. Multiphase Flow Modeling of Molten Steel and Slag Flow for Different Tundish Configurations. In IConAMMA_2017, Materials Today: Proceedings **2018**, 5, 24915–24923. DOI: 10.1016/j.matpr.2018.10.291

[16] More, M., V., Saha, S., H., Marje, V., Balachandran, G. Numerical model of liquid metal flow in steel making tundish with flow modifiers. IOP Conf. Series: Materials Science and Engineerin1g2 3149516 (72809107) 012021 DOI:10.1088/1757-899X/191/1/ 012021

[17] Agarwal, R., Singh,M. K., Bachchan Kumar, R., Ghosh, B., Pathak, S. Extensive Analysis of Multi-Strand Billet Caster Tundish Using Numerical Technique. World Journal of Mechanics, **2019**, 9, 29-51. DOI:10.4236/wjm.2019.92003

[18] Tkadleckova, M., Michalek, K., Gryc, K., Hudzieczek, Z., Pindor, J., Strasak, P., Moravka, J. Comparison of Extent of the Intermixed Zone Achieved under Different Boundary Conditions of Continuous Billets Casting. METAL 2010: 19TH INTERNATIONAL METALLURGICAL AND MATERIALS CONFERENCE, Book Group Author(s): Tanger Ltd, 47-52, Published: **2010**. Document Type: Proceedings Paper.

[19] UserGuide ANSYS FLUENT, **2019**.

RATE OF REDUCTION AND DEGREE OF METALLIZATION OF MILL-SCALE SLUDGES, REDUCED IN THE TEMPERATURE RANGE OF 850-1050°C

Anna Konstanciak[1], Marcin Więcek[1], Jan Mróz[1]
[1]Department of Metallurgy and Metal Technology Czestochowa University of Technology Czestochowa, Poland
*Correspondence:konstanciak.anna@wip.pcz.pl

Abstract
Due to the amount of waste generated in the steel production process, attempts were made to reduce direct and indirect sludge. Studies on the reduction of iron oxides were carried out for selected fine-grained iron-bearing materials using carbon monoxide as a reducing agent. Industrial waste sludge was used. Indirect reduction was carried out in the temperature range of 950°C - 1050°C with variablebasicity, grain size and height of waste material samples. To assess the speed of the reduction process, tests using carbon monoxide were carried out. The degree of metallization of the tested materials was determined. An indirect reduction was carried out using hydrogen as a reducer and a mixture of carbon monoxide and hydrogen at extreme test temperatures of 850°C and 1050°C. Comparative pure hydrogen reduction tests were also performed.

Keywords: waste generated; sludge; reduction

1. Introduction

Since 2004 the steel production worldwide reaches the level of 1 billion tonnes; in 2018 1.808 billion tonnes of steel was produced – it showes an increase of 7% compared to 2017 (1.689 billion tonnes). In metallurgy production processes are consumed twice as much input materials as compared to those received as final products. During this processing, large amounts of post-production wastes are produced, namely the blast furnace and converter slags, blast furnace and converter gases, dust and blast furnace and steelmaking sludge, metallurgical pumice, mill scale and slag [1 - 4]. For economic reasons, steel production plants seek to develop these materials [5].

Sludges generated during iron and steel production are divided according to the following groups [6]:

a) clean ironbearing sludge (with iron content over 60 wt. %):
   - sludge from wet flue gas cleaning steel converters,
   - wet sludge from scraper through in sintering plant,
b) ironbearing contaminated sludge (of the iron content in the range of 24÷56 wt. %):
   - sludge from cleaning blast furnace gases,
   - other sludge derived from i.e. chemical neutralization, oily mill-scale sludge.

Due to the amount of waste being produced during the steel production processes, certain attempts were made to carry out direct and indirect reduction of ferrous waste materials. From the group of waste materials consisting of dusts, scales and sludges, sluge samples were selected for testing. Research tests on iron oxide reduction in selected ironbearing materials were performed by using carbon monoxide as a reducing agent. Industrial sludges were employed [7 - 11].

2. Research material

Four samples of sludge were collected, among which three fulfilled the given criterium of iron content exceeding 40 wt. %. Three samples met this criterium – Table 1. Two samples demonstrated high silica content – 22.18 and 19.04 wt. % [12].

Sludge grain composition in dry state is listed in Table 2. For sample no. 32, the largest share demonstrates the fraction in the range of 0.5 – 1.0 mm, which is uncommon for sludges. For this type of wastes, the greatest wt. demonstrate fractions with the smallest grains ranging from < 0.5 mm, as it is demonstrated for samples no. 14 and 16.

Table 1 Chemical composition of selected sludge samples (wt. %) [12].

Sample number	Type of component (wt. %)								
	Fe	C	CaO	SiO_2	MgO	Al_2O_3	Zn	S	CaO/SiO_2
14	59.87	4.92	0.84	22.18	0.28	2.89	0.5	0.27	0.04
16	62.76	1.88	1.02	19.04	0.28	1.45	0.4	0.5	0.05
32	78.17	3.36	0.18	0.58	-	0.38	-	0.1	0.31

Table 2 Granular composition of sludge (wt. %).

Grain fraction (mm)	Sample number		
	S14	S16	S32
< 0.5	89.65	81.98	36.97
0.5-1.0	7.34	9.25	56.39
1.0-2.0	1.70	2.27	6.64
2.0-3.0	0.80	1.80	0.00
3.0-5.0	0.45	1.67	0.00
> 5.0	0.05	3.02	0.00

Reduction testing was performed by using carbon monoxide and a mixture of carbon monoxide and hydrogen acting as a reducer used at temperatures of 850°C, 950°C and 1050°C on three thicknesses of sludge layers. The volume of the research material in a crucible with an internal diameter of 5.2 cm for particular heights receives following values of: 0.2 cm (4.25 cm^3), 0.5 cm (10.61 cm^3), and 1.0 cm (21.23 cm^3). The V/A parameter adopts values of: 0.2 cm, 0.5 cm and 1.0 cm, subsequently starting from the lowest layer height of the material - the geometric volume (V) of sludge, the geometric volume (A) of the sample.

3. Indirect reduction by using the carbon monoxide at the temperatures of 950°C and 1050°C

For S14, S16 and S32 – the three samples of sludges – research tests on reduction with carbon monoxide were performed at temperatures of 950 and 1050°C for samples with basicity of 0.04, 0.9 and 1.1. CaO was added as an additive to increase the sample basicity. It was assumed that in this temperature range and with such sludge grains (Table 3), it is possible to form compounds and eutectics that affect the speed of reduction.

Table 3 Share of grain fractions in the sludge samples (wt. %).

Grain fraction (mm)	Sample number		
	S14	S16	S32
< 0.5	89.65	81.98	36.97
0.5-1.0	7.34	9.25	56.39
Sum of two fractions	96.99	91.23	93.36

The sludge grain size in dry state are listed in Table 2. For this type of wastes, the largest mass share is indicated for fractions with the finest grains in the range of < 0.5 mm, as indicated samples no. 14 and 16. Figure 1 demonstrates reduction process of three sludge samples in two variants: I – the subject of reduction process were samples with various basicity (0.4 and 1.1) carried out at constant temperature of 950°C and the 2nd variant – slugde samples with similar basicity level of (0.9 and 1.1), however, at two different temperatures of 950 and 1050°C.

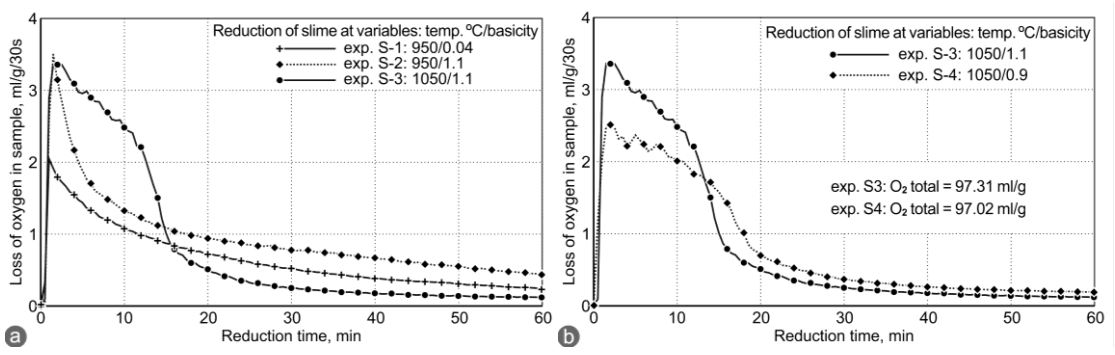

Figure 1 a, b The course of the reduction of mill-scale sludge at various temperatures and varying basicity.

As the data in Figure 1 a show, the curve of reduction for the sample with basicity of 1.1 tested at a temperature of 1050 °C (S-3 research test) differs significantly from other two research tests (S-1, S-2) carried out at a temperature of 950°C. The reduction rate does not decrease rapidly in the first minutes of the process, as it occurs in the case of research tests no. S-1 and S-2, however, it decreases gradually. It is associated with formation of new phases under the same conditions of basicity and temperature. Research tests performed at a temperature of 950°C demonstrated that the basicity does not significantly influences the reduction mechanism. Research on reduction of sludge with the basicity level of 0.9 showed that the reduction mechanism is shaped by the formation of liquid phases and despite the differences occuring in the speed of reduction process in the first minutes of the reaction, the final effect of reduction process after duration period of 60 min is very similar – the amount of oxygen being removed is 97.31 and 97.02 ml/g in the sample (Figigure 1 b).

The mineralogical tests being performed (in the Iron Metallurgy Institute in Gliwice) on samples S-2 and S-3, which indicated increased basicity, were subject to reduction processes at temperatures of 950 °C and 1050 °C, respectively. The tests demonstrated increased level of the glassy (liquid) phase in sample S-2, which was within the range of 9.8±2.8 wt. %, while in sample S-3 – 14.3±2.3 wt. %. It is worth mentioned, that the liquid phase occurs in the sample during reduction process at 950 °C. A change in this case is not remarkable in the course of the reduction process. The reduction speed increases as compared to the sample with 0.04 basicity. Therefore, it should be stated that an increased in the basicity of the sludge also affects the reduction rate at 950 °C.

Due to the fact that in the sludge, large amounts of fractions with grain lower than 0.5 mm can be observed, it should be assumed that such situation will hinder the reductor's access if the V/A ratio, namely the geometric volume (V) of sludge is too high in the geometric volume (A) of the sample. For a crucible with internal surface area of 52 mm and a sludge sample layer height of 2.5 and 10 mm, the V/A parameter adopts following values listed in (Table 4).

Table 4 The height of reduced material layer and the corresponding value of the parameter V/A.

Height of layer (mm)	2	5	10
Surface A (cm^2)	21.23	21.23	21.23
Volume V (cm^3)	4.25	10.61	21.22
Parameter V/A (cm)	0.20	0.50	1.00

To evaluate the impact of this indicator on the reduction process, three reduction experiments by using carbon monoxide were carried out at 950 ° C (S14 sludge sample) at varying sample heights. Results of these research tests are presented in Figures 2 a, b.

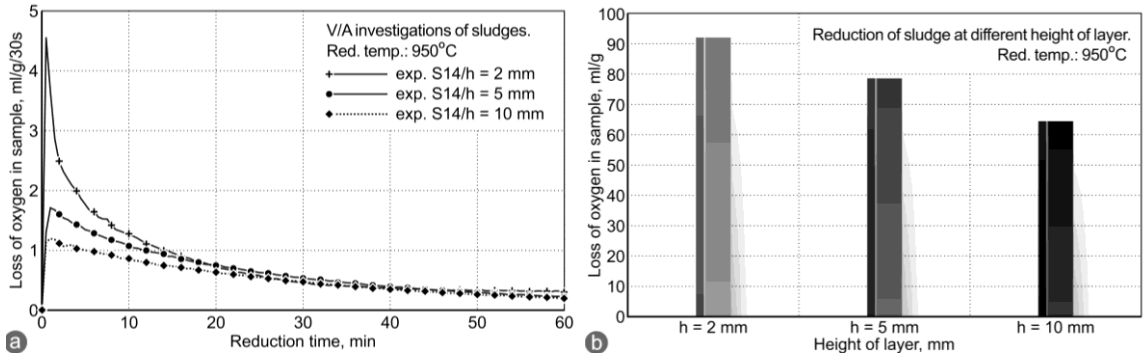

Figure 2 a, b The course of the reduction of mill-scale sludge at various temperatures and varying basicity.

As it can be observed in Figure 2 a, the reduction rate is the highest for the ration of V/A = 0.2, resulting in the highest amount of oxygen being removed from the sample, which equals to 91.9 ml O_2/g (Figure 2 b). For V/A = 1.0, the amount of oxygen being removed is lower and amounts to 64.4 ml of O_2/g. Such results indicate that for small fractions, the reduction process speed depends mostly on the availability of the reducer in wt. of the material being reduced. As the layer height increases, gas penetration in the sludge layer becomes more difficult. In reference to the conditions occurring in the rotary furnace, this indicates the need to intensify the process of material mixing and mass exchange inside the furnace.

The index of metallic iron was also determined in samples S4, S5 and S6 being subject to the reduction process. The reduction conditions and obtained ratio of sample metallization are summarized in Tables 5 and 6 and shown in Figure 3. As it can be observed in Figure 3, as the V/A ratio increases, the metallization process decreases. A convergence between the impact of the V/A ratio and the reduction ratio can be seen – Figure 2 b, which is caused by a high advancement of metallization and reduction processes. In such cases, the reduction mechanism is no longer relevant for shaping the relationship between the ratios of reduction and metallization.

Table 5 Conditions for the indirect reduction of sludge samples (no. 14) with using a carbon monoxide.

Designation of the experiment	S4	S5	S6
Temperature(°C)	950	950	950
Height of layer h (mm)	2	5	10
Grain fraction(mm)	whole	whole	whole
Basicity (CaO/SiO_2)	0,04	0,04	0,04
Reduction time (min)	60	60	60
Reducer	CO	CO	CO

Table 6 Results of chemical analyzes on iron content and iron metallization degree in indirect reduction of sludge samples (no. 14) with using a carbon monoxide.

Designation of the experiment	S4	S5	S6
Fe_c (wt. %)	54.7	52.5	51.7
$Fe_{met.}$ (wt. %)	40.2	36.9	33.6
Fe(II+III) (wt. %)	14.5	15.6	18.1
Metallization degree (%)	73.5	70.3	65.0

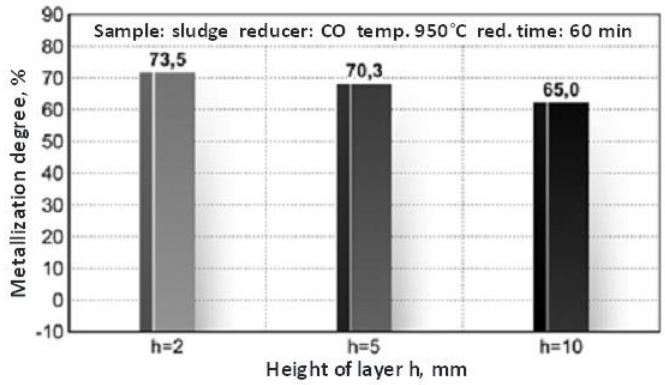

Figure 3 The course of the reduction of mill-scale sludge at various temperatures and varying basicity.

4. Indirect reduction of sluges by using a mixture of carbon monoxide and hydrogen at temperatures of 850 °C and 1050 °C

Ironbearing waste material – sludge (sample no. 16) with a grain size of < 0.5 mm and 3 – 5 mm, which was subject to reduction by using a mixture of CO- H_2 50:50 vol. %. Hydrogen as an iron oxide reducer is thermodynamically characterized by a greater degree of utilization of its reducing properties compared to carbon monoxide. Reduction process was carried out at boundary temperatures within the adopted testing of 850°C and 1050°C. Comparative research tests were also carried out on reduction by using pure hydrogen under the same process conditions – see Table 7.

After the reduction process, samples were subject to chemical analysis for the presence of total iron, metallic iron, as well as divalent and trivalent iron in the Analytical Chemistry Laboratory at the Institute of Ferrous Metallurgy in Gliwice. Table 8 presents results of determinants for particular samples, while Figures 4-6 indicate graphical interpretation of their average degree of metallization.

Figure 4 presents graphical interpretation of results on reduction with pure hydrogen. By increasing the reduction temperature by 200°C, the degree of metallization was significantly affected. At the temperature of

850°C the metallization degree was 44.4%, while at 1050°C – 55%. Such a result proves that for the reduction of sludge with a grain fraction of < 0.5 mm, being conducted by using pure hydrogen, the temperature is a key factor that causes an increase in the level of metallization in the waste material subject to reduction. However, for the grain fraction ranging 3.0-5.0 mm, the difference in results is within the margin of error accepted in the research testing (5% rel.), which proves that in this case the temperature has no significant effect on the degree of metallization – Figure 5. For this case, it seams most likely that the factor that controlls the reduction process is the transport of reagents inside the sludge graines and not the chemical activation of the reduction reaction, being related to the process temperature.

Table 7 Conditions for intermediate reduction of sludge (sample no. 16) using pure hydrogen and a mixed gases 50% vol. CO + 50% vol. H_2.

Designation of the experiment	Parameter						
	Temp., °C	Sample mass (g)	Height of layer (mm)	Grain fraction (mm)	Basicity (CaO/SiO_2)	Reduction time (min)	Reducer
1A-16	850	39.66	10	< 0.5	0.05	60	H_2
1B-16	850	41.04	10	< 0.5	0.05	60	H_2
1C-16	850	42.63	10	< 0.5	0.05	60	H_2
2A-16	1050	40.40	10	< 0.5	0.05	60	H_2
2B-16	1050	35.70	10	< 0.5	0.05	60	H_2
3-16	850	19.86	10	3-5	0.05	60	H_2
4-16	1050	16.67	10	3-5	0.05	60	H_2
5A-16	1050	43.53	10	< 0.5	0.05	60	$CO+H_2$
5B-16	1050	41.42	10	< 0.5	0.05	60	$CO+H_2$
6A-16	850	43.08	10	< 0.5	0.05	60	$CO+H_2$
6B-16	850	41.12	10	< 0.5	0.05	60	$CO+H_2$

Table 8 Results of determinations for the presence of Fe_c, $Fe_{met.}$, Fe^{2+} and Fe^{3+} after reduction of sludge samples with hydrogen and a mixed gases 50% vol. CO + 50% vol. H_2.

Designation of the experiment	Parameter						
	Temp., °C	Reducer	Fe_c (wt. %)	$Fe_{met.}$ (wt. %)	Fe(II+III) (wt. %)	Metallization degree (%)	Average of metallization degree (%)
1A-16	850	H_2	70.0	31.3	38.7	44.7	44.4
1B-16	850	H_2	70.9	33.2	37.7	46.8	
1C-16	850	H_2	70.2	29.3	40.9	41.7	
2A-16	1050	H_2	74.1	38.9	35.2	52.5	55.0
2B-16	1050	H_2	73.9	42.6	31.3	57.6	
3-16	850	H_2	74.5	34.3	40.2	46.0	46.0
4-16	1050	H_2	77.2	33.6	43.6	43.5	43.5
5A-16	1050	$CO+H_2$	69.7	24.8	44.9	35.6	35.4
5B-16	1050	$CO+H_2$	70.9	25.0	45.8	35.3	
6A-16	850	$CO+H_2$	67.6	26.1	41.5	38.6	38.1
6B-16	850	$CO+H_2$	64.9	24.4	40.5	37.6	

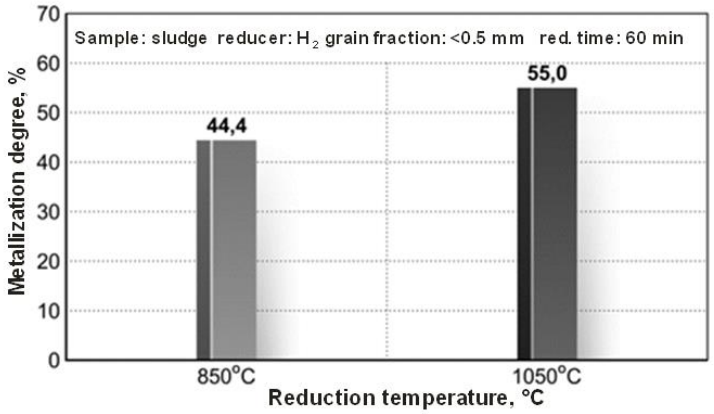

Figure 4 Results of sludges reduction of fraction grain < 0,5 mm by hydrogen at temp. 850 °C and 1050 °C.

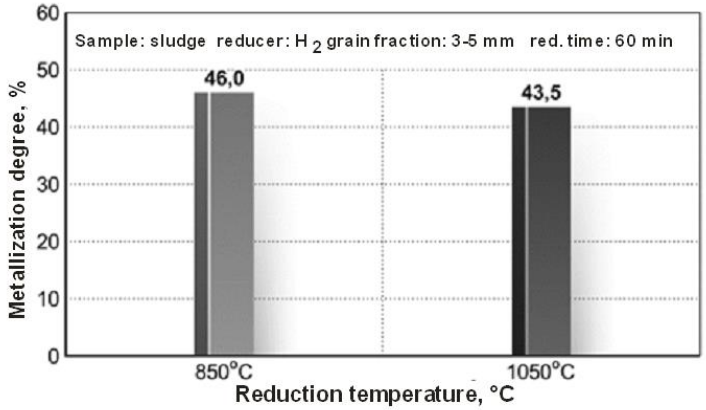

Figure 5 Results of sludges reduction of fraction grain 3-5 mm by hydrogen at temp. 850 °C and 1050 °C.

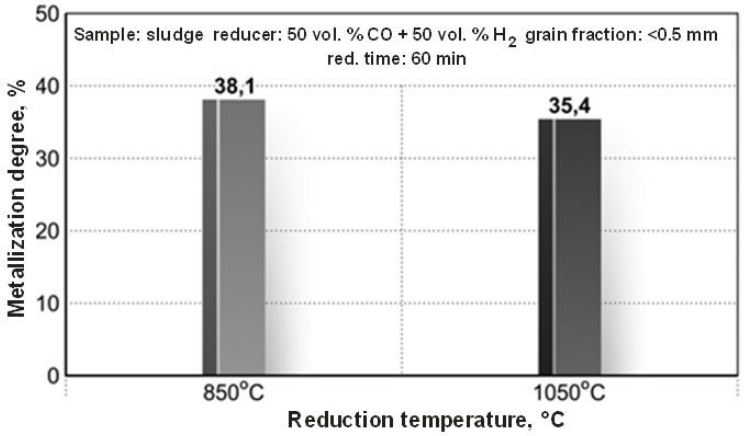

Figure 6 Results of sludges reduction of fraction grain < 0,5 mm by (50 vol.% CO + 50 vol.% H_2 at temp. 850 °C and 1050 °C.

The results of sludge reduction - by using a mixture of CO - H2 50:50 vol. %, which are the average of replicate testing indicated in Table 8 – demonstrate that by increasing the reduction temperature level from 850°C to 1050°C a slight decrease in the degree of metallization from 38.1 to 35.4% is observed – Figure 6. An increase in temperature that evokes an adverse effect on the degree of metallization, when using CO - H2 50:50 vol. % mixture as a reducing agent should be interpreted by the course of equilibrium curve as a function of temperature reduction by using such a mixture. An increase in the reduction temperature results in a slight decrease in the equilibrium concentration of the reduction gas product, which correlates with the decrease in the amount of metallic iron, being formed.

5. Results and discussions

Research testing on reduction for sluge indicates that increased basicity significantly changes the process at the temperature of 1050°C, while the course of the reduction curve indicates a change in the mechanism of the reduction process as a result of accurance of easy-reduction phases. A change in basicity of sludge samples from 0.9 to 1.1 did not significantly affect the reduction process. During research testing of fine fractions of sluge in the stationary layer, the reduction speed was largely dependent on the possibility of contact of the test material grains with the gas-reductor. Gas penetration becomes more difficult as the height of the sludge layer increased.

6. Conclusion

The aim of the researh tests was to determine reduction conditions under which the research materials remain in the solid state during the reduction process in a rotary furnace. The result of the research was to determine the maximum temperature at which the sintering process occurs in the reduced ironbearing materials. The result of not exceeding the set temperature in the rotary furnace should guarantee the smooth transport of the test material and adequate reduction speed. Another important factor in reduction process is the area of reaction, which is expressed by the grain composition and bulk density of ironbearing waste materials. The chemical composition, and first of all – the basicity being defined as the ratio of $\%CaO/\%SiO_2$, influences the reduction process, as well. By increasing the basicity the speed of reduction process can be boostered as a result of forming easy-to-reduce ferrite phases. However, the formation of liquid phases promotes agglomeration of reduced graines, thus limiting the area of the reaction process. It is also crucial to determine differences in reduction properties of carbon monoxide and hydrogen, depending on the type of waste materials being tested in the context of employing the mixture of these gases for industrial applications.

Acknowledgement

This research was funded by [The National Center for Research Development] grant number [No. 245969].

References

[1] Borowski, G. Określenie właściwości fizyczno-mechanicznych materiałów drobnoziarnistych w celu ich zagospodarowania. *Postępy Nauki i Techniki,* **2009**, 3, 67-82.

[2] Karwat, B. Recykling odpadów poprodukcyjnych w hucie surowcowej stali. *Hutnik – Wiadomości Hutnicze* **2010**, 10, 596-599.

[3] Konstanciak A. 2009. Odpady z produkcji surówki wielkopiecowej. *Prace Instytutu Metalurgii Żelaza*, **2009**, 5, 26-29.

[4] World Steel Association. World Steel in Figures 2019. *Brussels. Belgium*, **2019**.

[5] Mróz, J., Francik, P., Budzik, R. Niektóre problemy recyklingu materiałów odpadowych w hutnictwie żelaza i stali. *Hutnik – Wiadomości Hutnicze*, **2016**, 7, 327-332.

[6] Mróz, J. Recykling i utylizacja materiałów odpadowych w agregatach metalurgicznych. Częstochowa. *Wydawnictwo Politechniki Częstochowskiej*, **2006**.

[7] Więcek Marcin: Analiza eksperymentalna redukcji pośredniej i bezpośredniej zgorzeliny w zakresie 900-1050°C. Praca doktorska, *Politechnika Częstochowska, Częstochowa* **2019**.

[8] Monazam E. R., Breault R. W., Siriwardane R.: Reduction of hematite (Fe2O3) to wüstite (FeO) by carbon monoxide (CO) for chemical looping combustion, *Chemical Engineering Journal*, **2014**, 242, s. 204-210.

[9] Wang Y. D., Hua X. N., Zhao C. C., Fu T. T., Li W., Wang W.: Step-wise reduction kinetics of Fe2O3 by CO/CO2 mixtures for chemical looping hydrogen generation, *International Journal of Hydrogen Energy*, **2017**, 42, s. 5667-5675.

[10] Benchiheub O., Mechachti S., Serrai S., Khalifa M. G.: Elaboration of iron powder from mill scale, *Journal of Materials and Environmental Science*, **2010**, 1(4), s. 267-276.

[11] Mechachti S., Benchiheub O., Serrai S., M. E. H. Shalabi: Preparation of iron powders by reduction rolling mill scale, *International Journal of Scientific & Engineering Research*, **2013**, 4/5, s. 1467-1472.

[12] Mróz J., Więcek M., Konstanciak A., Kwintal-Ogórek P., Posiadało S., Soszek E.: Reduction of iron-bearing wastes in the temperature ranges 850-1050°C by mixtures of carbon monoxide, AISTech 2017 Iron and Steel Technology, *Association for Iron and Steel Technology*, **2017**, s. 121-133.

Session - Energy Transformation in Industry

MATHEMATICAL MODEL OF HEAT TRANSFER IN NON-OXIDISING FURNACE

René Atyafi[1*],Augustín Varga[1], Gustáv Jablonský[1]
[1]Faculty of Materials, Metallurgy and Recycling, Technical University of Košice, 04200 Košice, Slovakia;
augustin.varga@tuke.sk, gustav.jablonsky@tuke.sk
*Correspondence: rene.atyafi@tuke.sk; Tel.: +421-55-602-3228

Abstract
Created mathematical model partially described here allows processing of static state simulations of continuous direct-fired annealing furnace operation in different configurations. It allows the evaluation of the effects of variant operating modes, production speeds or heated body dimensions on the resulting temperature fields. A part of the heat treatment technology for steel strip at a specific continuous hot-dip galvanising line is a non-oxidising furnace. A comparison of measurement data from the furnace to simulation results of the referential configuration demonstrates the accuracy of the model. The other two simulations provide a test of the applicability of configurations that offer more intense heat transfer. Since the presented model requires low computational power, it is also suitable for operational control at the real plant. A heat transfer intensification upgrade of the non-oxidising furnace was suggested based on the interpretation of the simulation outputs. High combustion temperatures indicate that installation of more powerful burners is not an optimal form of increasing the heating capacity. Elongation of the burner section increases the heat exchange surface and is more suitable for achieving the desired effect.

Keywords: hot-dip galvanising line; heat transfer modelling; emissivity; direct-fired furnace; view factor

1.Introduction

Maintenance of competitiveness level in the galvanised sheet steel production industry stimulates the operators of older plants to increase the energy efficiency and production capacity. However, diverse engineering restrictions might often limit productivity growth. Based on the conclusions of internal studies of the hot-dip galvanising line (GL) in question, we figured that the restrictive factor that governs the effort to increase its production speeds is the heating capacity of the installed annealing technology. It is composed of horizontal continuous annealing furnaces (HCAF) (Figure 1). Those have to ensure optimal heat treatment of the strip and sufficient cleanliness of its surfaces. The processed steel passes through the non-oxidising furnace (NOF), reduction furnace (RF) and cooling sections. Subsequently, it enters the zinc bath at a temperature above the zinc melting point. Current performance conditions of the technology limit the maximal processing speed of the referential assortment sample to 50 $m.min^{-1}$. Data collected for this study indicate that the heat capacity of the reduction furnace, cooling performance, drive mechanisms and machinery construction can handle the production of the referential product at speed around 65 $m.min^{-1}$. However, the current heat capacity of the NOF would be insufficient.

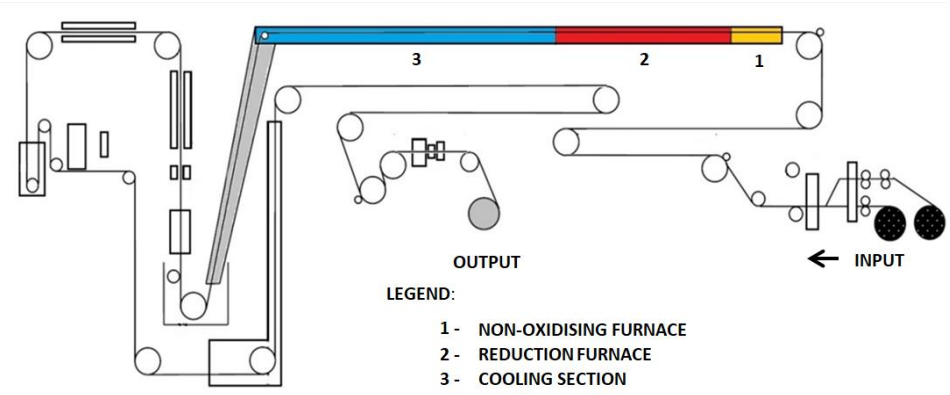

Figure 4 Technological scheme of hot-dip galvanising line.

1.1 Non-oxidising furnace

In the system of the HCAF at the GL in question, the NOF provides continuous heating in the annealing process and cleaning of the strip surfaces from rolling emulsions and other oils from preceding technological steps. Since the NOF is a direct-fired furnace, those oils oxidise at high temperatures in the fuel combustion flame [1]. Furthermore, the substoichiometric combustion of natural gas produces flue gas with partly non-oxidising properties [2]. The flue gas flows counter-currently to the steel and suppresses the formation of the oxide layer on the strip surfaces, that would otherwise form at these temperatures. The actual strip temperature exiting the chamber is mainly up to 500 °C and is dependent on the strip dimensions, its speed and actual performance of the furnace. Temperature control is realised by fuel throttling in two regulation zones. Each zone feeds 12 burners. This method can be used to regulate overall chemical power input in a range between 3 - 5 MW. Operation at the higher boundary of the spectrum is not sufficient enough for heating strips at higher mass flow levels (mostly thicker sheets at greater velocities). On the contrary, operation at the lower boundary creates suboptimal conditions for oxidisation of the surface impurities (oils and emulsions). Therefore, our goal was to assess the effect of alternative power distribution on overall process parameters in a static state operation of NOF utilising numerical modelling. Furthermore, these alternatives ought to provide higher intensity heat transfer and optimal control of the temperature fields. They also ought to optimise the furnace for a higher mass flow of the steel.

1.2 Existing modelling approaches

Numerical modelling of continuous annealing furnace can be approached by several methods. One of them is CFD modelling, which provides calculations in high-resolution temperature and velocity fields. Therefore, it demands high computational power even for solutions to already simple problems. Consequently, it is unsuitable for real-time process control. It is often used for computation of pinpointed local processes or overall heat transfer coefficient [3]. Less power-demanding models potentially usable as prediction models for real-time control are often based on analytical, empirical, and energy balance methods [4-8]. Transient model of vertical direct-fired continuous annealing furnace presented in Strommer 2014 [8] is based on material and enthalpy balances. The combustion model computes one stage combustion right at the burner nozzle. The authors also considered the effect of the water-gas shift reaction chemical equilibrium on flue gas composition and combustion temperature. Therefore, the method provides a more accurate estimation of overall heat transfer conditions. The model described here follows the first principles of radiative and convective heat transfer, the theory of gaseous fuel combustion and the principles of material and enthalpy balance. Considered were only static state heat transfer and one stage combustion without the impact of water-gas shift reaction.

2. Methods and modelling setup

The processes of heating bodies inside the furnace chamber can be distinguished into internal and external heat exchange. Double-sided heating of sheet metal bodies produces small enough temperature differential, which allows neglecting the internal exchange. The external transfer in the NOF realises in a mostly indirect radiative regime. The substoichiometric natural gas combustion products are considered to be the energy carrier. The energy transfers to surfaces of the strip and wall lining by mostly radiation but also convection. Most of the heat flux emitted to the walls reflects to the steel surfaces. The remaining flux transfers through the lining out to the environment. Computation of the energy accumulated in the heated body by flue gas and lining radiation, in such chamber, bases on the following expressions [9-10]:

$$Q^{R}_{acc,m} = \sigma_0 \cdot \varepsilon_{fg-l-m} \cdot \left({T_{fg}}^4 - {T_m}^4\right) \cdot S_m \tag{1}$$

$$\varepsilon_{fg-l-m} = \frac{\varepsilon_{fg} \cdot \varepsilon_m \left[1 + \varphi_{l-m} \cdot \left(1 - \varepsilon_{fg}\right)\right]}{\varepsilon_{fg} + \varphi_{l-m} \cdot \left(1 - \varepsilon_{fg}\right) \cdot \left[1 - \left(1 - \varepsilon_{fg}\right) \cdot \left(1 - \varepsilon_m\right)\right]} \tag{2}$$

Where σ_0 is Stefan-Boltzmann constant, ε_{fg-l-m} is combined emissivity factor of flue gas and wall lining, T_{fg} – flue gas temperature, T_m – strip temperature, S_m – heat exchange surface, ε_{fg} – flue gas emissivity factor, ε_m – strip emissivity factor, φ_{l-m} - view factor between wall lining and the strip.

Newton's law of cooling describes heat accumulation due to convection (3). The Nusselt criterium value is used to determine the convective heat flux coefficient magnitude. Its value is obtained through an empirical

expression for turbulent flow that is a function of Reynold's number and the criterium of Prantl (3-4). The Reynold's number for turbulent flow of the atmosphere inside the furnace is also based on empirical expressions describing the flow inside ducts and pipes.

$$Q_{fg-m}^{C} = \alpha_{fg-m}^{C} \cdot S_m \cdot \left(\bar{t}_{fg} - \bar{t}_m\right) \tag{3}$$

$$\alpha_{fg-m}^{C} = \frac{Nu \cdot \lambda}{l_{ch}} \tag{4}$$

$$Nu = f(Re, Pr) \tag{5}$$

The term α_{fg-m}^{C} is convective heat flux coefficient; S_m is the surface of heat exchange; $\bar{t}_{fg}$ is mean temperature of the atmosphere; $\bar{t}_m$ is mean temperature of the strip. The term Nu represents the value of the Nusselt criterium; λ the value of thermal conductivity of the atmosphere; l_{ch} is the characteristic dimension of the flow and terms Re and Pr represent the value of Reynold's and Prantl's criterium.

Temperature record obtained through a thermocouple located inside a furnace is affected by many sources of influence. Those are atmosphere temperature and intensity of its turbulent flow, location of the thermocouple inside the chamber and also the temperature of the walls which encompass the thermocouple. Therefore, the value recorded during a measurement cannot be understood as the temperature of the atmosphere. Computation of the theoretical value takes into consideration the radiation along the length of the furnace and also convection. Radiative heat flux from each computing zone is determined through view factors of surfaces inside these zones (6)[11]. The calculation realises for each wall of the lining and surface of the strip individually and the integral boundaries discretisation bases on the zonal divisions of the furnace.

$$\varphi_{\mathrm{p-e}} = \frac{1}{\pi} \cdot \iint_{\mathrm{x_1 y_1}}^{\mathrm{x_2 y_2}} \frac{\mathrm{Z^2 dx \cdot dy}}{(\mathrm{Z^2 + X^2 + Y^2})^2} \tag{6}$$

Index p represents the heat exchange surface; e a sufrace element located at the place of the thermocouple; X,Y,Z are spacial coordinates of the heat exchange surface.

2.1. Computational model of horizontal continuous furnace

This numerical model bases on zonal energy balance, the material balance of combustion and heat exchange conditions. Besides input parameters loading and output variables processing the program consists of following procedures:

- zonal material balance processing
- zonal iterative heat transfer computation (Figure 2)
- aggregate energy balance processing
- calculation of the theoretical thermocouple temperature

Following algorithm describes the iterative heat transfer computation. It stems from the final strip temperature estimate and artificial temperature gradient along the length of the zone. In each zone, the calculation is performed as follows:

1 loading the input values
2 entry strip temperature and exit atmosphere temperature estimation and calculation of the theoretical combustion temperature
3 calculation of the heat losses through the walls
4 calculation of the enthalpy difference of the strip
5 calculation of the exit atmosphere temperature
6 wall lining temperature computation
7 computation of the total heat flux on the strip
8 calculation of the entry temperature of the strip

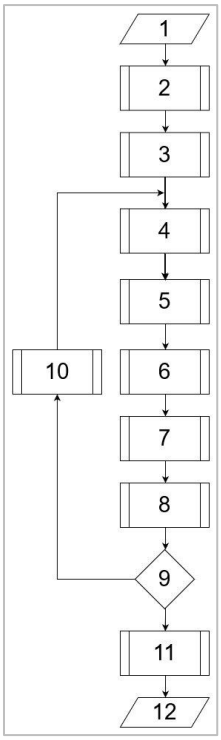

Figure 5 Iterative heat transfer computation model.

9 accuracy check of the interpolated entry strip temperature
10 entry strip temperature interpolation
11 exit-boundary atmosphere enthalpy calculation
12 outputting the temperatures in the zone

After the calculation has been performed in each zone, the programme checks the value of calculated material temperature at the furnace inlet. The program adjusts the outlet temperature of the strip until the required accuracy of material inlet temperature is achieved. The outputs of the model are the profiles of material, lining, furnace atmosphere temperatures and theoretical value of temperature on thermocouples located at selected positions. Other outputs are: heat flows in the furnace space, heat balance items, furnace atmosphere composition in individual zones.

2.2. Modelling setup

Table 1 lists some input data and dimensions of the reference material. The numerical model described above allowed us to simulate steady-state heating through the following configurations of the burner system:

- Configuration A - represents the current state of the device in real operation (24x200kW, material feed at 50 $m.min^{-1}$),
- Configuration B - operation with burners of higher power output (24x300 kW, material feed rate of 65 $m.min^{-1}$),
- Configuration C - extended burner zone with lower output at the furnace end section (24x250 kW + 8x200 kW, material feed rate at 65 $m.min^{-1}$).

Table 2 Overview of some input data.

Item	Length (m)	Width (m)	Height (m)	Emissivity (-)	Initial temperature (°C)	Volume flow rate ($m^3.h^{-1}$)
Furnace chamber	18.7	1.8	1.5	0.7	-	-
Material (strip)	-	1.255	0.0015	0.35	25	-
Combustion air	-	-	-	-	370	4162*
Fuel	-	-	-	-	25	481*
HNx atmosphere	-	-	-	-	750	313.6

*at 5 MW

3. Results and discussion

The results obtained by simulating the operating state in configuration A were compared to the values recorded during a real operation (Figure 3).

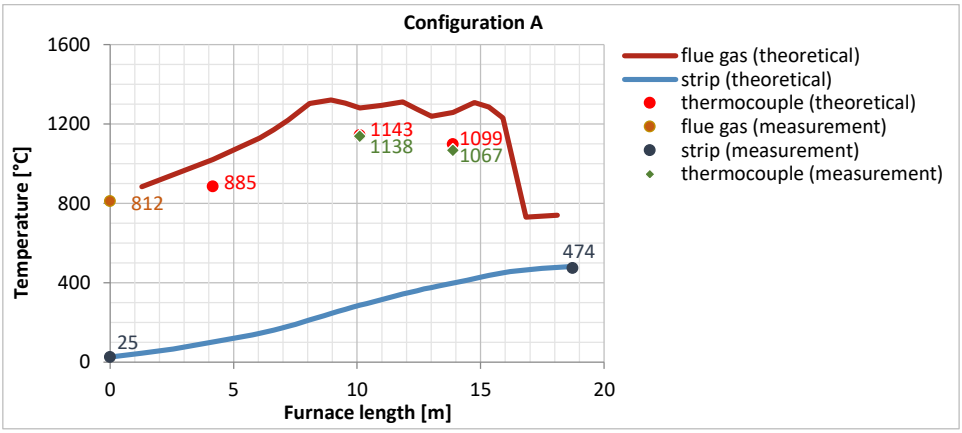

Figure 6 Temperature profile in configuration A in comparison to measurement records. Residence time 22,5 s.

The course of temperatures along the length of the NOF, as well as theoretical values of temperature on thermocouples, largely correlate to measurement values. The material temperature at the furnace outlet was calculated with a deviation of +1.7%, the flue gas outlet temperature with a deviation of +2.6% and the theoretical temperature values on thermocouples with a deviation of +3%. The source of these inaccuracies may be the fuel consumption value, which is the input variable of the model. Its measurement was processed by recording the values from the gas meter at the specified time interval. Other sources could be the method of calculating the heat losses through the walls of the furnace or the effect of the adopted geometric and other simplifications. The simulation results of the temperature field distribution achieved utilizing this method were considered satisfactory. Therefore, using the developed model, we proceeded to simulations of individual designs for optimization of heating at higher production speed, while the flue gas temperature profile in configuration A serves as a reference. It allows evaluating the degree of temperature increase in the chamber, due to the higher furnace performance in alternative configurations.

As expected, the simulation output of configuration B indicates the reach of higher combustion temperatures and more intensive heat exchange conditions as a result of higher performance level (Figure 4).

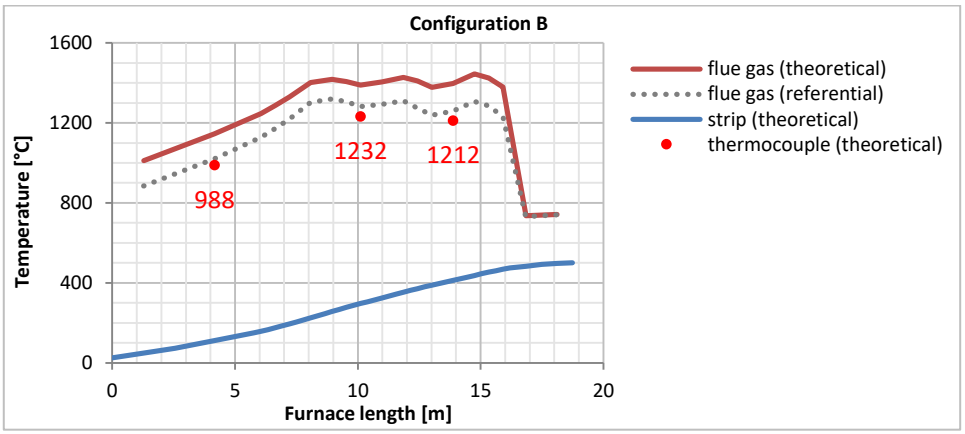

Figure 7 Temperature profile in configuration B. Residence time 17,3 s.

Particularly in the end part of the chamber, the flue gas can reach too high temperatures, causing accelerated degradation of the lining, eventually deformation of the support rolls or local melting of the material. These observations led to the idea to spread the heating power of the NOF over a larger length, using a higher number of lower power burners (Figure 5).

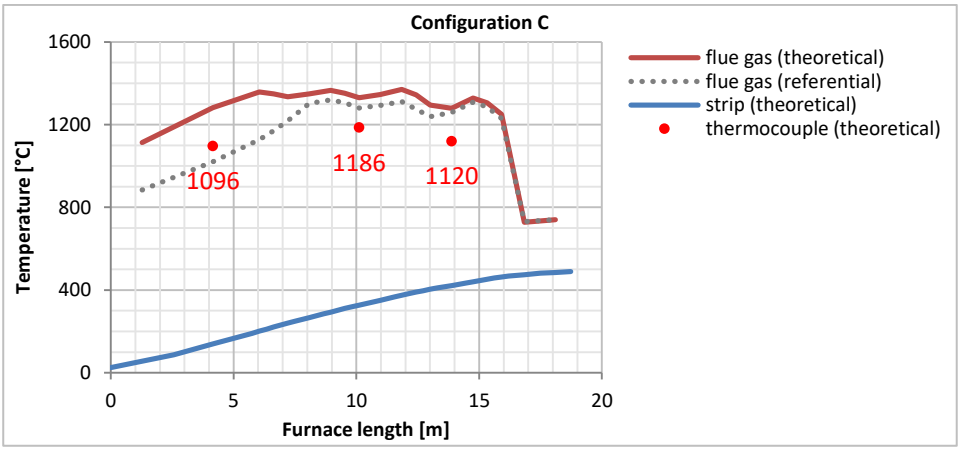

Figure 8 Temperature profile in configuration C. Residence time 17,3 s.

Simulation of the operation in configuration C allows to state that elongation of the burner section provides more linear temperature rise in the strip. Particularly in the initial heating phase, a more intense heat exchange occurs. Compared to the results for configuration B, the operation of lower power burners in the last zones produces flue gas at lower combustion temperature. The average values do not exceed the reference by more

than 60 °C and could be maintained below 1400 °C throughout the length of the furnace. In the reference state, the system achieves efficiency at around 50%. As a result of higher temperatures in the flue gas duct when operating at higher power, the furnace chamber becomes less efficient. In configuration B, efficiency drops to 48% and in configuration C to 44%. However, part of the heat loss can return to the process by preheating the combustion air.

4. Conclusion

The mathematical model presented here is based on the basic principles of heat and mass transfer, enthalpy balance and gaseous fuels combustion theory. It provides a calculation of heat transfer in a one-dimensional temperature field. The model was verified by a comparison of the reference state numerical analysis outputs with the values measured during a real operation. Furthermore, optimization adjustments were designed to increase the production capacity of the NOF. Simulations of these conditions have made it possible to assess that a simple increase in burner output is inappropriate given the reach of high combustion temperatures. Achieving optimal material and flue gas temperatures can be achieved by extending the burner zone but at the expense of the energy efficiency of the device. Implementation of ON/OFF regulation and burner cycling can ensure heating of thinner strips at lower furnace output. This type of regulation, step change of material type or other influences causes unsteady states during the furnace operation. They can only be taken into account in the calculations by creating a dynamic mathematical model of the aggregate.

References

[1] Tatič, M.; Lukáč, L. Industrial furnaces 1: Furnaces in metallurgy and engineering. Technical University of Košice. **2009**, 225, ISBN 978-80-553-0254-6 (in Slovak)

[2] Imose, M. Heating and cooling technology in the continuous annealing. Transactions of the Iron and Steel Institute of Japan. **1985**, 25, 911-932. [CrossRef]

[3] Su, F., Y.; Li, Z. Numerical Simulation of Temperature and Flow Field in Horizontal Continuous Annealing Furnace. Research Journal of Applied Sciences, Engineering and Technology. **2012**, 1322-1325. [CrossRef]

[4] Carvalho, S., R.; Ong, T., H.; Guimarães, G. A mathematical and computational model of furnaces for continuous steel strip processing. Journal of Materials Processing Technology. **2006**, 178, 379-387. [CrossRef]

[5] Hai. W.; Benschop, B.; Omar, B., D.; Frinking, F.; Speets, R. Furnace combustion and control renovation to improve the productivity of a continuous annealing line. Energy Procedia. **2017**, 120, 454-461.

[6] Wan, F.; Wang, Y.; Qin, S. Modeling of Strip Heating Process in Vertical Continuous Annealing Furnace. Journal of Iron and Steel Research, International. **2012**, 19, 29-36. [CrossRef]

[7] Yoshitani, N. Modelling and parameter estimation for strip temperature control in continuous annealing processes. Proceedings of the International Conference on Industrial Electronics, Control, and Instrumentation (IECON). **1993**, 469 – 474. [CrossRef]

[8] Strommer, S.; Niederer, M.; Steinboeck, A.; Kugi, A. A mathematical model of a direct-fired continuous strip annealing furnace. International Journal of Heat and Mass Transfer. **2014**, 69, 375-389. [CrossRef]

[9] Varga, A.; Jablonský, G.; Lukáč, L.; Kizek, J. Thermal engineering. Technical University of Košice. **2013**, 279, ISBN 978-80-553-1590-4 (in Slovak)

[10] Kazan, E. Industrial, Furnaces. Metallurgy. **1964** (in Russian)

[11] Hottel, H., C.; Sarofim, A., F. Radiative Transfer. New York: McGraw-Hill Book Company, **1967**. p. 520

CO_2 EMISSIONS IN LIME INDUSTRY

René Berta[1*], Ladislav Lukáč[2]
[1]Carmeuse Slovakia s.r.o., Slavec 179, 04911 Slavec, Slovakia; [2] Faculty of Materials, Metallurgy and Recycling, Technical University of Košice, 04200 Košice, Slovakia; ladislav.lukac@tuke.sk
*Correspondence: rberta@carmeuse.sk

Abstract
Lime industry is of one the industries that have two sources of CO_2 emissions, first from calcination process and second from fuel combustion. Reduction of CO_2 emission in the lime industry is possible in several ways. Increase of efficiency, the substitution of traditional fuels for its alternatives, lime application are three main way to decrease emission impact of lime industry nowadays. The optimal selection of technology and fuel mix brings a potentially significant reduction of CO_2 emissions from lime production.
Two third of emissions originate from raw material and the biggest potential reduction comes from Carbon Capture and Storage and Carbon Capture and Utilization.

Keywords: lime; steel industry; rotary kiln; shaft kiln; PFR kiln; renewable energy; alternative fuels

1. Introduction
The lime production process is based on a chemical reaction promoted by heating of calcium carbonate ($CaCO_3$) to produce quicklime (CaO). This reaction produces CO_2, which is inherent to process of de-carbonation of $CaCO_3$. Such a direct process emissions are 70% of total CO_2 emission from lime production process, these emission can not be avoid. The residual 30% of CO_2 emission comes from combustion of different types lime kilns. Modern lime kiln are very efficient, the energy efficiency is close to the limit. Around 38 % of lime is sold in EU for steel production. Although during production of lime CO_2 and other emission arise, the lime has many environmental applications for waste gas treatment. [1]

2. Cycle of lime
Lime is used in variety of application and products, these products are mostly recyclable. In steel industry recycling rate is 95% in other industries 65%. In case of flue gas treatment lime allows to create gypsum, which is used for building industry. [2,3]

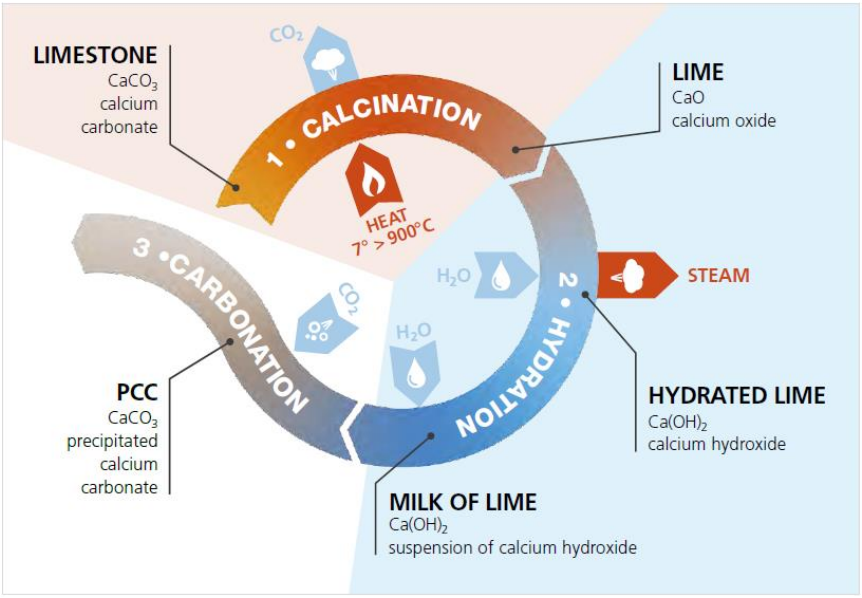

Figure 1 Cycle of lime.

3. CO_2 emission from different lime kilns

There are six main types use for lime production that are divided in two categories: vertical kilns and horizontal kilns.

Table 1 Different types of Kilns in EU [4,5].

Kiln orientation	Kiln type	Number of kilns (2013)
Horizontal	Long rotary kiln (LRK)	14
	Rotary kiln with pre-heater (PRK)	20
Vertical	Parallel flow regenerative kiln (PFRK)	183
	Annular shaft kiln (ASK)	67
	Mixed feed shaft kiln (MFSK)	86
Other kiln (OK)		469

The other kilns type include types like double-inclined shaft kilns, travelling grate kilns and rotating hearth kilns. The efficiency of the kilns depends on several factors like kiln type, feed size, limestone type, fuel and required residual CO_2.

Table 2 Overview of heat consumption range [4, 5, 6].

Kiln orientation	Kiln type	Heat use for quicklime production (GJ/t)
Horizontal	Long rotary kiln (LRK)	6.2 – 9,2
	Rotary kiln with pre-heater (PRK)	5.1 – 7.8
Vertical	Parallel flow regenerative kiln (PFRK)	3.2 – 4.2
	Annular shaft kiln (ASK)	3.3 – 4.9
	Mixed feed shaft kiln (MFSK)	3.4 – 4.7
Other kiln (OK)		3.5 – 7.0

The overview graph (Figure 2) shows minimum energy consumption in comparison with the range of energy consumptions of horizontal and vertical kilns.

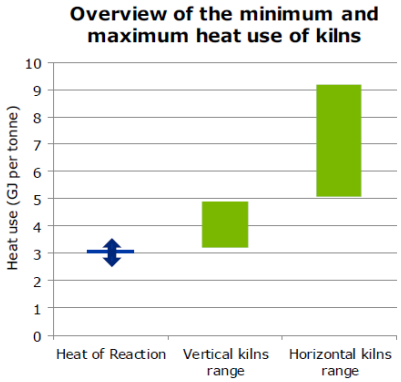

Figure 2 Overview of minimum and maximum heat use of kilns [3].

Table 3 Comparison of best energy efficiencies achieved by new large furnaces [3].

Process:	**Energy efficiency**
Parallel flow regenerative lime kilns	80-90%
Rotary cement kilns with pre-heaters and pre- calciners	68%
Cross-fired regenerative glass melting	49%
Brick kiln	68%
Steel electric arc furnace	70%
Steel re-heating	75%

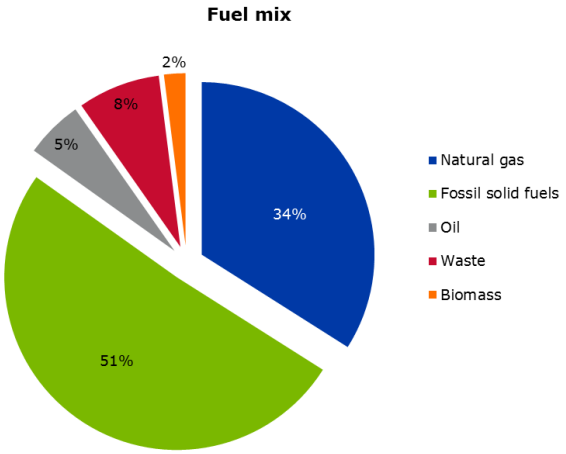

Figure 3 Fuel mix in lime industry in EU -2012 [8].

To generate the energy for the lime production process, fossil fuels are burned. The combustion of fossil fuels causes CO2 emissions. The vast majority of emissions from fossil fuel combustion originate in the kilns. No focus is given in this Roadmap on the CO_2 emissions in other parts of the production process, because of their relatively small size compared to the emissions in the kiln :

- The emissions during the downstream processing and hydration account for around 1.5% of total CO_2 emissions [3];
- Emissions during mining and stone preparation account for around 0.7% of total CO_2 emissions [3].

In addition to the emissions attributed to the energy consumption of the lime production process, this is also a source of CO_2 emissions. These emissions are constant and amount to 0.785 tonne CO_2 per tonne of lime and 0.913 tonne CO_2 per tonne of dolime [4] (in case of complete conversion of limestone and dolomite and no other impurities).

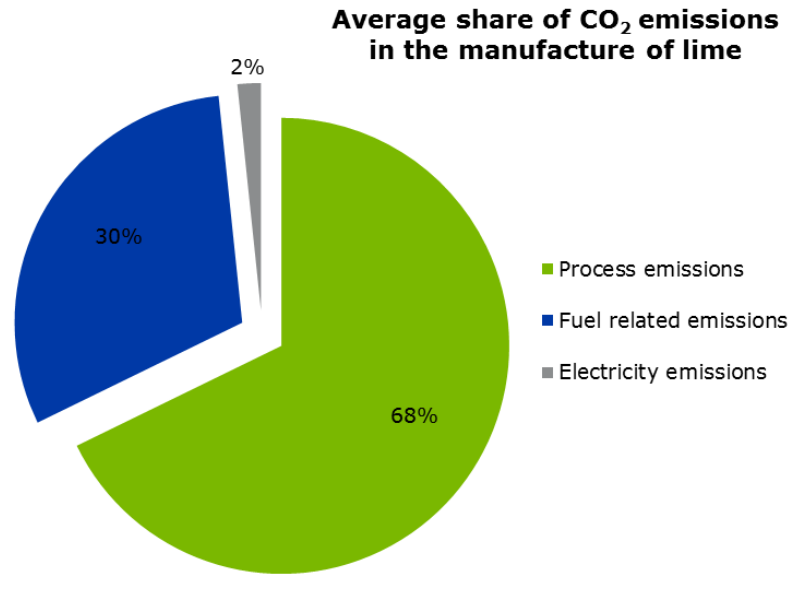

Figure 4 Average share of various CO_2 sources in lime manufacture for 2010 [8].

Table 4 Average CO2 intensities for various lime products in 2010 [8].

Lime product:	Process emissions (tonne CO_2 per tonne lime product)	Combustion emissions (tonne CO_2 per tonne lime product)	Electricity emissions (tonne CO_2 per tonne lime product)	Total emissions (tonne CO_2 per tonne lime product)
Quicklime	0.751	0.332	0.019	1.092
Dolime	0.807	0.475		1.301
Sintered dolime	0.913	0.635		1.567

Total direct carbon dioxide emissions is around 26Mtonne CO_2.

4. Mitigation of CO_2 in lime production

The average fuel use to produce quicklime is 4.25 GJ/tonne, while the heat of reaction – for a typical quicklime quality – is 3.03 GJ/tonne [3]:, 71% of the average fuel use. Theoretically, the potential for energy efficiency improvement for quicklime is therefore limited to 29%; the rest of the fuel is simply needed to provide the energy used in the reaction. This is a theoretical potential, as in reality a driving force is always required to get the reaction going. It is to be regarded as the "impossible to achieve upper limit of energy savings potential". The potential for fuel savings is shown in Figure 5. [2,8]

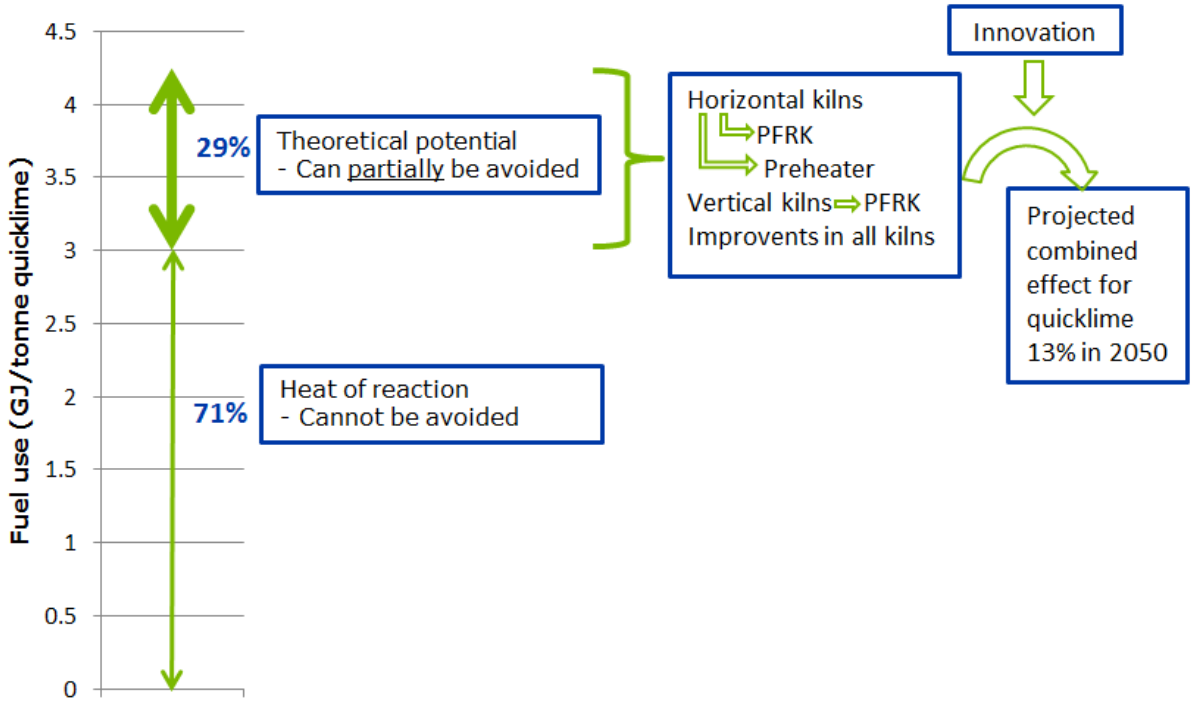

Figure 5 Potential reduction of fuel use and combined effect in 2050 for quicklime [8].

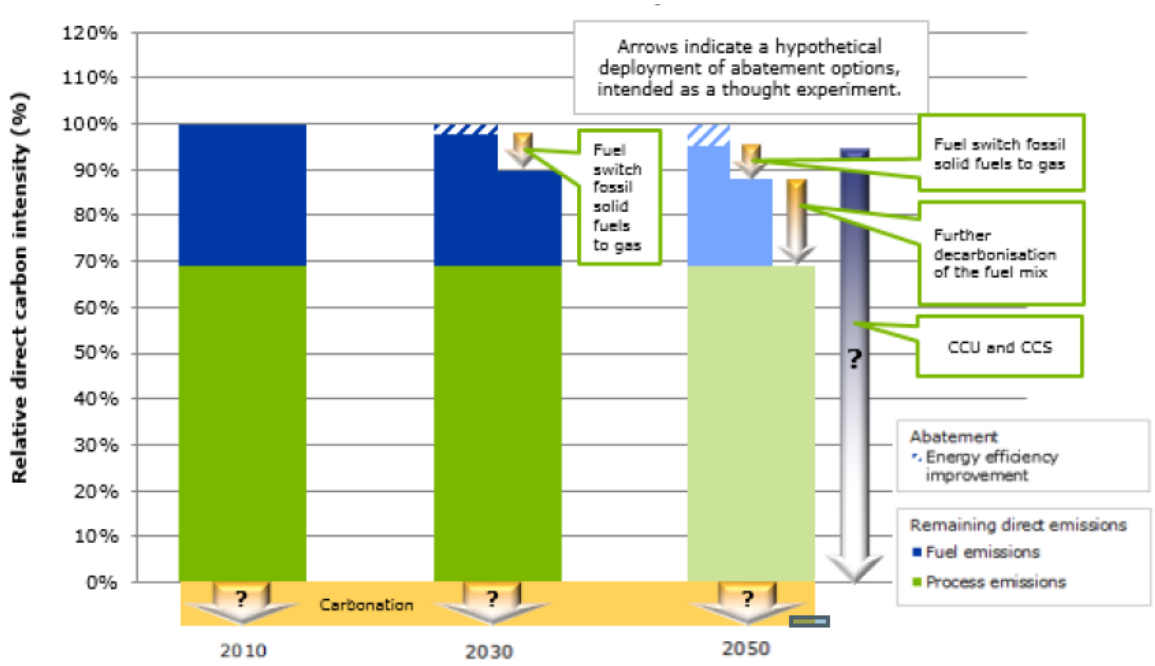

Figure 6 Potential reduction CO_2 emission with different technologies.

Options of decreasing CO_2 footprint [5]:

- Switch from horizontal to parallel flow regenerative kilns
- Switch from long rotary kilns to preheater rotary kilns
- Improved use of waste heat
- use waste as fuel:
  Waste currently accounts for 8% of the total energy content of fuels used in the lime production process.
- Use of gas instead of solid fuels:
  The current fuel mix contains 34% natural gas and 51% fossil solid fuels. Switching from fossil solid fuels use to natural gas would reduce the CO2 intensity of lime production because gas has a lower emission factor than fossil solid fuels.
- Use of gas instead of fossils
- Use of biomass as fuel.
  In case all fuel needed for EU non captive lime production by EuLA members would be supplied by biomass, an order of magnitude calculation shows that the amount of land needed to produce this biomass would be between 800 km2 and 21.000 km2. For Europe, this rough order of magnitude area would be 6.000 km^2
- Use of electricity to heat kilns
- Solar heat:
  For solar thermal technologies to provide the heat needed in the calcination process, the heat quality should be at least 900°C. In the future, high-temperature Central Receiver Systems (CRS) with pressurised air could reach temperatures up to 1000 °C. A prototype receiver demonstrated a receiver temperature up to 1000 °C (DLR, 2005). Due to differences in the composition of the atmosphere and the weather, good irradiation circumstances for CRS are usually found in arid and semi-arid areas with reliably clear skies (typically at latitudes between 15° to 40°, North or South) (IEA, 2010). Thus the most southern parts of Spain and Italy, as well as Greece and Turkey could become viable locations for solarpowered lime production.
- Carbon capture and storage technologies
- Carbon capture and utilization

5. Conclusion

The optimal selection of technology and fuel mix brings potentially significant reduction of CO_2 from lime production. Two third of emissions originates from raw material and the biggest potential reduction come from Carbon Capture and Storage and Carbon Capture and Utilization. The most economical way is to work efficiency,

References

[1] Innovation in the lime sector. Available online: https://www.eula.eu/2017-eula-innovation-report/ (accessed on 10 September 2019).

[2] Innovation in the lime sector 2.0. Available online: https://www.eula.eu/2018-eula-innovation-report/ (accessed on 10 September 2019).

[3] IMA – Europe (2014) Lime Recycling Available online: https://www.eula.eu/lime-recycling-sheet/ (accessed on 10 September 2019)

[4] Innovation in the lime sector 2016 Available online: https://www.eula.eu/2016-eula-innovation-report/ (accessed on 10 September 2019)

[5] OATES, J.: Lime and Limestone, 1998 WIlley, 475 s

[6] BOYTON, R.: Chemistry and technology of lime and limestone, 1980 WIlley, 578 s

[7] Innovation in the lime sector 2013 Available online: https://www.eula.eu/2013-eula-innovation-report/ (accessed on 10 September 2019)

[8] A competitive and efficient lime industry. Available online: https://www.eula.eu/category/resources/publications/(accessed on 10 September 2019).

[9] 2018-2019 Activity report EULA. Available online: https://www.eula.eu/2018-2019-eula-activity-report/(accessed on 10 September 2019)

[10] Competitiveness of European Cement and Lime Sectors 2018 Available online: https://ec.europa.eu/growth/content/competitiveness-european-cement-and-lime-sectors_en (accessed on 10 September 2019)

DEVICE FOR REGULATION OF THE FLAME LENGTH IN THE THERMAL AGGREGATE

Róbert Dzurňák[1*], Ján Kizek[1]
[1]Faculty of Materials, Metallurgy and Recycling, Technical University of Košice, 04200 Košice, Slovakia;
jan.kizek@tuke.sk (J.K.);
*Correspondence: robert.dzurnak@tuke.sk; Tel.: +421-55-602-3228

Abstract
At present, the modernization of thermal aggregates is aimed at increasing energy efficiency and reducing the amount of technology emissions. One such way is the enrichment of combustion air with oxygen. Increasing the oxygen in the combustion air leads to an increase in the combustion temperature and to the reduction of the amount of fuel to achieve the same performance. The result of this change is to reduce of amount emissions. In the article the authors approached the issue of combustion of gaseous fuels with oxygen enrichment of combustion air. They focused on the design of the combustion device (burner) given achieving a constant flame length at various concentrations of enriched oxidizer. The positive effect of flame length preservation during the heating of the charge material in the thermal aggregate was confirmed by experimental measurements and mathematical simulations. The evaluation criteria are the temperature field in the furnace space, the amount of emissions generated and the combustion rate of the gas-air mixture in the burner.

Keywords: oxygen enhanced combustion; burner; air nozzle; flame length

1. Introduction

Current trends show that energy-demanding industrial units require more attention. Despite extensive research and finding new ways of increasing the energy efficiency in industrial facilities is aggregate efficiency remains low. Global energy and environment policies push manufacturers towards increasing the thermal efficiency of thermal equipment while reducing emissions from technological processes. The current trend in the operation of these types of thermal aggregates is air-fuel combustion, in which fuel is combusted with oxygen-enriched air or oxy-fuel combustion [1,2]. The issue of oxy - combustion was largely addressed by Baukal, who reviewed in the publications [3,4] the effects and methods of using increased oxygen concentration in the oxidizing agent in the process of combustion and heat exchange in thermal aggregates. The main advantage of using increased oxygen concentration in the combustion process is the increase in combustion temperatures. Figure 1 shows the graphical dependence of the theoretical combustion temperature and theoretical combustion temperature with dissociation from the oxygen concentration in the oxidizing agent. Warmer flue gases heat the batch material more quickly, causing an increase in the production of the thermal aggregate. The disadvantage, however, is the lower production of combustion products from the combustion process, which in turn affects the proportion of heat transfer by convection. The decrease in the amount of flue gas produced by burning $1m^3$ of natural gas is shown in Figure 1. In pure oxygen combustion, the amount of flue gas produced is approximately 3.6 times less than in air combustion. The reason is the elimination of nitrogen from the combustion process in the thermal aggregate. Building on the knowledge of Baukal, an experimental thermal aggregate was designed and constructed at the Technical University of Košice, Faculty of Materials, Metallurgy and Recycling, at the department of Thermal Technology and Gas Industry (TTaGI) to investigate the effect of oxy-combustion on heat exchange in an experimental thermal aggregate. The findings of this research were published in a book [5]. In terms of heat exchange and temperature field distribution, the effects of oxy-combustion were found to be negligible as the distance from the burner gradually increased. The same trend was observed by the authors in the publication [6]. On the other hand, increasing the oxygen concentration led to a shortening of the flame front, thereby moving the temperature field distribution closer to the burner. Based on this information, a burner was developed at the TTaGI department, which intensified heat exchange in the heat generator by shifting the flame front. The flame front was moved to the area that was detected when burning with air. This type of burner has been successfully tested on an experimental rotary melting furnace for aluminium processing. Previous results from the research were published in a journal [7].

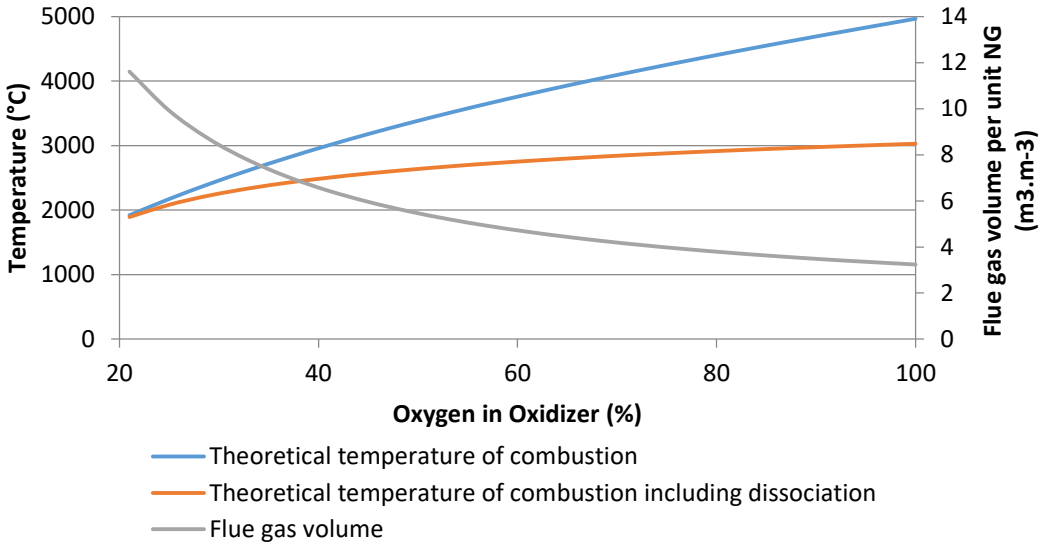

Figure 1 Theoretical combustion temperature including dissociation and flue gas volume per unit of NG - Natural Gas as a function the oxygen concentration in the oxidizer (calculated on the basis of the mathematical model).

2. Experimental device

The objective of the research was to analyse the heat transfer and aluminium-melting process in the experimental facility when the flame front is shortened. This is caused by the increase in the oxygen concentration in the oxidising agent within the range of 21 to 50 %. Experiments were carried out on the tilting rotary kiln (Fig.2) with the inside diameter of 305 mm and length 607mm. The angle of inclination of the experimental model during the measurement was 7%. In total 16 thermocouples of type K (NICr-NiAl) PTTK-TKb-60-2-SP were located in the furnace. The measurement uncertainty stated by the manufacturer is at the level of +/- 2.5 °C at the temperature of 1200 °C. The aim of the thermocouples was to monitor continually the change in the temperature field in the combustion chamber, lining, stack and charge. The experimental model was statically fixed due to the placement of thermocouples around the circumference of the casing and did not rotate during the measurement. The flue gas composition was analysed by the flue gas analyser TESTO-350XL. Other relevant parameters related to the furnace operation were recorded by the furnace control system. The charge was formed of the aluminium ingots with the dimensions 5 x 10 x 2.5 cm. The total charge weight was 15 kg. To achieve the comparability of the individual measurements, the melting was finished when achieved was the temperature of charge at the level of 740°C.

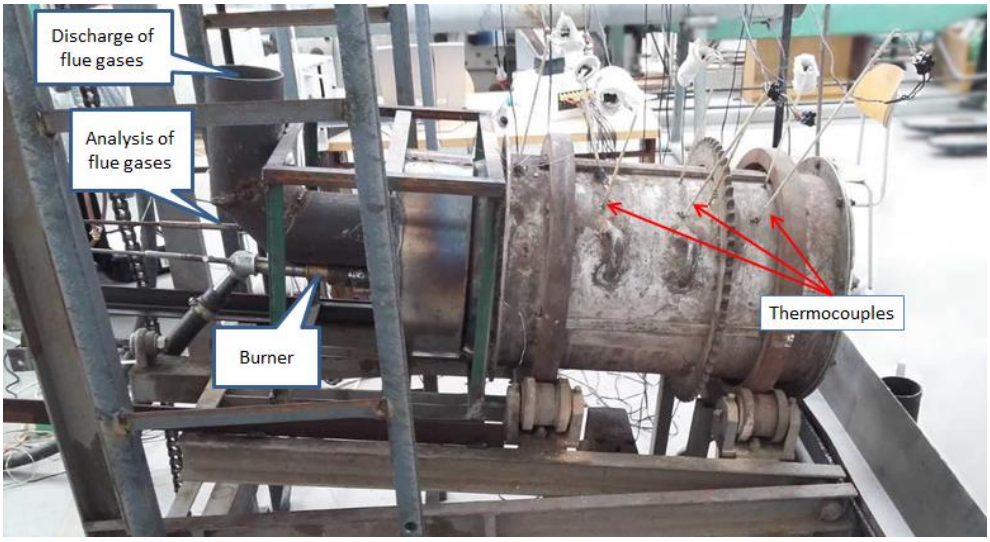

Figure 2 Experimental model of the tilting rotary kiln.

2.1 Device for regulation flame length

The burner is based on a device which gradually changes the diameter of the air nozzle based on the required oxygen concentration in the combustion process. The device has been designed to compensate the outflow orifice when the oxygen concentration in the oxidizing agent changes with respect to the change in the amount of flue gas produced according to figure 1. and the combustion rate of the gas-air mixture. The combustion rate of the gas-air mixture for the change in oxygen concentration is given equation by (1) for methane-based gaseous fuels. Equation 1 was determined empirically based on experimental measurements and the coefficients were determined by regression analysis [7].

$$u_n = -8.4\text{x}10^{-7}\ O_2^3 - 1.0898\text{x}10^{-4}\ O_2^2 + 0.06228767\ O_2 - 0.94666177 \quad (1)$$

Where: O_2 - is the oxidizer oxygen concentration (vol. %)

The experimental measurements were carried out using a burner with 13.5 kW input power for the natural gas combustion. Due to the shortening of the flame front at higher concentrations of oxygen in the oxidation mixture, the outlet diameter of the burner was modified during the experimental research according to oxygen concentrations in the oxidizer at the constant fuel flow. The burner orifice was modified (according to the equation (2) [8]), so that the flame length was the same for each examined level of oxygen enrichment of the oxidizer. On the basis of the equation (2), the flame length in air fuel combustion was set to 42 cm. The increase of the oxygen concentration results in the reduction of the combustion mixture amount, and hence the outlet rate of the mixture w_m decreases. For the purpose of studying the impact of the increased oxygen concentration in the air on the combustion process, an upstream burner was selected. The burner consists of a closed gas tube with a diameter of 8 mm, with four holes with the diameter of 2.5 mm transversally drilled along the perimeter to ensure better mixing of fuel and oxidizer. Construction modifications of the burner consisted in producing an optimised air nozzle for each examined level of oxygen enrichment of the oxidizer. The increase of the oxygen concentration was ensured by injecting oxygen into the combustion air inlet.

$$L_{fl} = r\sqrt{\left(\frac{w_m}{u_n}\right)^2 - 1} \quad (2)$$

Where L_{fl} - is length of flame (m), r - is diameter of the burner outlet orifice (m) ,w_m - is outlet rate of the mixture (m.s^{-1}) ,u_n - is normal combustion rate of the oxidising agent and gas mixture (m.s^{-1}).

Table 3 Volume flows of the inlet media depending on the oxygen concentration in the oxidiser.

Parameter	Unit	Value				
Burner power	kW	13.5				
Excess of combustion air	-	1.1				
Oxygen enrichment	%	21	25	30	35	40
Gas flow	m^3.h^{-1}	1.32	1.32	1.32	1.32	1.32
Air flow	m^3.h^{-1}	14.33	11.42	8.89	7.07	5.71
Oxygen Flow	m^3.h^{-1}	-	0.61	1.14	1.52	1.8
Diameter of Nozzle (D1)	m	0.044	0.026	0.023	0.019	0.016

The advantages of using a flame length control device for various oxygen enrichment of the oxidizing agent are shown in Figure 3. by varying the efficiency of the thermal aggregate. The efficiency of the device was defined by equation 3[7]. Within the range of combustion of natural gas with the oxidant enrichment at the level of 21% -30% at the air nozzle there is a linear increase in efficiency. The efficiency gain in this case is 6%. When optimizing the outflow through the flame length control device, the increase in the oxidation agent enrichment range is 10%. It can be seen from Figure 3 that, when using a flame length control device, it is possible to reduce the oxygen concentration in the oxidizing agent to achieve comparable efficiency to using an air nozzle

at higher concentrations. Thus, in addition to increasing the efficiency of the heat generator, it is possible to reduce the input costs of its operation.

$$\eta = \frac{Q_{UH}}{Q_{CV}.\dot{V}_G.\tau}.100 \quad (3)$$

Where: Q_{UH}- is useful heat use for melt aluminium batch (kJ);Q_{CV}- is calorific value of natural gas (kJ*m^{-3});V_G - is volumetric flow of natural gas (m^3*s^{-1});τ – is time (s).

In the case of a technological process such as melting aluminium ingots in rotary drum furnaces, the Q_{UH}, Q_{CV} and V_G components can be considered constant. The effect of the oxidant enrichment will only affect the heating rate of the batch material, which means that the time required to melt the batch will decrease as the concentration in the oxidant increases.

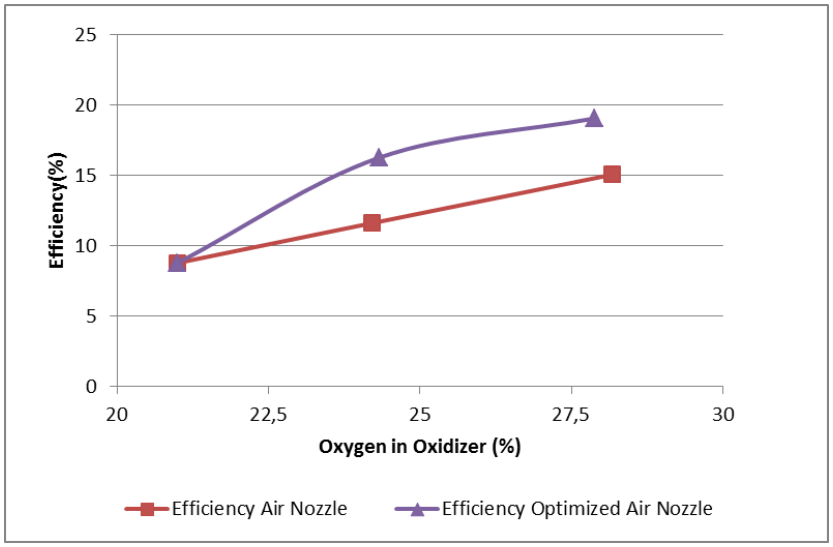

Figure 3 Comparison of the energy efficiency depending on the oxidizer oxygen concentration and burner type (calculated on the basis of the measurement results).

3. Mathematical modeling

The influence of the air nozzle diameter on the combustion process in the physical model of the rotary furnace can be determined on the basis of the mathematical modelling results. Mathematical modelling enables investigation of the flame shape, flue gas flow, temperature field distribution, heat flow to the charge and the distribution of concentrations of individual components under the stabilised conditions [9,10,11].

The mathematical model was developed in Ansys Fluent 17.2. The mathematical model of the physical model was discretized on a computational network, which was optimized for correct results. The combustion space was created by means of tetrahedral grids and was concentrated in the area of the walls and burner where larger gradients were assumed by the prismatic layer, which ensured correct formation of the velocity field. The computing network contained 5 prismatic layers. The accuracy of the number of prismatic layers as well as the setting of the prismatic layer algorithm was verified by cold model simulation, where the Y + parameter was monitored and compared in post-processing. The batch was created using a 10 mm side hexahedral grid to ensure correct calculation of the thermal gradients per charge and to minimize the impact of the grid on the result. The total computing network consists of almost a million cells. The network quality rating based on skewness was a maximum of 80%, which is defined as good based on parameters.

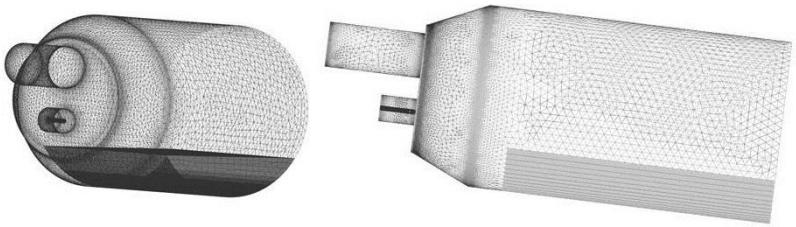

Figure 4 Mesh of mathematical model.

Boundary conditions are an auxiliary function in solving CFD model, which solves differential equations in models. The correct definition of boundary conditions is the basis for correct results of the mathematical model. The Realizable k-ε model was used to calculate the turbulent flow. For the combustion model, the Methan Air WGS global reaction scheme was used with the nitrogen emission calculation module on. Adjustment of the flow rate of fuel and oxidizing agent (Table 1) was set according to the results of the statics of natural gas combustion with the oxidation agent enrichment at an excess of oxidizing agent m = 1.1 and a fuel consumption of 1.31m^3 * h^{-1}.

The results of the mathematical modelling confirmed the hypothesis that the increase of oxygen concentrations in the oxidizer causes the shortening of the flame. Figure 6 (on the left) illustrates the temperature fields at the ordinary air nozzle diameter and oxygen concentrations in the oxidizer within the range from 21% to 50%. On this basis, the flame shape and the temperature distribution in the combustion chamber related to the changes of oxygen concentrations in the oxidizer can be determined. The results of the CFD simulations suggest that for this particular type of a burner with the conventional air nozzle, the oxygen enrichment of the oxidizer cannot exceed 50% during the combustion process. When the oxidizer oxygen concentration is higher, backflash into the burner or possible thermal damage to the burner orifice can occur.

On the basis of the mixture combustion rate, a constant flame length can be maintained by optimizing the burner air nozzle diameter. The results of the mathematical modelling shown in Figure 4 (on the right) confirmed the possibility of optimizing the air nozzle diameter, when the oxidizer is enriched in accordance with the equation (2).

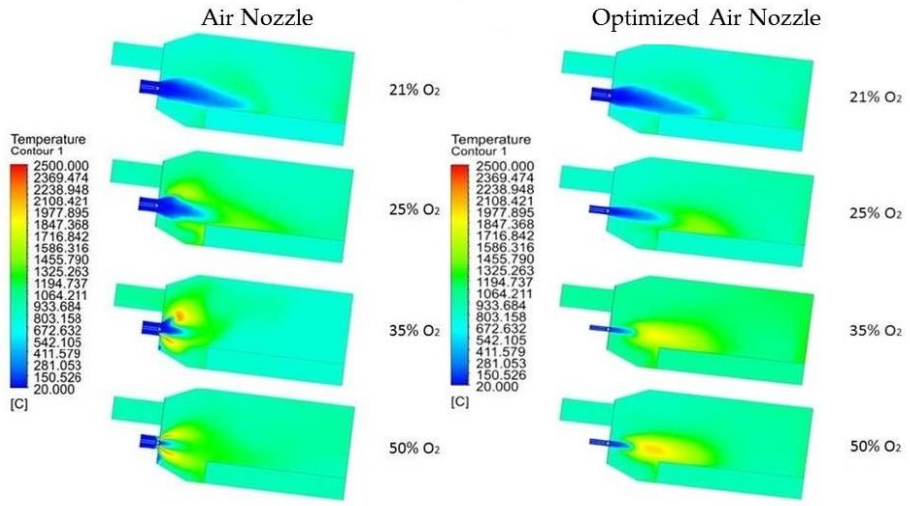

Figure 5 The temperature fields of the experimental device using ordinary air nozzles (on the left) and optimized air nozzles (on the right) for various levels of the oxidizer oxygen enrichment.

Based on the results of mathematical modelling, we can determine the effect of increased concentration on the distribution of the temperature field around the charge material. Shifting the flame queue towards the charge causes temperatures to rise at the flue gas-charge material interface. In experimental measurements it is not possible to measure the change in the temperature field over the whole area at this point, so

mathematical modelling is a suitable tool for this analysis. Figure 5 shows the average temperature values at the flue gas-charge material interface. From the analysis of the temperature changes at this interface and the results of the heat balance of experimental measurements, it can be assessed that the increase in the efficiency of the thermal aggregate is directly proportional to the temperature change at the flue gas-charge material interface.

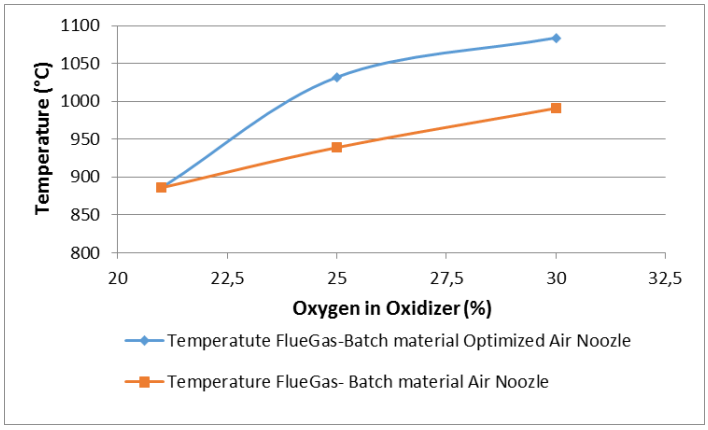

Figure 6 Comparison of the average temperature on the interface Flue Gas- Batch material depending on the oxidizer oxygen concentration and burner type (calculated on the basis of the mathematical model).

In connection with the change in combustion rate, the change in the flow rate of the flowing media also plays an important role. In the air nozzle, the kinetic energy of the oxidant stream is reduced, thereby significantly affecting the actual mixing of the resulting combustible mixture at the burner mouth. From Figure 6, it is evident that at a simulated oxygen level in the oxidizing agent of 30%, due to a change in the ratio of flowing media in a given burner, the combustible mixture cannot be transported further away from the burner mouth. In the case of an optimized air nozzle, the kinetic energy of the oxidizing agent stream remains approximately the same and the oxidizing agent stream entrains the natural gas into the space above the charge where combustion takes place. Worse mixing of the mixture of natural gas with an oxidizing agent can be deduced from the CO emission results, which arise mainly due to insufficient oxidation of the natural gas molecules in the combustion process. The constituents oxidize CO emissions as a result of high temperatures in the heat aggregate and reach only trace concentrations at the flue gas outlet. Based on the results of mathematical modelling, the CO emission concentration at the optimized air nozzle is 0.3ppm and at the air nozzle 7.7ppm. These values cannot be considered relevant due to the absence of experimental measurement results. However, it is believed that by better mixing the mixture and prolonging the residence of the flue gas in the furnace space, the CO emission will be less for the optimized air nozzle.

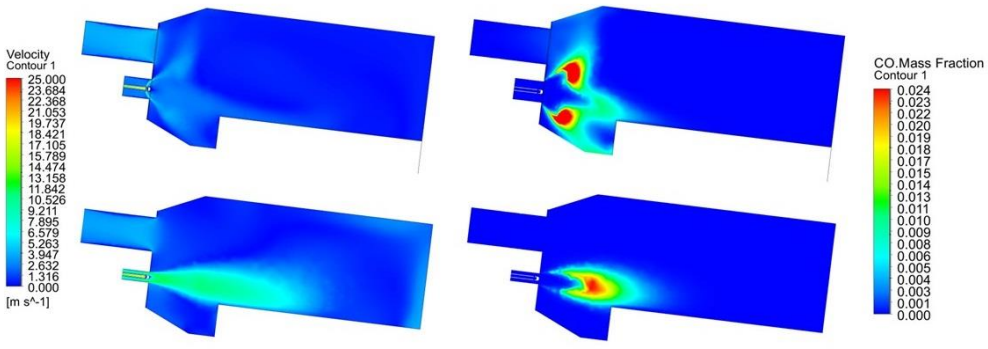

Figure 7 Velocity and CO mass fraction in experimental device using air noozle and optimized air noozle for 30% concentrations of oxygen in oxidizer.

4. Conclusion

Based on the result experimental measurement and mathematical modelling of device for regulation flame length it can be stated that a suitable optimisation of the air nozzle at increased oxygen concentrations in the oxidizer leads to better combustion condition and improve energy efficiency of thermal aggregate. From the environmental point of view, the main benefit is the reduction of emissions released to the atmosphere. With the expected improvement of the thermal efficiency of thermal aggregate using the optimized air nozzle, the experimental measurements performed show that further research in this field is possible. The results obtained reflect trends in EU energy policy and, therefore, research in the field is useful and highly topical.

Acknowledgement

This publication was supported by the VEGA 1/0691/18 project and obtained results are a part of the solution from this grant project.

References

[1] OECD Organization for economic Cooperation and Development (2010), Material case study 2: Aluminium, in OECD Global Forum on Environment. Available online: https://www.oecd.org/env/waste/46194971.pdf (accessed on 10 October 2018).

[2] R. D.Naranjo, J.Kwon, R.Majumdar, W. T. Choate, Advanced melting technologies: Energy saving concepts and opportunities for the metal casting industry, 2005. U.S Department of Energy, Available online: https://www1.eere.energy.gov/manufacturing/resources/metalcasting/pdfs/advancedmeltingtechnologies.pdf (accessed on 12 October 2018)

[3] Baukal CH.E. Oxygen- Enhanced Combustion, 2nd ed.; CRC Press, Boca Raton, USA, 2013; ISBN 9781439862285.

[4] Baukal CH.E. *Industrial burners handbook*, 1st ed.; CRC Press, Boca Raton, USA, 2004; ISBN 9780203488805.

[5] Jablonský G.; Pástor M.; Dzurňák R. Enriching the combustible mixture with oxygen in practice (in Slovak). TU of Košice, Košice, 2015; ISBN 978-80-5532414-2

[6] Poskart A.; Radomiak H.; Niegodajew P.; Zajemska M.; Musiał D. The Analysis of Nitrogen Oxides Formation During Oxygen - Enriched Combustion of Natural Gas. Arch. Metall. Mater. 2016, 61, 1925–1930. DOI: 10.1515/amm-2016-0309

[7] Dzurňák, R.; Varga, A.; Kizek, J.; Jablonský, G.; Lukáč, L. Influence of Burner Nozzle Parameters Analysis on the Aluminium Melting Process. Appl. Sci. 2019, 9, 1614. DOI: 10.3390/app9081614

[8] Fík,J.: Natural gas Tables,diagrams,equations,calculations (in Czech),ČSTZ,2006;ISBN 8086028224

[9] Rimár, M. Kulikov, A.: NOx formation in combustion of gaseous fuel in ejection burner / - 2016. In: AEaNMiFMaE 2016. - S.l. : AIP, 2016 P. 020051-1-020051-6. - ISBN 978-0-7354-1402-0 - ISSN 0094-243X

[10] Kulikov, A.; Fedák, M.; Abraham, M.; Váhovský, J.: Study of the gaseous fuel combustion respect to the O2 concentration and NOx formation / - 2018. In: Advances in Thermal Processes and Energy Transformation. Roč. 1, č. 1 (2018), s. 23-26 . - ISSN 2585-9102.

[11] Nieckele A.O.; Naccache M.F.; Gomes M.S.P. Numerical Modeling of an Industrial Aluminum Melting Furnace. J. Energy Resour. Technol. 2004, 126, 72–81. DOI: 10.1115/1.1625396

POSSIBLE USE OF WASTE HEAT FOR THE ELECTRIC POWER PRODUCTION

Peter Ďurčanský[1*], Andrej Kapjor[1] ,Jozef Jandačka[1]
[1]Faculty of Mechanical Engineering ,University of Žilina Univerzitná 8215/1 Žilina 01026, Slovakia
*Correspondence: peter.durcansky@fstroj.uniza.sk; Tel.:+421- 41- 513 - 2860

Abstract
A necessary condition for energy efficiency is to increase the efficiency of existing facilities, including heat recovery. The supply of thermal energy in our country is currently heavily dependent on the import of energy sources. The constant increase in the prices of energy resources leads to a reassessment of the relationship of consumers to efficient use of all types of energy and to savings in its production. Therefore, in order to further develop the economy and to ensure an adequate quality of life, it is necessary to increase energy security by effective use of low and medium potential thermal energy sources. This is the main objective, why the recovery of waste heat is becoming a necessary trend. Of the various options, the heat recovery from waste air and flue gas using a heat recovery exchanger is currently most commonly used. Industrial waste heat can be considered as the most important secondary energy source. This paper presents the possibilities of utilizing waste heat for the purposes of electricity production.

Keywords: waste heat; heat recovery; hot air engine

1. Introduction

Heat recovery is used in many technical fields and is often referred as recuperation, although recuperation can be considered as recovery of any form of energy. An important area of heat recovery is industry, typically the metallurgical industry. In metallurgy, air entering the blast furnaces, which is preheated by the waste heat of the working gases, is a clear example. It is also possible to use waste heat in various chemical and drying processes, but also for the production of ferroalloys and ceramic insulators, or in the food industry during milk pasteurization. [1] Current trends show that more than 96% of the steel produced in the world is processed by continuous casting. In view of this, there is a naturally increasing pressure on producers of refractory materials used in the continuous casting process. The process of using heat recovery is one of the ways to reduce the cost of heat energy through heat exchangers. Heat exchangers in heat exchangers are usually involved in all three ways of heat transfer (conduction, convection, radiation). The most common are those exchangers where the flow prevails, so the design and thermal calculation of the exchangers is based on the general laws of thermokinetics and fluid mechanics. In addition to industrial technologies, it is possible to use heat recovery also for heating and air-conditioning systems of apartment and family houses. One of the other solutions without negative consequences on the environment may also be the use of alternative energy sources in micro-cogeneration, especially hot-air engines and their use in combined heat and electricity production, while heat supply can be external, not only from renewable sources, but also from waste heat.

2. Hot air engines

Hot air engine is a heat engine in which atmospheric air is used as the working substance. It uses the expansion and compression of air influenced by its temperature change, which makes possible to convert heat to mechanical energy. Stirling engine is a heat engine which can be described as reciprocating engine with external combustion, with two interconnected linear spaces with different temperatures. [2] They work with a closed circulation of the working substance, which is alternately heated and cooled. As the working gas can be used air, but is preferable to use helium or hydrogen for their smaller molecular weight and higher thermal conductivity, making it possible to achieve a higher efficiency of the machine. The engine operates between two reservoirs of heat supply and heat dissipation to working substance in the system at constant temperature (as in the Carnot cycle). The engine consists of a cylinder with two pistons on each side and regenerator in the middle. Ericsson engine is similar to the Stirling engine with the difference that to working substance is heat not supplied and not collected isochoric but isobaric. The principle of Ericsson engine operation consists on engine that contains two cylinders with pistons of different sizes. This engine allows complete separation of working substance - air and combustion products and effectiveness of the device significantly increases the regenerator like at Stirling engine. [3]

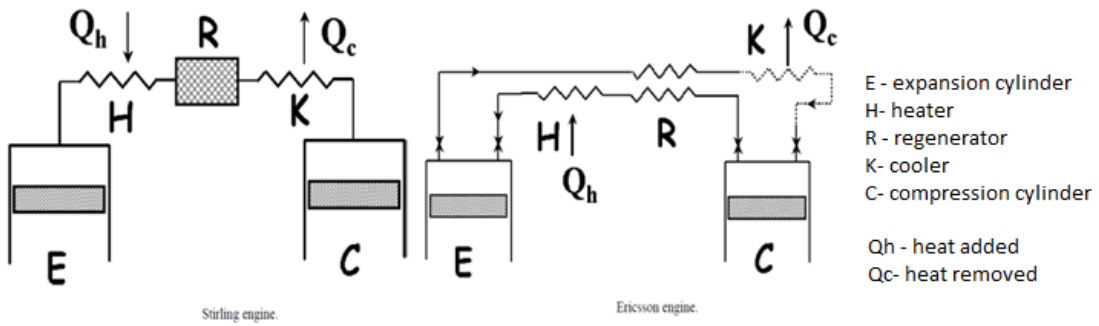

Figure 1 Stirling engine and Ericson engine.

2. Numerical simulation

The Stirling engine is theoretically divided into five characteristic control volumes, according to Fig. 1: expansion cylinder (E), heater (H), compression cylinder (C), regenerator (R), and cooler (K). These are represented by control volumes, the advanced adiabatic model, worked out according to [3], is based on the basic equations of mass and energy equilibrium, with a state equation applied to each control volume. The working gas mass is defined by ideal isothermal Schmidt analysis [4], where this analysis is taken into account as first step. The calculation is performed for the Stirling engine of the Cleanergy C9G cogeneration unit. The engine design is a two-piston engine of the alpha model with a phase shift of 90 °. The heatsink, heater and regenerator are tubular exchangers. The working medium is helium.

Ericsson engine simulation is similar to the Stirling engine activity with the difference that to working substance is heat not supplied and not collected isochoric but isobaric. For this purpose, numerical model was developed with help of Matlab Thermolib library, as shown in Fig. 2.

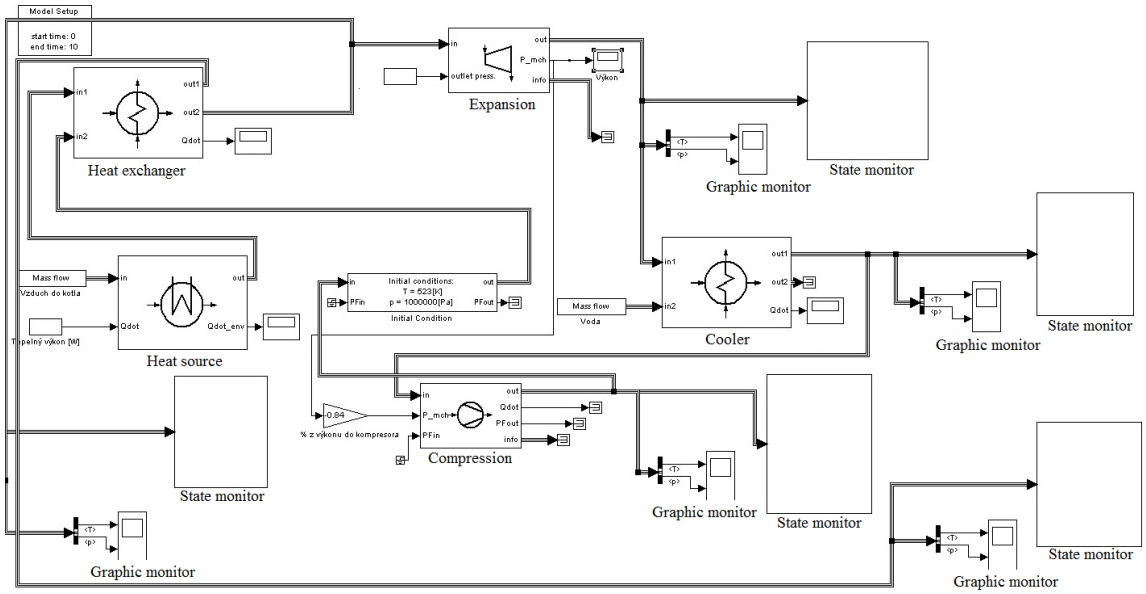

Figure 2 Block diagram of Ericson engine in Simulink.

For the calculation it is necessary to know at least the initial values of working temperatures, which are the result of adiabatic processes and enthalpy flow. The only clue to their correct selection is that their end-of-cycle values should be equal to their respective values at the start of the cycle. [5], [6] To evaluate the potential electrical power of the cogeneration unit, a performance characteristic was constructed from the inlet temperature on the heater and the mean working pressure of the medium in the engine. The theoretical electrical power can be calculated even for small temperature differences between the heater and cooler. The

mechanical parts of the engine only come into contact with clean air, which is advantageous in terms of service life. The proposed hot-air Ericsson engine will be a double-acting double-cylinder with mass flow of 50 g/s. Each cylinder will have a compression volume at the bottom of the cylinder and an expansion volume at the top. The maximum circulation temperature behind the heater-heat exchanger will be 500 ° C. [7], [8] The lowest circulation temperature will be considered at 90 ° C at the chiller outlet. [9]

3. Results

The calculation of the Stirling engine was made for the Stirling hot air engine, which is part of the Cleanergy C9G cogeneration unit. The engine is a two-cylinder with V-shape cylinder arrangement, with displacement of 160 ccm, using helium as the working medium. The heat source is a gas burner at the top integrated with the combustion chamber in one unit made of stainless steel. The used material must be characterized by high strength and high temperature resistance, which is conditioned by the purity of the base material. [10] Natural gas, LPG and treated gas from the biogas plant can be used as fuel. The electric power of this motor is from 2 to 9 kW. The heat output varies from 8 to 25 kWt when the working gas pressure is changed. Unit noise is less than 58 dB. Total efficiency at max. load is declared by the manufacturer at 96%, of which 25% represents electrical efficiency. The calculation was carried out at different engine operating pressure settings as shown in the following Figure 3, according to heat source temperature as the main variable. There we can see the change of net power output of the engine, that varies from 800 up to 5000 W. Every line represents another working medium pressure. As we can see, the pressure plays significant role in net power output and has maybe more impact than temperature.

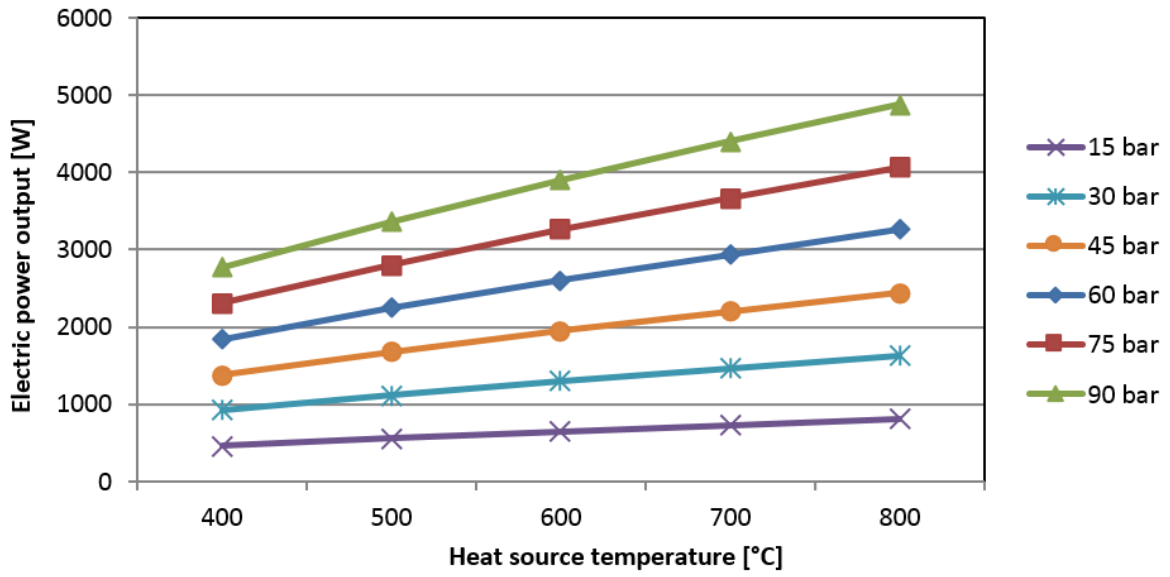

Figure 3 Stirling engine net power output.

The calculation of the proposed hot-air Ericsson engine was performed with help of Matlab – Thermolib. State changes of the working substance at all points in the working cycle were calculated, from these calculations we determined the basic operating parameters - maximum operating pressure of 2.5 MPa in the high-pressure branch and 1 MPa in the low pressure branch. The Ericsson engine was simulated only for one pressure, due to the high temperature dependence of the power output. Higher pressures are also possible to achieve, but there is problem with operating time. In Figure 4 we can see very strong dependence of Ericsson engine on temperature.

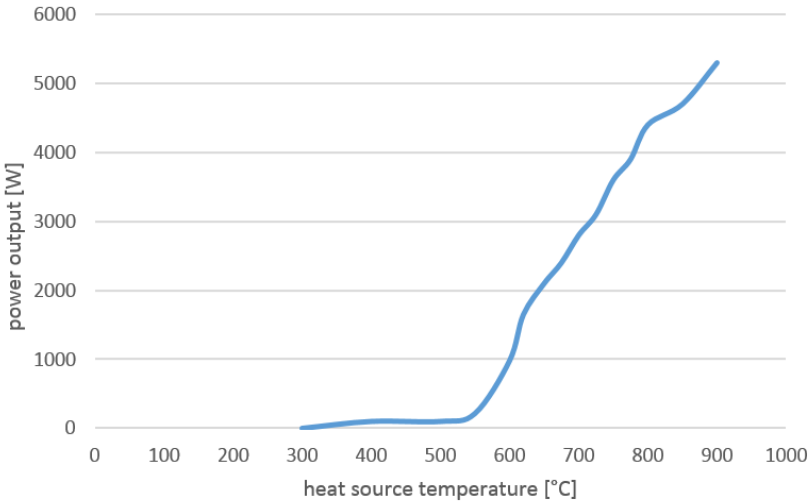

Figure 4 Ericsson engine net power output.

4. Conclusion

Within the current trend in life and global technology development, there is an increasing demand after innovative solutions for the production of pure and less-carbon energy. Searching for such technologies which will achieve high energy efficiency of production and meet strict requirements, whether standards or users, represents the future in the production and supply of buildings energy. One of the alternatives that seeks to promote as a modern resource and the replacement for conventionally available technologies is use of waste heat. Use of this kind of energy for heating is well known topic and is used in many companies. But electricity production from heat due to high procurement price, up to 30 times higher than commonly available technologies, and also operating costs of these high-end technologies are unfavorable circumstances that lead to the conclusion that the facilities are not in the present time and present state in research field competitive compared to the traditional way of electricity supply. One solution is the current experimental research of cheaper types of materials for use in such technological devices, as hot air engines are.

Acknowledgement

Work on article has been financially supported by the project VEGA 1/0479/19 “Influence of combustion conditions on production of solid pollutants in small heat sources”, and project VEGA 1/0233/19 Structural modification of burner for combustion of solid fuels in small heat sources.

References

[1] Masaryk, M., Gróf, G., Pospíšil, J., Hernik, B., Lepszy, S. Green energies in V4 countries. 1st. ed. Bratislava, Porta Danubiana, 2014. 123 p. ISBN 978-80-971479-1-4.

[2] Finkelstein, T., Organ, J. A. *Air engines*, 2001, Three Park Avenue, New York, ISBN 0-7918-0171-3

[3] Urieli, I. - Berchowitz, D. M. 1984. Stirling cycle engine analysis. Bristol: Hilger

[4] Karafiát, J. a kol. Sborník technických řešení zdrojů s kombinovanou výrobou elektřiny a tepla. Ortep 2006, Praha.

[5] United States Patent n. 5 894 729, date: apr. 20, 1999

[6] Bonnet S., Alaphilippe M., Stouffs P.: Energy, exergy and cost analysis of a micro-cogeneration system based on an Ercsson engine.

[7] Organ, A. J. Stirling Cycle Engines. London: John Wiley & Sons, Ltd., 2014. 272 s. ISBN 978-1-118-81843-5

[8] NEMEC, P., HUŽVÁR, J. Proposal of heat exchanger in micro cogeneration unit, configuration with biomass combustion, Materials science and technology, 2011, ISSN 1335-9053

[9] KLIMEŠ, L.; CHARVÁT, P.; HEJČÍK, J. Comparison of the energy conversion efficiency of a solar chimney and a solar PV-powered fan for ventilation applications. ENERGIES, 2018, roč. 11, č. 4, s. 912:1 (15 s.) ISSN: 1996-1073.

[10] Bul’ko, B., Molnár, M., Demeter, P., Pribulová, A., Futáš, P. Study of the influence of intermix conditions on steel cleanliness, Metals, Volume 8, Issue 10, 19 October 2018, Article number 852

MODIFICATION OF LIQUID FESI75 FERROSILICON LADLE REFINING TO IMPROVE ITS PURITY

Stanisław Gil[1*], Wojciech Bialik[1], Bolesław Machulec[1], Sławomir Kozłowski[2]
[1]Faculty of Materials Engineering and Metallurgy, Silesian University of Technology, Katowice, Poland, EU, , wojciech.bialik@polsl.pl, boleslaw.machulec@polsl.pl,
[2]Re Alloys Ltd., Łaziska Górne, Poland, EU, slawomir.kozlowski@realloys.pl
*Correspondence: stanislaw.gil@polsl.pl

Abstract

The paper presents a proposed modification of liquid FeSi75 ferrosilicon ladle refining with technical gases to improve its purity. Depending on the requirements, refining gases can be oxygen, air or oxygen-enriched air. Compression gas will be delivered to liquid metal through a gas lance or, optionally, through a specially designed porous plug located in the ladle bottom (the gas lance was used in the experiments). Physical model studies have shown that the optimal depth of lance immersion should be 2/3 of the metal height in the refining ladle. Chemical composition analyses of individual fractions of both ordinary and refined FeSi75 ferrosilicon after the process of mechanical milling and sieving have confirmed the presented mechanism of carbon removal during ferrosilicon refining through floatation of SiC carbide inclusions in liquid metal bath using slag-forming CaO, Al_2O_3, MgO carriers. The most considerable changes in refined ferrosilicon chemical composition refer to elements with a high oxygen affinity that form oxidation-related slag (Ca, Al).

Keywords: Ferrosilicon; submerged arc furnace; casting ladles; improving purity of alloy

1. Introduction

Global economy requires continuous improvement of a product and reduced costs of its production. Similar policies also refer to the metallurgical industry, although the need of product improvement is more difficult to satisfy in this field. Implementation of sometimes minor innovations may significantly improve the product quality and result in considerable economic benefits. Due to their properties, iron-silicon alloys are widely used in the metallurgical and chemical industries. The most popular ferrosilicons are FeSi65 and FeSi75 types, used in the steel industry for steel deoxidation and as alloy additives. Silicon is a component of many steel and alloy types, including spring, bearing, stainless, heat-resistant and electrical steels as well as structural steels for the construction industry. It can also be applied in processes of silicothermic reduction of oxides. Depending on the temperature, in equilibrium conditions of the binary system Fe-Si, a few iron-silicon compounds (silicides), such as FeSi, $FeSi_2$, Fe3Si7, Fe_5Si_3, Fe_2Si and FCC or BCC iron matrix-based solid solutions (Figure 1) that precipitate during the solidification process, can be found [1]. Industrial-type ferrosilicons also contain small amounts of other elements, such as Al, Ca, Mg, Mn, Cr, Ti, P or S, which are impurities. Their fractions depend of the quality of raw materials and physicochemical processes that occur during electrothermal reduction of silica with carbon in a submerged arc furnace [2]. Therefore, ferrosilicon should be considered a multicomponent system. In a finished alloy, these impurities may appear in various phases in the form of non-metallic and intermetallic compounds. A small fraction of carbon in ferrosilicon is important when the alloy is used in manufacturing of high-quality, special-purpose steels. Carbon is particularly unwelcome in certain alloy steels due to carbide formation, leading to depletion of alloy component in ‘pericarbide’ zones and resulting in poorer strength, plastic and anticorrosive properties. As quality requirements for steel increase, there is a higher demand for ferrosilicon with a very small carbon content.

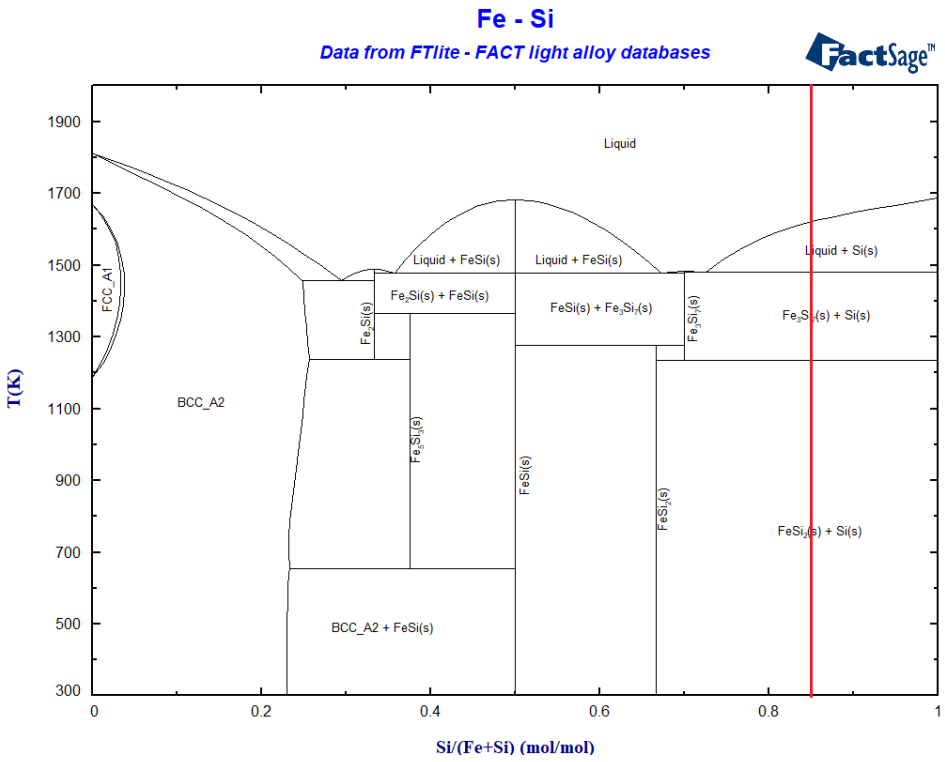

Figure 1 The equilibrium system Fe-Si available for the FactSage users, obtained with the use of FTliht database (of light alloys) [1].

In ferrosilicon, carbon mainly occurs as carbide SiC which is one of the intermediate products in the process of silica reduction with carbon. For most elements, the solubility limit in solid-state silicon and ferrosilicon is small and dissolved elements precipitate as inclusions or form intermetallic compounds during solidification. Carbon solubility in liquid silicon and ferrosilicon, in equilibrium with SiC(*s*), depends on temperature and decreases at lower temperatures. This results in precipitation of secondary SiC(*s*) inclusions in liquid alloy [3-6]. In addition to silicon carbide, ferrosilicon may contain other carbides of such trace elements as Ti, Ca, Al or Mg (e.g. TiC, CaC_2, Al_4C_3, Al_4SiC_4, MgC_2, Mg_2C_3). Carbon solubility in silicon is not high but some amounts may dissolve in other phases that are iron-matrix solutions.

2. Composition and parameters of technical gases solution blown into the refining ladle

One of the ways of non-metallic inclusion content reduction in liquid metal is its refining in a ladle through technical gas purging. Gas bubbles, moving to the liquid metal surface, facilitate flow of non-metallic inclusions. Depending on the type of process, refining gases can be inert gases or their mixtures with other gases as well as nitrogen, oxygen, air or oxygen-enriched air. In addition to stirring of metal bath alone or metal bath with refining slag, gas can participate in oxidation of additives. Compressed gas can be delivered to liquid metal through a porous plug located in the bottom of the refining ladle or through a gas lance. The scheme of a ferrosilicon refining system with a gas lance immersed in liquid metal is presented in Figure 2. Physical model studies [7] have shown that the optimal depth of lance immersion should be 2/3 of the metal height in the refining ladle. Assuming that for the ladle in Figure 2, containing 8 Mg (tons) of FeSi75 ferrosilicon, the height of metal surface is about 1600 mm, the gas lance head should be located at the depth of approximately 1000 to 1200 mm. Due to the decarbonisation process, a non-graphite lance is recommended. Therefore, an air-cooled lance is suggested. In addition, to ensure a properly high gas outflow velocity, enabling volume penetration of liquid metal by gas streams, the lance should be fitted with a replaceable head with holes of appropriate diameter and shape. Pressure of gas delivered to the lance must overcome hydrostatic pressure of the metal bath and flow resistance of the lance head nozzles resulting from required outflow velocity.

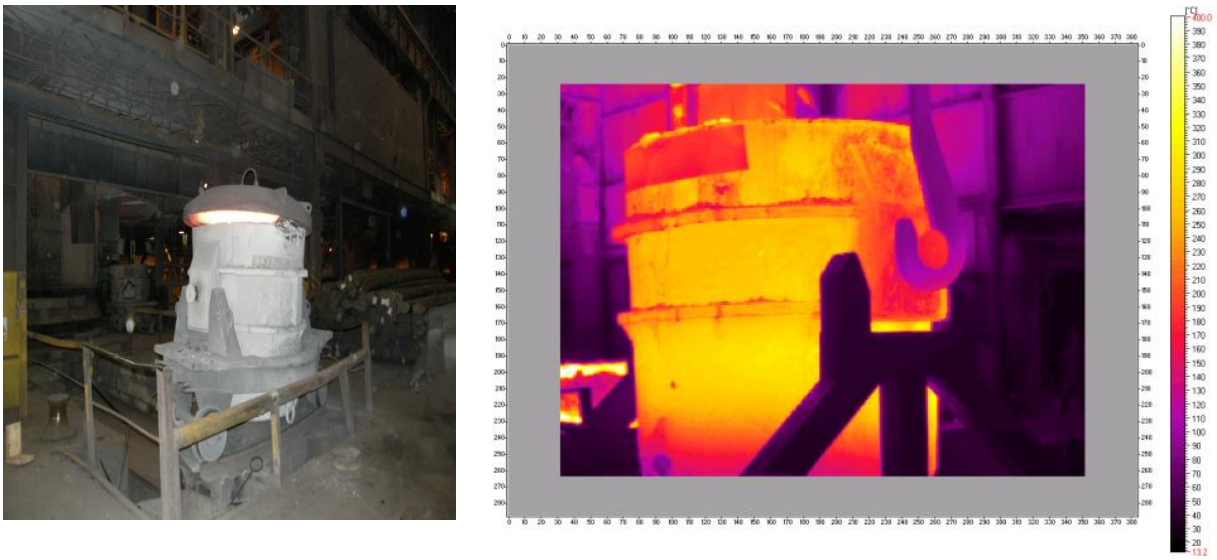

1 refining ladle, 2 gas lance in a thermal cover, 3 gas lance head,
4 refining gas stream, 5 cover of the ladle, 6 refinery gas connector

Figure 2 Photos and scheme of a refining ladle with a gas lance.

Hydrostatic pressure can be calculated using the following formula:

$$p = g \cdot h \cdot (\rho_a - \rho_g), \quad (1)$$

where: p – hydrostatic pressure, Pa; g – gravitational acceleration m s^{-2}; h – depth of lance immersion in liquid, m; ρ_a – alloy density, kg m^{-3}; ρ_g- gas density, kg m^{-3}. Because the gas density in formula (1) is far smaller than the alloy density, it can be neglected in engineering calculations. Assuming the FeSi75 ferrosilicon density at 1450 °C is 3400 kg m^{-3}, the formula (1) result suggests that hydrostatic pressure does not exceed $4 \cdot 10^4$ Pa, but in the case of lance fitted with a nozzled head, a higher pressure of $1.5 \cdot 10^5$ to $2.5 \cdot 10^5$ Pa is required to overcome nozzle resistance and to ensure properly high gas outflow velocity. In industrial practice, to achieve the effect of smooth metal bath stirring with no metal splashing out of the ladle, gas pressure should be adjusted in an experimental manner by observation of liquid bath surface in the ladle. To reduce radiation heat loss to the environment, the ladle is fitted with a cover containing a slot for outflowing gases. Based on the mechanism of carbide inclusion removal from the metal bath (mediated by slag resulting from dissolved Al, Ca,

Mg oxidation), natural air, oxygen-enriched air or pure oxygen can be the best refining gases. Industrial experiences from previous years, related to liquid ferrosilicon dealumination with the use of INJECT oxidising refining method [8], show that with application of appropriate silica-based synthetic slags, oxygen use for Al, Mg, Ca oxidation is not necessarily associated with silicon loss. This is due to chemical reactions between slag and liquid metal in the oxidising environment [8]:

$$[\mathrm{Al}] + \frac{3}{4}(\mathrm{SiO_2}) = \frac{3}{4}[\mathrm{Si}] + \frac{1}{2}(\mathrm{Al_2O_3}), \qquad \Delta \mathrm{H}_{1723} = -131.325\ \mathrm{kJ} \tag{2}$$

$$[\mathrm{Ca}] + \tfrac{1}{2}(\mathrm{SiO_2}) = \tfrac{1}{2}[\mathrm{Si}] + (\mathrm{CaO}), \qquad \Delta \mathrm{H}_{1723} = -170.594\ \mathrm{kJ} \tag{3}$$

Reactions (2) and (3) are highly exothermic, which additionally improves the thermal balance of refining process and enables its longer duration. Therefore, a combination of ferrosilicon decarbonisation and dealumination processes is worth considering. Smaller additive contents in ferrosilicon are beneficial for its durability, which is related to formation of a smaller 0–3 mm subgrain amount in the mechanical milling process. Additionally, reduced Al contents in the alloy may result in a higher sale price. The above considerations show that the use of inert gas for the refining process is not advisable because the same effect of metal bath stirring in the ladle can be achieved when compressed air is applied for liquid metal purging. In addition to pressure, another important parameter to determine is the size of refining gas stream. With no exothermic reactions, gas that flows through liquid metal leads to its cooling. It has been confirmed by results of previous attempts to purge liquid metal with compressed oxygen-enriched air using a bath-immersed lance of the 45 mm inner diameter [9]. The report does not contain detailed data on refining gas consumption or composition but the measurement values demonstrated a faster temperature decrease of about 3.5 K min^{-1} during the refining process while the same parameter during smelting with no gas purging reached a mean value of 2.0 K min^{-1}. The tests did not result in expected refining improvement compared to smelting without refining gas purging. Therefore, pure oxygen is suggested to be used in further refining attempts by means of gas purging. To estimate the quantitative gaseous oxygen requirements, Table 1 data were used and it was assumed that after the refining process in oxidising environment, a higher Al and Ca content reduction should be achieved to ensure a final Al content in the alloy of less than 0.5 %. Chemical composition analyses of individual fractions of both ordinary and refined FeSi75 ferrosilicon after the process of mechanical milling and sieving have confirmed the presented mechanism of carbon removal during ferrosilicon refining through floatation of SiC carbide inclusions in liquid metal bath using slag-forming CaO, Al_2O_3, MgO carriers. The most considerable changes in refined ferrosilicon chemical composition refer to elements with high oxygen affinity that form oxidation-related slag (Ca, Al). In stoichiometric calculations, it is assumed that mean Al content will be reduced from 0.9 % to 0.45 % while Ca content: from 0.1 % to 0.05 %, which (with the weight of liquid metal bath of 8 Mg) is, respectively: 36 kg of Al and 4 kg of Ca. Thus, the overall gaseous oxygen requirement for Al and Ca oxidation is 33.62 kg (23.53 m_n^3). Assuming a 15-minute period of oxygen purging, the stream of refining gas in the form of gaseous oxygen should correspond to about 0.037 kg s^{-1} (1.6 m_n^3 min^{-1}). In reality, some gaseous oxygen will only be used for warm metal bath stirring as, due to kinetic issues, not all amounts of gas delivered to the ladle can undergo chemical reactions. It can be assumed, however, that as a result of liquid metal stirring, some metal bath-dissolved Al and Ca amounts can participate in slag-metal reactions (2) and (3) without gaseous oxygen. After the process of metal bath purging with oxygen, the ladle should remain still for 10 minutes so that slag and carbide inclusions can emerge to the bath surface. The exothermic effect of Al and Ca oxidation with gaseous oxygen results in slower metal cooling and ensures longer duration of the refining process.

Table 1 Chemical composition changes for individual fractions of ordinary and refined FeSi75 ferrosilicon following the process of mechanical milling and sieving [9].

Grain range (mm)	Fraction (mm)	Chemical composition (wt. %)										
		Al	Ca	Ni	Ti	C	Cu	Cr	Fe	Mn	P	Si
ordinary 10 - 60	> 60	1.51	0.270	0.038	0.123	0.053	0.110	0.018	24.4	0.196	0.023	73.2
	40 - 60	1.44	0.256	0.036	0.116	0.067	0.107	0.021	23.5	0.181	0.024	74.2
	20 - 40	1.42	0.263	0.036	0.121	0.061	0.109	0.028	23.8	0.186	0.023	73.9
	10 - 20	1.47	0.282	0.036	0.116	0.113	0.110	0.019	23.1	0.182	0.023	74.5
ordinary 3 -10	< 10	1.55	0.346	0.035	0.123	0.138	0.109	0.015	23.3	0.188	0.024	74.1
	5 - 10	1.57	0.332	0.035	0.119	0.137	0.113	0.015	23.3	0.185	0.024	74.1
	3 - 5	1.51	0.295	0.036	0.120	0.123	0.116	0.013	23.4	0.184	0.024	74.1
	< 3	1.69	0.295	0.042	0.165	0.099	0.145	0.016	26.2	0.225	0.024	71.0
ordinary 0 - 3	> 3	1.59	0.330	0.036	0.119	0.152	0.114	0.013	23.2	0.183	0.024	74.2
	1 - 3	1.64	0.302	0.037	0.131	0.125	0.118	0.016	23.9	0.191	0.024	73.5
	< 1	1.79	0.338	0.037	0.140	0.112	0.120	0.015	25.3	0.204	0.024	71.8
refined 10 - 60	40 - 60	0.82	0.109	0.036	0.107	0.008	0.128	0.012	24.1	0.192	0.028	74.3
	20 - 40	0.79	0.087	0.038	0.104	0.011	0.132	0.015	24.6	0.198	0.028	74.0
	10 - 20	0.74	0.101	0.038	0.109	0.011	0.132	0.013	24.9	0.200	0.028	73.6
refined 3 - 10	5 - 10	0.84	0.117	0.038	0.106	0.008	0.131	0.017	24.2	0.195	0.028	74.2
	3 - 5	0.86	0.097	0.038	0.109	0.008	0.129	0.012	24.6	0.198	0.028	73.9
	< 3	0.81	0.077	0.034	0.101	0.012	0.125	0.013	23.8	0.189	0.026	72.3
refined 0 - 3	> 3	0.93	0.101	0.034	0.100	0.013	0.116	0.024	24.1	0.186	0.026	74.3
	1 - 3	1.05	0.113	0.037	0.111	0.021	0.129	0.027	24.6	0.199	0.026	73.6
	< 1	1.26	0.147	0.038	0.122	0.045	0.131	0.019	25.5	0.211	0.025	72.4

3. Conclusion

1. The process of solid carbon inclusion removal from the metal bath is affected by slag inclusions of CaO, Al_2O_3, MgO that form as a result of element oxidation during the contact of liquid metal with oxygen. These slags almost entirely moisten SiC carbide and ensure floatation of carbide inclusions in liquid ferrosilicon.
2. One of the ways of non-metallic inclusion content reduction in liquid metal can be its refining through metal purging with technical gases. Gas bubbles that move to the metal bath surface facilitate flow of non-metallic inclusions to the surface. The use of inert gas for the refining process is

not advisable. The same effect of metal bath stirring in the ladle can be achieved using compressed air for liquid metal purging but oxygen purging is recommended.

3. Oxygen is suggested to be the refining gas. Ferrosilicon decarbonisation can be combined with its dealumination. Smaller aluminum contents in ferrosilicon are beneficial for its durability, which is related to formation of a smaller 0–3 mm subgrain amount in the mechanical milling process. Additionally, reduced Al contents in the alloy may result in a higher sale price.
4. For gas purging, a ceramic-coated, air-cooled lance of the 45 mm inner diameter is recommended. To ensure a properly high gas outflow velocity, enabling volume penetration of liquid metal by gas streams, the lance is recommended to be fitted with a replaceable head with holes of appropriate diameter and shape.
5. At the optimal immersion depth of the lance in the metal bath (1–1.2 m), hydrostatic pressure of metal does not exceed $4 \cdot 10^4$ Pa. To achieve the effect of smooth metal bath stirring with no metal splashing out of the ladle, gas pressure should be adjusted in an experimental manner by observation of liquid bath surface in the ladle. When the lance is fitted with a nozzled head, higher pressure of $1.5 \cdot 10^5$ to $2.5 \cdot 10^5$ Pa will be required to overcome nozzle resistance and to ensure properly high gas outflow velocity.

Acknowledgement

The authors acknowledge the support of research project "Innovative technology for the production of ferrosilicon with silicon content min. 75% and ultra-low carbon content max. 0.02% " (Project No POIR.01.01.01-00-0052/17), funded by the Intelligent Development Operational Program 2014-2020.

References

[1] Różański, P. Wykonanie obliczeń termochemicznych z wykorzystaniem oprogramowania FactSage dotyczących równowagi w układzie Fe-Si-O-C w celu ustalenia warunków rafinacji węgla w stopie FeSi75. Sprawozdanie z pracy badawczej Nr B0-1605/BS/2018 wykonanej w IMŻ na zlecenie Politechniki Śląskiej. Gliwice, 2018.

[2] Machulec, B.; Bialik, W. Comparison the physico-chemical model of ferrosilicon smelting process with results observations of the process under the industrial conditions. *Archives of Metallurgy and Materials* **2016,** *61,* 265-270.

[3] Lauri Holappa, L.; Louhenkilpi S. On the role of ferroalloys in steelmaking. The 13th International Ferroalloys Congress: *Efficient technologies in ferroalloy industry*. Almaty, **2013**, 1083-1090.

[4] Panic, B. Influence of the bed type on the flow resistance change during the two-phase (gas plus powder) flow through the descending packed bed. *Archives of Metallurgy and Materials* **2014**, *59*, no. 2, 795 – 800.

[5] Grigorovich, K.V; Shibaev, S.S.; Kostenko, I.V. Ferroalloys for clean steels production and quality specifications. The 12th International Ferroalloys Congress: *Sustainable Future*, Helsinki, **2010**, 929-934.

[6] Merder, T.; Pieprzyca, J.; Warzecha, M.; Warzecha, P. Application of high flow rate gas in the process of argon blowing through steel. *Archives of Metallurgy and Materials* **2017**, *62*, no. 2, 905-910.

[7] Zubov, V.L.; Gasik, M.I. Electrometallurgy of ferrosilicon. Physical Chemistry and Technology. Dnepropetrovsk: System Technologies Publication, 2002.

[8] Schei, A.J.; Tuset, J.K.; Tveit, H. Production of High Silicon Alloys. Trondheim, 1998.

[9] Kozłowski, S. Raport z procesu rafinacji odwęglającej FeSi75. Re Alloys, 2016 (not published).

ASSESSMENT OF THE ENERGY POTENTIAL OF SOLAR ENERGY IN INDUSTRIAL APPLICATIONS

Miroslav Rimár[1], Jakub Váhovský[1*], Olha Kulikova[1]

[1]Faculty of manufacturing technologies with the seat in Prešov, Technical University of Košice, 04200 Košice, Slovakia; miroslav.rimar@tuke.sk (M.R.); olha.kulikova@tuke.sk (O.K.)

*Correspondence: jakub.vahovsky@tuke.sk; Tel.: +421-55-602-6335

Abstract

The submitted paper deals with possibilities of solar energy application in metallurgical industry. The paper presents comparison of the most significant presently working devices which use solar energy concentration. The experimental part is focused on the measurements of the incident solar energy in selected localities in Slovakia. The results provide the theoretical potential for the solar energy application in similar devices, taking into account the sunshine duration as well as the amount of potential energy.

Keywords: solar energy; concentration; solar radiation; energy potential

1. Introduction

In recent years, changes in climatic conditions are also evident in Slovakia. These changes are directly linked with the amount of emissions produced and the pollutants entering to the air. The main producers of pollutants are metallurgical plants, where a number of harmful substances are released during the processing and production of metallic and non-metallic materials. Therefore, there is pressure to reduce emissions by increasing the use of renewable energy sources. These norms are given at the level of both national and European legislation. To meet the stricter criteria, it is necessary to choose an appropriate energy source. Natural conditions, geographical location and infrastructure are decisive factors in deciding on the choice of an alternative energy source. Metallurgy is characterized by high-energy processes, which directly represents a significant problem in supplementing or fully replacing them. This paper evaluates the potential of solar energy in Slovakia as a possible source usable in the metallurgical industry. During the analysis of the potential of electricity production were used photovoltaic panels, as well as solar radiation technologies of medium and high concentration. The evaluation is carried out for selected agglomerations in Slovakia, both in terms of annual operating characteristics of potential production and in terms of local conditions. The use of solar energy has been increasing in recent years, but it is mainly the construction of photovoltaic power plants and small home solar systems. Slovakia is characterized by high segmentation of the relief, which is an important factor in evaluating of the using of solar energy. Other important factors are the amount of incident radiation and the length of sunshine, which depend on the position of the Earth in relation to the Sun.

1.1 Solar radiation

Solar radiation reaches earth's surface consists of three forms of radiation: direct solar radiation, diffuse solar radiation and reflected radiation [1]. The amount of incident sunlight varies during the year and depends on several factors such as declination of the earth, geographical location, season, weather and daylight duration. The inclination and orientation of the collectors are playing an important role in capturing direct radiation. The angle of inclination of the solar collectors is determined according to the operation of the solar system [2]. We know three types of operations: summer operation (20 – 35 °C), winter operation (50 – 75 °C) and year-round operation (35 – 50 °C). In Slovakia, the average annual intensity of solar radiation varies in the interval of 1000 - 1250 kWh/m^2. The distribution of the intensity of solar radiation in Slovakia is shown in Figure 9.

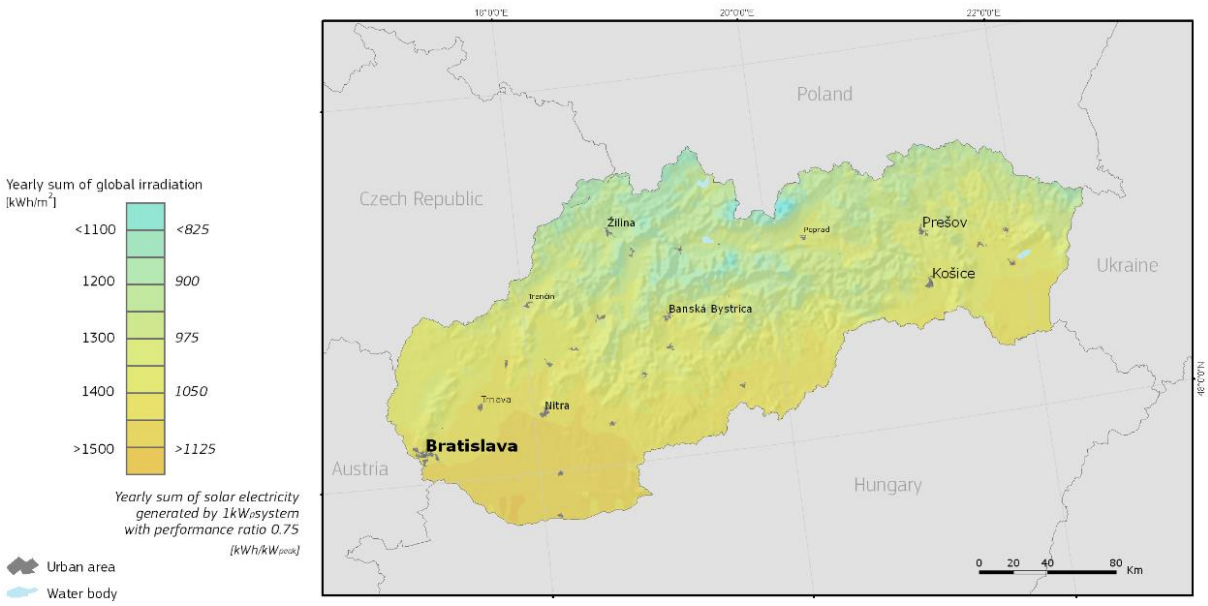

Figure 9 Average annual intensity of solar radiation in Slovakia [3].

2. Experimental Material and Methods

Basically there are two possibilities for conversion solar energy into another form of energy: conversion into electrical or thermal energy. The conversion into electrical energy is divided into direct and indirect conversion [4]. By direct conversion of solar energy we convert the acquired energy directly into electrical energy. And the principle of transformation of solar energy into thermal energy and then with help of other devices into electrical energy is used in case of the indirect conversion of solar energy into electrical energy. Indirect conversion systems are achieves higher efficiency than direct conversion systems. Solar systems, which are operates on the principle of indirect conversion, concentrate the solar radiation by mirrors on a small area where heat accumulates to generate electricity. These solar systems are uses direct radiation, which concentrate in one place – solar receiver. Four basic types of solar systems are used for concentration of solar radiation [5][6][7]:

1. The central tower systems are composed of a large number of parabolic mirrors, which reflecting solar radiation at one point on top of the thermal tower, solar receiver. The mirrors are controlled and follow the movement of the sun during the day and therefore constantly direct solar radiation to the solar receiver of the central tower. In this solar receiver the heat is transferred to the liquid, which is converted into steam, and then generates electricity by driving steam turbines. Heat at the top of the tower is transferred to the thermal storage tank due to the liquid circulation and can also be taken for other industrial equipment. The temperatures in the thermal tower range from 540 °C to 1480 °C;

2. The parabolic trough systems are concentrating the solar radiation into the center of the tube, which is located in the solar receiver of the parabolic mirrors. The whole solar system is turned towards the sun and oil is used as the heat transfer medium. The oil is heated up to 400 °C and is gradually pumped through the heat exchangers, so that the high-temperature steam is produced and it drives the generator;

3. The parabolic dish systems are using a set of dish-shaped parabolic mirrors and concentrate solar radiation into the solar receiver of the dish. In the solar receiver of the dish there is an absorber where the liquid is heated up to 1000 °C. And subsequently this liquid is used to generate electricity in a turbine. It is the most efficient solar system due to its high optical efficiency and low energy loss;

4. The solar updraft tower is working on heating the air under the greenhouse principle. The subsequently heated air creates an air flow that flows through the chimney and drives the wind turbine. Part of the solar radiation heats the salt water tanks. These tanks maintain airflow even without sunlight and allow the plant to operate at night.

The solar concentrators can also be used to reach very high temperatures, which can also be used in high-energy consumption metallurgical processes. Equipment which can utilize such high temperatures are called

solar furnaces [8]. It is a system of spherical shape covered with mirrors, which concentrates solar radiation on a small area. Mirrors are placed opposite the spherical part of the device and they reflect the radiation to the concentrating part. The focal point temperature of the device can reach 3800 °C. The solar furnace can be used to melt steel or produce hydrogen fuel.

At present, concentrated solar thermal energy is not widely used in the production of iron and steel. It is mostly used to verify experimental operating regimes aimed at monitoring of process efficiency, technological aspects, economic indicators as well as environmental impacts. The environmental aspects are currently assessed not only from direct impacts on pollutant production but also from the impact of the environmental footprint from the implementation of the components themselves in the system. There are several concentration solar systems in Europe that are mainly used for testing and experimenting [9][10]:

1. Platform Solar de Alméria - a solar system located in Spain, where are 2 types of solar systems, namely linear parabolic mirrors with an achievable temperature from 120 °C to 500 °C and a pair of solar towers with heliostatic fields of 10000 m^2 and 4000 m^2, with temperature range from 250 to 1100 °C;

2. PROMES - Odeillo solar oven - located in France, it is the world's largest 1000kW solar furnace. The solar furnace consists of a parabolic mirror with an area of 2000 m^2 and an array of mirrors (10000). This furnace can reach temperatures in excess of 3000 °C. In the whole complex there are ten small solar ovens with an output of 1-2 kW and one kiln with an output of 6 kW;

3. Solar Research Division - Cologne – 25 kW solar furnace;

4. Solar Technology Laboratory - Zurich – 40 kW solar furnace.

3. Results and discussions

To select the evaluated sites were chosen cities where are located the largest metallurgy plants and secondary metallurgical producers. These places are located in different parts of Slovakia and have different climatic and relief conditions. Data were obtained from the PVGis database [3]. Figure 2 and Figure 3 shows the energy of solar radiation in individual cities and the average intensity of solar radiation in July and December. These averages were obtained for the period from 2007 to 2016. The intensity of radiation for July is given as the intensity for a 35 °C inclined panel and for December - 55 °C. Areas of Kosice and Sládkovičovo receives more of solar radiation energy, comparing with Podbrezová and Oravský Podzámok which areas have by almost 13 - 14 % less energy. However, an important indication is the distribution of the amount of solar radiation energy in the summer and winter half year. In the summer half year, the most solar radiation is obtained from the Sládkovičovo and Košice regions. Comparing with them the locality of Oravský Podzámok receive by 14 % less solar radiation and in Podbrezová this value is lower by up to 20 %. The lower values of solar radiation are caused by the northern position and the severely rugged relief.

In the winter half year, the amount of solar radiation is significantly lower and it is only from 33 % to 38 % of the annual amount. The differences between the sites are smaller and the northern ones can approach with the southern ones. The areas of Sládkovičovo, Kosice and Podbrezová have almost the same amount of solar radiation. Such equipoise in the amount of solar radiation is caused by frequent weather inversions and fogs that occur in the winter half-year and focus mainly on the lower lying areas. Another factor is the air pollution by metallurgical companies, which is often seen mainly in the form of industrial snow, especially in winter.

Figure 4 shows the share of diffuse radiation in global radiation in 2016 in the regions of Košice (SE SR), Podbrezová (Middle SR), Oravský Podzámok (N SR), Sládkovičovo (SW SR). For solar systems, the direct solar component is particularly important. More of direct radiation received the southern regions of Slovakia, in this case in the areas of Sládkovičovo and Košice. The graph shows that in the summer half the proportion of diffuse radiation in global ranges from 40 % (Sládkovičovo, Košice), 45 % (Podbrezová) to 50 % (Oravský Podzámok). In the winter half-year, the amount of diffuse radiation increases significantly what results that its share in global radiation will also increase. In the area of Sládkovičovo the maximum is 69 %, Košice and Podbrezová – 75 % and Oravský Podzámok up to 80 %, which indicates that the amount of solar radiation usable for solar systems is insignificant.

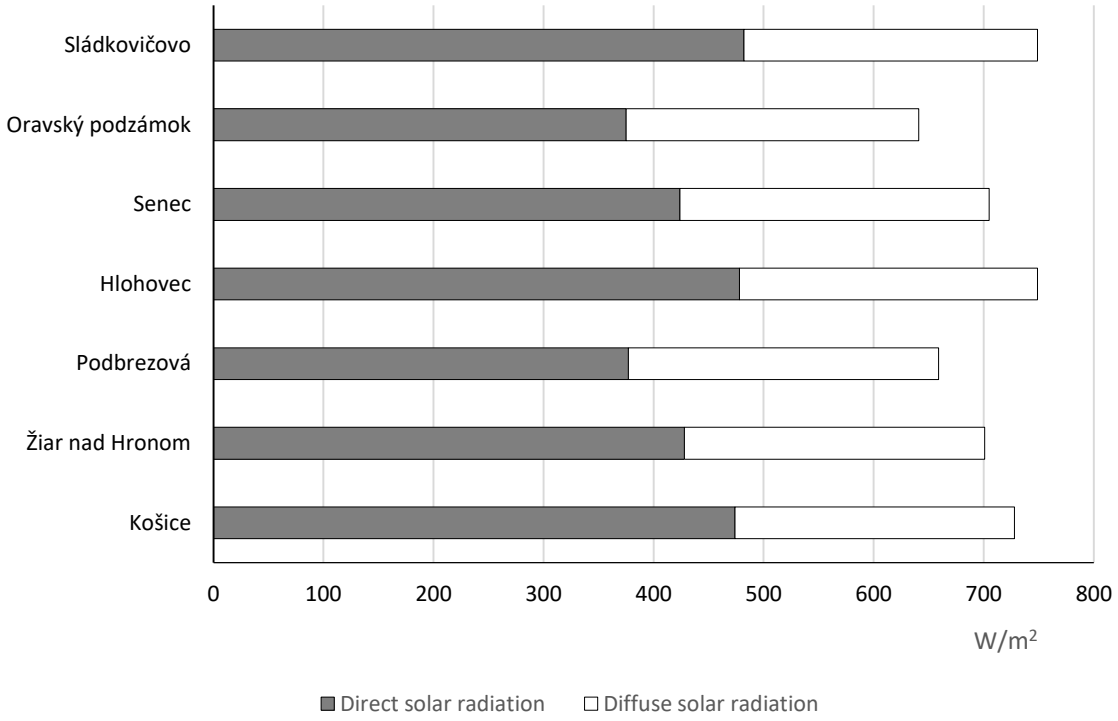

Figure 10 Average solar radiation in selected locations – July.

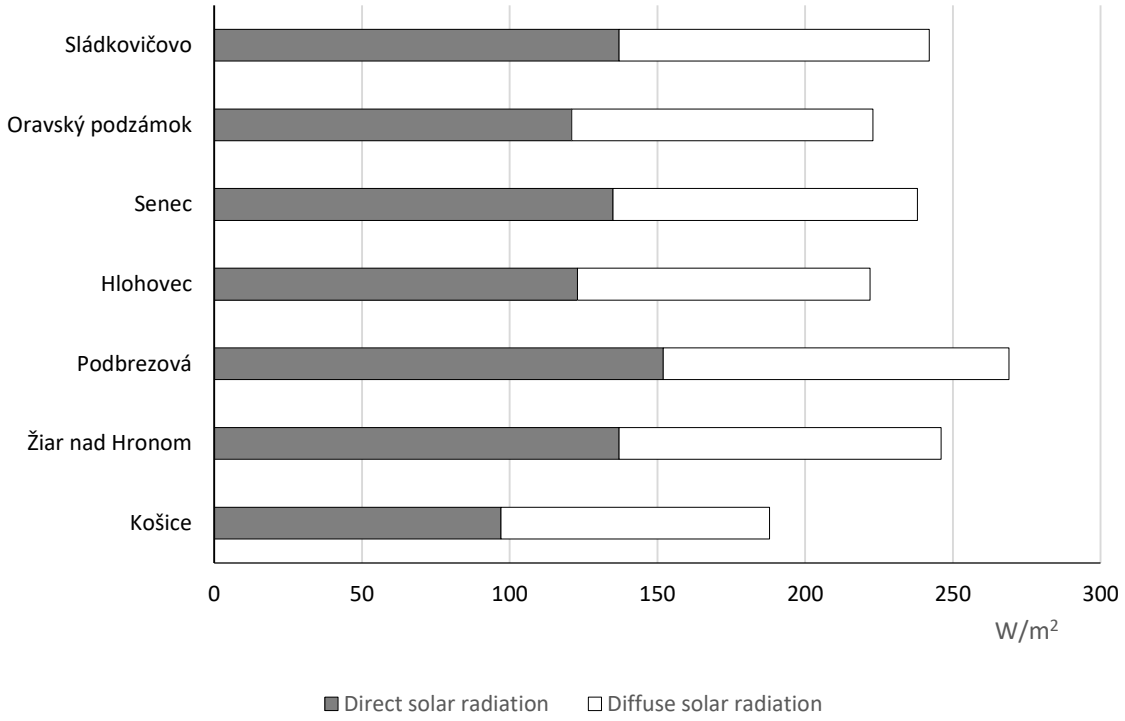

Figure 11 Average solar radiation in selected locations – December.

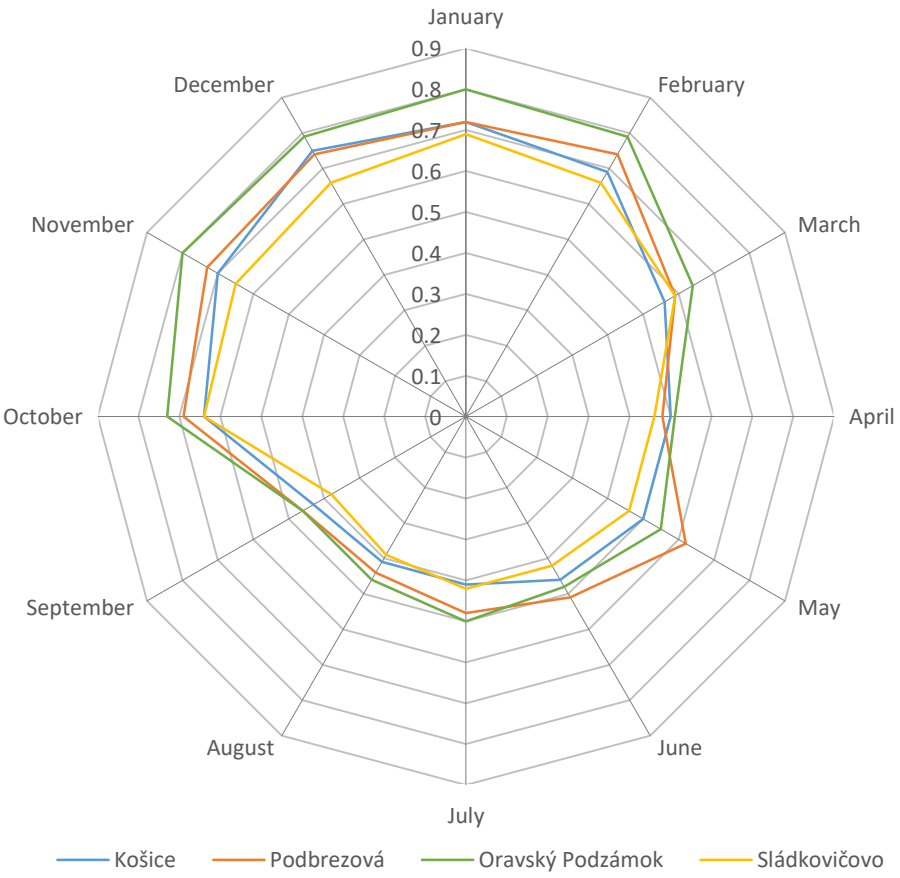

Figure 12 The share of diffuse radiation during the year.

It is possible to use two types of systems to utilize the solar energy, namely photovoltaic systems or solar thermal systems. Photovoltaic systems work on the principle of direct conversion of solar energy into electricity. Solar thermal systems use indirect conversion of solar energy, which means that they firstly convert the sun energy to thermal energy and then use the thermal energy to generate electricity. The efficiency of photovoltaic power plants varies from 3 % to 14 % depending on the type of panels, while for solar thermal power plants it is from 20 % to 30 %. This implies that solar thermal power plants require significantly smaller area for the panels for the same amount of energy comparing to photovoltaic panels. The potential of solar radiation for solar thermal systems is greatest in the summer half year, for the southern regions from April to September and for the northern regions from June to September. In the winter half year, the proportion of diffuse radiation in global radiation is high, which is not an ideal condition for using solar thermal systems. Experimental and research activities are also taking place in the northern latitudes (Cologne), so there is a potential to use these systems in areas with less solar radiation in future.

4. Conclusion

The current climate change is caused by high level of emissions and air pollutants. One of the major emitters and pollutants is the metallurgical sector. There are processes with high-energy consumption used in metallurgy and the equipment of such processes is not easy to replace. The purpose to reduce emissions helps to increase the use of renewable energy sources. One renewable resource of energy is solar, which can be applied in almost all parts of the world and has enormous potential for the future. There are several projects around the world which are using technologies that concentrate solar radiation. Utilization of solar radiation energy requires conditions regarding the amount of incident direct radiation and is not applicable in every region of the world. In Slovakia, the climate and relief conditions for using solar systems are very diverse. During the year, the length and angle of incidence of solar radiation changes significantly. The rugged relief, altitude and natural conditions also have a high impact on the amount of incident radiation. The proportion of diffuse radiation in the winter half of the year ranges from 70 % to 80 % of global radiation in selected areas, which means very low utilization level of solar radiation. Therefore, sometimes, it is not possible to provide

sufficient energy from this source all year round for high-energy consumption processes. The use of technologies based on the concentration of solar energy can be used during the summer half year (from 4 to 6 months), depending on the location. The use of solar energy is also possible through PV systems for electricity generation. PV systems are widespread throughout Slovakia and are now a stable source of electricity generation.

Acknowledgement

The authors would like to thank the KEGA grant agency for supporting research work and co-financing the project KEGA 004TUKE-4/2018.

References

[1] Vrtek, M. Sluneční energie, Ostrava 2012. Available online: https://kke.zcu.cz/export/sites/kke/old_web/_files/projekty/enazp/21/IUT/140_Slunecni_energie_-_Vrtek_-_P3.pdf

[2] Skalík, L. Zvyšovanie výkonu a účinnosti solárnych kolektorov v obytných budovách. TZB HAUSTECHNIK 1/2012. Available online: https://www.asb.sk/stavebnictvo/technicke-zariadenia-budov/solarne-kolektory/zvysovanie-vykonu-a-ucinnosti-solarnych-kolektorov-v-obytnych-budovach (accessed on 15 August 2012).

[3] European Commission, Photovoltaic geographical information system, 2017. Available online: https://re.jrc.ec.europa.eu/pvg_download/map_index.html

[4] Boleman, T.; Fiala, J. Obnoviteľné zdroje energie, Trnava 2009. Available online: http://www.prirodnejavy.eu/sub/energia.pdf

[5] Pavlović, T. M.; Radonjić, I. S.; Pantić, S. L. A review of concentrating solar power plants in the world and their potential use in Serbia. Renewable and Sustainable Energy Reviews, Volume 16, Issue 6, August 2012, Pages 3891-3902. doi: https://doi.org/10.1016/j.rser.2012.03.042

[6] Barlev, D.; Vidu, R.; Stroeve, P. Innovation in concetrated solar power. Solar Energy Materials and Solar Cells, Volume 95, Issue 10, October 2011, Pages 2703-2725. doi: https://doi.org/10.1016/j.solmat.2011.05.020

[7] European Commision. Eurpean Research on Concentrated Solar Thermal Energy. 2004, 39pp. Available online: https://ec.europa.eu/research/energy/pdf/cst_en.pdf

[8] Rodriguez, J.; Cañadas, I.; Zarza, E. New PSA High Concetration Solar Furnace SF 40. AIP Conference Proceedings 1734, 070028. 2016. doi: https://doi.org/10.1063/1.4949175

[9] Fernández-González, D. ; Ruiz-Bustinza, I.; González-Gasca, C.; Noval, P. J.; Mochón-Castaños, J.; Sancho-Gorostiaga, J.; Verdeja, F. L. Concentrated solar energy applications in materials science and metallurgy. Solar Energy, Volume 170, August 2018, Pages 520-540. doi: https://doi.org/10.1016/j.solener.2018.05.065

[10] The European Alliance SolLab. Alliance of European Laboratories for Research and Technology on Solar Concentrating Systems. Available online: https://www.sollab.eu/index.html

ANALYSIS OF THE ENERGY CONSUPTION DURING THE ELECTRIC ARC PROCESS

Piotr Migas[1*], Michał Moskal[2*], Mirosław Karbowniczek[1], Jacek Czyż[2]
[1]AGH-University of Science and Technology, Faculty of Metals Engineering and Industrial Computer Science, 30 A. Mickiewicza Av., Krakow, Poland; mkarbow@agh.edu.pl; pmigas@agh.edu.pl;
[2]COGNOR SA Branch HSJ in Stalowa Wola, Kwiatkowskiego 1, Stalowa Wola, Poland; mmoskal@hsjsa.pl,
*Correspondence: pmigas@agh.edu.pl, mmoskal@hsjsa.pl

Abstract
Electrical energy consumption and optimization of the chemical energy contribution in the process of melting the charge in the electric arc furnace is a decisive importance in steel production costs. The development of mathematical model that takes into account the relationships of electrical and chemical energy input or output to the steel production process, especially in industrial conditions, is not easy. This is mainly due to the fact that it is not possible to measure some parameters, such as eg. thermal losses. Analysis of the energy consumption, using industrial technological data of the electric arc furnace with a nominal capacity of 45 Mg was presented in this paper. The developed model makes it possible to calculate the theoretical demand for electric energy needed for the process and to compare this quantity with the measured values. In the case of furnaces with lower production capacity it seems necessary to more accurately characterize energy efficiency and the ability to control and optimize the production process.

Keywords: electric arc process; energy consumption; modelling of energy demand

1. Introduction

A modern electric arc furnace during its operation (steelmaking) uses a few energy sources. They can be generally broken down into: energy transferred by means of electricity – burning arc, and by means of chemistry – combustion of fuels and exothermic reactions. The main aspect of its economic and efficient operation in the production conditions is the optimisation of proportion of electrical and chemical energy consumption. In addition, it is very important to effectively use the energy introduced into the process, including the application of the slag foaming process. The foundation of analysis of these issues is the conducted heat balance of the steelmaking process in the electric arc furnace [1, 3].
Each of the process components impacts the energy efficiency. A proper method of loading the charging basket with scrap is to protect the furnace bottom against damage during charging, to reduce the likelihood of electrode breaking and to ensure a fast melting process. In addition, selecting scrap with a suitable form influences the kinetics of its melting, which translates into energy efficiency of the process and the time of a single melting process [4].
The electrical energy is the basic source of heat necessary to carry out the melting process in an electric arc furnace. Modern processes, in particular as regards production of common carbon steels, contain aspects intensifying the scrap melting process, in order to reduce the melting time. It is possible thanks to the application of various methods of adding chemical energy. Here we have gas-oxygen burners, oxygen lances, after-burning lances, introducing recarburization agents, etc. Another important method of process intensification, and at the same time reduction of the electric power consumption is increasing the furnace transformer power and improving the energy utilisation ratio. It is because only a part of the electrical energy transformed to heat in the burning arc is used for the execution of a metallurgical process. The ratio of energy utilisation largely depends on the arc “uncovering”, or “holding” the thermal energy radiating within the melt. At the initial phase of scrap melting the burning arc is covered with scrap, and the whole thermal energy from the arc is effectively utilized to heat and melt the scrap. However, at the final melting phase and at the subsequent melting process stages, the burning arc is not covered with the scrap, and a substantial part of the generated thermal energy radiates to the furnace walls and little amount of it is directly used for the process execution [1-4].

2. Heat balance of the steelmaking process

The impact of process parameters and the EAF design on the demand for electrical energy is schematically presented in Fig. 1.

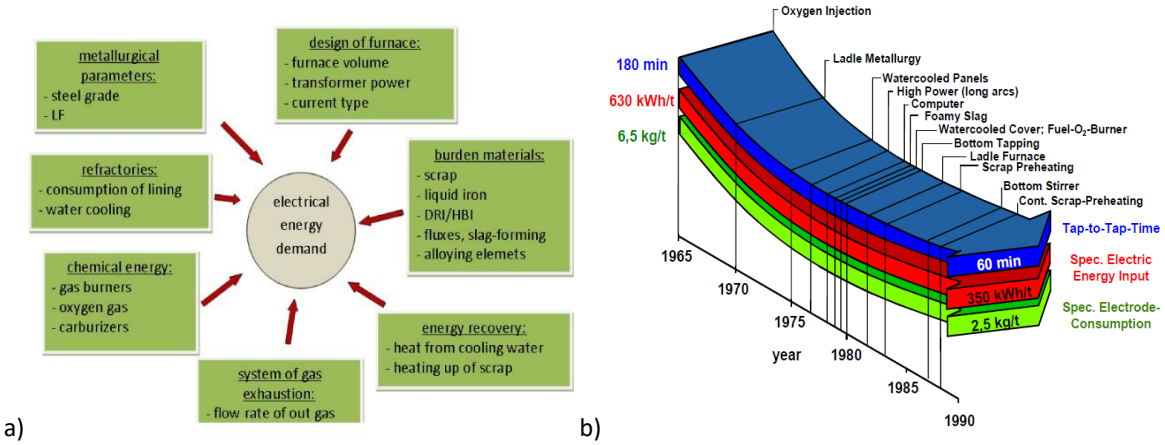

Figure 1 Process and design parameters of the EAF influencing the demand for electrical energy a) and their optimisation b) [1, 5].

The following factors influence the demand for electrical energy in the steelmaking process in the EAF (Fig. 1a): amount, type and quality of charge materials, furnace design parameters, possibility of thermal energy recovery, flue gas exhaust system, refractories, chemical energy, and metallurgical parameters. The three main indicators (melting time, energy consumed for a heat, electrode consumption) optimized in the process are presented in Fig. 1 b).

Effective, efficient and economic operation of an EAF during steel production can only be performed if the all above mentioned technological factors are optimally selected, taking account of the furnace design parameters, type and quality of the available scrap and the manufactured steel range. The main goal of the production process is usually to minimize the electrical energy consumption while optimally utilizing the chemical energy.

In order to determine the complete heat balance of the EAF process it is necessary to know the volumes of all heat sources and the volumes of heat accumulated in the liquid steel, slag and all heat losses. In practice, determining the full heat balance is very difficult, primarily, because the values of all components of heat loss cannot be accurately determined. The primary components of the EAF melting process heat balance are presented in Fig. 2.

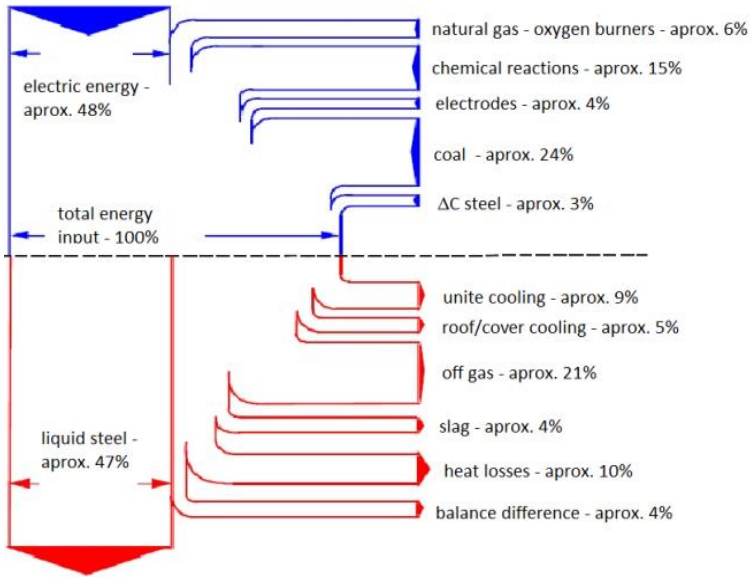

Figure 2 General diagram of the heat balance of steel melting in an electric arc furnace [6].

The process heat sources are: electrical energy, heat from the burner gas combustion, exothermic reaction heat, heat of exothermic reactions occurring during oxidation of graphite electrodes, physical heat of charge materials [1].

At the output side in the heat balance there are: physical heat of liquid steel, physical heat of slag, physical heat

of gases, heat of endothermic reactions, heat loss for water cooling, heat loss by radiation and convection of the outer surface of the furnace shell and roof, electrical loss related to heat loss resulting from the current flow in a conductor [1].
Estimating the component volumes at the input side in the heat balance does not pose problems. Determining the volumes of components on the output side of the balance is more problematic, it concerns in particular the volumes of individual losses. In the most general form, the heat balance equation can be written as follows:

$$\sum \mathrm{Q_{in}} = \sum \mathrm{Q_{out}} \tag{1}$$

where: the left hand side of the equation means the total input heat, and the right hand side means the total output heat. A heat balance of the EAF operation in the industrial conditions is prepared on the basis of process parameter data and statistical values. Generally, the equation components can be written as follows:

$$\Sigma \mathrm{Q_{input}} = \mathrm{E_{el.}} + \mathrm{E_{chem}}; \qquad \Sigma \mathrm{Q_{output}} = \mathrm{Q_{liq.\,steel}} + \mathrm{Q_{slag}} + \mathrm{Q_{out\,gas}} + \mathrm{Q_{heat\,loss.}} \tag{2}$$

One of general methods of energy analysis of the EAF operation is a model developed in 1992 by Köhle S. [7]. Modified in the subsequent years (1999-2002), the model presents a linear function between the electrical energy demand in the steelmaking process, and various, most influencing process parameters. The model, in its general form is a linear equation (3) [5]:

$$W_R = 375 + 400 \cdot \left[\frac{G_E}{G_A} - 1\right] + 1000 \cdot \frac{G_Z}{G_A} + 0{,}3 \cdot [T_A - 1600] + 1{,}0 \cdot (t_S + t_N) - 8 \cdot M_g - 4{,}3 \cdot M_L - 2{,}8 \cdot M_N + 80 \cdot \frac{G_{DRI}}{G_A} - 350 \cdot \frac{G_{HM}}{G_A} - 50 \cdot \frac{G_{Shr}}{G_A} + NV(W_V\text{-}W_{Vm}) \tag{3}$$

where: W_R – unit electrical energy demand, kWh/Mg, W_V – unit thermal loss of the melting, kWh/Mg, W_{Vm} – average value of unit heat loss in the furnace water cooling system, kWh/Mg, G_A – weight of metal tapped from the furnace after melting, Mg, G_E – weight of ferrous materials per heat, Mg, G_Z – weight of slag-forming materials per heat, Mg, G_{DRI} – weight of DRI materials (DRI/HBI) per heat, Mg, G_{Shr} – weight of shredded scrap in the charge, Mg, M_g– unit consumption of natural gas per heat, m^3/Mg, M_L – unit consumption of gaseous oxygen per heat, m^3/Mg, M_N– unit consumption of gaseous oxygen for afterburning CO in the furnace per heat, m^3/Mg, T_A – metal temperature in the furnace before tapping, °C, t_S– furnace operating time „under current" during melting, min, t_N– furnace operating time „without current" during melting, min., NV - constant. (0.2-0.4).However, the most updated form of the modified Köhle model is equation 4 in the form [7]:

$$W_R = -152.56 + 4.2146 \cdot G_E - 5.0795 \cdot G_A - 1.447 \cdot G_{HDRI} - 1.3039 \cdot G_{CDRI} - 1.9784 \cdot G_{Scrap} + 3.0905 \cdot \frac{G_A}{G_E} + 0.48352 \cdot t_{ttt} + 4.8648 \cdot t_S - 0.46807 \cdot t_N - 0.31964 \cdot t_{prep} - 0.0040591 \cdot M_{O2} + 6.8737 \cdot G_{chC} + 4.7919 \cdot G_{injC} + 3.9598 \cdot G_{Lime} + 1.3675 \cdot G_{Dolo} + 3.8739 \cdot P_{AVG} \tag{4}$$

The nature of the equation remains linear, however the nature of process variables influencing the electricity demand has substantially changed in terms of quality. For instance, the temperature component occurring in equation (3) does not appear in this equation.
It is apparent that new models of furnace operation optimisation have been created or the existing ones have been modified. The numerical models developed to identify the electrical energy demand in the EAF should be user friendly.
Work on the optimization of steel melts in an EAF in terms of energy is continuously carried out, in particular when shortage of energy prevails in the world. The new models include the influence of more and more process parameters – equation (4). The extended Logar model [5, 6, 8], based on solving a set of ordinary differential equations identifying the EAF thermal state can be another example.

3. Analysis of process parameters from the point of view of energy efficiency of charge melting

One of the objectives set for the conducted analysis of energy consumption was the identification of heat losses in the conditions of the furnace analysed. The values of these losses cannot be calculated/estimated

from the measured furnace process parameters, it is caused by lack of measurements of necessary physical and process variables.
In order to analyse energy efficiency of the charge melting process in an EAF in the conditions of Cognor S.A. HSJ Branch in Stalowa Wola, a database was prepared on the basis of the selected process parameters.
The set initial databases contains 147 records, where the main "unit" is a single heat. Each heat (record) includes results of temperature measurements and oxygen activity in the melt, consumption of electrical energy, gas and oxygen and recarburization agent, foaming agent, slag-forming materials and deoxidizers, as well as the melting time including the weight of the obtained metal and other production indicators. The database also contains set chemical constitutions of slag samples (final) taken during melting.
The equation describing the amount of energy obtained by oxidation of elements (from scrap) was used for computing (5):

$$E_M = \sum_M (M_S * \frac{M_{AM} * aver\%_{MO.s} * 1000\frac{kg}{Mg}}{100\% * M_{AMO}} * E_{jM}) \quad (5)$$

where: M_s – mass of slag [Mg], M_{AM} – metal atomic weight, $aver\%_{MO.s}$ – average metal oxide content in slag [%]; M_{AMO} – atomic weight of a specific metal oxide, E_{jM} –unit oxidation energy of a specific element [kWh/kg]. (where *M = Cr, Mn, Fe, Al., Si*). For operation conditions of the electrical steelmaking shop analysed, the general Köhle model (3) – for electrical energy demand – was modified and next utilized. As some process parameters, which are not measured or not used in a given furnace, occur in the equation (3), the equation was modified to the form (6):

$$W_R = 375 + 400 * \left(\frac{G_E}{G_A} - 1\right) + 1000 * \frac{G_Z}{G_A} + 0{,}3 * (T_A - 1600) + 1 * t_s + t_N - \left(\sum_M \left(M_s * \frac{M_{AM} * aver\%_{MO.s} * 1000\frac{kg}{Mg}}{100\% * M_{AMO}} * E_{jM}\right) + 11 * M_G + M_c * 2{,}73\right) * F_L \quad (6)$$

where: F_L – heat loss indicator [kWh/Mg], M_c– weight of the carburising agent in the charge [kg].
The following modifications of the equation were made: the (4.3*M_L) component, representing the heat of combustion of elements in the melt per Nm^3 of the supplied oxygen, was removed and replaced with the heat of combustion for each of significant elements in the melt (*Al, Cr, Si, Mn, Fe* – equation (5)). The conversion coefficient referring to the natural gas combustion was changed from 8 kWh/Nm^3 to the value declared by the gas supplier – 11 kWh/Nm^3. Next, heat coming from oxidation of carbon brought into the process with recarburizing agents in the charge was taken into account, also the heat loss indicator in the process was included. Generally, the variable – thermal loss of a heat is an estimated value, or it is calculated theoretically (or determined from measured parameters). In this case it is calculated by comparing the values of electrical energy Real and Mod – so that the difference between the mean values of actual electricity consumption and the mean values calculated from the formula is as low as possible. It arises from the fact, that taking into account the formulas (1) and (2) – the real consumption of the electrical energy is the only measured energy value at the input side and it appears that only the F_L estimation – relative to this value, is justified.

Figure 3 shows a comparison of actual values of electrical energy utilisation with model values for two versions of the Köhle model (Köhle 2002 and Modified). The straight line presents the actual values obtained in the furnace. As can be noticed, the earlier version of the "Köhle 2002" model gives results, which are mostly below the actual values. However, the "Modified" model seems to better describe the actual data. Figure 3 shows also the average values of electrical energy demand obtained with the same method: av. Real – actual furnace data, av. Kohl2002 – earlier model, av. Modified – used last version of the model. As can be seen, the average values of energy for the actual energy = 341.26 kWh/Mg and the computed energy from the Modified model = 340.99 kWh/Mg – in Figure 3 – the points overlap.

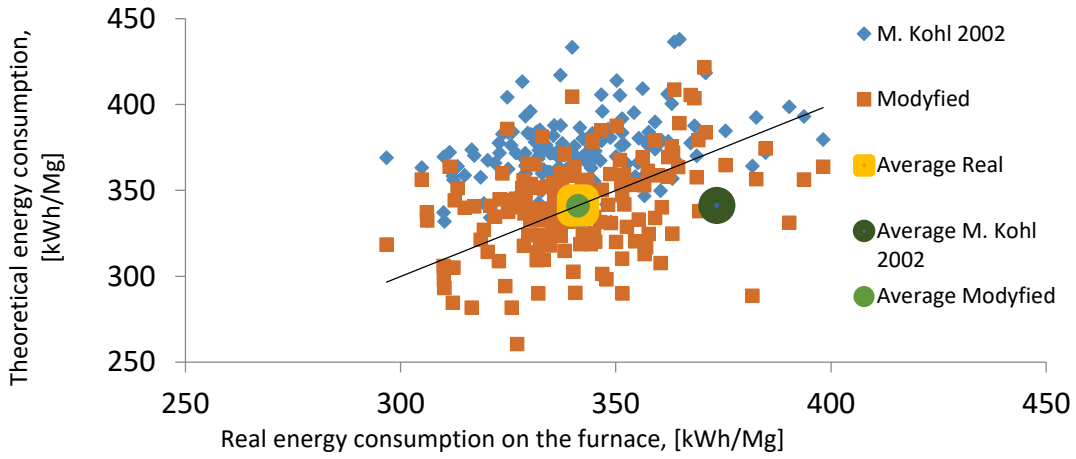

Figure 3 Comparison of the model and real values of demand for electrical energy.

During the conducted analyses and tests, the estimate measurements of the slag mass tapped from the furnace for a single heat were made, in the actual conditions this value was 10-14 Mg.

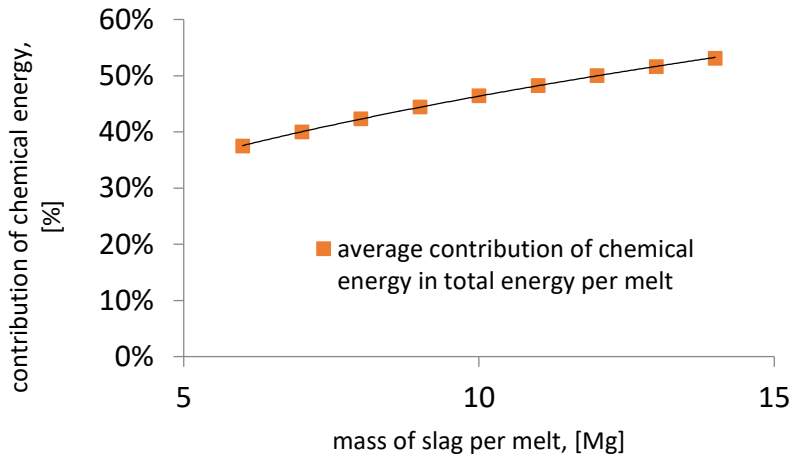

Figure 4 Change in the contribution of chemical energy vs. the mass of slag per melt.

On the basis of the weighted slag, changes in the energy demand per heat were simulated, the assumed changes in slag weight in heats were from 6 to 14 Mg. Figure 4 shows the change in the chemical energy share as a function of the slag weight change. As the slag weight per heat increases, the average share of chemical energy in the total energy utilised in specific conditions during melting increases.
Figure 5 shows the change in the electrical energy demand as a function of changes in total energy for various slag weights. As the slag weight in the furnace increases, the total energy demand increases, and the electrical energy demand also increases. If the electrical energy cannot be obtained, this shortage is compensated by an increase in the chemical energy share in the system (Fig. 4).

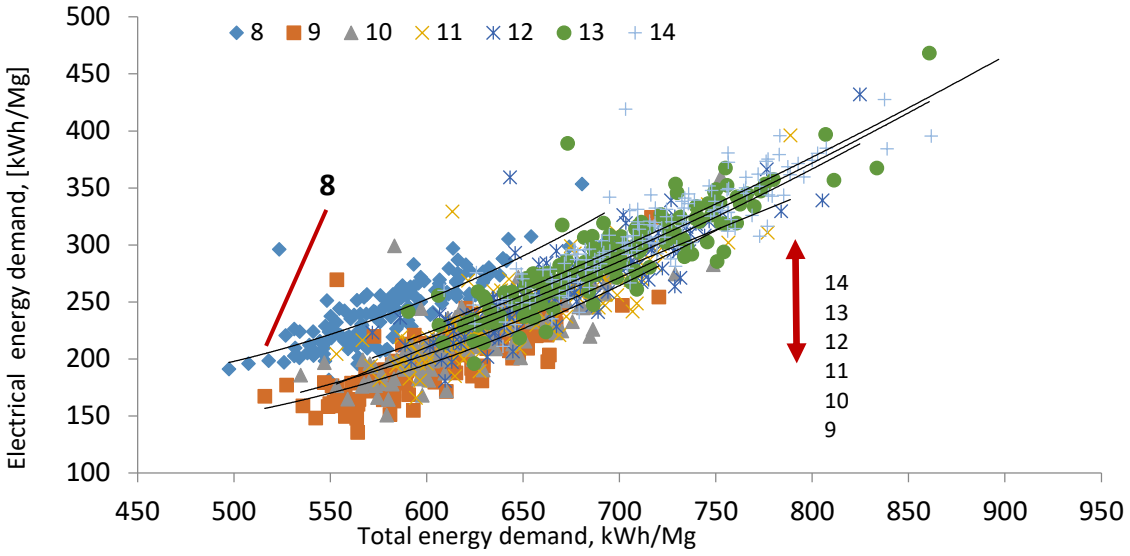

Figure 5 Change in the electrical energy demand vs. the total energy demand.

Using the Köhle (3) equation the demand for the electrical energy was calculated, next it was compared to the actual value of electrical energy consumed in the furnace. The difference between these values is presented in Fig. 6.

As can be seen on figure6 the zero value of differences between the reality and the model can be determined from the regression equation, and it is 178.11 kWh/Mg (for α=0.05, R=0.837, N=145). For this value, one can assume the selected model fits the actual values (for the electrical energy demand per heat).

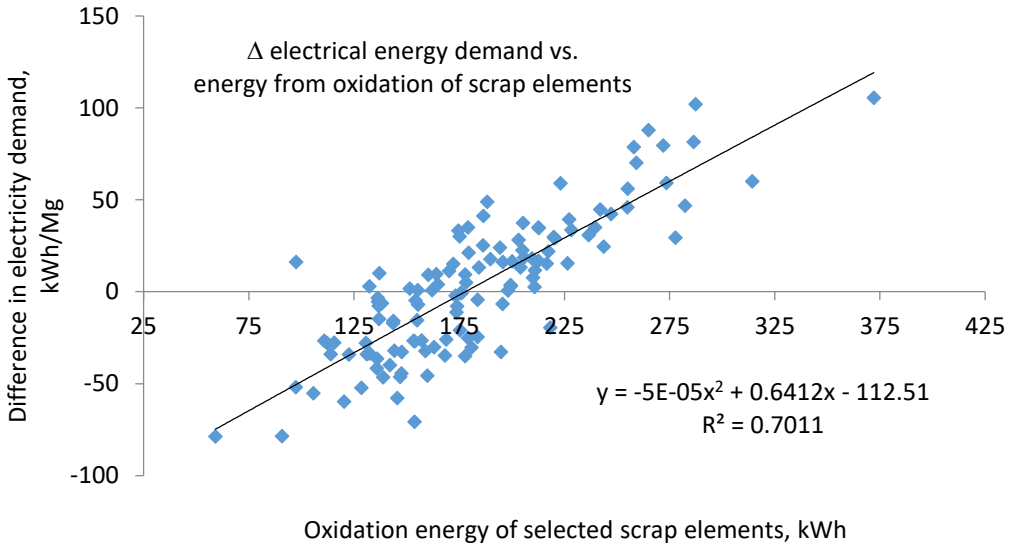

Figure 6 Change in differences of energy values between the actual values and the values calculated as function of energy from oxidation of elements in the scrap.

4. Conclusions

The following conclusions and observations can be drawn, on the basis of the conducted calculations, simulations and analyses:

1. The share of calculated chemical energy – depending on the slag amount – is within the range 40-50%. This value is comparable with other furnace units described in literature (although concerning bigger nominal capacities)

2. The selected Model describing the energy system of the furnace analysed "gives a good response" to changes in the chemical energy (oxidation of elements). Figure 5 – compensation of chemical energy by an increase in the electricity demand can be seen.

3. The sensitivity of the model to the energy originating from the heat of oxidation of the metal bath constituents, is shown on Figure 6 – underestimations of the chemical energy are directly related to the divergence of values of the measured electrical energy in relation to the calculated demand, and vice versa – the real values higher than the computed ones are related to the computed high value of energy from oxidation of elements contained in the metal bath.

It is necessary to continue the development of the model, or its modifications, reconstructions, followed by verification of the computed heat loss with measurements of measurable parameters – real heat losses of the heat, for the furnace analysed.

Acknowledgement

The research was conducted with the financial support as part of the Project: No POIR.01.02.00-00-0207/17, title: „Innovative manufacturing process for a very high metallurgical purity steel for the most critical applications in the automotive industry".

References

[1] Karbowniczek M.: Stalowniczy piec łukowy, wydawnictwo AGH, **2015**,

[2] Blachnik M., Wieczorek T., Mączka K., Kopeć G.; Identification of Liquid State of Scrap in Electric Arc Furnace by the Use of Computational Intelligence Methods; ICONIP 2010, **2010**, Part II, pp. 700–707,

[3] Bergman K., Gottardi R.: Design criteria for the modern UHP electric arc furnace with auxiliaries., Ironmaking and Steelmaking, **1990**, vol 17, No. 4, s. 156-159

[4] Jianghua Li.; Kinetics of steel scrap melting in liquid steel bath in an electric arc furnace; A Thesis Submitted to the School of Graduate Studies in Partial Fulfillment of the Requirements For the Degree Doctor of Philosophy, McMaster University, **2007**,

[5] Pfeifer H., Kirschen M.: Thermodynamic analysis of EAF energy efficiency and comparison with a statistical model of electric energy demand, materiały konferencji EEC 2005 Birmingham, 9-11.05.**2005**

[6] Logar V, Dovžan D., Škrjanc I.; Modeling and Validation of an Electric Arc Furnace: Part 2, Thermo-chemistry; ISIJ International, Vol. 52 **2012**, No. 3, pp. 413–423,

[7] Kirschen M, Zettl K. M., Echterhof T. Pfeifer H.; Models for EAF energy efficiency, Electric Steelmaking, www.steeltimesint.com, **2017**,

[8] Logar V, Dovžan D., Škrjanc I.; Modeling and Validation of an Electric Arc Furnace: Part 1, Heat and Mass Transfer; ISIJ International, Vol. 52, **2012**, No. 3, pp. 402–412,

Session - Non Ferrous and Non - Metallic Materials

THERMAL ANALYSIS OF CAST IRON - POSSIBILITIS OF USE IN FOUNDRY AND ITS RESTRICTION

Marianna Bartošová[1*], Martina Hrubovčáková[1], Iveta Vasková[1], Alena Pribulová[1]

[1]Faculty of Metallurgy, Technical University of Košice, 04200 Košice, Slovakia; martina.hrubovcakova@tuke.sk (M.H.); iveta.vaskova@tuke.sk (I.V.); alena.pribulova@tuke.sk (A.P.)

*Correspondence: marianna.bartosova@tuke.sk; Tel.: +421-55-602-3140

Abstract

The solidification of cast iron is the complex process. The influence of solidification process on the final quality of the cast is significant. Cast iron production is a difficult process with a many number of variables. For cast iron foundries, to produce quality castings, is important appropriate pouring temperature (but also thermal process of melting), chemical composition, effective inoculation and modification, casting time, etc. - they have a great effect on solidification. One of the process which allowed to observe solidification of alloys is the thermal analysis.

Thermal analysis is based on the recording and evaluation of a cooling curve, used to determine solidification characteristics of cast iron. In the foundries, various types of test cup are used to sense the cooling curves. Using cup with tellurium there is possibility to take off typical temperature values from cooling curve (liquidus temperature – min., max., solidus temperature) and following statistical correlation functionality to assess the value of carbon, silicon content and carbon equivalent. By using cup without tellurium (liquidus temperature – min., max., eutectic temperature – min., max., solidus temperature), relative relations between metallurgical quality of melting cast iron and final cast quality.

This article deals possibilities of use thermal analysis in various metallurgical processes and its restriction. The aim of this research is to study reliability of thermal analysis results of cast iron.

Keywords: thermal analysis; solidification of cast iron; cooling curve; quality control

1. Introduction

The thermal analysis can be defined as "...the analysis of a change in a sample property (thermodynamic properties, materials properties, chemical composition or structure), which is related to an imposed temperature alteration" [1].

Thermal analysis is the recording and interpretation of the temperature variation in time of a cooling or heated material. Recent developments in thermal analysis instruments make it possible to precisely measure and visualise the events within the solidification of iron samples. Data generated from thermal analysis can be used to study composition, processing effect, chill and microstructure. The shape of the cooling curve measured by a thermocouple mounted in a thermal analysis sample cup reflects the solidification process of the melted cast alloy for the given solidification conditions. The cooling rates measured in degrees per second at different stages of the solidification sequence can be analysed and correlated with the properties of the castings to be produced from the same melt. Chronologically, the major parts of the curve are pre-liquidus, austenitic arrest, dendritic growth, eutectic solidification, end of freezing and the austenite transformation region. The normal cooling curve gives basic information about the solidification. Additional information can be obtained from the first derivative (DT/dt) of the curve [2-5].

Thermal analysis is not something new in foundry praxis. Nevertheless, it can be stated, that not all possibilities, which analysis can provide are being exploited. Nowadays, the devices for thermal analysis are based on top apparatus and software equipment. In addition to characteristics of cooling curves and other qualitative indicators, it is possible to use the devices for collection of the measurement results from different laboratories (results of chemical analysis, mechanical properties, structural analysis etc.) and also statistic evaluation of collected data. The known fact is, that it is necessary to make production process as stable as possible to obtain reliable results by thermal analysis. It is known and used in praxis, that via thermal analysis it is possible to quickly establish basic chemical composition - %C, %Si, Sc. However, from cooling curves and their characteristics it is possible to obtain information about crystallization and graphitization processes during solidifying and cooling of the sample of cast iron, in other words it is possible to obtain information about metallurgical quality of molten cast iron before casting. Current literature is greatly focusing on this application. This application can provide valuable knowledge and important manufacturers of devices for thermal analysis

are equipping their analysers with software that can evaluate metallurgical state of molten metal and also predict final structure and mechanical properties of cast iron after cooling [2-4, 6, 7].

The thermal analysis cooling curves can be used for optimisation of inoculation in ductile iron. The minimum eutectic temperature should be greater than 1140°C to avoid primary carbides in ductile iron, and the angle at the end of solidification in cooling rate curve (VPS) should be between 25 and 45°C to avoid secondary carbides. Furthermore, computer-aided cooling curve analysis can be used for evaluating latent heat evolved during solidification. Iron castings produced with identical chemical composition can have considerable variations in mechanical properties. With thermal analysis, it is possible to predict such variations and correct the melt before pouring [5].

The use of thermal analysis of cast iron is in practical condition still problematic. In published papers [8-10] was stated, based on the results of thermal analysis of cast iron from different practical problem is, as it was mentioned before, that the process stability is not sufficient in the tested foundries and therefore a lot of influencing factors is causing unreliability of obtained results [3, 11, 12].

2. Experimental Procedures

All measurements were realized by ductile cast iron production (EN-GJS-500-7) in the operating conditions in the foundry. The initial melt was prepared in 8 tonne middle frequency induction furnace with acid brickwork. The composition of used charge was: pig iron SOREL, hematite and steel scrap. After preheating on 1500°C the molten metal was treated by method Tundisch Cover (into 2 t ladle).

Foundry alloy FeSiMg (with 5% of Mg) in quantity of 3 kg (it is 1.9 – 2% of the weight of molten metal) was used as a modifier. The treated molten metal was inoculated by pouring into foundry ladle according technological rules. 300 kg molten metal was leaved in the treated ladle because of experiments. From this 20 kg were used for the experiment without inoculation (melting No. 11, 21, 31, … 81 – see Table 1), next 20 kg of molten metal was inoculated with smaller quantity of inoculation (sampling of cast iron No. 12, 22, 32, ... 82) and next 20 kg of molten metal was inoculated with higher quantity of inoculant (No. 33, 43, 53, … 83). Metallurgical conditions of molten metal were changed by the quantity and quality of used inoculants. The overview of metallurgical treatment of cast iron from observed 8 melts shows Table 1.

Table 1 Used quantity and kinds of modification and inoculation additives by treatment of tested cast irons.

Number of melts	Modification	Inoculation
11	38 kg FeSiMg	-
12	+ 1 kg CeMM	0.2% Barinoc
21	38 kg FeSiMg	-
22		0.2% Barinoc
31	38 kg FeSiMg	-
32		0.2% Barinoc
33		0.3% Barinoc
41	38 kg FeSiMg	-
42		0.1% FeSiCe MM40
43		0.3% FeSiCe MM40
51	38 kg FeSiMg	-
52		0.2% Superseed
53		0.3% Seperseed
61	38 kg FeSiMg	-
62		0.2% Barinoc
63		0.4% Barinoc
71	38 kg FeSiMg	-
72		0.2% Barinoc + 0.1% FeSiCeMM
73		0.4% Barinoc + 0.1% FeSICeMM
81	38 kg FeSiMg	-
82		0.2% Foundrysil + 0.1% FeSiCeMM
83		0.4% Foundrysil + 0.1% FeSiCeMM

Table 2 shows the chemical composition of tested cast irons which was realized by spectral analysis. Degree of eutectic saturation (S_c) shows that all tested cast irons were hypereutectic.

Table 2 Chemical composition of tested cast irons.

Sample number	C [%]	Si [%]	Mn [%]	S [%]	P [%]	Mg [%]	S_c
11	3.84	2.35	0.39	0.020	0.056	0.089	1.0940
12	3.70	2.48	0.43	0.025	0.054	0.087	1.0708
21	3.66	2.33	0.41	0.016	0.050	0.079	1.0437
22	3.82	2.28	0.38	0.018	0.048	0.071	1.0817
31	3.98	2.21	0.36	0.021	0.051	0.086	1.1223
32	3.70	2.24	0.36	0.017	0.044	0.075	1.0456
33	4.12	2.09	0.35	0.014	0.049	0.083	1.1486
41	3.74	2.41	0.37	0.013	0.047	0.067	1.0707
42	3.80	2.50	0.35	0.019	0.045	0.059	1.0962
43	3.81	2.49	0.35	0.015	0.046	0.063	1.1005
51	3.74	2.36	0.38	0.016	0.048	0.071	1.0663
52	3.73	2.52	0.39	0.020	0.046	0.069	1.0779
53	3.82	2.48	0.41	0.021	0.043	0.072	1.0918
61	3.79	2.41	0.39	0.023	0.048	0.078	1.0868
62	3.85	2.54	0.40	0.028	0.045	0.069	1.1197
63	3.68	2.60	0.39	0.024	0.047	0.061	1.0768
71	3.75	2.39	0.38	0.018	0.046	0.065	1.0751
72	3.72	2.59	0.38	0.014	0.045	0.065	1.0871
73	3.83	2.75	0.37	0.013	0.041	0.062	1.1366
81	3.79	2.47	0.37	0.019	0.045	0.080	1.0948
82	3.85	2.68	0.38	0.020	0.045	0.073	1.1351
83	4.11	3.02	0.37	0.022	0.041	0.091	1.2530

Apparatus TERMOCARB assembled on the Department of Foundry in Miscolc University in Hungary was used for the analysis. Shell pots "Quick – cup" without telur were used, it has enabled to achieve grey solidification. Collected variations of temperature by cooling of samples were registered via converter ADAM by software GENIE. It was not used any software for reading of characteristic temperatures on the cooling curves. The results of the thermal analysis are shown in the Table 3.

Three testing Y-blocks for the testing of mechanical properties and metallographic analysis were poured from every melt, the first after modification treatment, the second one after inoculation with smaller quantity of inoculating agent and third after bigger part of inoculation agent.

3. Results and Discussions

As it was already above mentioned, it is possible to divide the use of thermal analysis in foundry praxis into 3 parts:

- Setting of basic chemical composition – amount of C, Si and degree of eutectic saturation Sc,
- Evaluate the effect of inoculation,
- Evaluate the final quality of castings.

This article covers the evaluation of inoculation effect with the use of thermal analysis. Figure 1 shows the cooling curves of cast iron, before inoculation - cooling curve 61, inoculated with 0.2% inoculant Barinoc - 62 and inoculated with 0.4% Barinoc - 63. From the picture it can be seen, how the shape of cooling curve by the influence of inoculation had changed. Liquid area and also eutectic area had moved to higher temperatures, over 1140 °C. Such change of cooling curve in eutectical area, as result of inoculation effect, is awaited. Mainly the increase of minimum eutectical temperature TE_{min} is important for stabile solidification. This increase of TE_{min} after inoculation is closely connected with increase of graphitizing nuclei.

Table 3 The results of the thermal analysis (Possibilities of evaluation of field of liquidus on the cooling curve were not the same in all cases. Field of liquidus is characterized either only TL or minimal and maximal TL.).

Sample number	TL [°C]	TL_{min} [°C]	TL_{max} [°C]	TE_{min} [°C]	TE_{max} [°C]	TS [°C]
11		1144.5	1146.3	1131.6	1134.3	1079.9
12		1148.4	1149.5	1145.3	1146.6	1073.1
21		1131.7	1132.5	1132.5	1137.5	935.3
22		1138.2	1139.2	1135.6	1137.6	1080.9
31		1130.8	1132.5	1132.5	1137.9	1090.2
32		1137.4	1139.1	1134.7	1138.3	1091.5
33	1150.8			1145.8	1146.4	1091.8
41		1138.9	1139.3	1135.6	1137.1	1075.0
42		1139.1	1139.3	1136.6	1139.2	1097.1
43	1156.2			1148.4	1150.6	1106.7
51	1163.6			1131.2	1138.7	1094.0
52	1151.8			1147.7	1149.6	1099.9
53		1143.3	1143.5	1142.8	1143.1	1083.2
61		1128.8	1130.0	1128.3	1133.6	1095.5
62		1153.0	1153.1	1147.0	1148.3	1094.6
63	1159.5			1148.3	1150.4	1096.5
71		1131.9	1133.1	1131.2	1135.1	1058.3
72		1146.0	1146.9	1144.8	1145.3	1093.9
73	1160.1			1147.3	1149.2	1093.4
81		1141.0	1141.6	1135.3	1136.1	1089.9
82	1155.0			1146.2	1147.2	1093.1
83	1174.1			1148.4	1150.7	1099.8

TL – liquidus temperature, TL_{min} – minimum liquidus temperature, TL_{max} – maximum liquidus temperature, TE_{min} – minimum eutektical temperature, TE_{max} – maximum eutektical temperature, TS – solidus temperature

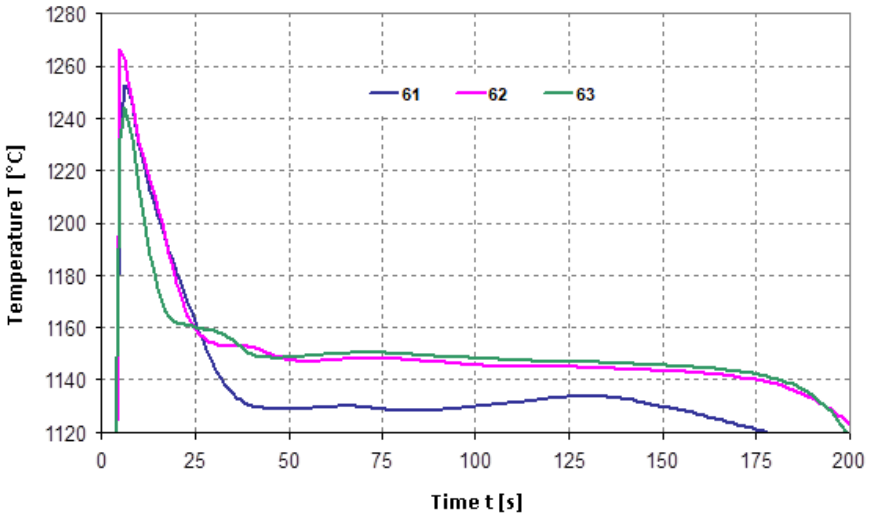

Figure 1 The cooling curves of cast iron (melt 6).

On Figure 2 can be seen, that by melting 2, 3 and 4 (melts 22, 32 and 42) had not came to awaited increase of minimum eutectic temperature TE_{min}. According to these results, it would be possible to assume, that inoculation in these cases was not effective.

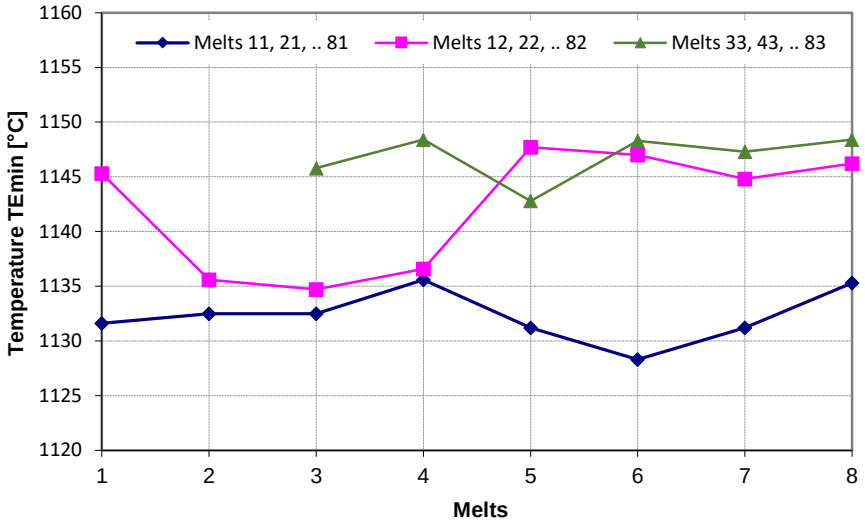

Figure 2 The measured values of minimum eutectic temperature (Table 3).

Inoculation increases the amount of graphitizing nuclei in melt. Insufficiency of graphitizing nuclei causes undercooling by eutectical solidification with the formation of improperly excluded graphite, eventually undercooling under metastabile eutectic temperature and occurence of carbides. Results of metalographic analysis (Table 4) did not prove significantly lower amount of graphite spheroids and event the presence of carbides in structure of observed melts, what should be result of low temperature TE_{min}.

Table 4 The metallographic analysis results.

Sample number	Shape of graphite	Size of graphite [µm]	Number of graphite particles/mm²	Ferrite content [%]
11	VI	55	65	30
12	III,V, VI	55	62	55
21	VI	55	53	30
22	VI	35	85	55
23	III, V, VI	25	98	80
31	V	55	79	55
32	VI	55	90	55
33	VI	35	94	80
42	VI	25	178	80
53	III,V,VI	55	82	80
61	III,V,VI	55	60	15
62	VI	25	144	80
63	VI	25	240	94
71	VI	55	50	15
72	VI	25	115	100
73	VI	25	183	80
81	V	55	58	55
82	VI	35	96	55
83	VI	25	182	80

III – vermi-graphite, V – incomplete spheroidal graphite, VI – spheroidal graphite

4. Conclusions

In special literature it is known for a long time, that information about inoculation effect – amount and activity of graphitizing nuclei are got from course of cooling curve in area of eutectical change. Content of graphitizing nuclei in melt can be measured with the use of minimum eutectical temperature TE_{min} of coolilng curve. The higher the TE_{min} is, the higher is the amount of graphitizing nuclei. This is evident on increased amount of graphite spheroids in structure of ductile cast iron.

Low temperatures TE_{min} after inoculation (melts 22, 32 and 42) should indicate improper inoculation and by that low amount of graphite spheroids, presence of carbides and breach of mechanical properties. Results of

metalographic analysis and mechanical tests did not prove that. Chemical composition of these melts (Table 2) do not significantly differ from other melts. The type and amount of inoculant was used also in other observed melts, where this effect had not proved.

For correct use of thermal analysis by high stability of production process is needed to secure qualified personnel for correct taking of samples. Another important factor is the choice of suitable tools, testing cups and machines and also their calibration. According to F. Hanzig, the deviation by measurements can move up to +/- 9,90 °C in summary. Maximal accuracy of measurement can be achieved by optimalization of single elements of measurement chain (thermocouples, compensation lead, compensation cold joint, A/D converter) [13].

References

[1] Hemminger, W.; Sarge, S. M. Definition, Nomenclature, Terms and Literature. *Handbook of Thermal Analysis and Calorimetry Vo.1.*: Amsterdam, Netherlands. Elsevier Science B. V., **1998**, 8-14.

[2] Stefanescu, D. M. Thermal Analysis – Theory and Applications in Metalcasting. *International Journal of Metalcasting* **2015**, 9 (1), 7-22. [*DOI*: 10.1007/BF03355598]

[3] Diószegi, A.; Svensson, I. L. On the problems of thermal analysis of solidification. *Journal of Materials Science and Engineering A* **2005**, 413, 474-479. [DOI: 10.1016/j.msea.2005.09.052]

[4] Gedeonová, Z.; Jelč, I. Metalurgia liatin. 2000, Košice: HF TU v Košiciach.

[5] Vasudev, D. S. Thermal Analysis of Ductile Iron Casting. Advanced Casting Technologies. 2018 [DOI: 10.5772/intechopen.72030]

[6] Rio Tinto Metal & Titanium Inc. Cabanne, P. M. Thermal Analysis: A useful technique for the foundryman. Available online: http://www.sorelmetal.com/de/publi/PDF/103_(2006).pdf (accessed on 16 September 2019).

[7] Santorini, F.; Powell, C. Gründe für die Anwendung der Thermischen Analyse bei der Produktion von Grau- und Sphäroguss. Giesserei-Rundschau. 2011, 58 (11/12), 273-277.

[8] Bartošová, M.; Stríž, T.; Eperješi, Š. Skúsenosti zistené pri hodnotení kvality LGG pomocou termickej analýzy. In: Quo vadis zlievarenstvo 2015. Technical university of Košice. 12-14.

[9] Bartošová, M.; Pribulová, A. Experiences with commercial thermoanalysator used in the foundry. Acta Metallurgica Slovaca 2005, 11(3), 29-32. [DOI: 10.12776/ams.v20il.273]

[10] Bartošová, M.; Pribulová A. The study of cooling curves of nodular cast iron. In: 7th International Foundrymen Conference: Advanced foundry materials and technologies 2006, University of Zagreb. 5-9

[11] Li, Y.; Wang, O. Intelligent evaluation of melt iron quality by pattern recognition of thermal analysis cooling curves. Journal of Materials Processing Technology. 2005, 161, 430-434. [DOI 10.1016/j.jmatprotec.2004.07.078]

[12] Anjos, V. Use of Thermal Analysis to Control the Solidification Morphology of Nodular Cast Irons and Reduce Feeding Needs. Dissertation thesis. Duisburg-Essen. Faculty of Engineering, University of Duisburg-Essen, Germany. 2015. 187.

[13] Rio Tinto Metal & Titanium Inc. Hanzig, F. Qualitätsüberwachung von Eisenschmelzen durch thermische Analyse. Available online: http://www.sorelmetal.com/de/publi/PDF/103_DE.pdf (accessed on 16 September 2019).

HYDROMETALLURGICAL TREATMENT OF METAL-BEARING WASTES USING NON-FERROUS METALS

Silvie Brožová[1*], Monika Zbránková[1], Jaroslav Havránek[2]

[1]Faculty of Materials Science and Technology, VŠB-Technical University of Ostrava, 708 00 Ostrava-Poruba, Czech Republic; silvie.brozova@vsb.cz

[2]VITKOVICE CYLINDERS a.s., Ostrava, Czech Republic

*Correspondence: silvie.brozova@vsb.cz; Tel.: +420-59-732-3311

Abstract

The article deals with further possibilities of processing of metal-bearing wastes in the form of steel dust by hydrometallurgy. The main part of the research focused on the development of suitable technology of leaching of steel dust to obtain selected non-ferrous metals, mainly zinc and lead for economic and environmental reasons. Laboratory experiments were carried out to verify a suitable leaching agent in the form of high-temperature acid leaching and neutralizing leaching. From the results of the experiments, a suitable technology for processing steel dust was proposed.

Keywords: hydrometallurgy; metal-bearing waste; steel dust

1. Introduction

The dust from steel furnaces (steel dust) was experimentally processed by the process of melt reduction. The aim of these works was to assess the effect of self-reducing briquettes (prepared from steel dust) on the cupola furnace charges, and, above all, to verify the degree of reduction of iron oxides. At the same time, the behaviour of zinc in these processes was monitored, and the efficiency of its removal was monitored [1].

While some authors [2-3] propose to recycle dust and sludge in the technological cycle of pig iron and steel production, it should be noted that such solutions are not promising in terms of environmental protection and ever more stringent permissible emission standards. During the recycling of contaminated dust and sludge, the zinc and lead accumulate, and their contents increase, especially in the blast furnace charge. This means that part of the enriched and trapped dust that is non-recyclable must be landfilled appropriately. The previous works [4] and the average composition of steel sludge produced in tandem furnaces [5] show that dust and sludge are a fine pulverulent substance generated in the production of pig iron and steel. The concentrations of iron, zinc, lead, cadmium, copper, manganese, chromium, carbon, sulphur, Al_2O_3, CaO, MgO and K_2O vary in a relatively narrow range, depending on the type of raw materials processed. However, in terms of the zinc content of the dust and sludge, the dependence on the proportion of galvanized scrap in the charge and the phase of the technological cycle in the production of steel in an oxygen converter or tandem furnace is significant [5].

At present, there is an urgent need for an immediate solution aimed at reducing the amount of waste generated in the production of pig iron and steel and minimizing waste deposited in landfills. Making steel production more environmentally friendly is a fundamental trend of current industrial production, which not only benefits the more efficient use of processed raw materials but also contributes to reducing the environmental problems that arise when landfilling steel waste [6-15].

The presented experimental study examines the possibilities of processing enriched steel dust by the hydrometallurgical method. The main part was focused on verification of suitable methodology of hydrometallurgical treatment of steel dust with the aim to obtain non-ferrous metals of interest, especially zinc and lead. In the next part, laboratory tests were carried out, which verified the leaching of recycled steel dust in the form of high-temperature acid leaching.

2. Overview of technologies for processing steel dust and sludge

The issue of processing fine-grained metallurgical waste (FGMW) is so relevant and topical that it has been addressed by many leading companies operating in the field of metallurgy of iron and steel. The companies focused on the reprocessing of these wastes in the metallurgical cycle while removing non-ferrous metals such as zinc and lead [16-17]. In recent years, the “Waelz” process has become the most important process for processing the electric arc furnace dust. In the “Waelz” process (Figure 1), sand and fine coke are deposited

together with the dust pellets. At temperatures up to 1200°C, zinc, lead, alkali and chlorine evaporate and are trapped in electrical filters for hot gas processing. The larger, non-evaporated part of the pellets and sand forms “Wälz” slag, which must be disposed of. The minimum amount of processed material of the profitable plant is approximately 40,000 tons per year. Existing plants can process around 80,000 tons per year and unit. The BSN process was developed and tested in the laboratory of Badische Stahlwerke AG (now Südweststahl GmbH - SWS). This development is based on the evaporation of metals and metal compounds in dust pellets in indirectly heated rotary kilns. The SWS patent (PCT/EP93/00747 and P4209891.2) is based on the discovery that lead is present in electric arc furnace dust as lead chloride and can be separated from zinc oxide at temperatures above 900°C.

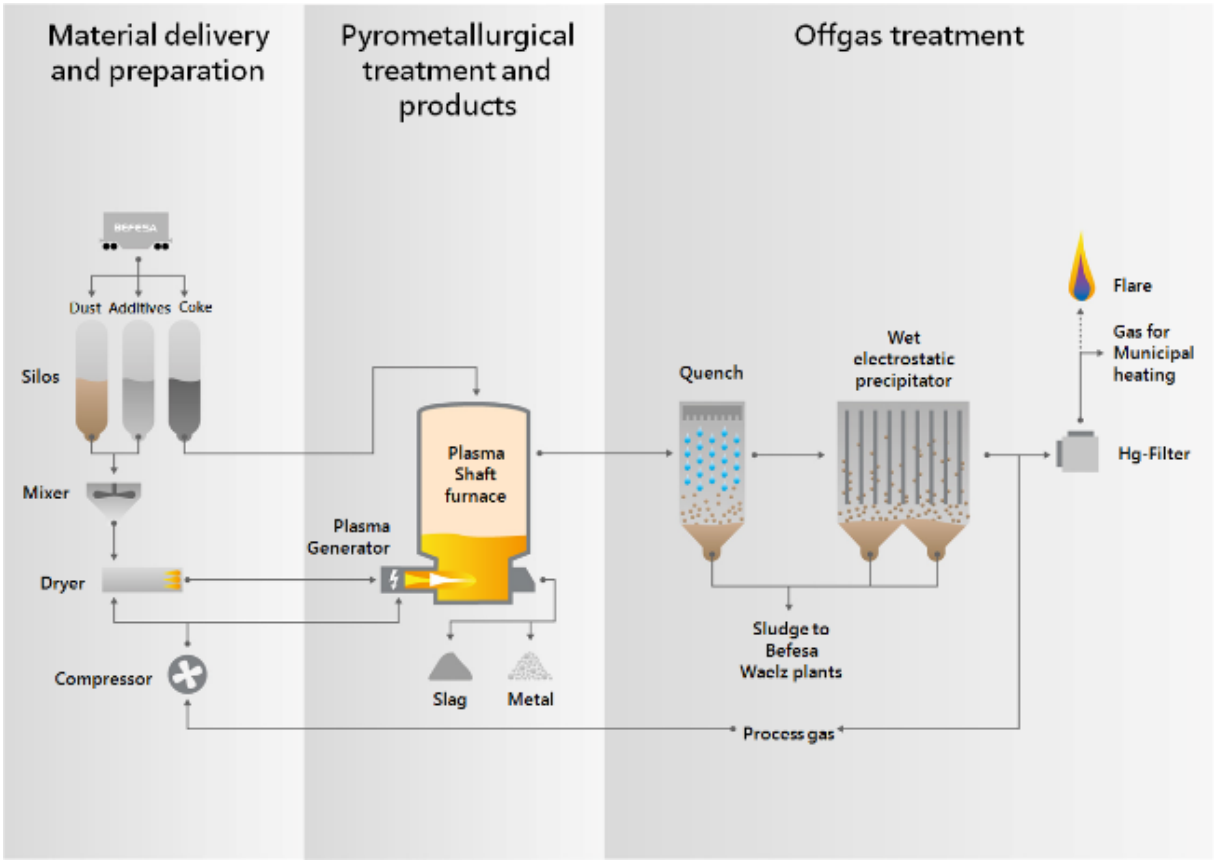

Figure 1 The SDHL Waelz process is composed of the following process steps [18].

KAWASAKI Steel corp. has developed the fine-grained metallurgical waste processing technology (EAF - dust) and pickling sludge containing Cr. This technology was originally used for the production of ferrous alloys. The operation of the Chiba steel mill for commercial use began in 1994. [10] The technology is based on a shaft furnace, with a coke-filled shaft, with two rows of exhausts, with direct pneumatic charging of the powder material through the upper exhaust without agglomeration. Air for the furnace is enriched with oxygen to intensify heat production. The furnace gases, including the vaporized metals, are cleaned in a hot cyclone and then cooled with water in Venturi tubes. The products are metal, i.e. Fe, Ni and Cr alloy with C ≈ 4 - 5%, SiO_2 - CaO - Al_2O_3 slag and scrubber condensate with Zn ≈ 60%. The gas is used to preheat the air.

The company Scandust in Lanskrona, Sweden, uses similar technology, i.e. a shaft furnace filled with coke. The heat source is a plasma burner with independent plasma flame and pneumatic charging of EAF-dust in front of the burner. Dust is sprayed with water in Venturi tubes, the product is so-called “hot metal”, i.e. Fe, Ni and Cr alloy with C ≈ 4 - 5%, which is bought by the FGMW producer, slag based on SiO2 - CaO - Al2O3, generator gas used to heat the town of Landskrona, and the zinc concentrate [18].

The company Horsehead Resource Development Co. has developed a flame reactor for processing EAF dust in which natural gas or pulverized coal is used as the heat source and reducing agent and uses pure oxygen for combustion. In this case, EAF dust is pneumatically added to the flame space; the volatile metals are

evaporated and condensed as oxides in the condenser. The method of condensation is not specified; it is probably a shower of water [19-24].

Krupp Edelstahlprofile GmbH uses FGMW injection on the steel level below the slag in the furnace about 10 minutes after the slag has melted and a continuous foamed layer is formed. FGMW dissolves in slag without noticeable problems. It is partially reduced, passes into steel and volatile metals evaporate. For each melt, a batch of 1.5 t of FGMW was added, with no appreciable effect on the course of the process (no overall furnace capacity and condensation method is given) [25-26].

The company Voest-Alpine Linz, Austria, uses recycling technology in its own steel converter in its FGMW processing technology. FGMW is added to the charge in the form of briquettes (a similar principle was used during the tests in 1985 the New Metallurgical Plant in Ostrava, Ing. Melecký's report) [19-26]. Vaporized metals are trapped in an electrostatic precipitator. Zinc circulates in this technology until enrichment is sufficient for processing in zinc production technology. The same methods of FGMW recycling in the company's own steel technology (electric arc furnace), until sufficient enrichment (min. 40% Zn in recycled sludge with minimum iron content) are used, for example, by Ugine Savoie in France. Due to the repeated cycling of the dust and thus the high Zn content in the dust, the recycling technologies are, with respect to work hygiene, highly dependent on the quality of operation of the separators [27].

3. Laboratory experiments

Within the laboratory tests, the possibility of leaching of enriched steel dust (ESD) was verified. High-temperature acid leaching technology was used. Three samples of ESD were used, which were prepared by a precisely defined amount of lead and zinc inserted into the furnace aggregate together with the ESD. The captured dust was used as input material for hydrometallurgical processing. Table 1 shows the chemical composition of selected elements of interest (%) of three laboratory samples.

Table 1 The chemical composition of selected elements of interest (%) of three laboratory samples.

Sample n.	Fe [wgh. %]	Zn [wgh. %]	Cu [wgh. %]	Pb [wgh. %]
1	64	3	0.071	0.82
2	55	14	0.081	1.1
3	32	35	0.088	4.8

Based on Table 1, it can be stated that by its composition, Sample 1 represents the original steel dust without enrichment. Samples 2 and 3 are taken at various stages of the melting process.

The above-mentioned prepared samples were leached at 92-95°C in a beaker for 2 and 4 hours. The leaching agent was a sulfuric acid solution in the range of 40, 60, 80 $g.dm^{-3}$. The liquid to solids ratio is 5: 1. In the experiment was used 2 molar sulfuric acid solution. The leaching results are shown in Table 2. They indicate relatively rapid kinetics of the conversion of the individual metals of interest into the leachate.

Table 2 The leaching results.

Sample n.	concentration of the solution H_2SO_4	L:S	Temperature [°C]	metal of interest	2 hours	4 hours
3	2M	5:1	92	Fe [ppm] Zn [ppm]	0.098 0.1242	0.4237 0.1514
3	2M	5:1	95	Fe [ppm] Zn [ppm]	1.733 0.2145	1.9774 0.2293
2	2M	5:1	92	Fe [ppm] Zn [ppm]	0.215 0.2458	0.634 0.324
2	2M	5:1	95	Fe [ppm] Zn [ppm]	0.935 0.125	1.458 0.148

Overall, the tests performed can be evaluated as follows:

a) The raw material shows excellent kinetics and the transfer of the metals of interest into the leachate
b) It is difficult to change the leaching kinetics to influence the transfer of iron into the leachate, with a required zinc leaching efficiency of about 95%, the transfer of iron into the leachate is nearly 90%.

c) Suitable leaching conditions are high-temperature acid leaching at 92-95°C and a sulfuric acid content above 40 g.dm^{-3}.

d) Sample 3 is suitable for hydrometallurgical treatment.

4. Pilot verification

Based on the results of laboratory tests, pilot tests were performed in the metallurgical plant. Individual test materials weighing 200 kg were produced during the recycling of steel dust in the tandem furnace charge. Samples with higher contents of zinc and lead were prepared by adding zinc and lead waste to the tandem furnace charge.

Pilot verification of leaching kinetics of ESD was carried out in a prepared apparatus with a volume of 2.5 m^3 with heating to 92-95°C and stirring. Sulfuric acid in the range of 40, 60, 80 g.dm^{-3} was used as a leaching agent.

The leaching kinetics of the ESD was monitored during the tests. Leachate samples were taken. The results are shown below, which shows:

a) Iron and zinc transfer kinetics are sufficiently rapid to transfer both metals into the leachate efficiently.

b) Sufficient sulfuric acid content in the leaching solution is 60 g.dm^{-3}.

c) Pilot tests verified the laboratory experiment with the possibility of shortening the leaching time.

5. Conclusion

Due to the inhomogeneity of the input material, but also the effort to achieve the optimum ratio of zinc: iron (2:1) in the product of hydrometallurgical processing, the methodology with pre-treatment of the feedstock is suitable. The result of hydrometallurgical processing is a leach containing metals of interest - zinc and iron. These can then be used as secondary raw material.

Within the experiment, an approximate material and energy balance was carried out to assess the costs of obtaining metals of interest, and to design a suitable processing technology.

Acknowledgements

The work has been prepared within the framework of the project No. SP 2019/128 and project No. SP2019/43 Specific research in metallurgical, materials and process engineering.

References

[1] Majerčák, Š. Blast furnace charge, Alfa/SNTL, 1986

[2] Kursa M., Leško J., Kret J., Botula J., Krištofová D. A Kárník T. Characteristics and possibilities of processing fine-grained metallurgical waste. Metallurgical sheets, 7-8, 1999, p.130-136.

[3] Baran L., Šonovský P., Michálek J., Kučerová R. Steel sludge-source of raw material by metallurgy. Waste recycling VIII, TU-VŠB Ostrava, 2003, p.273-277.

[4] Imriš, I., Klenovčanová A., Imriš, M. Steelmaking flue dust – Source of Mmetels or waste.Trade steel.sem.1/15, 1998, Linz 22-24 April 1998.

[5] Klein, K.H. at al. The BSB process to recycle zine and Lead fume dust. Trade Steel.sem.1/29, 1998, Linz 18 Frebruary 1998.

[6] Brožová, S., Ingaldi, M., Šperlín,I. Economical aspects of high-temperature heating utilization for industrial waste treatment. METAL 2013 - 22nd International Conference on Metallurgy and Materials, Conference Proceedings 2013, Brno, Pages 1735-1739, ISBN: 978-808729441-3

[7] Kardas,E., Brožová, S., Pustějovská, P. The evaluation of efficiency of the use of machine working time in the industrial company - case study. MANAGEMENT SYSTEMS IN PRODUCTION ENGINEERING, 2017, Vol. 25, Issue 4, p. 241-245. DOI: 10.1515/mspe-2017-0034. ISSN: 2450-5781

[8] Jonšta,P., Váňová,P., Brožová,S., Pustějovská,P. Hydrogen embrittlement of welded joint made of supermartensitic stainless steel in environment containing sulfane. Archives of Metallurgy and Materials, 2016, Vol. 61, Issue 2A, p. 709-711. DOI: 10.1515/amm-2016-0121. ISSN: 17333490

[9] Kardas,E., Brozová,S. Situation in waste treatment in Poland. METAL 2013 - 22nd International Conference on Metallurgy and Materials, Conference Proceedings 2013, Brno, Pages 1773-1778. ISBN: 978-808729441-3

[10] Brožová,S. Possibility of using pyrolysis and plasma during disposal of plastic parts of electric waste. International Multidisciplinary Scientific GeoConference Surveying Geology and Mining Ecology Management, SGEM, Albena, Bulgaria, 2013, Pages 423-428. DOI: 10.5593/SGEM2013/BD4/S18.018. ISSN: 13142704

[11] Findorak R., et al.: The effect of charcoal addition on iron-ore sintering emission, International Multidisciplinary Scientific GeoConference Surveying Geology and Mining Ecology Management, SGEM, 2, Bulgaria, 2013, pp 629-636.

[12] Džupková M., et al.: Evaluation of selected technological and ecological parameters of sinter production (2011) Acta Metallurgica Slovaca, 17 (4), pp. 269-275.

[13] Bernasowski M., Theoretical Study of the Hydrogen Influence on Iron Oxides Reduction at the Blast Furnace Process, Steel Research International, Germany, vol. 85, no.4, pp 670-678, 2014.

[14] Baricova D., et al., Steelmaking slag - waste or valuable secondary raw material, 13th International Multidisciplinary Scientific GeoConference, SGEM Albena, Bulgaria, 2013, pp 437-442.

[15] Fröhlichová M. et al., Influence of biomass on the structure of iron ore sinter. International Multidisciplinary Scientific GeoConference Surveying Geology and Mining Ecology Management, SGEM, Albena, Bulgaria, 2015, pp 615-620

[16] Hara, Y., Ishiwata, N., Itaya, H., Miyagawa, S.: Development of a smelting reduction process for electric arc furnace dust recycling. La Revue Métallurgie - CIT, March 1998, pp. 369-375.

[17] Bounds, C.,O., Pusateri, J.,F. EAF dust processing in the gas-fired flame reactor. Lead-Zinc-Tin`90 - World Symposium, Anaheim, California, February 1990.

[18] Steffes, B., Drissen, P., Kuhn, M. Optimization of the dust cycle in KEP EAF steel shop. Seminar on economic Aspects of Clean Technologies, Energy and Waste management in Steel Industry. Linz, Austria, April 1998.

[19] Heiss, J., Fritz, B., KohL, B. Development of dust-recycling at Voest-Alpine Stahl Linz GmbH from 1989 to 1997. Seminar on economic Aspects of Clean Technologies, Energy and Waste management in Steel Industry. Linz, Austria, April 1998.

[20] Jursová, S., Pustějovská, P., Brožová, S. Study of reducibility and porosity of metallurgical sinter. Alexandria Engineering Journal, Volume 57, Issue 3, p. 1657-1664. **DOI:** 10.1016/j.aej.2017.03.007. ISSN: 1110-0168

[21] Oujezdsky, A., Sliva, A., Brazda, R. Using ICT in education: measuring systems interfaced to computers. In *9th International technology, education and development conference*. Madrid: INTED Proceedings, 2015, pp. 7509-7512. ISBN:978-84-606-5763-7.

[22] Sliva, A., Samolejova, A., Brazda, R., Zegzulka, J., Polak, J. Optical parameter adjustment for silica nano and micro-particle size distribution measurement using mastersizer 2000. *MICROWAVE AND OPTICAL TECHNOLOGY*. 2003, vol. 5445, pp. 160-163. DOI: 10.1117/12.558761. ISBN:0-8194-5368-4.

[23] Fedorko. G., Pribulová, A., Futáš, P., Baricová, D., Demetr, P. Compacting of fly dusts from cupola and electric arc furnace. Metalurgija. 2012. vol. 51, no. 1, p. 63-66. ISSN 0543-5846.

[24] Pribulová, A., Futáš, P., Rosová, A., Demetr, P., Baricová, D. Influence of foundry dust on moulding mixtures quality. Metalurgija. 2013. vol. 52, no. 1, p. 51-54. ISSN 0543-5846.

[25] Sliva, A., Brazda, R., Prochazka, A., Martynkova, G., Barabaszova, K. Study of the optimum arrangement of spherical particles in containers having different cross section shapes. *Journal of nanoscience and nanotechnology*. 2019. vol 19, iss. 5, pp. 2717-2722. DOI: 10.1166/jnn.2019.15873. ISSN: 1533-4880.

[26] Slíva, A., Brázda, R., Procházka, A., Martynková, G., Brabašová, K. Investigation of geometric properties of modified titanium white by fluidisation for use in the process of transport, handling, processing and storage. Journal of nanoscience and nanotechnology. 2019. vol 19, iss. 5, pp. 2997-3001. DOI: 10.1166/jnn.2019.15872. ISSN: 1533-4880.

[27] Legemza, J et al. Modelling of mass and thermal balance and simulation of iron sintering process with biomass. In: Metals. Basel: Multidisciplinary Digital Publishing Institute. Vol. 9, n. 9 (2019), p. 1-18 [online]. – ISSN 2075-4701

FLOTATION CONCENTRATE AS A CARBONACEOUS MATERIAL FOR APPLICATIONS IN COPPER PYROMETALLURGY PROCESSES

Maciej Jodkowski[1*], Jerzy Łabaj[1], Leszek Blacha[1]

[1]Faculty of Materials Engineering and Metallurgy, Silesian University of Technology, ul. Krasińskiego 8, 40-019 Katowice, Poland, jerzy.labaj@polsl.pl; blacha@polsl.pl

*Correspondence: maciej.jodkowski@polsl.pl

Abstract

Evaporation of volatile components of liquid metal phenomenon could occur during every single metal and their alloys melting and in their refining process as well. As many researches proved the type of gas atmosphere used affects the rapidity of that process, especially, when is carried out under atmospheric pressure. In the given article the results of researches of zinc evaporating rapidity during its melting proceeds in atmospheres of helium, carbon monoxide and helium-carbon monoxide mixture are shown.

Keywords: alloys melting; refining process; zinc evaporating

1. Introduction

Research conducted for many years indicate the possibility of use fine carbon fractions as well as the variety of waste carbonaceous material as a raw material in many industry branches. They could be used mainly as:

- ingredients of carbons mixtures and energy fuel
- self-contained energy fuel for specific technological process
- materials for soil and rockmass sealing

Bearing that all in mind, it turned out that metallurgical industry is also interested in finding alternative carbonaceous additives, which could replace coke and coke breeze used mainly in metallurgy extraction processes. That interest is caused by economic aspects, since price of that two basic batch additions has been significantly rising for a couple of years. In pyrometallurgy processes coke and coke breeze are fuel, which burns up and provides warmth. It is necessary for heating and melting batch materials and in course of chemical reactions (mainly endothermic reduction reactions of metal oxides). They also act as reducing agent, which delivers the certain amount of CO oxide necessary in indirect reduction of oxide metal compounds, which are the basic ingredients of batch processed in given process. An example of process in which fine-grained carbonaceous material could be used in domestic metallurgical industry is processing copper slag which comes into existence in suspension process held in KGHM „Polska Miedź" [1]. That slag, which contains 12-16wt.% of copper is processed in electric furnace. Coke is added partially during filling the furnace of converter slag and suspension slag and during the last phase of releasing slag and Cu-Pb-Fe alloy [2]. Presently, the share of coke used in the process is about 0.3 Mg per Mg of copper contained in slag. Currently in KGHM „Polska Miedź" is used coke peas with a grain size of 10-25mm.

In the given paper the results of laboratory research of slag reduction process from suspension process using carbon flotation concentrate and coke breeze are shown.

2. Research materials

Industrial slag containing 11.6 wt.% Cu; 3.25 % mas. Pb and 10.63 wt.% Fe was used in research. As materials – reducing agents – were used carbon flotation concentrate and coke breeze. Carbon flotation concentrate is a fine-grained carbonaceous material which occurs in coal flotation process. Flotation is enriching method, in which disassociation of varied materials grains in which the grain separation of a mixture of different minerals occurs on the basis of differences in the surface properties of these minerals, further increased by the use of flotation reagents. The separation consists on taking of hydrophobic grains by air bubbles (not wetted by water) on the surface of suspension. Non-floating grain (hydrophilic) remains in suspension or form sediment [3,4]. Flotation concentrate is carbon with parameters similar to coarse coals and its only disadvantage is granulation. The results of analysis concerning composition and energy values used in the reducing agents tests were shown in the Table 1. Additionally calcium carbonate was used as batch ingredient, which accelerates slag decoppering process.

Table 1 Results of the research of the carbonaceous materials used in reduction processes.

Research material	Sulfur content, wt.%	Humidity content, wt.%	Calorific value, kJ/kg	Volatile parts content, wt.%	Ashes content, wt.%
Flotation concentrate	0.45	26.5	20 824	22.03	8.71
Coke breeze	0.54	0.5	30 000	0.9	11.5

3. Research methods

The melting process and reducing of copper slag was carried out in two separate resistance furnaces. The first furnace, marked as „I" was used to melt slag in Al_2O_3 melting crucible. In the second furnace, marked as „II" the melting crucible was heated with a backfill consisting of a mixture of limestone and a selected reducing agent. The moment of flooding the backfill with slag melted in furnace „I" was considered to be the beginning of the experiment . The process was carried out up to 8 hours. After the process the melting crucibles were let to cool down together with the furnace. Batch additions (the reducing agents and limestone) were added in the amounts corresponding to those used in the industrial process conditions. Cu-Pb-Fe alloy received after the reduction process as waste slag as well have been subjected to chemical analysis.

4. Research results and their report

Tables 2 and 3 list the compositions of Cu-Pb-Fe alloys obtained after reduction processes carried out when using a carbon flotation concentrate and coke breeze, while tables 4 and 5 list the composition of waste slags obtained after reduction processes.

Table 2 Composition of Cu-Pb-Fe alloys obtained after the slag decoppering process with the use of carbon flotation concentrate.

Batch ingredients, g			Duration of melting, h	Alloy weight Cu-Pb-Fe, g	Chemical composition of the alloy wt.%		
Slag	Reducing agent	Limestone			Cu	Pb	Fe
1 000	30	70	1	132	77.03	13.65	2.25
1 000	30	70	2	153	71.76	21.16	4.88
1 000	30	70	3	161	70.23	15.31	4.97
1 000	30	70	5	166	72.57	13.72	6.03

* mean values from three experiments

Table 3 Composition of Cu-Pb-Fe alloys obtained after the slag decoppering process with the use of coke breeze.

Batch ingredients, g			Duration of the smelting, h	Alloy weight Cu-Pb-Fe, g	Chemical composition of the alloy wt.%		
Slag	Reducing agent	Limestone			Cu	Pb	Fe
1 000	30	70	1	181	73.60	13.39	0.07
1 000	30	70	2	209	66.50	14.01	0.72
1 000	30	70	3	217	78.80	17.02	1.92
1 000	30	70	5	124	78.60	15.11	4.12
1 000	30	70	8	142	78.87	12.09	5.06

* mean values from three experiments

Table 4 Composition of slags obtained after the slag decoppering process with the use of carbon flotation concentrate.

Batch ingredients, g			Duration of melting, h	Chemical composition of slags wt.%		
Slag	Reducing agent	Limestone		Cu	Pb	Fe
1 000	30	70	1	0.87	1.28	14.46
1 000	30	70	2	0.66	0.73	10.83
1 000	30	70	3	0.38	0.56	9.23
1 000	30	70	5	0.40	0.53	2.56

* mean values from three experiments

Table 5 Composition of slags obtained after the slag decoppering process with the use of coke breeze.

Batch ingredients, g			Duration of melting, h	Chemical composition of slags wt.%		
Slag	Reducing agent	Limestone		Cu	Pb	Fe
1 000	30	70	1	1.56	1.57	14.25
1 000	30	70	2	0.52	1.01	11.72
1 000	30	70	3	0.40	0.56	8.73
1 000	30	70	5	0.25	0.45	3.79
1 000	30	70	8	0.29	0.44	4.01

* mean values rom three experiments

The results summarized in tables 2-5 are graphically shown on Figure 1-4.

After an analyse of results of all tests, there could be stated that while using both of reducing agents were obtained a high level of oxide reduction for copper and lead, which were contained in the output slag. In case of copper, after just one hour of the reduction process the slag obtained contains less than 1.56 wt.% of this metal, when, after 5 hours – less than 0.4%. There should be mentioned that in industrial conditions these values are at the level of 0.5-0.6 wt.%. Time extension to 8 hours, when using coke breeze as a reducing agent has a little effect on the copper content results, both, in the alloy and in slag.

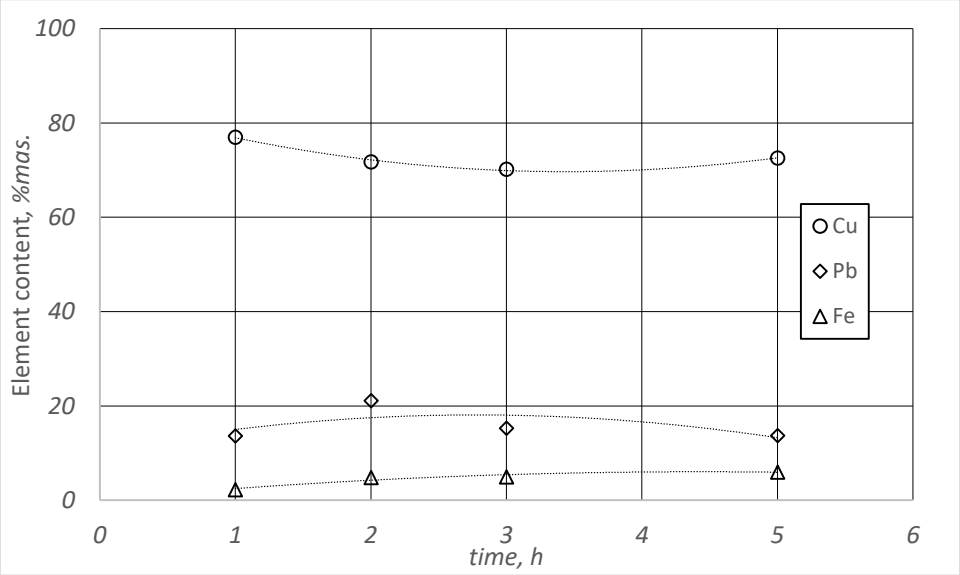

Figure 1 Copper, lead and iron content in Cu-Pb-Fe alloy using carbon flotation concentrate as a reducing agent.

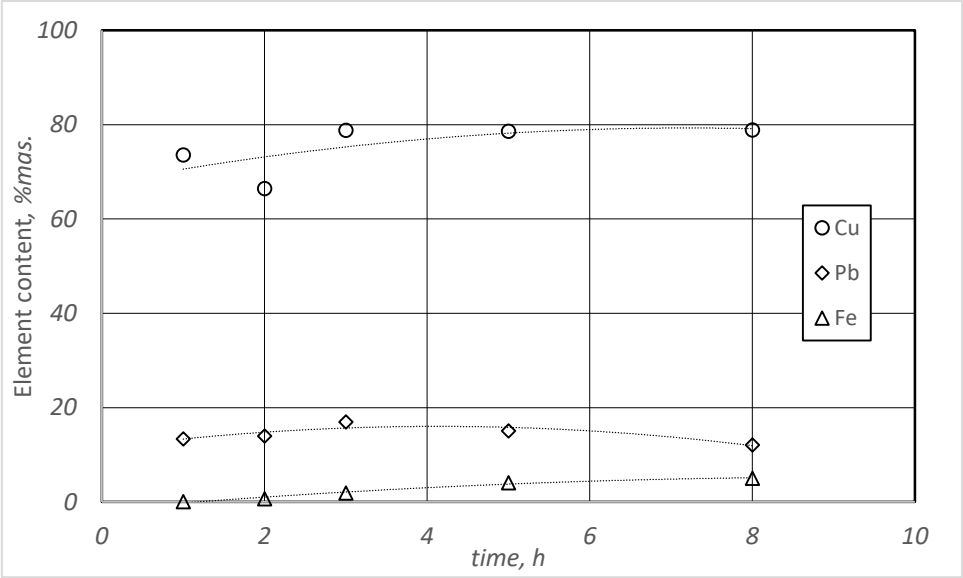

Figure 2 Copper, lead and iron content in Cu-Pb-Fe alloy using coke breeze as a reducing agent.

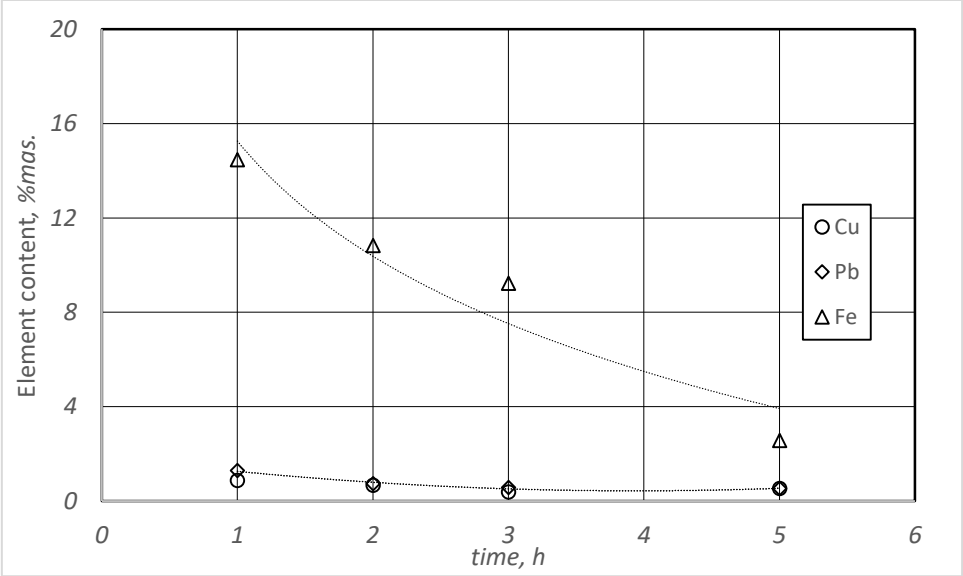

Figure 3 Lead and iron copper content in waste slag obtained for alloy using with the use of carbon flotation concentrate as a reducing agent.

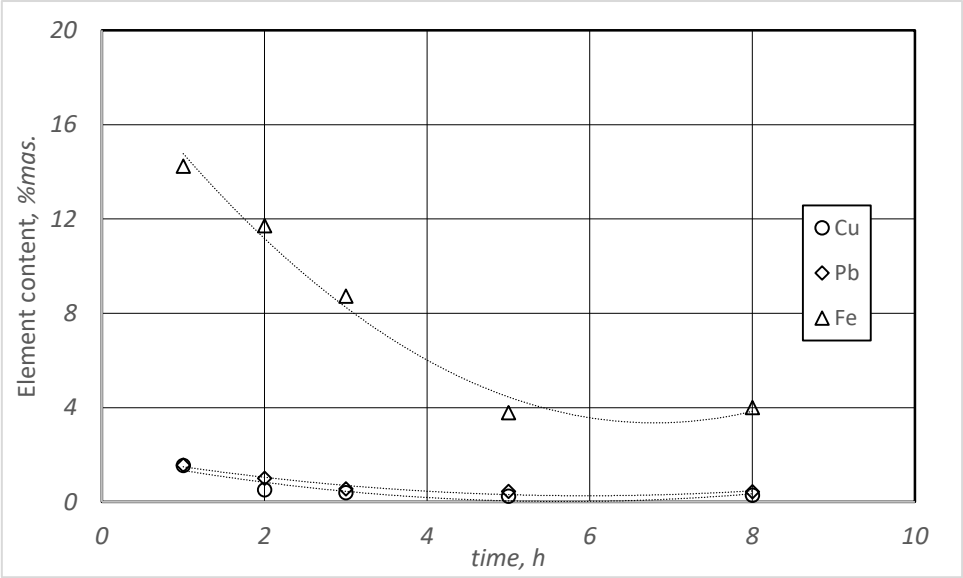

Figure 4 Copper, lead and iron content in waste slag when using coke breeze as a reducing agent.

So called decoppering level can be used as an factor of the effectiveness of the analyzed process. The value of this factor determines the dependence:

$$S_{Cu} = \frac{C^0_{Cu} - C^t_{Cu}}{C^0_{Cu}} \cdot 100 \quad (1)$$

where: C^0_{Cu} ; C^t_{Cu} - respectively initial copper content in the slag and copper content in the slag after time h.

From the data presented in the figure 5, it results that for all experiments high values of this factor were obtained. Therefore for tests with usage of coke breeze as a reducing agent this factor ranged from 86.5% to 97.8% and while using flotation concentrate as a reducing agent values of the factor ranged from 92.5% to 96.7%.

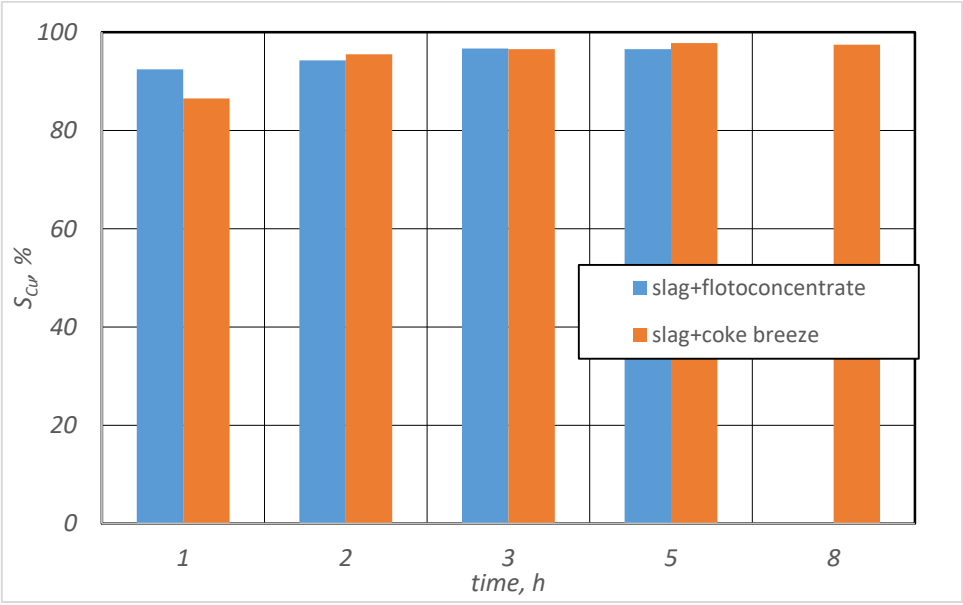

Figure 5 The change of slag decoppering level as a function of the duration of the reduction process.

5. Conclusion

Basing on the results of experimental slag smelting from a flash furnace, using flotation concentrate and coke breeze as a reducing agents could be stated that:

- when using in research carbon flotation concentrate the decoppering level was obtained on the range of 92.5% after one hour and about 97% after 5 hours of the pyrometallurgical process.
- when using coke breeze the decoppering level takes values respectively 86.5% and 97.5%
- in both reducing agents cases after one hour of the reduction process the obtained waste slags containing less than 1.5 wt.% Cu and after 5 hours – below 0.4 wt.% Cu.
- in the case of lead for both reducing agents the reduction of this metal in slag was obtained on the level below 0.6 wt.% Pb in tests carried out for 5 hours.
- results received for copper and lead removing from slag during its reduction in melting were at a similar level as results receiving in industrial conditions.

Acknowledgement

Research results were developed basing on accomplished grant PBS/A5/21/2012 entitled: „Research technological assumptions of the reducing agent selection and batch material preparation in the suspension slag smelting process in electric arc furnace on an industrial scale" financed by The National Centre for Research and Development.

References

[1] KGHM Polska Miedź S.A., 2007 Lubin

[2] M. Kucharski: Pirometalurgia Miedzi. 2003, Kraków

[3] M. Janicki, Ł. Bartkowicz, B. Zakręcki, P. Kowalczuk: „BEZKOLEKTOROWA FLOTACJA WĘGLA KAMIENNEGO WOBECNOŚCI SPIENIACZY"; III Polski Kongres Górniczy, Mineralurgia i wykorzystanie surowców mineralnych, J.Drzymała, P. Kowalczuk (red.), 14-16 września 2015, Wrocław, 52-60.

[4] M. Lenartowicz, B. Grynkiewicz-Bylina: BADANIA LABORATORYJNE FLOTACJI WĘGLA W OBECNOŚCI ODCZYNNIKA RFK−X , Górnictwo i Geoinżynieria • Rok 34 • Zeszyt 4/1 • 2010, 129-134

USE OF WASTE FROM COAL MINING IN Fe-Si-Al ALLOY PRODUCTION PROCESSES

Sławomir Kozłowski [1], Wojciech Bialik [2], Stanisław Gil [2], Łukasz Banasik [1]
[1]Re Alloys Ltd., Łaziska Górne, Poland, EU, slawomir.kozlowski@realloys.pl, lukasz.banasik@realloys.pl
[2] Faculty of Materials Engineering and Metallurgy, Silesian University of Technology, Katowice, Poland, EU, stanislaw.gil@polsl.pl, wojciech.bialik@polsl.pl
*Correspondence: stanislaw.gil@polsl.pl, Re Alloys Ltd., Łaziska Górne, Poland, EU

Abstract
The article presents issues related to the use of industrial waste, especially this generated in mining and processing of hard coal as charge material in the electrothermal reduction of silicon and aluminum oxides in a six-electrode submerged arc furnace. A broad qualitative and quantitative analysis of various industrial waste, characterized by the closest to the optimal content of compounds of silicon, aluminum, iron, "hard" carbon and trace elements that allow the use of the raw material in the production of FeSiAl alloy, was performed. The paper presents results of tests carried out in an electric furnace equipped with two 7.75 MVA transformers where iron alloys with silicon and aluminum, with Al content of 4 ÷ 20 % mass and Si content of 55 ÷ 75 % mass, were obtained using a clay-bearing mineral substance from hard coal mining as raw material and high-ash fine coal as a reducer.

Keywords: ferrosilicon-aluminum; submerged arc furnace; carbothermic reduction process; utilization of industrial wastes

1. Introduction

Ferrosilicon-aluminum belongs to a class of complex ferroalloys which, in addition to iron, contain two or more other chemical elements. So far, this alloy has been produced using two technologies. In the first method, conventionally manufactured metallic FeSi is combined with liquid aluminum. This enables production of a material with high Al content. A significant disadvantage of the method is a great aluminum loss during the manufacturing process. The other method is analogical to conventional FeSi production through carbothermic reduction of silicon- and aluminum-containing raw materials in submerged arc furnaces; it was patented in the USA in the second decade of the 20th century [1]. In the carbothermic reduction process, conventional raw materials (bauxites, kaolinites or waste materials from another process) can be used as the source of aluminum. Utilization of waste in the production of ferrosilicon-aluminum is an attractive opportunity for its disposal and can result in an additional economic effect. The most commonly considered waste is generated during production of refractory materials, ceramics and sialon ceramics. In Polish ferroalloy industry, the most useful waste materials to be utilized are mineral residues from the process of hard coal and non-ferrous metal ore upgrading. An additional advantage is the potential for using low-quality types of coal with high ash content to reduce oxides contained in gangue and other mining industry waste materials. Complex ferroalloys are utilized during production of modern steels and their application may result in technology simplification.

2. Production process

Until the middle 1950s, the scale of FeSiAl alloy production used to be minor due to a small market demand. This mainly resulted from granulometric instability of the stored alloy and reluctance of technologists to use a new steel deoxidizer. Ferroalloy-related literature from the first half of the 20th century also neglected problems with FeSiAl production in its description or it was very scarce [2]. Methodical research, carried out in the Soviet Union in 1950s, resulted in the description of a ferrosilicon-aluminum production technology using various raw materials, including industrial waste [3, 4, 5]. In Poland, the interest in the use of complex FeSiAl ferroalloys dates back to 1980s [6]. A potential for industrial waste utilization in the process of their production was also considered [7]. Further research was continued in the 2010s and resulted in development of the FeSiAl production technology with the use of industrial waste [8]. Ferrosilicon-aluminum manufacturing in the submerged arc furnace is based on Al_2O_3 and SiO_2 reduction with carbon according to the following reactions [9, 10]:

$$SiO_2 + 2C = Si + 2CO, \quad (1)$$

$$3Al_2O_3 + 9C = 6Al + 9CO. \quad (2)$$

The description of a complex process using only two reactions is strongly simplified but the analysis of all reactions in the furnace goes far beyond the scope of this paper. As in the ferroalloy production technology used by Re Alloys company, the iron source is scale formed during hot working of steel, a simplified reaction should be added to reactions (1) and (2):

$$FeO + C = Fe + CO. \quad (3)$$

Chemical compositions of the most common FeSiAl alloys are presented in Table 1.

Table 1 Chemical compositions of specific FeSiAl types [11].

Sort	Mass fraction, %						
	Si		Al		P	S	C
	min	max	min	max	max	max	max
FeSi65Al4-6	63	67	4	6	0.03	0.01	0.2
FeSi65Al6-8	63	67	6	8	0.03	0.01	0.2
FeSi75Al6-8	72	78	6	8	0.03	0.01	0.2
FeSi55Al10-15	54	59	10	15	0.03	0.01	0.2
FeSi55Al15-20	54	59	15	20	0.03	0.01	0.2

Iron content in FeSiAl results from content of primary elements Si, Al and other and it doesn't measure. It's always calculated as the rest in chemical contents.

Due to a small production scale that results from specific orders, a manufacturer can change the alloy chemical composition to some extent on the client's request. The alloys are also categorized according to the grain classes which are shown in Table 2.

Table 2 Granulometric composition of FeSiAl produced [11].

Size grade	Size grain, mm	Undersize, % mass	Oversize, % mass
1	100 - 315	20	10
2	75 - 200	20	10
3	35 - 100	18	10
4	10 - 75	18	10
5	3,15 - 35	8	10
6	3,15 - 10	10	10
7	3,15 - 6,3	10	10
8	< 3,15	-	10

The raw materials used for production of FeSiAl alloys were clay- and silicon-bearing materials which need to demonstrate proper mechanical and thermal strengths. These properties should ensure stable granulometric composition of the charge material during its transport and weighing as well as in the furnace bath (while exposed to high temperatures and mechanical load) [12]. The test material was waste from fossil fuel processing and demonstrated variable compositions that depended on its delivery time. The material characteristics are presented in Table 3.

Table 3 Chemical composition of the clay-bearing raw material (called 'aggregate' in the technology) [8].

Date of measurement	Composition, % mass				Chemical composition of the mineral residues, % mass						
	A	V	W	C	SiO_2	Al_2O_3	Fe_2O_3	CaO + MgO	TiO_2	S	P_2O_5
Accepted for the balance	88.0	9.17	0.61	2.23	64.22	22.25	5.01	-	1.04	-	0.06
25 Aug 2017	82.1	11.3	2.9	6.5	67.00	27.47	4.73	2.59	1.10	0.069	0.108
30 Aug 2017	87.9	9.7	1.7	9.3	62.72	24.06	4.98	2.75	0.92	0.077	0.139
12 Sep 2017	84.0	9.5	4	7.5	65.93	26.18	3.57	2.42	0.95	0.083	0.099
22 Sep 2017	80.7	10.8	5.3	10.6	64.42	25.40	4.31	2.89	1.02	0.084	0.104
10 Oct 2017	89.2	7.7	3.6	3.6	70.07	24.02	3.96	2.48	0.48	0.151	0.105
24 Oct 2017	82.6	10.3	5	8.8	60.51	25.06	4.83	3.11	1.01	0.098	0.173
23 Nov 2017	78.7	10.3	0.1	0.1	62.05	23.85	5.37	2.93	1.50	0.089	0.119
23 Dec 2017	88.9	9	2.8	3.5	72.84	29.84	6.21	3.12	0.54	0.037	0.146

A – ash content, V – volatile content, W – moisture content, C – fix carbon content

A missing amount of silicon in substrates was supplemented with quartzite which contains over 98 % of SiO_2. Fine coal with high amounts of the mineral substance (up to 28 % mass) was used as a reducer. Its chemical analyses are presented in Table 4.

Table 4 Fine coal characteristics [8].

Date of measurement	Composition, % mass				Chemical composition of the mineral residues, % mass						
	A	V	W	C	SiO_2	Al_2O_3	Fe_2O_3	CaO + MgO	TiO_2	S	P_2O_5
Accepted for the balance	22.5	39.8	6.5	31.3	49.01	24.48	9.66	6.33	1.04	1.64	0.130
28 Aug 2017	24.4	31.6	15.0	29.0	46.68	26.89	7.42	4.08	0.89	3.20	0.090
30 Sep 2017	18.6	34.3	14.6	32.5	41.94	22.58	17.20	5.75	0.81	3.76	0.108
23 Nov 2017	22.7	29.3	16.1	31.9	44.93	22.03	9.69	5.77	0.79	3.17	0.101
23 Dec 2017	28.8	29.2	15.4	26.6	50.35	25.35	6.25	3.85	0.83	2.47	0.104

A – ash content, V – volatile content, W – moisture content, C – fix carbon content

The use of fine coal with a dominant fine grain fraction reduces post-reaction gas outflow from the charge bed, which may influence the element yield [13]. A missing amount of the fine coal in the reduction reaction was supplemented with hard coal (pea coal granulate) containing far higher amounts of 'hard carbon' C_{fix} than the fine coal does, which additionally improves gas permeability of the charge bed. The raw materials, weighed in adequate proportions, were charged into a six-electrode submerged arc furnace where the process of reduction was carried out using electric energy as the heat source. The resulting alloy was removed (every two hours on average) from the furnace, through the tapping holes, to the ladle. Compositions of the alloys produced are presented in Table 5.

Table 5 Characteristics of FeSiAl types produced during project execution [8].

Reference period	Alloy type	Weight, Mg	Chemical composition, % mass				
			Si	Al	Ti	Ca	P
Cycle I	FeSi65Al4-6	415.34	65.04	4.39	0.33	0.43	0.021
Cycle II	FeSi65Al6-8	436.89	65.03	6.40	0.32	0.71	0.020
Cycle III	FeSi75Al6-8	356.47	72.75	6.18	0.36	0.58	0.024
Cycle IV	FeSi55Al10-15	264.75	59.07	10.93	0.86	0.66	0.029
Cycle V	FeSi55Al15-20	184.98	58.21	15.02	0.88	1.33	0.032

The values of unit electricity consumption during FeSiAl production are presented in Figure 1.

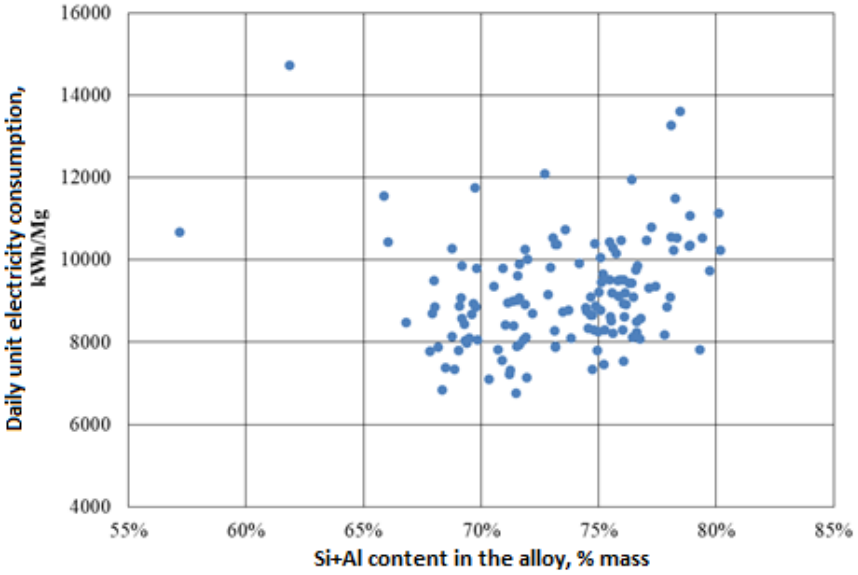

Figure 1 Daily unit electricity consumption versus Si and Al contents in FeSiAl [8].

Energy consumption in the process depends not only on the technology and raw materials, but also on a human factor related to the furnace operation. This factor can be partially responsible for significantly different rates of unit energy consumption presented in Figure 1. The rates of unit electricity consumption are similar to those observed during production of FeSi with an analogical Si content [12].

3. Conclusions

The research and experiments conducted confirmed the theses assumed for development of complex FeSiAl ferroalloy production technology:

The waste material, in the form of mining waste, can be used as a cheap and effective source of aluminum and silicon oxides during production of FeSiAl with Al content up to 20 %.

High-ash fine coal can partly replace good-quality coals in reduction blends provided that proper technological procedures are followed. In the perspective, it is possible to be used, at the industrial scale, in production of a number of alloys containing 55 to 75 % Si and up to 20 % Al.

The six-electrode submerged arc furnace ensures sufficient energy flux concentration in the furnace bath that enables adequate reduction of Al_2O_3 and SiO_2.

The rate of unit electricity consumption during FeSiAl production is comparable to analogical values observed during FeSi production. To achieve such a result, stable chemical compositions and granulation of substrates are necessary.

Due to the use of waste substrates, the analysis of FeSiAl production costs, based on experimental studies, demonstrated comparable costs to those for production of standard FeSi with the Si content close to the fraction of Si + Al in FeSiAl.

Acknowledgement

The research was carried out with co-financing under the Intelligent Development Operational Program 2014 - 2020 I Priority axis "Support for conducting R&D works by enterprises", Measure 1.2, Sectoral R&D program: INNOSTAL. The study was based on the results of the project implementation. "Development of an innovative technology for the production of iron alloys with silicon and aluminum based on industrial waste, especially from mining", project number POIR.01.02.00-00-0178 / 16.

References

[1] Patent USA nr US 1369298 A „Production of ferrosilicon aluminium” Authors: William B D Penniman, Roy S White. Date of Publication: 22.02.1921.

[2] Durrer R., Volkert G. Die Metalurgie der Ferrolegierungen. Springer-Verlag, Berlin/Göttingen/Heidelberg 1953.

[3] Yeliutin V.P., Pavlov Yu. A., Lievin B. Ye. Proizvodstvo fierrosplavov. Gosudarstviennoye nauchno-tiehnicheskoye izdatielstvo litieratury po chiornoy i cvietnoy metallurgii, Moskva 1951.

[4] Gasik M.I., Liakishev N.P., Yemlin B.I. Tieoriya i tiehnologiya proizvodstva fierrosplavov. Metallurgiya, Moskva 1988.

[5] Ryss M.A. Proizvodstvo fierrosplavov. Metallurgiya, Moskva 1975.

[6] Szydło A., Jastrzębski R., Piechocki F. Wybrane aspekty teoretyczne i praktyczne zastosowania FeSiAl w procesie odtleniania stali. *Hutnik* 1981, nr 8-9, 371-375.

[7] Sosnowski R.; Podbioł S., Kasprzyk H., Toborek P. Ocena możliwości otrzymywania stopów FeSiAl z popiołów lotnych elektrowni. *Hutnik* 1981, nr 11-12, 463-468.

[8] Projekt POIR.01.02.00-00-0178/16 ,,Opracowanie innowacyjnej technologii produkcji stopów żelaza z krzemem i glinem na bazie odpadów przemysłowych zwłaszcza pozyskiwanych z górnictwa”

[9] Elliott J., Gleiser M. Thermochemistry for Steelmaking. Vol. 1. London 1960.

[10] Snitko Yu. P. et al. Razrabotka i opyt osvoyeniya vniepiechnoy tiehnologii polucheniya fierrosilikoaluminiya v usloviyah OAO „Kuznieckiye fierrosplavy”. Nr 3. Novokuznieck 1997.

[11] Instrukcja technologiczna nr ReA 6/2016 „Wytwarzanie FeSiAl w piecu XIV”.

[12] Machulec B., Bialik W. Comparison the physico-chemical model of ferrosilicon smelting process with results observations of the process under the industrial conditions. *Archives of Metallurgy and Materials* 2016, Vol. 61, No. 1, 265 – 270.

[13] Gil S., Góral J., Ochman J., Saternus M., Bialik W. An experimental study on the air and gas removal method in a model of furnace for ferroalloy production. *Metalurgija* 2014, Vol. 53, No. 4, 447 – 450.

SOLUTION OF NON-CONFORMITIES IN THE CASE OF ALUMINIUM CASTINGS MADE IN METAL MOULDS

Ivana Kroupová[1*], Petr Lichý[1], Isabel Nguyenová[2], Miroslav Dostál[2]

[1]VSB – Technical university of Ostrava, Faculty of Materials Science and Technology, Department of Metallurgy and Foundry, 17. listopadu 2172/15, 708 00, Ostrava – Poruba, Czech Republic; petr.lichy@vsb.cz; ivana.kroupova@vsb.cz

[2] Brembo Czech s.r.o.; Isabel_Nguyenova@cz.brembo.com; Miroslav_Dostal@cz.brembo.com

*Correspondence: ivana.kroupova@vsb.cz; Tel.: +420-59-699-4321

Abstract

The contribution is aimed at identifying and eliminating defects occurred during gravity casting of aluminium alloys into metal moulds. The actual experiment of the work consists of analysis and processing of data about the defects formed directly in the production, with which the manufacturer of components for the automotive industry is confronted. The paper deals specifically with two types of pitman castings. These parts are important safety features of the vehicle and are subject to high quality demands. Based on the production data the most frequently occurring defects and examples of their elimination are described.

Keywords: aluminium alloy, casting defect, gravity casting, automotive

1. Introduction

The fields of application of aluminium alloys are currently very broad, especially in the automotive industry the use of Al-based alloys tends to steady growth. On the part of car manufacturers it is emphasized to reduce the weight of produced cars. The reduction of weight leads to fuel savings, to reduce harmful emissions and thus the car manufacturers meet environmental protection standards. The main reasons for this use are the low specific weight of aluminium alloys, their corrosion resistance and sufficient strength of the manufactured components. This also involves increasing emphasis on the quality of these parts (castings).

To achieve a high quality casting (the casting with a minimum of defects – non-conformities) is important for increasing the life and competitiveness of cast parts and it is the goal of every foundry plant. However, this fact is influenced by a number of parameters – from input material, metallurgical processing, through the used casting technology, to the actual processing of the final product. A technology very frequently used for the production of parts cast from aluminium alloys in large-scale production is gravity casting into permanent moulds. This technology is technically and economically undemanding and it allows to quickly obtain a large number of products with sufficient quality. However, this state can be only achieved after appropriate optimisation of the casting cycle and the casting parameters. At the same time it is necessary during the entire process to correctly identify the forming defects for the possibility of their further elimination [1].

2. Experimental materials and methods

The experiment is aimed at analysing the non-conformities of castings cast from aluminium alloy, namely two types of aluminium castings of pitmans (type 1 and 2), which were produced by gravity casting technology in metal moulds. This technology can be described as a simple but progressive and productive method of manufacturing castings from aluminium alloys. This method is used where it is necessary to cast larger series and volumes of castings cast mainly from materials with lower casting temperature. A permanent metal mould is used here with metal cores or cores made from moulding mixtures.

The studied castings were made of the AlSi7Mg alloy [2]. The 3D model of castings is shown on Figure 1 and 2. These are castings of chassis components – the heads of seating the wheel bearing which are hollow. When making these castings the cores produced by Croning technology are used.

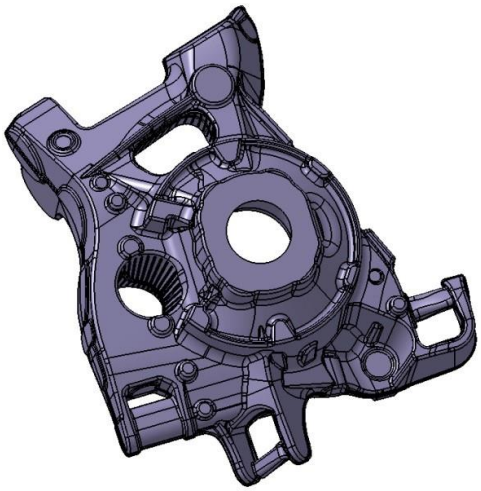

Figure 1 A pitman casting – type 1.

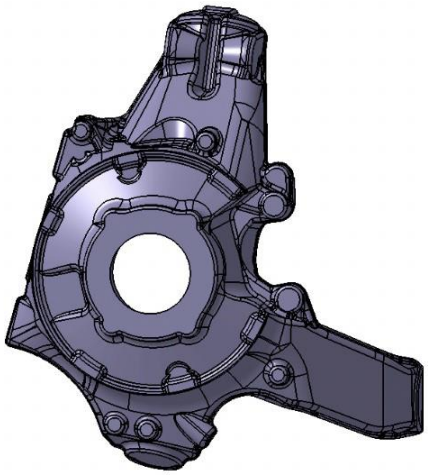

Figure 2 A pitman casting – type 2.

Data from the whole year 2018 production were available for two specific types of castings (the type 1 and 2). In these data the individual metal doses were included which were used for the production of castings. A month in which the dose was worked was added to these doses. Influence of individual seasons on the occurrence of non-conformities was solved marginally. Subsequently these data were sorted according to the individual production operations in which a possible non-conformity or other deficiency could be detected. Consecutive operations were ordered as follows: casting, manual cutting, cutting, grinding, X-ray inspection, belt grinding, blasting and penetration checking. For individual metal doses the number of castings which passed the given operation and the number of non-conforming pieces of castings after detecting the defect were known. For each metal dose was also known the casting machine on which the dose was cast and also the mould indication was known.

3. Results and discussions

Based on the provided operating data the dependencies between the casting type, the metal dose and its non-conformity expressed as a percentage were created. Allowed operating non-conformity of castings was 3%. The results under the permissible operational non-conformity were also included in this experiment. Possibilities to eliminate the most frequent defects were also consulted.

The casting of the type 1

Micro-shrinkage cavities (Table 1) and gas holes occurred most frequently in the case of castings of the type 1. The total number of studied metal doses for these castings was 22, of which 6 were below 3% (permitted operational non-conformity). From the total number of doses the 72% of them contained micro-shrinkage cavities and the average non-conformity of the cast parts with the micro-shrinkage cavity defect was 7.1%. An example of a defect of micro-shrinkage cavity type in a casting can be seen on Figure 3.

Table 1 Percentage occurrence of micro-shrinkage cavities in castings of the type 1.

Metal dose	Number of castings	Occurrence of micro-shrinkage cavities [%]
1	469	3.0
2	683	6.6
3	687	4.1
4	376	5.6
5	481	6.7
6	416	5.5
7	137	7.3

8	**605**	**8.4**
9	**521**	**8.4**
10	**150**	**9.3**
11	**340**	**3.8**
12	**545**	**9.0**
13	**577**	**9.5**
14	**830**	**9.0**
15	**391**	**5.9**
16	**634**	**12.3**

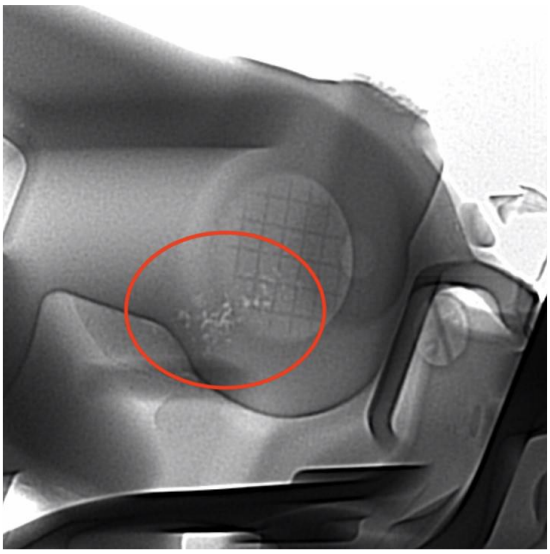

Figure 3 Picture of the X-ray inspection showing the micro-shrinkage cavities.

Another type of the non-conformity – gas holes or trapped gas – occurred in the casting of the type 1 from the total number of doses in 32% (Table 2). The average non-conformity of cast pieces with the gas hole defect was 4.3%. An example of a defect of a gas hole type in a casting of the type 1 can be seen on Figure 4.

Table 2 Percentage occurrence of gas holes in castings of the type 1.

Metal dose	Number of castings	Occurrence of gas holes [%]
1	698	3.3
2	374	3.7
3	769	5.3
4	328	4.6
5	474	3.6
6	914	4.2
7	663	5.7

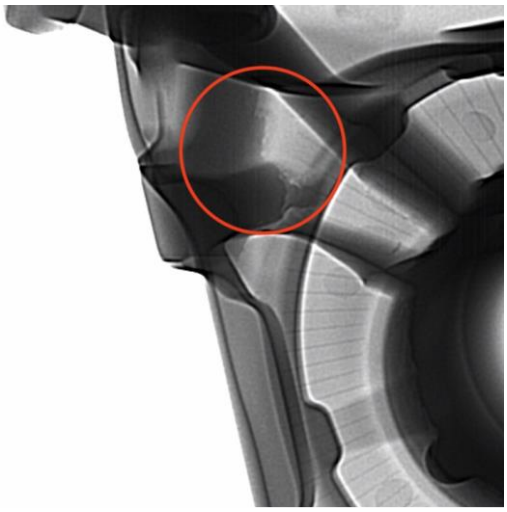

Figure 4 Picture of the X-ray inspection showing the gas holes.

In the case of a micro-shrinkage cavity defect this appeared often and all the time in one place of the casting. Several possible measures have been proposed to eliminate this defect. The first step was to enlarge the risers, another procedure was the introduction of the so-called grooving to increase the liquid metal's fluidity. However, neither of these solutions resulted in a complete elimination of the micro-shrinkage cavity defect. This defect is still in the solution, it is designed further procedure of its possible removal, namely cooling the casting in the given problematic location.

When solving the measures for an emerging non-conformity of the gas hole an error has been determined in the production data. The error consisted in wrong evaluation and determination of the non-conformity. The reason for this error is insufficient training of operators in the plant. So this non-conformity is still in the solution [2 - 4]. Several measures are proposed to eliminate gas holes – changes of the shape of the structure or more intense degassing of the mould.

The casting of the type 2

According to the achieved results the most common defects of shrinkage porosity and cold cracks type were found on the castings of pitmans of the type 2. For these castings the total number of 36 metal doses was studied. Of the total number of cast metal doses there were cold cracks in 16% (6 doses) (see Table 3) and the average non-conformity of cast pieces with the cold crack defect was 6.2%. An example of a defect of a cold crack type in a casting of the type 2 can be seen on Figure 5.

Table 3 Percentage occurrence of cold cracks in castings of the type 2.

Metal dose	Number of castings	Occurrence of cold cracks [%]
1	268	3.0
2	940	4.5
3	603	6.8
4	349	7.2
5	567	7.6
6	629	7.8

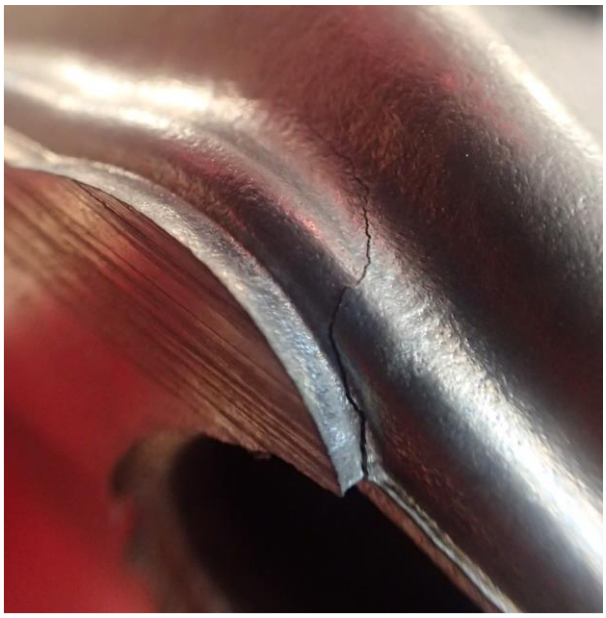

Figure 5 Picture of the cold crack in the casting of the type 2.

Another type of defect in these castings (type 2) were micro-shrinkage cavities. Of the total number of cast metal doses the micro-shrinkage cavities appeared in 50%. The average non-conformity of cast pieces with this defect was 5.4% (Table 4).

Table 4 Percentage occurrence of micro-shrinkage cavities in castings of the type 2.

Metal dose	Number of castings	Occurrence of micro-shrinkage cavities [%]
1	992	4.1
2	740	3.4
3	122	5.7
4	700	5.4
5	542	3.8
6	77	9.1
7	961	5.6
8	538	3.5
9	773	3.6
10	225	6.2
11	358	3.6
12	376	5.9
13	146	10.3
14	608	3.3
15	1160	3.3
16	848	3.1
17	752	13.4
18	834	3.5

Cold cracks in the pitman castings of type 2 were formed during the knocking-out of cores and cutting of these castings. As a measure to reduce the occurrence of this non-conformity the studied castings began to be "pre-cut" in the area of the riser – just in these places a cold crack appeared. The proposed measure helped to eliminate the mentioned non-conformity. However, for the conditions of the foundry operation this meant one additional operation which was not counted in the price of the resulting casting. Therefore it started to look for a solution after which it would not be necessary to perform this operation and would not have to increase the casting price. The design was modified when the transition area between the casting and the riser was enlarged. Subsequently tests were carried out on several cast pieces which again passed the knocking-out and cutting operations without prior pre-cutting. The castings were inspected on both X-ray and penetrating

checking with a positive result – the defect was eliminated by changing the design. Currently the company discusses this change of shape with the customer.

4. Conclusion

A detailed analysis of the production data was carried out as a part of the contribution experiment. Based on the provided operating data the dependencies between the casting type, the metal dose and its non-conformity were created expressed as a percentage. Permitted operating non-conformity of castings was 3%. It could be noted from the processed results that the most frequently occurring defects were gas holes, the occurrence of which ranged from 3.3% to 5.7%. Other common defects were micro-shrinkage cavities and cold cracks. In castings of the type 1 the average occurrence of micro-shrinkage cavities was 7.1% and for the type 2 castings the average occurrence was 5.4%. In addition for castings of the type 2 the occurrence of the cold crack defect was characteristic – in average 6.2%.

For manufacturers of automotive components the production volume and quality of manufactured castings are crucial. Equally important, however, is the precise preservation of production data for the subsequent possibility of elimination of possible forming non-conformities. Nowadays, especially when casting large series of castings, the problem is to observe the overall production process of each cast piece. The goal is to use casting marks that will remain in the entire production process and this will record specific operations each time. This would result in a more accurate keeping of data and production data for the possibility of solving the already established non-conformities.

Acknowledgement

This research was funded by the project of MEYS CZ.02.1.01/0.0/0.0/17_049/0008399. This work was carried out in the support of projects of “Student Grant Competition” numbers SP2019/43 a SP2019/148.

References

[1] Lichý, P.; Kroupová, I.; Radkovský, F.; Nguyenová, I. Possibilites of the controlled gasification of aluminum alloys for eliminating the casting defects. In: METAL 2016: 25th Anniversary international conference on metallurgy and materials. Tanger, Brno, **2016**, 1474-1479.

[2] Pastirčák, R.; Ščury, J. Effect of Pressure on the Crystallisation of AlSi7Mg Alloy. *Arch. Metall. Mater.* **2017**, 62; 4, 2193-2198. DOI: 10.1515/amm-2017-0323

[3] Dobrzański, L. A., Krupiński, M. Sokołowski, J. H., Zarychta, P. Włodarczyk-Fligier, A. Methodology of analisis of casting defects, *Journal of Achievements in Materials and Manufacturing Engineering*, 18 (2006) 267-270.

[4] Sviželová, J.; Tkadlečková, M.; Michalek, K.; Walek, J.; Saternus, M.; Pieprzyca, J.; Merder, T. Numerical modelling of metal melt refining process in ladle with rotating impeller and breakwaters. Archives of Metallurgy and Materials **2019**, 64, 2, 659-664. DOI: 10.24425/amm.2019.127595

[5] Michalek, K.; Tkadlečková, M.; Socha, L.; Gryc, K.; Saternus, M.; Pieprzyca, J.; Merder, T. Physical modelling of degassing process by blowing of inert gas. Archives of Metallurgy and Materials **2018**, 63, 2, 987-992. DOI: 10.24425/122432

EVAPORATION OF METALS IN INERT ATMOSPHERES

Jerzy Łabaj[1*], Leszek Blacha[1], Maciej Jodkowski[1]

[1]Faculty of Materials Engineering and Metallurgy, Silesian University of Technology, ul. Krasińskiego 8, 40-019 Katowice, Poland, leszek.blacha@polsl.pl; maciej.jodkowski@polsl.pl

*Correspondence: jerzy.labaj@polsl.pl

Abstract

Evaporation of volatile components of liquid metal phenomenon could occur during every single metal and their alloys melting and in their refining process as well. As many researches proved the type of gas atmosphere used affects the rapidity of that process, especially, when is carried out under atmospheric pressure. In the given article the results of researches of zinc evaporating rapidity during its melting proceeds in atmospheres of helium, carbon monoxide and helium-carbon monoxide mixture are shown.

Keywords: alloys melting; refining process; zinc evaporating

1. Introduction

As the tests provided by many authors taken from literature data proved, the pressure in the melting system significantly affects the rapidity of metal evaporation [1-3]. Generally there could be distinguished four pressure ranges affecting the process. The first range is pressure, in which the rapidity of metal evaporating achieves maximal value and does not change when it is decreased. This is a process of free evaporation, because the atoms or molecules of the evaporating metal do not collide with the gas molecules and thus move at the same rapidity at which they left the interphase surface. The second range of the pressure is where the process rapidity is controlled only by mass transport phenomena in the liquid phase. Analysing Figure 1, on which are presented kinetic curves obtained for the manganese evaporation process from iron [4] and copper from iron [5]. There could be stated that pressure ranges for which the process is determined by mass transport in the liquid phase were similar in both cases and amounts below 10 Pa. The pressure increase in the system above that value changes the stage determining the analysed process. This applies to pressure reaching up to several hundred Pascals. In that pressure range the process rapidity is determined by the mass transport phenomenon in the liquid phase and in the gaseous phase as well. That means that the type of gas should have a visible effect on the metal evaporation rapidity carried out in the pressure of 101325 Pa, in an inert and reducing gas atmosphere. On the Figure 1 and 2 examples of experimentally determined kinetic curves of the process of evaporation of copper and manganese from liquid iron with marking pressure range for which the determined process was a mass transport in gaseous phase were shown.

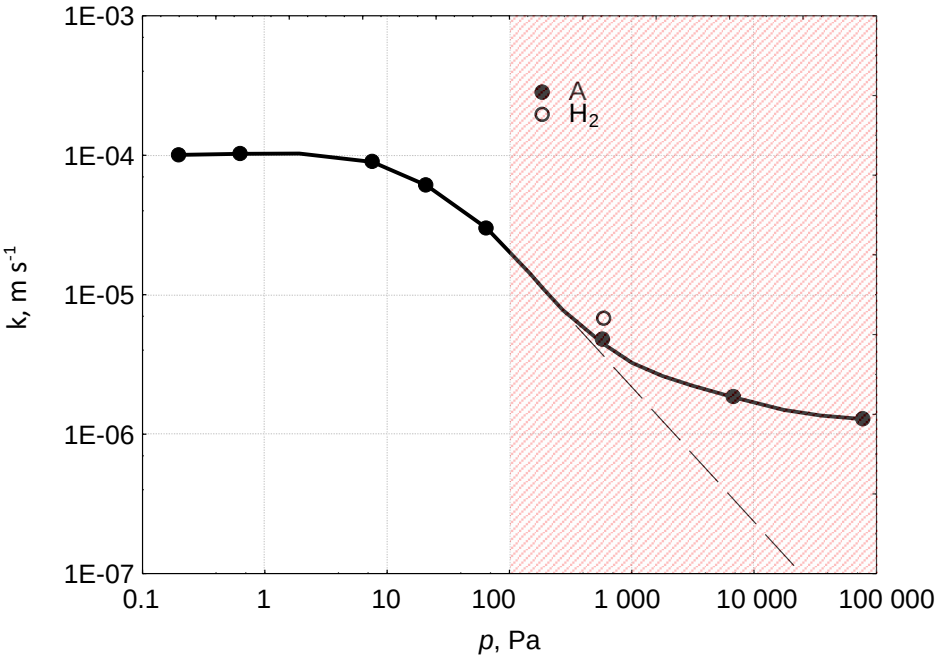

Figure 1 Influence of pressure on the overall coefficient of mass transport for manganese evaporation from iron [4].

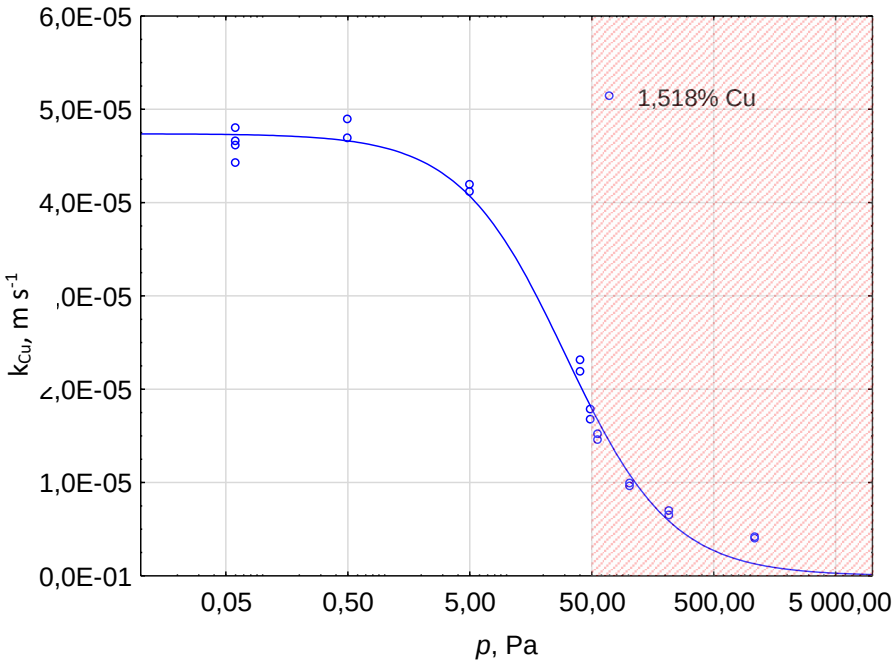

Figure 2 Influence of pressure on the overall coefficient of mass transport for the copper-iron evaporation process [5].

2. Research methods

The researches aimed at determining the rate of evaporation of zinc in a specific atmosphere were carried out by thermogravimetric method, with pressure of 101 325 Pa, in the helium, carbon monoxide and helium-carbon monoxide mixture atmosphere. During the measurement the sample's temperature, weight loss and duration of the measurement were recorded. The sample's mass loss was read for isothermal conditions when

the sample reached the desired temperature. As the material in the test the rectified zinc (the purity of 99.99% Zn) was used.

Measurements were carried out in alundum crucibles with an internal diameter of 6.5 mm. the samples mass was about 4 g. During the tests zinc vapours condensation on the working elements of thermobalance was not observed. Temperature ranges in which measurements were carried out amounted from 948 K to 1023 K.

4. Research results and their report

On the Figure 3-5 exemplified relative mass losses of zinc samples determined from measurement data for experiments carried out in gas atmosphere and 973K and 1023 K respectively are shown [6].

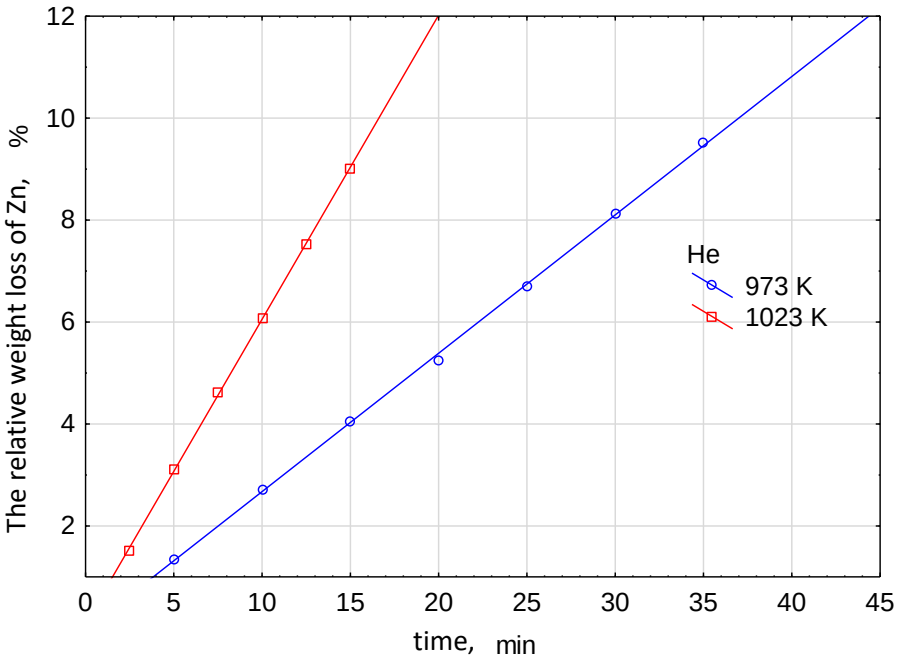

Figure 3 Relative weight loss of zinc obtained for the tests carried out in helium.

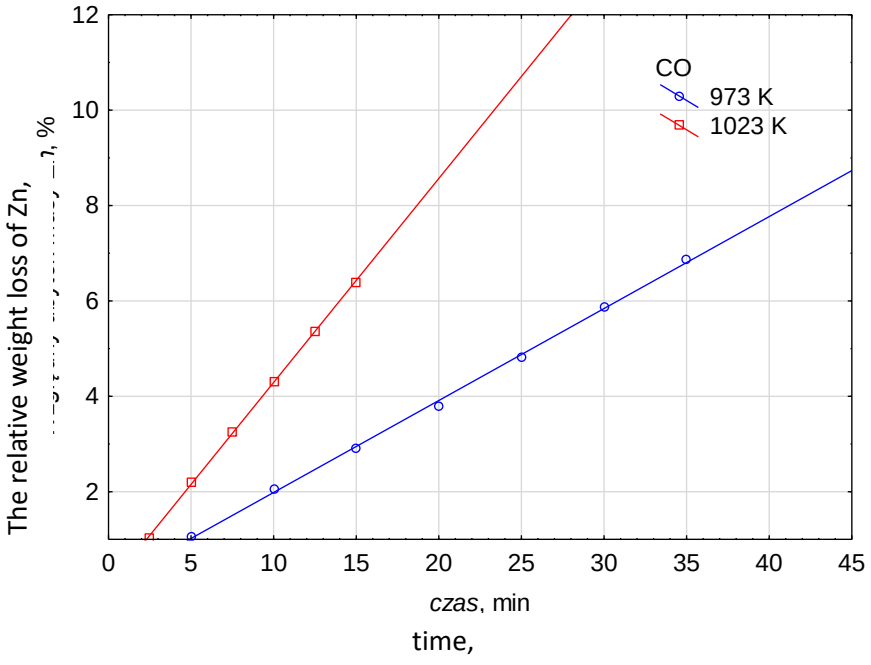

Figure 4 The relative weight loss of zinc obtained for the tests carried out in carbon monoxide.

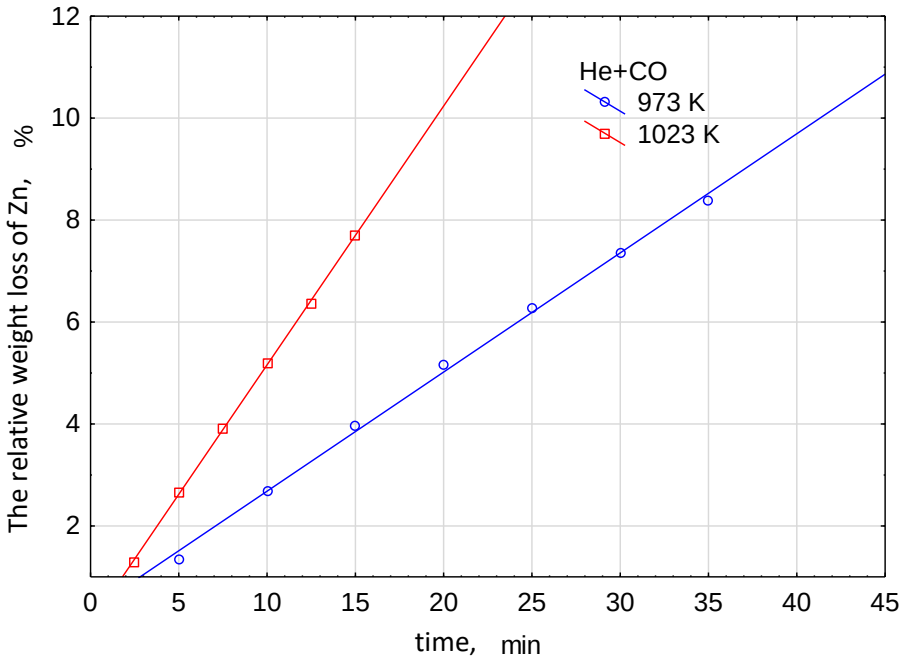

Figure 5 Relative weight loss of zinc obtained for the tests carried out in helium-carbon monoxide mixture.

Results obtained from all tests based on the measurement showed that in the case of using helium atmosphere the higher relative weight loss of zinc was observed for the same temperature than in the case of measurements carried out in CO atmosphere or He+CO mixture. For a more complete analysis of the obtained measurement results, the average values of the zinc density evaporating flux were determined. They were presented in table 1. The graphical interpretation of the zinc flux density changes for all used atmospheres in the temperature ranges from 948K to 1023 K were presents on the Figure 6.

Table 1 Average density values of the zinc evaporating flux.

The type of used atmosphere	Temperature K	Stream density Zn, mg min^{-1} cm^{-2}	
		Test 1	Test 2
He	948	23.6	22.8
He	973	32.9	33.07
He	998	54.0	53.1
He	1023	72.7	73.1
CO	948	14.05	14.50
CO	973	23.80	23.90
CO	998	28.6	31.2
CO	1 023	51.2	51.8
He+CO	948	18.08	18.30
He+CO	973	29.5	28.8
He+CO	998	42.4	42.7
He+CO	1 023	59.6	63.4

Data presented in Table 1 show, that temperature increase of the process from 948K to 1023K caused an increase in the zinc flux density in the case of helium from 22.8 to 73.1 mg cm^{-2} min^{-1}; in the case of CO from 14.05 to 51.8 mg cm^{-2} min^{-1} and in the case of He+CO mixture from 18.08 to 63.4 mg cm^{-2} min^{-1}. It could be stated that obtained values of zinc flux density followed the relationship:

$$N_{Zn\text{-}CO} < N_{Zn\text{-}He+CO} < N_{Zn\text{-}He} \quad (1)$$

Talking about the metal evaporating process in the inert gas atmosphere it must be noted that as the gas pressure decreases we observe a significant increase in the rate of evaporation [7]. The maximum value of the

density of the evaporating metal stream is observed in the case of a process carried out under ideal vacuum conditions. It can be determined from the dependence [8]:

$$\dot{N}_{Max} = \frac{p^o}{\sqrt{2\pi MRT}} \quad (2)$$

where: p^0- equilibrium pressure of evaporating metal, Pa; T- temperature, K; R- gas constant, J mol^{-1} K^{-1}

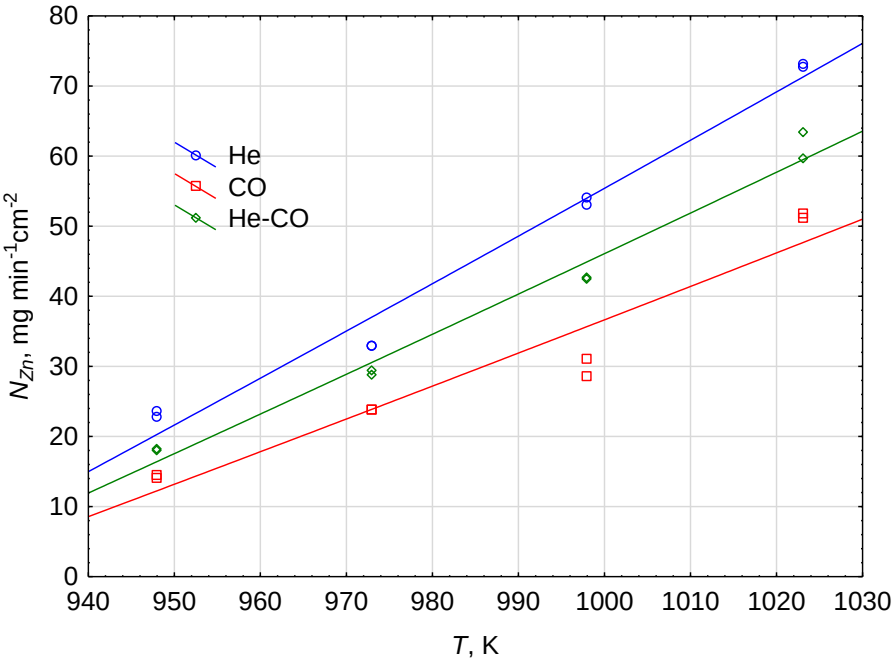

Figure 6 Changing of the density of the evaporating zinc stream in the temperature range of 948-1023 K.

Using the relationship (2) and thermodynamic data of the HSC Chemistry [9], the value of zinc flux density N_{Max} was estimated. It was in the interval: 1124 – 3212 mg $cm^{-2}min^{-1}$ for the temperature ranges 948K - 1023K.

On the Figure 7 change of values of zinc vapor diffusion coefficients in the atmosphere: helium, carbon monoxide and He+CO mixture was shown [6]. The diffusivity values were estimated from the Enskong-Chapman relationship [10]. From the data presented in this figure it follows that the value of the discussed vapor diffusion coefficients of zinc in the gas phase clearly depends on the type of atmosphere. For helium, the zinc vapor diffusion coefficient is almost 3.9 times higher than for CO and 2.4 times higher than for He+CO. We can therefore write down that there is a relationship between these diffusion coefficients:

$$D_{Zn\text{-}CO} < D_{Zn\text{-}He+CO} < D_{Zn\text{-}He} \quad (3)$$

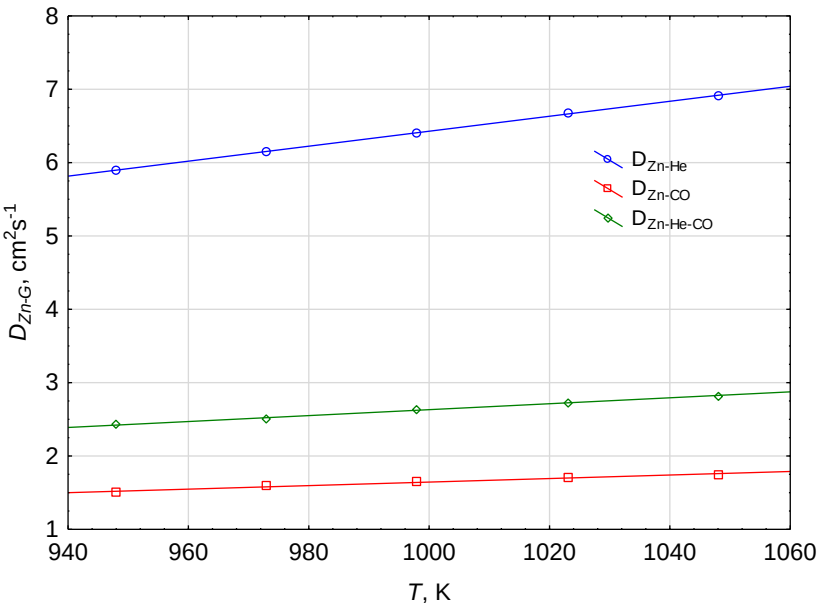

Figure 7 Change the diffusivity of zinc vapours in the atmosphere: helium, CO and helium-CO mixture for temperature range of 948-1023 K.

5. Conclusion

The conducted studies of the zinc evaporation process in various gas atmospheres showed a significant impact of the type of atmosphere on the speed of the analyzed process. The highest rate was observed for the helium atmosphere and the lowest for CO. The values of the density of the zinc evaporating flux determined from the obtained measurement data were within the analyzed temperature range in the range 22,8-73,1 mg·cm^{-2}·min^{-1} for helium; 18.08 – 63.4 mg·cm^{-2}·min^{-1} for He+CO mixture and 14.05 – 51.8 mg·cm^{-2}·min^{-1} for CO. Such a clear impact of the type of the used gas atmosphere confirms that the process of metal evaporation carried out in inert and reducing gases has diffusion control. The evaporation process values obtained constituted only up to 2.5% of the maximum values observed for evaporation processes carried out under ideal vacuum conditions.

References

[1] Blacha L., Łabaj J.: „Factors determining the rate of the process of metal bath components" , Metalurgija, 2012, vol. 51, No. 4, 529-533.

[2] Turkdogan E.T., Grieveson P., Darken L.S.: "Enhancement of Diffusion-limited Rates of Vaporization of Metals" The Journal of Physical Chemistry, 1963, vol. 67, 1647-1654, https://doi.org/10.1021/j100788a048

[3] Turkdogan E.T.: "The Theory of Enhancement of Diffusion-limited Vaporization Rates by a Convection-condensation Process" Transaction of the Metallurgical Society of AIME, 1964, vol.230, 740-749.

[4] Ward R.G.: "Evaporative losses during vacuum induction melting of steel" , Journal of the Iron and Steel Institute, 1963, vol. 1, 11-15.

[5] Łabaj J.: Kinetyka parowania miedzi z ciekłego żelaza, Wydawnictwo „Oldprint" 2010.

[6] Blacha L.: Sprawozdanie z pracy badawczej NB-68/RM3/08 „Kinetyka parowania cynku w atmosferze obojętnej i redukcyjnej" , Politechnika Śląska (niepublikowane)

[7] Fromm E.: „Reduction of Metal Evaporation Losses by Inert Gas Atmospheres" Metallurgical Transactions A, 1978, vol. 9A, 1835-1838, https://doi.org/10.1007/BF02663416

[8] Richardson F.D.: Physical Chemistry of Melts in Metallurgy, Academic Press, London 1974

[9] HSC Chemistry VER.6.1. Copyright (C) Outocumpu Research Oy, Pori Finland

[10] Wroński S., Pohorecki R., Siwiński J.: Przykłady obliczeń z termodynamiki i kinetyki procesów inżynierii chemicznej, WNT Warszawa 1979

THE POSSIBILITIES OF REFINING ALUMINIUM ALLOY MELTS USING GRAPHITE ROTORS

Petr Lichý[1*], Ivana Kroupová[1], Markéta Baierová[2], Tomáš Obzina[1], Jaroslav Štefánek[2]
[1]VSB – Technical university of Ostrava, Faculty of Materials Science and Technology, Department of Metallurgy and Foundry, 17. listopadu 2172/15, 708 00, Ostrava – Poruba, Czech Republic; petr.lichy@vsb.cz; ivana.kroupova@vsb.cz; tomas.obzina@vsb.cz
[2]JAP INDUSTRIES s.r.o., Bystřice 1260, 739 95 Bystřice, Czech Republic; marketab@jap.cz
*Correspondence: petr.lichy@vsb.cz; Tel.: +420-59-699-4321

Abstract
The contribution is devoted to the issue of refining aluminium melts. The theoretical part focuses on the sources of pollution and their influence on the quality of the melt and the final casting. For refining the AlSi7Mg0.3 alloy two types of graphite rotors and a different type of refining gas (argon and nitrogen) were used in the experiment. Results are evaluated from the point of view of the gassing value (Dichte Index). At the same time the microstructure of samples before and after refining was monitored. The results showed that the use of argon as a refining gas is more effective. In terms of use under real operating conditions, it is also necessary to assess the economic aspect.

Keywords: aluminium alloy; degassing; microstructure; Dichte Index

1. Introduction

The input material, the method and processing of the melting itself and the final treatment of the melt with the refining processes are decisive for obtaining a sufficient quality of cast parts. The input materials are mainly the pigs of the given chemical composition and return materials (residues of the gating system including risers and non-conforming castings). The problems are then chips from machining the aluminium castings, which can be very heavily polluted with organic substances (e.g. oil emulsions residues). These are used to achieve a higher economic efficiency of the production. This fact, however, often leads to consequent problems, which include an increased degree of gassing of the melt with hydrogen, a higher proportion of inclusions and the related waste castings [1]. In this case it is then necessary to use a more effective method of refining the melt [2].

An important requirement for the entire refining process, i.e. the removal of gas and inclusions from the melt, is to be as short as possible, but also as effective as possible to avoid an unnecessary downtime in the production [3]. This requirement is also important from the point of view of energy and economy intensity.

2. Experimental Materials and Methods

Nitrogen and argon gases were used in the experiment as refining media. To determine their efficiency both types of gases were tested on two types of rotors from the company JAP INDUSTRIES s.r.o. (Ltd.) marked J8 and F2A (Figure 1) at 500 rpm.

Both rotors were tested with the AlSi7Mg0.3 alloy [4]. The flow rate of the degassing medium was 10.5 $l.min^{-1}$, the melt temperature 710 °C, the ambient temperature 21 °C and air humidity of 28%. The rotor was located in the melt 150 mm above the crucible bottom.

Figure 1 Used graphite rotors (J8 – left, F2A right).

The cycle for evaluating the refining effectiveness is given in Table 1. To ensure a higher number of measurements and simulation of real conditions of operation the melt was after each refining gassed with

hydrogen using a mixed gas (H_2 + N_2). After each step the samples were taken (marked J for the rotor J8 and marked F for the rotor F2A, supplemental A letter then indicates samples obtained with the use of argon – JA and FA) which were evaluated for the purity from the point of view of microstructure of cast samples and the Dichte Index (DI). DI is a characteristic number for the melt quality of an aluminium melt sample [5,6]. The melt sample pair densities – the one resulting from the vacuum density test (D_{80mbar}) and the one from hardening under atmospheric pressure (D_{atm}) – are related to each other on the basis of the Equation 1.

$$DI = ((D_{atm} - D_{80mbar})/D_{atm}) * 100\ [\%] \quad (1)$$

Table 1 Tested refining cycle.

Order	Step	Time of the operation [min]	Marking the samples			
			Rotor J8 (nitrogen)	Rotor F2A (nitrogen)	Rotor J8 (argon)	Rotor F2A (argon)
1	After melting	-	J1	F1	JA1	FA1
2	Refining N_2	3	J2	F2	JA2	FA2
3	Gassing with H_2+N_2	6	J3	F3	JA3	FA3
4	Refining N_2	6	J4	F4	JA4	FA4
5	Gassing with H_2+N_2	6	J5	F5	JA5	FA5
6	Refining N_2	3	J6	F6	JA6	FA6
7	Gassing with air	5	J7	F7	JA7	FA7
8	Refining N_2	6	J8	F8	JA8	FA8
9	Gassing with air	5	J9	F9	JA9	FA9
10	Refining N_2	3	J10	F10	JA10	FA10
11	Gassing with H_2+N_2	5	J11	F11	JA11	FA11

3. Results and Discussions

Microstructures of obtained samples are shown in Figures 2–9. Figures 2, 4, 6 and 8 show the samples of materials before refining. Figures 3, 5, 7 and 9 then show the structure of samples after refining for 3 minutes. Figures. 3 and 5 are samples with using nitrogen and Figures. 7 and 9 with using argon as a degassing medium. In all cases it is evident that after refining there is a significant reduction of the amount of defects, i.e. gas bubbles and oxidizing inclusions. However, this effect is difficult to quantify. For this reason the gassing degree by determining the DI value was also evaluated. The obtained DI values depending on the used type of rotor and the refining gaseous medium are shown in the chart in Figure 10.

From the measured values it is evident that after the 1st refining cycle (step 2) using argon there is a more rapid reduction of the DI value than in the case of using nitrogen. In the case of using the J8 rotor the decrease of the DI value is by 81%, for the F2A rotor it is then by 66% in comparison with the starting state of gassing the melt.

In the case of using nitrogen the DI value is also reduced, but less pronounced. The specific values are 42% when the J8 rotor is used and 7% for the F2A rotor.

In the next tested steps the difference between the used rotors and gases is gradually reduced. These steps also included gradual gassing that followed every refining process. Gassing was carried out with mixed H_2+N_2 gas and it aimed at achieving higher DI values for the possibility of more refining cycles. This made it possible to use the prepared melt to perform more measurements.

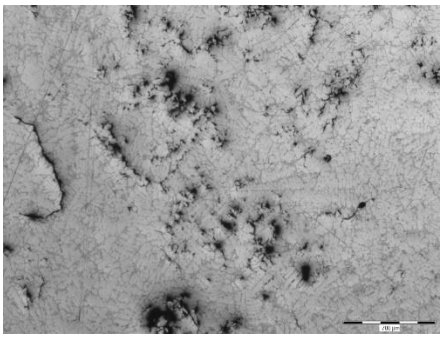

Figure 2 Microstructure of the J1 sample.

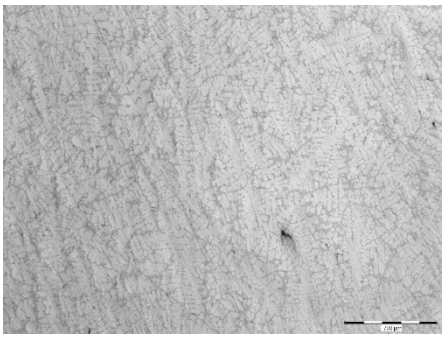

Figure 3 Microstructure of the J2 sample.

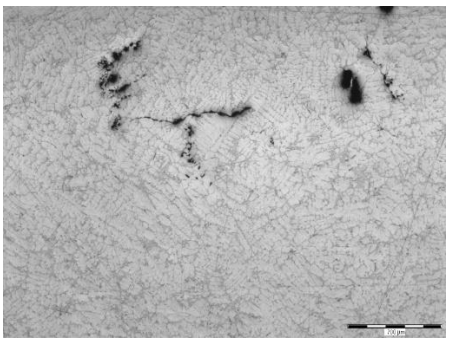

Figure 4 Microstructure of the F1 sample.

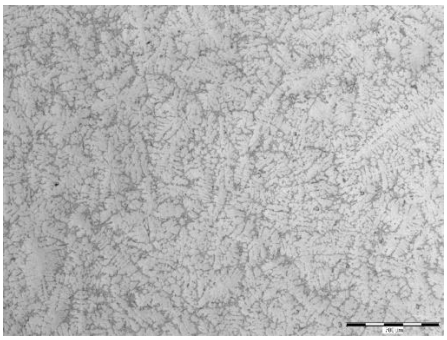

Figure 5 Microstructure of the F2 sample.

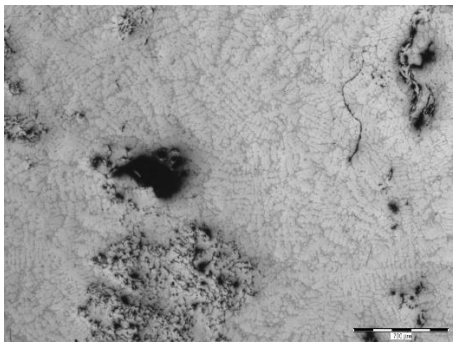

Figure 6 Microstructure of the JA1 sample.

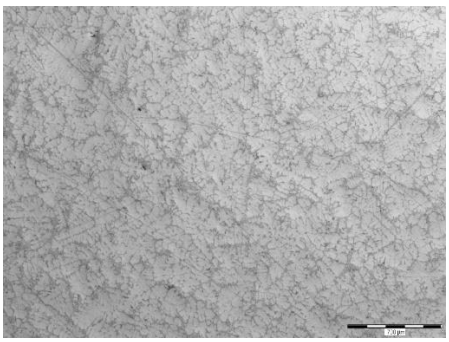

Figure 7 Microstructure of the JA2 sample.

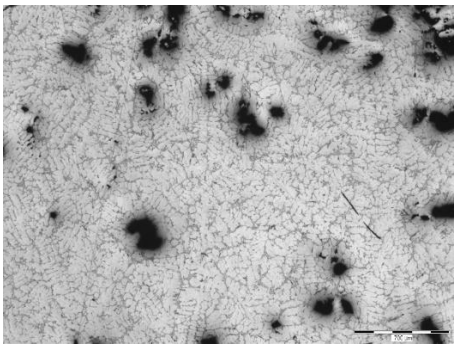

Figure 8 Microstructure of the FA1 sample.

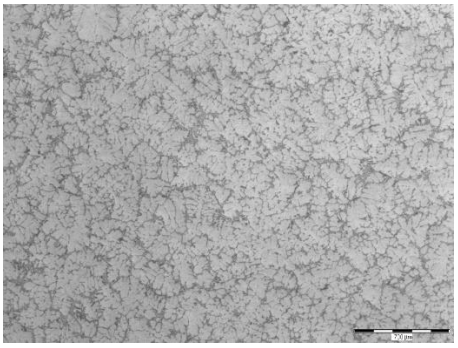

Figure 9 Microstructure of the FA2 sample.

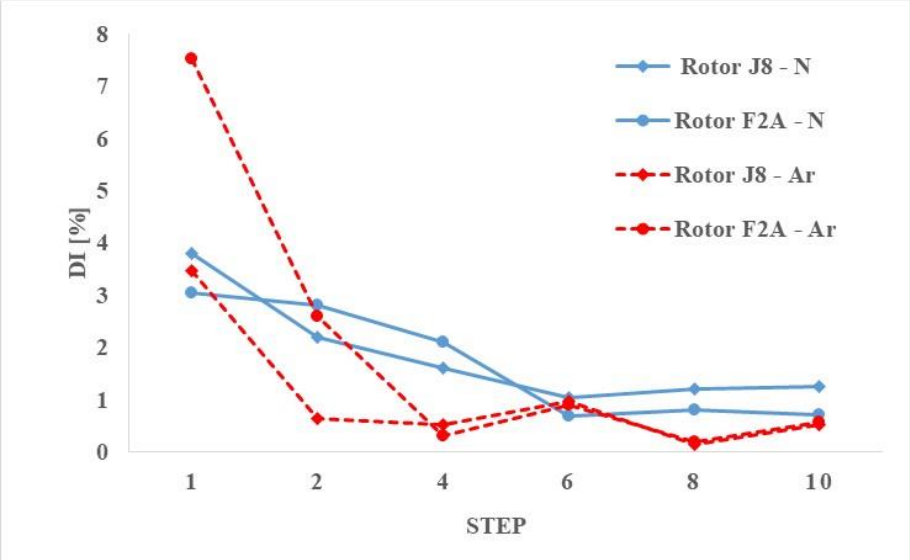

Figure 10 The DI determined in dependence on the refining step and the rotor and gas type.

4. Conclusion

The work was focused on refining the melt of the AlSi7Mg0.3 aluminium alloy. Two types of rotors marked J8 and F2A supplied by the company of JAP INDUSTRIES s.r.o. (Ltd.) were verified in combination with two refining gases – argon and nitrogen. With the use of refining conditions the argon showed significantly higher efficiency. From the point of view of the rotor type the use of the J8 type is then more effective. The most significant reduction of the gassing degree of the evaluated DI was in the case of a combination of the J8 rotor and argon as a refining gas. The least significant reduction of the DI value was then in the case of a combination of the F2A rotor and the use of nitrogen.

For an objective assessment the work will continue with the use of modified conditions of refining cycles and other types of aluminium alloys. In the conditions of foundry production the economic aspect must also be evaluated as the acquisition costs of argon are higher.

Acknowledgement

This research was funded by the project MPO TRIO FV 10080. This work was carried out in the support of projects of “Student Grant Competition” numbers SP2019/43 a SP2019/148.

References

[1] Cagala, M.; Břuska, M.; Lichý, P.; Beňo, J.; Špirutová, N. Influence of Aluminium-Alloy Remelting on The Structure and Mechanical Properties. *Materiali in Tehnologije* **2013**, 47, 2, 239-243.

[2] Michalek, K.; Tkadlečková, M.; Socha, L.; Gryc, K.; Saternus, M.; Pieprzyca, J.; Merder, T. Physical modelling of degassing process by blowing of inert gas. *Archives of Metallurgy and Materials* **2018**, 63, 2, 987-992. DOI: 10.24425/122432.

[3] Sviželová, J.; Tkadlečková, M.; Michalek, K.; Walek, J.; Saternus, M.; Pieprzyca, J.; Merder, T. Numerical modelling of metal melt refining process in ladle with rotating impeller and breakwaters. *Archives of Metallurgy and Materials* **2019**, 64, 2, 659-664. DOI: 10.24425/amm.2019.127595.

[4] Pastirčák, R.; Ščury, J. Effect of Pressure on the Crystallisation of AlSi7Mg Alloy. *Archives of Metallurgy and Materials* **2017**, 62; 4, 2193-2198. DOI: 10.1515/amm-2017-0323.

[5] Czekaj, E.; Nykiel, J.; Kwak, Z.; Garbacz-Klempka, A.; Nykiel, M. The Influence of Selected Refining Methods of AlSi7Mg0.3 Silumin on its Quality Index. *Archives of Foundry Engineering* **2018**, 18, 2, 72-78. DOI: 10.24425/122505.

[6] Djurdjević, M.B.; Odanović, Z.; Pavlović-Krstić, J. Melt quality control at aluminum casting plants. *Metall. Mater. Eng.* 16(1), 63–76 (2010) Vol 16 (1) 2010 p.63-76

INFLUENCE OF BASIC PRODUCTION PARAMETERS ON MECHANICAL PROPERTIES OF CORES PRODUCED BY C-METHOD

Václav Merta[1*], Jaroslav Beňo[1], Isabel Nguyenová[2], Miroslav Dostál[2]

[1]VSB - Technical University of Ostrava, Faculty of Materials Science and Technology, Department of Metallurgy and Foundry, 17. listopadu 2172/15, Ostrava-Poruba, 708 00, Czech Republic; vaclav.merta@vsb.cz, jaroslav.beno@vsb.cz

[2]Brembo Czech, s.r.o., Na Rovince 875, Ostrava-Hrabová, 720 00, Czech Republic, Isabel_Nguyenova@cz.brembo.com; Miroslav_Dostal@cz.brembo.com

*Correspondence: vaclav.merta@vsb.cz; Tel.: +420-59-699-4321

Abstract

Croning process (C-method) has its roots in the 1940s and marks the beginning of the chemistry of the foundry core production. Although at present the cold processes in the production of cores predominate and this process of core production seems long overdue, the cores so produced and in particular their applications have their place in the common foundry practice in the production of cast parts. It is a technology that allows the production of very shaped cores with high mechanical properties, which cannot be produced by commonly available and most commonly used processes (eg PUR COLD-BOX). The aim of this paper is to determine the basic parameters of core production, respectively. optimization of methodology for evaluation of basic parameters of core mixture for production of cores by C-method.

Keywords: foundry; core making; croning process; C-method

1. Introduction

One of the key operations in the production of quality castings is the production of molds, respectively cores for casting cavities and holes in the casting. In particular, the cores are subject to high requirements both in terms of mechanical properties, thermal stability and resistance, and dimensional stability. As a standard, the core mixtures are prepared from new quality raw materials, except for the use of reclamation sands.[1] In addition, the cores are used not only for disposable (sand) molds, but are also used in die casting. Although cold processes (COLD-BOX methods) for the production of cores are prevalent today, cores produced by older processes which were at the peak of the application in the 1980s (HOT-BOX processes) also retain a significant position, including so-called C-method (Croning). [2] It is a technology that allows to produce very complex and thin-walled cores with high mechanical strengths not only cold but also hot. In addition, it is possible to produce hollow cores, hence the evacuation of gases emitted by the decomposing organic binder is positively influenced and at the same time the disintegration of these cores is improved. [3] These types of cores can be found today mainly in the production of automotive parts such as water jackets, suction channels, wheel suspension, etc., side by side with new types of cores [4]

However, it is necessary to observe the manufacturing process and be aware of the basic properties of the so-called coated mixture, which is used in the production of cores by the C-method. As the principle of the C-method is melting of phenol-formaldehyde resin, in which are the individual grains of sand coated, if technological processes are not followed, a number of foundry defects can occur. The most common defects include, for example, gas defects due to insufficient curing of the core mixture, the formation of non-metallic inclusions (dropping of the uncured core mixture), cracking of the cores and hence dimensional inaccuracies of the pre-formed holes and cavities, and so on. [3] The aim of this paper is to determine the basic parameters of core production, respectively optimization of methodology for evaluation of basic parameters of core mixture for production of cores by C-method.

2. Experimental Materials and Methods

For the design of the experiment and verification of the critical process parameters, a resin coated sand (RCS) was used in the experiment for the production of test samples, which is a mixture of silica sand coated with a novolak phenolic resin.

Test specimens for determining the bending strength (22.5 x 22.5 x 180 mm) were prepared on a laboratory core shooting machine LUT (Multiserw) suitable for production of HOT-BOX respectively. C-method. The experiment was carried out under the following conditions:

- Core box temperature - 250; 280 and 300 °C to 0.1 °C.
- Shooting pressure - 0; 0.1; 0.3 and 0.6 MPa
- Curing time - 1; 2 and 3 min

The bending strength was determined on the LRU-2e universal strength measuring device. The device is designed to measure the strength of molding mixtures on test specimens (test bars) in the raw, dried or cured state. The hot bending strength (immediately after removing core from the core-box) and cold bending strength (after cooling of the core) was determined.

3. Results and discussions

While observing the impact of the shooting pressure, the theoretical assumption that the resulting strength increases with increasing shooting pressure is confirmed. However, there is no significant difference between the shooting pressures of 3 and 6 bar. Therefore, with respect to the mechanical wear of the shooting machine, respectively core-boxes, the shooting pressure of 0.3 MPa seems to be optimal for most core types. Only in cases of complex shape and thin-walled cores production increase of the shooting pressure might be needed. The results of hot bending strength depending on the shooting strength are graphically illustrated in Figure 1.

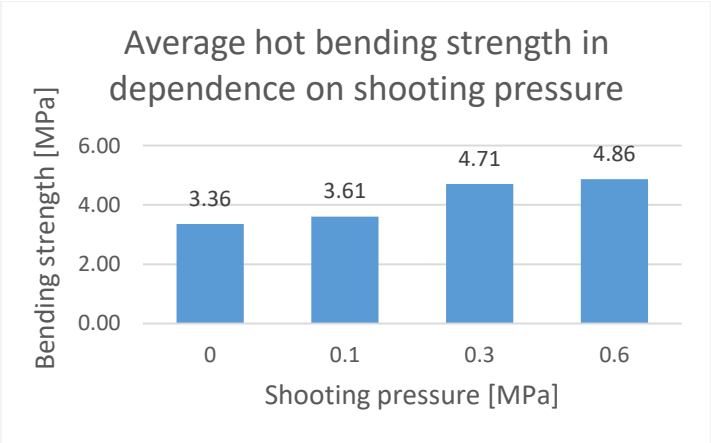

Figure 1 Hot bending strength in dependence on shooting pressure.

In Figure 2 there are graphically illustrated results of hot bending strength measurements taken on test specimens produced with the optimal shooting pressure - 0,3 MPa. From the results it is obvious that with increasing curing time the bending strength increases, as well as in case of increasing the core box temperature. However, it can be observed that the influence of curing time is stronger wherein the differences between 1 and 2 minutes of curing are relatively negligible and the best results are achieved with 3 minutes of curing, so that the curing time of 3 minutes can be considered optimal. On the other hand, the core-box temperature influence is also obvious but can be considered less signifficant as the differences are smaller in the observed rank of temperatures. And also, as the differences between 280 °C and 300 °C are relatively insignifficant, taking into account the cost of energy consumption and thermal wear of the core-box, the optimum core-box temperature is considered to be 280 °C.

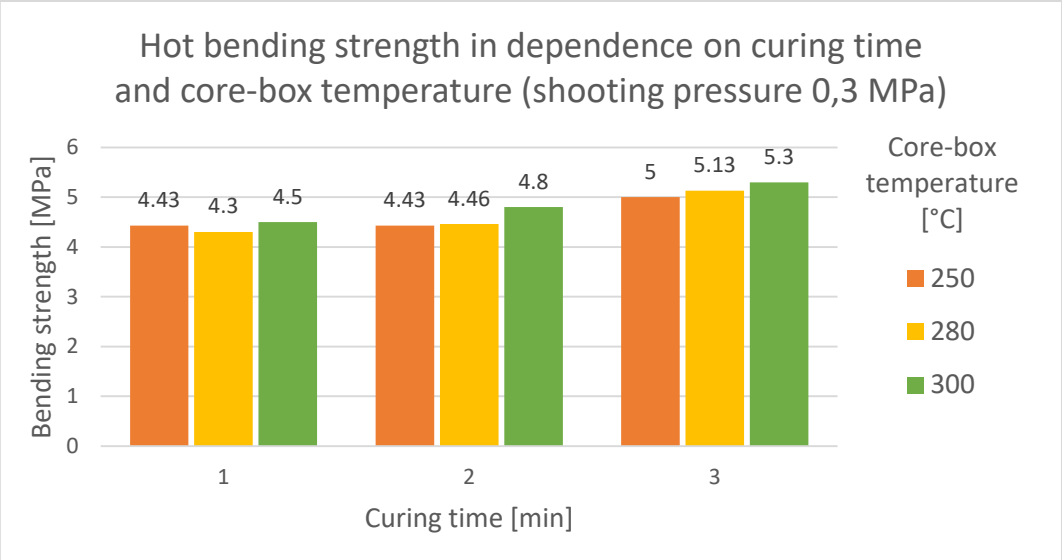

Figure 2 Hot bending strength in dependence on curing time and core-box temperature, measured on test specimens produced with optimal shooting pressure - 0,3 MPa.

Cold bending strength measurements were also carried out to clarify the influence of the monitored production parameters. In Figure 3. there are graphically illustrated results of cold bending strength measurements taken on test specimens produced with the optimal shooting pressure - 0,3 MPa. From the results it is obvious that the trends are the same as in case of hot bending strength measurements,with the only difference in slightly higher values of the resulting strengths. This confirms the validity of previous hypotheses. At the same time, it shows that under optimum conditions the cores produced by this method can achieve a bending strength of over 6 MPa.

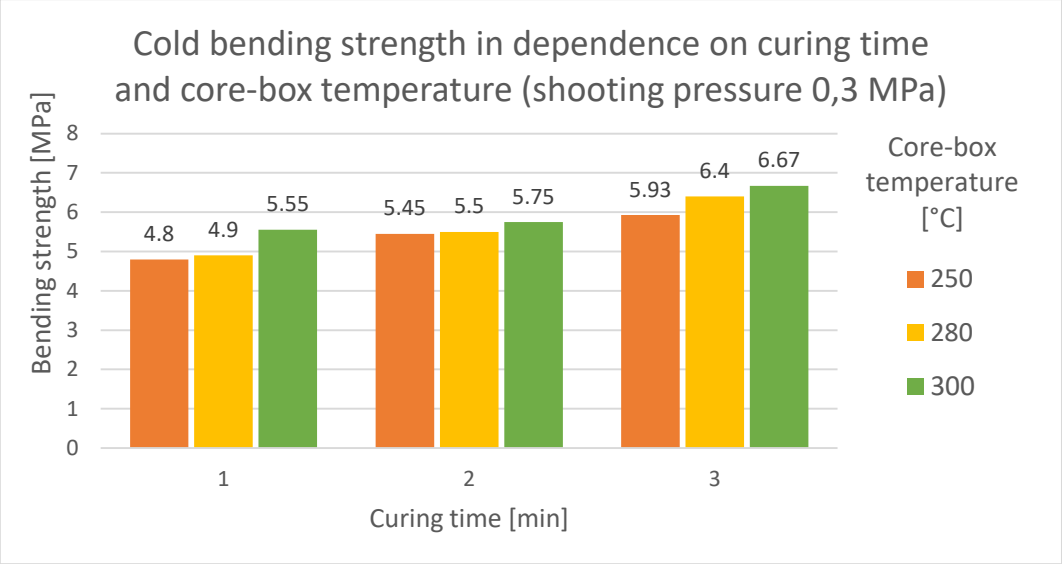

Figure 2 Cold bending strength in dependence on curing time and core-box temperature, measured on test specimens produced with optimal shooting pressure - 0,3 MPa.

4. Conclusion

In the course of the experiment, a series of bending strength measurements, both hot and cold, were carried out on test specimens in the form of test bars made by the C-method from the resin coated sand (RCS) under various process conditions. The aim of this measurement was to evaluate the influence of individual process parameters of this method on the resulting quality of the cores thus produced. The monitored parameters included shooting pressure, curing time and core-box temperature.

It is apparent from the results of the experiment that the resulting strength of the cores thus produced increases in parallel with the increase in any of these parameters. However, each of the monitored parameters acts with different intensity. Based on the analysis of the results, the following optimal values of the observed parameters were determined for the production of standard cores.

From the measured values, 0,3 MPa appears to be the optimum shooting pressure. When the pressure is increased to 0,6 MPa, there is only a minimal increase in flexural strength, while this increase would significantly increase the wear of production machines and equipment. The recommended curing time (melting of the mixture) is 3 min, especially with regard to the more complex cores. The optimum core-box temperature then appears to be 280°C. The difference in strength between 280°C and 300°C is minimal and the lowering of the temperature brings several positives. On the one hand, it is a reduction in the direct cost of heating the core-boxes. Furthermore, there will be less thermal wear of the core-boxes. This wear occurs mainly due to higher dilatation of the cores at higher temperatures. Therefore, most foundries prefer lower temperatures. In addition, the lower temperature will be compensated by a longer heating time, which will compensate for the uneven heating that occurs with this technology. It is not realistic to keep the core-box heating in such a state that the temperature field remains homogeneous.

Acknowledgement

This research was funded by the project of MEYS CZ.02.1.01/0.0/0.0/17_049/0008399. This work was carried out in the support of projects of “Student Grant Competition” numbers SP2020/39 a SP2020/64.

References

[1] Jelínek, P. Pojivové soustavy slévárenských formovacích směsí: (chemie slévárenských pojiv). [Ostrava: P. Jelínek], 2004, 241p. ISBN 80-239-2188-6.

[2] Carey, P.R. Sand Binder Systems Part X II – Hot Box, Warm Box, and Core Oil. Foundry, 1996, 3, 31-37.

[3] Fošum, J. Současný stav využívání skořepinových systémů pro výrobu forem a jader v českých slevárnách, Slévárenství, 2012, 60, 3/4, 98- 99, ISSN 0037-6825.

[4] Lichy, P.; Beno, J.; Lackova, P.; Morys, M. Influence of ecologically friendly cores on surface quality of castings based on magnesium alloys. Metalurgija 2014, 53, 3, 303-306.

DESIGN OF CASTING TECHNOLOGY USING SIMULATION PROGRAM

Filip Radkovský[1*], Václav Merta[2]

[1]Faculty of Materials Science and Technology, VSB - Technical University of Ostrava, 17. listopadu 2172/15, 70800, Czech Republic; filip.radkovsky@vsb.cz (Ing.); vaclav.merta@vsb.cz (ing.);

[2]VSB - Technical University of Ostrava, Faculty of Materials Science and Technology, Department of Metallurgy and Foundry, 17. listopadu 2172/15, Ostrava-Poruba, 708 00, Czech Republic; vaclav.merta@vsb.cz,

*Correspondence: filip.radkovsky@vsb.cz; Tel.: +421-597-324-204

Abstract

In this paper design and the optimization of foundry production of a porous metal are described. The formation of porous metal by infiltration of liquid metal into the mould cavity ensures the fastest and most efficient way of production. But even in this case, it is necessary to use correct and verified input data for manufacture process. For successful production the casting model should be firstly created using 3D drawing software and then the MAGMASOFT® 5.4 software for the numerical simulation should be applied. Utilization of MAGMASOFT® 5.4 provides optimisation of the whole manufacturing process. The accurate conditions for the real production of castings can be defined exactly by realisation of simulations of pouring and solidification. To create cavities in the casting the usage of sand cores is required. The bentonite mixture (UBM) should be used as the mould material. The following decrease of scrap rate during production saves time and incurred costs. Therefore the main aim of this research is to ensure the production of sound castings, which would be used in the field of power industry, specifically for heat exchangers manufacturing.

Keywords: porous metal; simulation program; casting; heat exchanger

1. Introduction

Porous metal in its internal structure has got purposely created cavities–pores. Materials can be divided according to the arrangement of internal cavities as regular or irregular ones. The internal structure of porous metals differs depending on the technology used. Porous metal can be produced in various ways, but the production is economically demanding, therefore it is good to deal with production by using casting technologies, where the lowest cost are expected. Thanks to that we can meet the technologies of forming the cavities with the aid of sand cores. Depending on the size, openness and the amount of pores the different behaviour in the field of thermal conductivity is observed. Open pores in the material increase thermal conductivity. This can be used for the design of heat exchangers. The principle is to let flow the fluid or gas through the open pores of the material, what will cool down or heat up the porous metal. To increase the economy of casting production of heat exchangers it is suitable to use the MAGMASOFT® 5.4 – Autonomous Engineering simulation program that represents a very mature tool for the simulation of all the casting operations from the beginning of pouring to the end of cooling process. With correct setting of the simulation program, boundary conditions and establishing the appropriate goals the critical points in the casting can be found in advance or unnecessary elements of the gating system can be removed, which otherwise burden the foundry with redundant cost of processing. [1, 2, 3].

2. Experimental Materials and Methods

Several variants of the heat exchanger in the environment of the ANSYS CFX simulation program was firstly analysed. Based on the calculations of heat transfer simulations the geometry with ball cores seems to be more efficient. A model of a casting and cores was created firstly as a drawing and then it was modelled with the Rhinoceros 4.0 program (see Figure 1 and 2) and inserted into the MAGMASOFT® 5.4 program. After production the sand cores will be settled in pairs next to each other and provided with prints. Material of the mould that will be used for the casting of the heat exchanger is the unit bentonite mixture (UBM). Casting weight is 4.72 kg with the volume of 1784.28 cm^3. The used material is the AlSi10Mg alloy [4, 5].

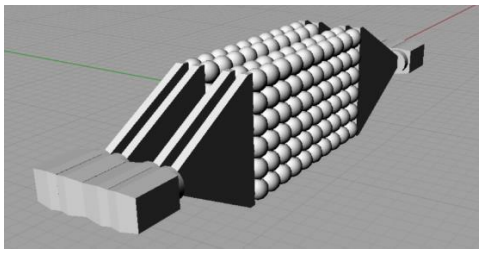

Figure 1 3D model of a sand core.

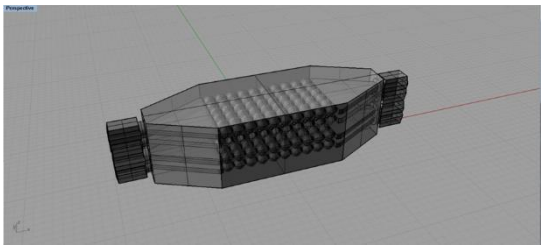

Figure 2 3D model of a casting with cores.

The next step was the creation of several different variants of gating systems and their comparison. Subsequently a suitable candidate for the design of experiments (DoE) analysis was chosen. Porosity in the casting, the optimum casting temperature of the metal, subsequently the metal temperature in the casting until the material solidification, the flow rate of metal in ingates and in the casting, microporosity, the ability of feeding the used risers, the size and shape of ingates and the casting time will be the monitored parameters. [6]

3. Results and discussions

From initial simulations that lasted nearly 120 h the one variant in was chosen as a suitable candidate for the DoE analysis because it achieved the low filling rates. Figure 3 shows a casting with the selected gating system and shrink hole in case that casting solidificated without usage of riser. Optimization was created based on the variables that were in the geometry itself, and namely the ingate width, the angle of overhang ending from the vertical wall up to a 30 ° incline, the riser diameter which was set to the values of the diameter of the bottom side of 40, 60 and 80 mm and the casting temperature. Altogether 144 pieces of variables were examined. Calculation time of the DoE analysis subsequently reached 192 hours. Of course, the calculation time could be shortened significantly by using a more powerful station (PC). The overall results of the analysis were recorded in the chart (Figure 4). Then the results were filtered.

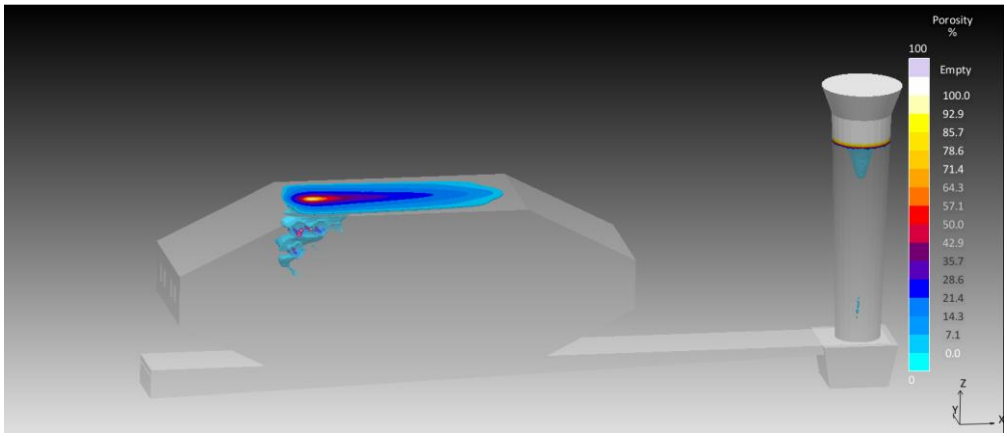

Figure 3 Porosity in casting without risers.

Following criteria were used for the choice of suitable candidates: reduction of porosity, minimum temperature in the casting, minimum temperature of the metal, lower rate in ingates, lower rate in the casting, reduction of microporosity, higher feeding ability of the riser, the usage of liquid metal. Longer filling time was chosen to comply with lower rates in ingates. The riser dimension was changed by its diameter, not height, due to testing of variants with sufficient feeding ability.

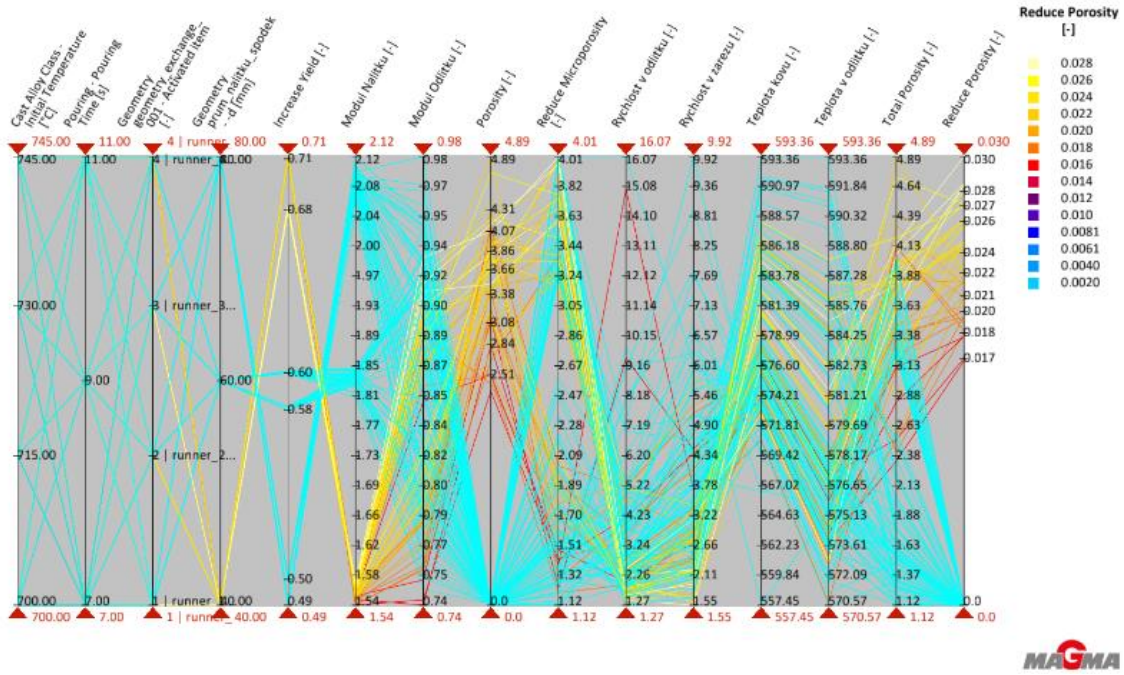

Figure 4 Unsorted results of the DoE analysis.

Versions 75 and 134 were subsequently added for comparison. The following (Figure 5) shows the flow rate in the distribution channel. Filling rates up to 0.5 m/s were recorded in the casting which is an acceptable border. There is no damage of cores and the filling is fast enough. The version 134 on the figure right shows lower rates than the more turbulent version 75 on the left. When choosing between the versions 75 and 134 it was decided in favour of the version 134. Although the version 75 showed better thermal node and a smaller drop in temperature, the riser was uneconomical. Further on the version 134 showed more continuous filling of the entire cavity. With regard to the drop in temperature in the 134 design two additional simulations were made in which the existing casting temperature compared to the newly modified one was evaluated. The initial casting temperature was 745 °C and there were too many temperature drops in narrow intercore areas. The temperature of a newly simulated sample was set to 755 °C. (Figure 6) shows the critical points in the original version 134 (on the left). On the left casting the places can be seen where in narrow spaces the temperatures of only 593 °C are reached. The casting on the right figure, however, maintains a fully cast all the time the temperature around 600 °C. Microporosity was also studied in both the above mentioned simulations. The results came out positive with a very low value of only 4% of the total volume, which was spread across the casting body.

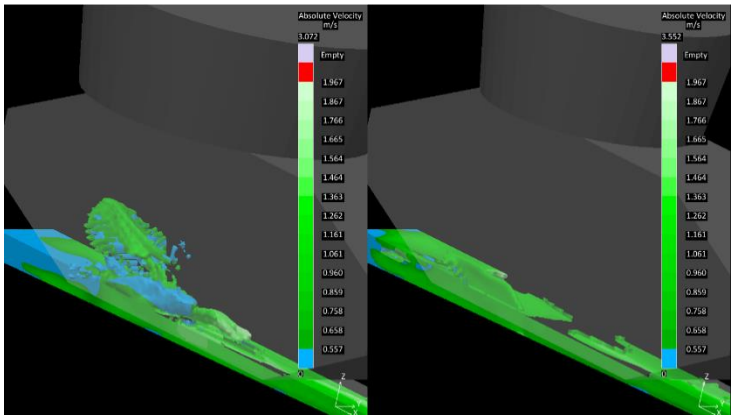

Figure 5 Rates in the distribution channel.

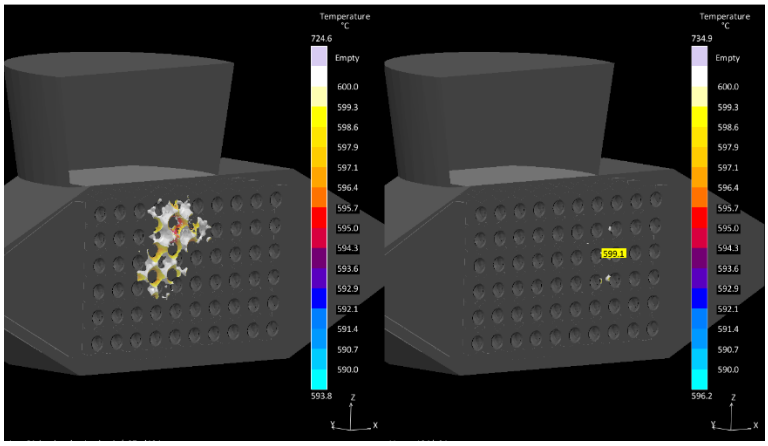

Figure 6 Critical points in version 134 left and new right. Casting temperature 745°C left and 755°C right.

4. Conclusion

A variant with a serial number 134, which was simulated under the casting temperature of 745 °C, was established as the winning design of the casting. Then the casting temperature was modified to 755 °C and once again compared with this variant. Increased casting temperature had a positive influence on the fluidity in the intercore areas, as it had been assumed. Therefore the casting temperature of 755 °C has been determined as the minimum for a successful casting of the tested sample of the heat exchanger. The riser size was sufficient to eliminate the thermal node and to compensate the material loss. At the same time the gating system allows the faster casting than simulated, which lasted 11 seconds. Common conditions in a foundry when the casting rate isn't strictly respected were taken into consideration and therefore the simulation calculated with a reserve. Acceleration of the casting time without the negative influence on the increase of the flow rate of metal in the mould cavity can be up to 15%.

Acknowledgement

This article was created within the project TH02020668 with financial support of the Czech Technology Agency.

References

[1] Lichý, P.; Bednářová, V.; Elbel, T., Casting routes for porous metals production, Archives of Foundry Engineering, Vol. 12, 2012, Issue 1/1012, ISSN 1897-3310

[2] Thomas-Sadowski, S., et al. Basic principles of gating & risering. 2nd ed. Schaumburg: American Foundry Society, c2008. ISBN 978-0-87433-315-2

[3] BANHART, J. Manufacture, characterisation and application of cellular metals and metal foams Available online: http://www.uniroma2.it/didattica/tbs2/deposito/Manufacture,_characterisation_and_application_of_cellular_metals_and_metal_foams.pdf (accessed on 1 September 2019).

[4] Lichý, P.; Elbel, T.; Kroupová, I.; Radkovský, F.; Preparation and evaluation of properties of cast metallic foams with regular inner structure, Archives of Metallurgy and Materials, 62 (2017) 3, 1643-1646, ISSN 1733-3490. doi: 10.1515/amm-2017-0251

[5] Kroupová, I.; Lichý, P.; Merta, V.; Lána, I. Use of Precursors for the Production of Cast Metallic Foams. . Materiali in Tehnologije, 53 (2019) 2, 189-191. ISSN 1580-2949. doi: 10.17222/mit.2018.141

[6] MAGMA GmbH. MAGMA GmbH Press Release: MAGMASOFT® 5.4 – Autonomous Engineering Available online: 1 – 10, https://www.magmasoft.de/export/shared/.galleries/pdfs_publications/2018_pm_en_magmasoft_rel_5_4.pdf (accessed on 1 September 2019).

APPARATUS FOR PROCESSING METALS OF LOOSE NATURE TENDING TO AIR OXIDATION, ESPECIALLY ALKALINE EARTH METALS

Aleš Slíva[1*], Robert Brázda[1]

[1]Faculty of Mechanical Engineering, VŠB-Technical University of Ostrava, 70800 Ostrava-Poruba, Czech Republic; ales.sliva@vsb.cz ; robert.brazda@vsb.cz

*Correspondence: ales.sliva@vsb.cz; Tel.: +420-59-732-5110

Abstract

The paper deals with an experience and a methodology of innovation process of a technical solution of apparatus for processing metals of loose nature tending to air oxidation, especially alkaline earth metals. The apparatus has been developed in an utility model. The aim of this technical solution is to design a device facilitating the process of treating rare earth metals in a way that would prevent their air oxidation and thus facilitate their handling in the next technological process. The utility model has been created of a standard device to prevent air oxidation without the use of protective devices and thus to facilitate their further handling. The paper has been carried out with an experience with master degree education of students in the subject Equipment in Processing Plant I., in which the apparatus for processing metals of loose nature tending to air oxidation, especially alkaline earth metals, has been developed. The education model can be used for a teaching of students in the subjects of innovation focus.

Keywords: innovation; rare earth metals; apparatus; oxidation

1. Introduction

Innovations of high degree of innovation, i.e. radical innovations are indispensable for the country's competitiveness since their considerable changes in the product [1], process or business model and therefore significantly supported by the EU member states. A significant share in the whole process of a product radical innovations plays young students of bachelor and master degree under the education process [2] with the aim of transferring of interesting innovative ideas [3] in the course in the form of interesting applied technologies resulting into original ideas for implementations of industrial and utility models or results with the highest protection level – licensed patent.

The rare earth metals (hereinafter referred to as "REM") have found significant and irreplaceable practical applications in industry and energy over the past 40-50 years due to the accelerating of new technologies, especially in the area of alternative energy sources [4-14]. There are strategic important in the area of electrical engineering, nanotechnology [15, 16], nuclear power, military technology, lasers etc. Despite their name, their occurrence on Earth is not *rare* at all. The most frequently represented cerium is the 26th element in the order of elemental composition of the Earth's crust and even the least common lutecium has 200 times higher content in comparison of gold. However, economically exploitable rare earth deposits are very rare due to their mostly low concentration in the deposit and the negative impacts of their mining and treatment on the environment [17-19].

2. Methodology of utility model development

Methodology of utility model development in education process in cooperation with students by the education process is described in the Figure 1. In the Figure 1, a problem needed to solve created by the education process is carried out the utility model in cooperation with an industrial company and an patent attorney supported by the university.

2.1. Innovation of equipment for treatment of bulk metals liable to air oxidation, especially rare-earth metals - state of the art

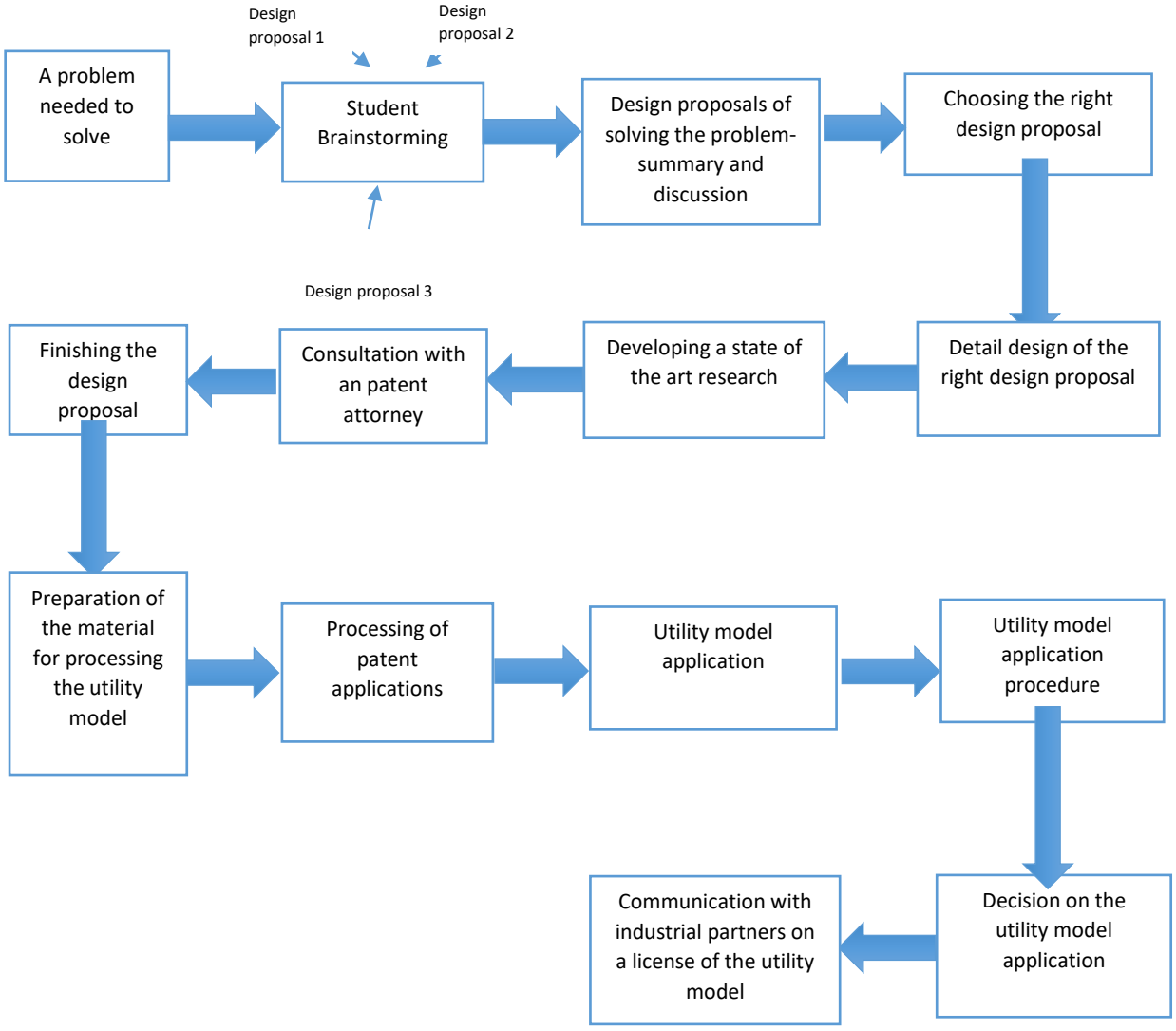

Figure 1 Methodology of utility model in education process.

The most frequently used possibility of REM surface treatment is the application of a protective coat in the form of other metals [10, 20-24], the so-called metal-plating, such as zinc, nickel, silver and gold plating. There are numerous technologies for the coat application [25], starting from brush painting, dipping, spraying, electrostatic painting, galvanization etc. The application of another layer of a different metal on the REM surface is an invasive method and it causes contamination in the following technological process.

The goal of the technical solution is to propose a design of equipment facilitating REM treatment in a way which would prevent their air oxidation, and thus facilitate handling of them in further technological process and particle characterization [26, 27].

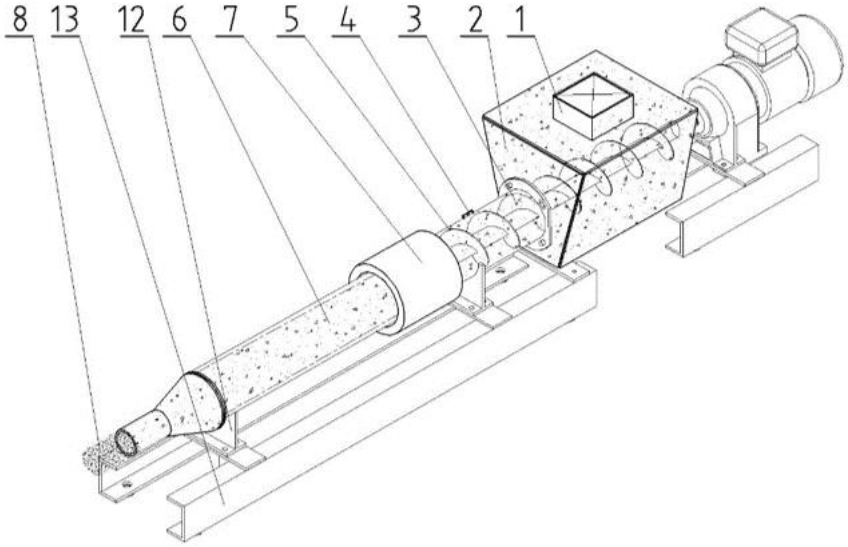

Figure 2 A design of the utility model of the bulk metal treatment equipment [10].

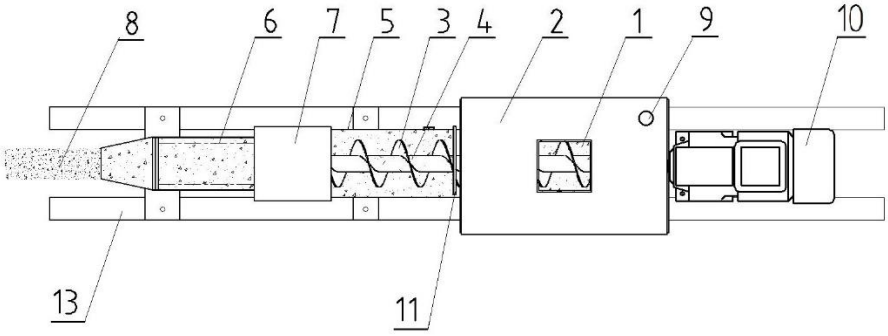

Figure 3 A design of the utility model of the bulk metal treatment equipment [10].

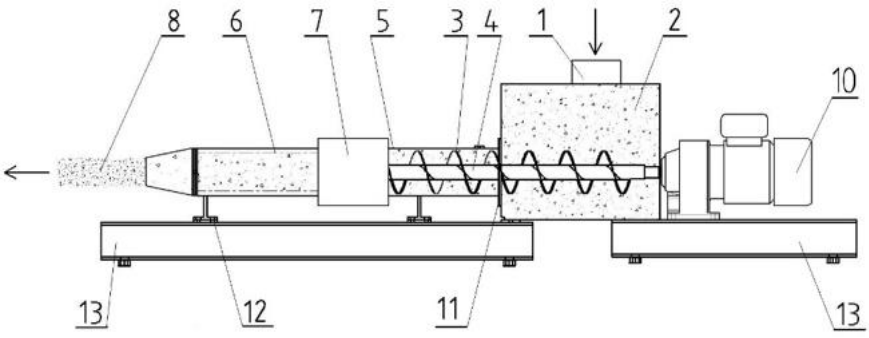

Figure 4 The front view of a design of the utility model of the bulk metal treatment equipment [10].

3. An example of technical solution of the utility model

In general, the equipment for treatment of bulk metals **6** liable to air oxidation, the treatment equipment especially for alkali-earth metals, is shown in **Figure 2** through **4.** The equipment of this embodiment consists of a load-bearing structure **13**, on which there is a storage tank **2** with a hopper **1**, which is equipped with a protective gas inlet **9**. A shaft **4** with a worm **3** goes through the storage tank, which reaches into a heated tube **5** with a flange **11**, by which the heating tube **5** is connected to the storage tank **2**, where the other end of the shaft **4** is connected with a drive **10**. Furthermore, on the heating tube **5** there is a heating system **7** that sintered the bulk metals **6** to the continuum of metal materials **8** and the tube is connected with a load-bearing structure **13** by means of supports **12**.

The utility model has been published in Espacenet database under European Patent Office [10].

5. Conclusion

In this paper, the methodology of utility model in the educated object has been explained from the very hint of a student, i.e. his/her idea, as far as to the work implementation in a form of a utility model. The main objective of the creation of the methodology was the student's familiarisation with the innovation procedures from the draft idea through the cooperation with the patent representative and the university.

There is described an exact way for finding a solution in the methodology formed into the Figure 1, including the steps necessary to be adopted for the utility model registration. A significant part of these procedures is an exact description of the concrete work – utility model: apparatus for processing metals of loose nature tending to air oxidation, especially alkaline earth metals starting from the state of the art in the form and findings of concrete similar constructions, over the publication of the utility model subject matter, including its description of functions and drawings, and ending with the composition of utility model claims necessary for filing the utility model application.

Acknowledgement

The paper has been done in connection with the Innovative and additive manufacturing technology – new technological solutions for 3D printing of metals and composite materials project, reg. no. [CZ.02.1.01/0.0/0.0/17_049/0008407] financed by the [Structural Founds of Europe Union] and the [SGS SP2019/101] Student Grant Competition – Transport Science and Research – Transport Simulation, Adhesive Models and Storage Processes project.

References

[1] Fries, J.; Hapla, T. Influence affecting the lifetime of belt conveyor's drive drums. *Tehnicki Vjesnik* **2018**, 25, 7-14. [CrossRef]

[2] Oujezdsky, A.; Sliva, A.; Brazda, R. *Using ICT in education: measuring systems interfaced to computers*; 9th International technology, education and development conference. Madrid: INTED Proceedings, **2015**, 7509-7512.

[3] Cep, R.; Janasek, A.; Sliva, A.; Neslusan, M.; Binder, M. Experimental tool life tests of indexable inserts for stainless steel machining. *Tehnicki vjesnik-technical gazette* **2013**, 20, 6, 933-940.

[4] Anderson, Nathaniel A; Hupalo, M.; Keavney, D.; Tringides, M.; Vaknin, D. Intercalated rare-earth metals under graphene on SiC. *Journal of Magnetism and Magnetic Materials* **2019**, 474, 666-670. [CrossRef]

[5] 5Aoki, Y.; Habazaki, H.; Konno, H. Interconversion between rare-earth metal (III) chromates (V) and low-crystalline phases by reduction with methanol and oxidation in air. *Chemistry of Materials* **2003**, 15, 12, 2419-2428. [CrossRef]

[6] Barisic, D.; Buschmann, D., A.; Schneider, D.; Maichle-Moessmer, C.; Anwander, R. Rare-earth-metal pentadienyl half-sandwich and sandwich tetramethylaluminates-synthesis, structure, reactivity and performance in isoprene polymerization. *Chemistry European Journal* **2019**, 25, 18, 4821-4832. [CrossRef]

[7] Charalampides, G.; Vatalis, K.; Karayannis, V.; Baklavaridis, A. *Environmental defects and economic impact on global market of rare earth metals*; 20th Innovative Manufacturing Engineering and Energy Conference (IManEE): Kallithea, Greece, 2016, 161. [CrossRef]

[8] Hamza, A.; Mohammed F.; El-Aassy; Ibrahim E.; Guibal, E. Integrated treatment of tailing material for the selective recovery of uranium, rare earth elements and heavy metals. *Minerals Engineering* **2019**, 133, 18, 138-148. [CrossRef]

[9] Liu, R.; Chen, G. Characteristics of rare earth elements, Zr, and Hf in ore-bearing porphyries from the western Awulale metallogenic belt, Northwestern China and their Application in determining metal fertility of granitic

magma. *Resource Geology* **2019**, 69, 2, 193-210. [CrossRef]

[10] McLellan, B., C.; Corder, G., D.; Golev, A.; Ali, S., H. *Sustainability of the Rare Earths Industry;* 4th International Conference on Sustainable Future for Human Security (SUSTAIN), **2013**, Kyoto Univ, Kyoto, Japan. 20, 280-287. [CrossRef]

[11] Nigussa, K., N.; Stovneng, J. A. Alloy structure of rare earth Ce with Pt base metal, and the adsorption of CO. *Materials Research Express* **2019**, 6, 4. [CrossRef]

[12] Odintsov, V., V.; Koren, E. V. Tribological properties of dodecaborides of rare-earth metals. *Journal of Friction and Wear* **2018**, 39, 6, 483-486. [CrossRef]

[13] Oleneva, E.; Savosina, J.; Agafonova-Moroz, M.; Lumpov, A.; Babain, V.; Jahatspanian, I.; Legin, A.; Kirsanov, D. Potentiometric multisensor system for tetra- and hexavalent actinide quantification in complex rare earth metal mixtures related to spent nuclear fuel reprocessing. *Sensors and Actuators B-Chemical* **2019**, 288, 155-162. [CrossRef]

[14] Wuebbeke, J. Rare earth elements in China: Policies and narratives of reinventing an industry. *Resources policy* **2013**, 38, 3, 384-394. [CrossRef]

[15] Sliva, A.; Brazda, R.; Zegzulka, J.; Dvorsky, R.; Lunacek, J. Particle characterization of nanoparticle materials in water jet mill device. *Journal of Scientific Conference Proceedings* **2010**, 2, 1, 45-48. [CrossRef]

[16] Sliva, A.; Samolejova, A.; Brazda, R.; Zegzulka, J.; Polak, J. Optical parameter adjustment for silica nano and micro-particle size distribution measurement using mastersizer 2000. *Microwave and Optical Technology* **2003**, 5445, 160-163. [CrossRef]

[17] Brozova, S. *Possibility of using pyrolysis and plasma during disposal of plastic parts of electric waste;* International Multidisciplinary Scientific GeoConference Surveying Geology and Mining Ecology Management, SGEM, Albena, Bulgaria, **2013**, 423-428. [CrossRef]

[18] Brozova, S.; Drapala, J.; Kursa, M.; Pustejovska, P.; Jursova, S. Leaching refuse after sphalerite mineral for extraction zinc and cobalt. *Metalurgija* **2016**, 55, 3, 497-499.

[19] Brozova, S.; Ingaldi, M.; Sperlin, I. *Economical aspects of high-temperature heating utilization for industrial waste treatment;* METAL 2013 - 22nd International Conference on Metallurgy and Materials, Ostrava: TANGER. **2013**, Brno, 1735-1739.

[20] Hayes, Sarah M.; McCullough, Erin, A. Critical minerals: A review of elemental trends in comprehensive criticality studies. *Resources Policy* **2018**, 59, 192-199. [CrossRef]

[21] Jonsta, P.; Vanova, P.; Brozova, S.; Pustejovska, P. Hydrogen embrittlement of welded joint made of supermartensitic stainless steel in environment containing sulfane. *Archives of Metallurgy and Materials* **2016**, 61, 2A, 709-711. [CrossRef]

[22] Kardas, E.; Brozova, S.; Pustejovska, P. The Evaluation of Efficiency of the Use of Machine Working Time in the Industrial Company - Case Study. *Management Systems in Production Engineering* **2017**, 25, 4, 241-245. [CrossRef]

[23] Kardas, E.; Brozova, S. *Situation in waste treatment in Poland*; METAL 2013: 22nd International Conference on Metallurgy and Materials, Conference Proceedings, **2013**: Brno, 1773-1778.

[24] Meshram, P.; Pandey, B., D. Perspective of availability and sustainable recycling prospects of metals in rechargeable batteries - A resource overview. *Resources Policy* **2019**, 60, 9-22. [CrossRef]

[25] Dvorsky, R.; Lunacek, J.; Sliva, A.; Sancer, J. Preparation of silicon nanoparticular nanocomposite with thin interparticular tin matrix. *Journal of Nanoscience and Nanotechnology* **2011**, 11, 10, 9065-9071. [CrossRef]

[26] Sliva, A.; Brazda, R.; Prochazka, A.; Martynkova, G., S.;imha, Barabaszova, K., C. Study of the optimum arrangement of spherical particles in containers having different cross section shapes. *Journal of nanoscience and nanotechnology* **2019**, 19, 5, 2717-2722. [CrossRef]

[27] Sliva, A.; Brazda, R.; Prochazka, A.; Martynkova, G., S.;imha, Barabaszova, K., C. Investigation of geometric properties of modified titanium white by fluidisation for use in the process of transport, handling, processing and storage. *Journal of nanoscience and nanotechnology* **2019**, 19, 5, 2997-3001. [CrossRef]

[28] Slíva A.; Drápala J.; Brožová S.; Machovčák P.; Jonša P. CZ28113 (U1) Apparatus for processing metals of loose nature tending to air oxidation, especially alkaline earth metals. European Patent Office. Espacenet Database **2015**

STUDY OF THE TEMPERATURES OF PHASE TRANSFORMATIONS OF STEELS AND THEIR APPLICABILITY IN THE TECHNOLOGY OF STEEL CASTING

Michaela Strouhalová[1*], Karel Michalek[1], Bedřich Smetana[2]

[1]Faculty of Materials Science and Technology, Department of Metallurgy and Foundry, VSB-Technical University of Ostrava, 70800 Ostrava, Czech Republic; michaela.strouhalova@vsb.cz, karel.michalek@vsb.cz

[2]Faculty of Materials Science and Technology, Department of Physical Chemistry and Theory of Technological processes, VSB-Technical University of Ostrava, 70800 Ostrava, Czech Republic; bedrich.smetana@vsb.cz

*Correspondence: michaela.strouhalova@vsb.cz; Tel.: +420-59-732-4345

Abstract

A comprehensive experimental and theoretical study of the thermo-physical, thermodynamic, physico-chemical properties of steels and also the modeling of the processes of steelmaking it allow to achieve the top quality of the cast, semi-finished steel product, which is comparable or superior with the quality of world producers of these materials. The paper is focused on the study of phase transformations temperatures in different types of high-alloy steels during its solidification process. The field of the research reflects current world trends in the field of new steel grades, microstructure and mechanical properties of steel, subsurface and surface quality of final products, etc. The realization of highly specialized measurements of thermo-physical properties of steels, respectively the knowledge of phase transformation temperatures (liquidus and solidus temperatures) of steels, is the basic precondition for successfully understanding (manage) the process of cast of steels with the high internal homogeneity. Based on this information, important and significant parameters are specified in the whole technological flow of steelmaking production. Knowledge of those temperatures in combination with utilisation of the method of numerical modeling (setting of boundary condition of numerical simulation of steel solidification process) can then improve the quality of cast steel without any additional treatment.

Keywords: steel casting technology; phase transformation temperatures; direct thermal analysis; differential thermal analysis; high-alloy steels

1. Introduction

Current trends show that more than 96% of the steel produced in the world is processed by continuous casting. But the production of steels made by technology of ingot casting is still irreplaceable with regard to the specific requirements on the final shape of ingot, which can't to be made by continuous casting technology. Steel producers are in both cases exposed to naturally increasing pressure of customers to production of steels with top quality. One of the important aspect (factors) influencing the quality of cast steel is correct setting of parameters [1-3] of own casting process as the temperature of superheat of steel before casting, casting speed, casting temperature whose have an effect on character of solidification, structure of cast steel etc. Setting of those parameters depends on the knowledge of temperatures of phase transformations [4,5]. Most important phase transformation at steelmaking process is crystallisation of steel (phase transformation of steel from liquid to solid state), which has significant influence on process of own solidification of steel. Critical factors characterising the steel's behaviour during the solidification process are liquidus (T_L) and solidus temperature (T_S). These temperatures are important for the correct setting of casting and solidification conditions of steel yet and significantly affect the final quality of the cast steel. Experimental determination of the T_L and T_S temperature may lead to more precise determination of the width of the interval of steel solidification (two phase region). Liquidus (T_L) and solidus temperature (T_S) may be investigated by several ways. The most frequently used approaches are experimental determination of these phase transformation temperatures using thermo-analytical methods[6,7] and the second one is theoretical determination using various models implemented in commercial software applications [8,9]. Usually, it is not so easy to identify the phase transformations occurring in such multicomponent systems like steels in high temperature region (over 1000 °C). It is therefore appropriate to combine different approaches - experimental and theoretical and also with numerical simulations [10-12], because we can achieve more accurate results and thus better knowledge of eventual impacts of newly improved technological parameters to steel casting process and final quality of cast steel.

In this paper is an attention focused on study of liquidus and solidus temperatures of three steels grades by thermal analysis methods and their comparison with theoretical calculations of these temperatures by thermodynamic SW's. This work follows systematic study of T_L and T_S temperatures [13-16] of various types of steels (low alloy, special types of steels) and its measurement can lead to more accurately determine T_L and T_S temperatures for specific conditions of industrial partner.

2. Experimental methods, material's specification and experimental configuration of the analyses

For experimental investigation of T_L and T_S temperatures of steels in high temperature region were used two thermo-analytical methods – "Direct Thermal Analysis" method (method is often called Heating/Cooling curve Thermal Analysis) and Differential Thermal Analysis method (DTA).

Method of "Direct Thermal Analysis"[6,7] is based on a "direct" measurement of the temperature of studied sample during its controlled linear heating or cooling. The result of the experiment (analysis) is a heating or a cooling curve which expresses dependency of the temperature on time. During the phase transformation ongoing the temperature curve changes its otherwise linear progression. Deflection of the temperature curve from its baseline is observed. Temperatures of phase transformation is then possible to obtain by the interpreting such deflections from baseline for given experimental conditions.

The principle of Differential Thermal Analysis[6,7,17] (DTA) method is a measurement of the temperature difference between the measured sample and the reference. The reference can be an empty reference crucible or a reference crucible with a standard material. The sample and reference are exposed to the same setting of the temperature program (linear heating conditions usually). The result of DTA analysis is a DTA curve with expresses the dependency of the temperature difference between the measured sample and the reference. If the phase transformation occurs in the sample there is also a deflection of temperature curve from the baseline and the peak is formed. Temperatures of phase transformation is possible to obtain by the interpreting such peaks for given experimental conditions.

2.3 General material's specification - steel grades type overview

Experimental study of T_L and T_S temperatures were performed for three industrially produced steels grades:

- 15Cr18Ni - steel with increased susceptibility to crack formation during rolling of ingots,
- X22CrMoV12-1 - steel for turbine blades, with high demands on cleanliness and structure,
- X3CrMoNb 18-2 - ferritic magnetically mild steel, under development.

An overview of the selected elements of the chemical composition of studied steel grades is shown in **Table 1**.

Table 1 Chemical composition of steel samples (wt.%) provided by the project partner.

Steel grade	C	Mn	Si	P	S	Cu	Cr	Ni	Al	Mo	W	V	Ti	Co	B	Nb	N
15Cr18Ni	0.160	1.01	1.54	0.033	0.014	0.13	20.21	12.31	0.028	0.271	0.03	0.051	0.003	0.070	0.0040	0.009	0.0703
X22CrMoV12-1	0.212	0.65	0.34	0.012	0.004	0.03	11.59	0.57	0.008	0.87	0.00	0.33	0.00	0.01	0.0002	0.00	0.0110
X3CrMoNb18-2	0.016	0.68	1.04	0.029	0.008	0.05	18.66	0.29	0.030	1.71	0.01	0.06	0.01	0.02	0.0003	0.48	0.0174

2.1 Experimental apparatus and measurement configuration

Studied steel samples were analysed with the utilization of two experimental laboratory systems (apparatus) - STA 449 F3 Jupiter, manufactured by NETZSCH-Gerätebau GmbH, Germany, year of manufacture 2011 (**Figure 1**) for "Direct Thermal Analysis" method, Setaram SETSYS 18$_{TM,}$ manufactured by SETARAM Instrumentation, France, year of manufacture 2001, for DTA (**Figure 2**). The Netzsch STA 449 F3 Jupiter, experimental laboratory system used an 'S' type mono-couple sensor for T_L and T_S temperature detection. Steel samples were analysed in the regime of a cyclic experiments and under the linear heating and linear cooling conditions. During the cycling experiment is steel sample heated and cooled under the same experimental conditions first time in first cycle and the second time in the second cycle. The mass of the studied steel samples were approximately 21-23 g. Heating and cooling rate was 5 °C.min^{-1}. For each studied steel grade were measured two steel samples by "Direct Thermal Analysis" method. The second experimental laboratory system Setaram SETSYS 18$_{TM}$ were used the 'S' type tri-couple sensor for measuring the T_L and T_S temperatures.

The mass of the studied samples was approximately 200 mg. An empty corundum crucible was used as reference. On Setaram SETSYS 18_{TM} analyses under linear heating conditions was performed. Heating rate was 10 °C.min^{-1}. By DTA three pieces of steel samples of each steel grade was analysed.

Figure 1 Netzsch STA 449 F3 Jupiter.

Figure 2 Setaram Setsys 18_{TM}.

All studied steel samples were analysed in a corundum crucibles. The analyses were carried out in an inert atmosphere of argon of purity 6.0. The samples were machined to a desired shape according to requirements of each experimental apparatus and thermo-analytical method, then polished and cleaned by ultrasound in acetone.

Besides to analyses of studied steels were also performed calibration measurements for calculating values of temperature correction. Experimental T_L and T_S values were then corrected regarding to melting point temperatures of the pure standard metals - palladium for DTA and nickel for "Direct TA". Liquidus and solidus temperatures from DTA analysis were also corrected to influence of the heating rate and sample mass[18,19].

Summary overview of the experimental equipment and adjustment of experimental conditions of "Direct TA" and DTA analyses configuration is shown in the **Table 2**.

Table 2 Experimental conditions and configuration of DirTA a DTA measurements.

"Direct TA"	Sample mass (g.)	20-24	Linear heating, linear cooling temperature mode, cyclic experiments	Dynamic inert atmosphere (Ar 6.0)
	Heating / cooling rate	5 °C.min^{-1}	TG 'S' type mono-couple measuring sensor (rod)	Pt/PtRh 10 % thermocouple
DTA	Sample mass (mg.)	200	Linear heating temperature mode	Dynamic inert atmosphere (Ar 6.0)
	Heating rate	10 °C.min^{-1}	TG/DTA'S' type tri-couple measuring sensor (rod)	Pt/PtRh 10 % thermocouple

3. Results and discussions

Under the experimental conditions specified in **Table 2** was determined T_L and T_S temperatures of 15Cr18Ni, X22CrMoV12-1, X3CrMoNb18-2 grades of steel. The T_L and T_S temperatures (**Table 3** and **Table 4**) were carried out by evaluation of the thermo-analytical curves: curves heating and cooling curves and DTA curves. Tables summarise average (and corrected) values of liquidus (T_L) and solidus (T_S) temperatures determined by both thermo-analytical methods and their comparison with theoretically calculated T_L and T_S temperatures by thermodynamic SW's – Thermo-Calc and database TCFE8, version 2019a, IDS (version 1.3.1, year of manufacture 1997) and Computherm from Esi Group as a part of the Pro Cast software 2018.0 and database Visual Cast 13.5.5). T_L and T_S temperatures determined from "Direct TA" analyses are shown separately according to usage of experimental mode. Bold marked T_L and T_S temperatures in the **Tables 3** and **4** represent temperatures that were decided to be recommended for operating conditions.

Table 3 Experimental and calculated liquidus temperatures.

Steel grade	Experimental T_L temperature (°C)			SW prediction of T_L temperature (°C)		
	„direct TA“, heating	„direct TA“, cooling	DTA	Thermo-Calc	IDS	Computherm
15Cr18Ni	**1422**	1418	1420	1419	1398	1430
X22CrMoV12-1	**1491**	1488	1484	1493	1486	1494
X3CrMoNb18-2	1492	1490	**1493**	1506	1476	1505

Table 4 Experimental and calculated solidus temperatures.

Steel grade	Experimental T_S temperature (°C)			SW prediction of T_S temperature (°C)		
	„direct TA“, heating	„direct TA“, cooling	DTA	Thermo-Calc	IDS	Computherm
15Cr18Ni	1365	1381	**1353**	1363	1240	1363
X22CrMoV12-1	1416	1371	**1414**	1419	1402	1416
X3CrMoNb18-2	1456	1459	**1454**	1492	1413	1484

According to Tables 3 can be stated that experimentally determined T_L temperatures across both thermo-analytical methods shown close T_L values. Differences between them are at maximum 7 °C (X22CrMoV12-1). Differences between the results of thermo-analytical methods are related to different experimental conditions and character of their usage. More variable results show a comparison of experimental T_L values with theoretically calculated T_L values. There are also differences in tens degrees of Celsius (15Cr18Ni - IDS).

Similar situation is obvious for T_S temperature. Differences in values of T_S temperatures between thermo-analytical methods are relatively close, for Thermo-Calc and Computherm too, but IDS again shown some differences more tens degrees of Celsius between experimentally determined T_S temperatures and theoretically calculated T_S values. Software calculations represent more different conditions of determination of phase transformation temperature usually. Therefore, calculations don't cover all aspects of experimental conditions. They have some own simplifications, limits for inclusion of all elements of chemical composition into calculation etc.

For final operational recommendations were decided, that as relevant T_L and T_S temperature will be selected those values, which were experimentally determined by thermo-analytical methods. Not from thermodynamic calculations. It is always better to use experimental data and robust methodology of measuring rather to predicted data. Therefore, was as the final one proper T_L, resp. T_S temperature of each steel grade recommended that value which is the least critical in relation to negative impact in process of its implementation into steel casting technology. In the case of T_L, the highest value from was recommended (in relation to superheat setting of steel before casting). Solidus temperature which has to be implemented into the real conditions of industrial partner represents as the lowest T_S value (to prevent to reach the solidus temperature at which a steel not be in solid state). Determination of T_L and T_S temperatures allows to predict more accurate the width of temperature range of two-phase zone region (interval) as possible and allows more precise conditions for numerical simulation of the behaviour of the steel during its solidification process.

All experimental values, in general, show high level of consistency and low level of variability. It was shown that both thermo-analytical methods used are set correctly; the results are reproducible, comparable and close to the equilibrium. Obtained experimental temperatures by the thermal analysis can be used to optimize production and processing of analysed steel grades.

4. Conclusion

The paper was focused on the determination of liquidus (T_L) and solidus (T_S) temperatures for three industrially produced steel grades. Two dynamic thermo-analytical methods were used: "Direct Thermal Analysis (Heating/Cooling Curve Analysis) and the NETZSCH STA 449 F3 Jupiter experimental system, which allows to measure relatively large steel samples (over 20 g) and the DTA realised on Setaram SETSYS 18_{TM} experimental system and small steel samples (about 200 mg). Experimentally obtained values of T_L and T_S were also compared with the results (T_L and T_S values) predicted by software calculations in Thermo-Calc, IDS and Computherm.

On the basis of discussion were to operating conditions were recommended these experimental T_L and T_S temperatures:

1. 15Cr18Ni: T_L : **1422 °C**; T_S : **1353 °C**,
2. X22CrMoV12-1: T_L : **1491 °C**; T_S : **1414 °C**,
3. X3CrMoNb18-2: T_L : **1493 °C**; T_S : **1454 °C**.

The results can be considered relevant, but with regard to the specific conditions of the experiments. In real technological conditions, it is necessary to take into account the possible influence of other factors that can affect the resulting behaviour (samples may exhibit different behaviour in the real technological processes). It is necessary to proceed with caution when implementing the knowledge into the technological practice.

Systematic research of important thermodynamic data (phase transformation temperatures allow carry out the requirements of industrial partners and solve the specific operational requirements of metallurgical practice, solution of practical problems of real steel solidification associated with real operational problems and share on achieve the high requirements for quality of cast steel. A comprehensive approach allows solving real steel casting problems. Realisation of systematic analyses of different types of steel grades allows create a wider base of analysed steels in relation to experimental study of a technically important spectrum of steels, development of new steel grades, various modifications of steel grades.

This approach represent a direct connection to operating conditions and technological use in steel casting process: direct use of T_L to the superheat setting of steel before casting; more precise determination of T_L in relation with T_S can lead to the refinement of the interval of steels' solidification as well; implementation of the experimental T_L and T_S temperatures into numerical simulations to setting of boundary conditions of numerical modeling.

Parallel use of both different methods of thermal analysis allows reduce the disadvantages of each method and comparison with software calculations completes the complex illustration about results at the process of final decision of implementation of experimentally determined data (T_L and T_S) to operating conditions and achieved a more precise results, eliminating the neglect of one possible approach.

Acknowledgement

This research was funded with the support of project CZ.02.1.01/0.0/0.0/17_049/0008399 Development of inter-sector cooperation of RMSTC with the application sphere in the field of advanced research and innovations of classical metal materials and technologies using modelling methods and due to the financial support of project of Student Grant Competition No. SP2019/148 and SP2019/43.

References

[1] Koležnik, M.; Nagode. A.; Klancnik, G. et al. Effects of solidification parameters on the micro- and macrostructure of the X19CrMoVNbN11-1 steel. *Materiali in Tehnologije*. **2013**, *47*, 739-744. [CrossRef]

[2] Schweinichen, von P.; Chen, Z.; Senk, D. et al. Effect of different casting parameters on the cleanliness of high manganese steel ingots compared to high carbon steel. *Metallurgical and Materials Transactions A.* **2013**, *44*, 5416-5423. DOI: 10.1007/s11661-013-1949-7. [CrossRef]

[3] Sviželová, J.; Tkadlečková, M.; Michalek, K.; Gryc, K.; Socha. L. Influence of Casting Speed on Solidification of Continuously Cast Round Steel Billets. *Hutnické listy*. **2017**, *2*, 22-27. [CrossRef]

[4] Porter, D.A.; Easterling, K.E.; Sherif, M.Y. *Phase Transformations in Metals and Alloy,* 3rd ed.: CRC Press, Boca Raton, FL, USA, 2009.

[5] Zhao J.C. Methods for Phase Diagram Determination: Elsevier, Oxford, 2007.

[6] Gallagher, P.K. *Handbook of Thermal Analysis and Calorimetry: Principles and Practice*, 2nd ed.: Elsevier, Oxford, 2003.

[7] Hatakeyama, T.; Liu, Z. *Handbook of Thermal Analysis*: Wiley, London, 1998.

[8] Andersson, J.O.; Helander, T.; Höglund, L.; Shi,P.; Sundman, B. Thermo-Calc & DICTRA, Computational Tools for Materials Science. *Calphad*, **2002**, *26*, 273-312. DOI: 10.1016/S0364-5916(02)00037-8. [CrossRef]

[9] Miettinen, J; Louhenkilpi, S.; Kytönen, H.; Laine, J. IDS: Thermodynamic-Kinetic-Empirical Tool for Modelling of Solidification, Microstructure and Material Properties. *Math. Comput. Simul.* **2010**, *80*, 1536-1550. DOI: 10.1016/j.matcom.2009.11.002. [CrossRef]

[10] Sviželová, J.; Tkadlečková, M.; Michalek, K. Research of steel ingot casting and solidification using numerical modelling. In *METAL 2018: 27th International Conference on Metallurgy and Materials*. **2018**, 192-198. WOS:000461832200026 [CrossRef]

[11] Tkadlečková, M.; MichaleK, K..; Strouhalová, M.; Sviželová, J.; Saternus, M.; Pieprzyca, J.; Merder, T. Evaluation of approaches of numerical modelling of solidification of continuously cast steel billets. *Arch. Metall. Mater.* **2018**, *63*, 1003-1008. DOI: 10.24425/122435 [CrossRef]

[12] Tkadlečková, M.; Válek, L.; Socha, L.; Saternus, M.; Pieprzyca, J.; Merder, T.; Michalek, K.; Kováč, M. Study of Solidification of Continuously Cast Steel Round Billets Using Numerical Modelling. *Arch. Metall. Mater.* **2016**, *61*, 221-226. DOI: 61. 221-226. 10.1515/amm-2016-0041. [CrossRef]

[13] Gryc, K.; Strouhalová, M.; Smetana, B.; Kawuloková, M; Zlá, S.; Socha, L; MichaleK, K.; Tkadlečková, M.; Kalup, A.; Jonšta, P.; Sušovský, M. Determination of solidus and liquidus temperatures for bearing steel by thermal analysis methods. *Metalurgija*. **2017**, *56*, 385-388. [CrossRef]

[14] Smetana, B.; Zlá, S.; Kawuloková, M.; Gryc, K.; Strouhalová, M.; Kalup, A.; Tkadlečková, M.; Dobrovská, J.; Michalek, K.; Jonšta, P.; Sušovský, M.; Dostál, P.; Martiník, O.; Drozdová, Ľ. Temperatures of solidus and liquidus of tool steel. In *METAL 2016: 25th International Conference on Metallurgy and Materials*. **2016**, 91-96. WOS:000391251200011 [CrossRef]

[15] Kawuloková, M.; Zlá, S.; Dobrovská, J.; Smetana, B.; Kalup, A.; Strouhalová, M.; Vontorová, J.; Válek, L.; Rosypalová, S.; Francová, H. Phase transformations temperatures of real steel grade. In *METAL 2015*: *24th International Conference on Metallurgy and Materials*. **2015**, 636-641. WOS:000374706100100 [CrossRef]

[16] Martiník, O.; Smetana, B.; Dobrovská, J.; Zlá, S.; Kawuloková, M.; Gryc, K.; Drozdová, Ľ.; Dostál, P.; Martiníková, B. Experimental and Theoretical Assessment of Liquidus, Peritectic Transformation, and Solidus Temperatures of Laboratory and Commercial Steel Grades. *J. Phase Equilib. Diffus.* **2019**, *40*, 93-103. DOI: 10.1007/s11669-019-00707-1 [CrossRef]

[17] Boettinger, W.J.; Kattner, U.R.; Moon, K.V.; Perepezko, j.H. *DTA and Heat-flux DSC Measurements of Alloy Melting and Freezing*: National Institute of Standards and Technology, Washington, USA, 2006.

[18] Žaludová, M.; Smetana, B.; Zlá, S.; Dobrovská, J.; Watson, A.; Vontorová, J.; Rosypalová, S.; Kukutschová, J.; Cagala, M. Experimental Study of Fe-C-O Based System Above 1000 °C. *J. Therm. Anal. Calorim.* **2013**, *112*, 465-471. DOI: 10.1007/s10973-012-2847-8 [CrossRef]

[19] Žaludová, M.; Smetana, B.; Zlá, S.; Dobrovská, J.; Vodárek, V.; Konečná, K.; Matějka, V.; Matějková, P. Experimental Study of Fe-C-O Based System Below 1000 °C. *J. Therm. Anal. Calorim.* **2013**, *111*, 1203-1210. DOI: 10.1007/s10973-012-2346-y [CrossRef]

MODELLING OF MELT DEGASSING BY BLOWING OF INERT GAS THROUGH THE ROTATING IMPELLER

Josef Walek[1*], Karel Michalek[1], Markéta Tkadlečková[1], Jana Sviželová[1]
[1]Faculty of Materials Science and Technology, VŠB – Technical University of Ostrava, Ostrava, Czech Republic; karel.michalek@vsb.cz; marketa.tkadleckova@vsb.cz; jana.svizelova@vsb.cz
*Correspondence: josef.walek@vsb.cz; Tel.: +420 597 323 534

Abstract
Presented paper deals with the use of physical modelling to study the degassing process of aluminium melts in the refining ladle by blowing inert gas through a rotating impeller. The method of blowing inert gas, so-called refining gas, through a rotating impeller into the ladle presents the most common operational technology to reduce the content of impurities in a molten aluminium, e.g. hydrogen. The efficiency of this refining process depends on the creation of fine bubbles with a high interphase surface, their regular distribution and regular arrangement of bubbles in the whole volume of the refining ladle and with long period of their effect in the melt. Physical modelling represents the basic method of modelling and it makes it possible to obtain information about the course of refining processes. On the basis of obtained results, it is possible to predict the behaviour of the real system. This paper is aimed at the evaluation of laboratory experiments obtained by the method of physical modelling; attention is focused on the assessment of relevant parameters for the degassing process – mainly rotary impeller speeds and volume flow rate of inert gas.

Keywords: physical modelling; refining ladle; inert gas blowing; degassing of the melt; impeller

1. Introduction

Optimisation of the degassing process is difficult under operating conditions. Therefore, in laboratory conditions, so-called modelling is used, where the original work is replaced by the model. The technology of modelling is divided to two basic methods. In numerical modelling, the process is described by a mathematical model formed of a system of partial differential equations. In the case of physical modelling, a method is used, in which the real system is replaced by a tangible physical model, which is as close as possible to the behaviour of the real system. In this method, both the work and the model have the same physical substance. One of the advantages of physical modelling is the possibility of visual monitoring and evaluating the investigated process under review. The results achieved on the model can predict the real system behaviour. The combination of physical and numerical modelling is an optimal model research variant. Among the biggest consumers of aluminum alloys include engineering and automotive industries. In some applications, they can also replace structural steel. This alternative will achieve the preferred ratio of low density and good mechanical properties [1], [2], [3], [4], [5], [6], [7], [8].

2. Experimental conditions

Physical modelling of degassing the aluminium melt by inert gas blowing is quite widely used [9]. The decrease of hydrogen content in molten aluminium during refining with inert gas is simulated at physical modelling by a decrease of dissolved oxygen in model liquid (water). The main advantage of using water is primarily its low cost, good availability and especially because the fact that it has similar physical properties as liquid aluminium. The dynamic and kinematic viscosity of aluminium and water can be considered to be very close. A comparison of the basic parameters of aluminium and water is shown in Table 1.

Table 1 Comparison of basic physical parameters of the aluminium melt and water [1].

Parameter	Symbol	Unit	Aluminium	Water
Temperature	T	K	1023	293
Density	ρ	$kg \cdot m^{-3}$	2345	998.5
Dynamic viscosity	η	$kg \cdot m^{-1} \cdot s^{-1}$	0.00120	0.00101
Kinematic viscosity	ν	$m^2 \cdot s^{-1}$	$0.51 \cdot 10^{-6}$	$1.012 \cdot 10^{-6}$
Surface tension	σ	$N \cdot m^{-1}$	0.680	0.072

Laboratory experiments were conducted in accordance with the theory of similarity between the model and the work, based on the identity of Froude's criterion. It is necessary to observe in particular geometrical similarity of the work and its model, and dynamic similarity of fluid flow in work and in its model.

Experiments investigating degassing the metal melt by inert gas in refining ladle were performed in the Laboratory of Physical and Numerical Modelling at the Department of Metallurgy and Foundry, FMT (Faculty of Materials Science and Technology), of the VŠB – Technical University of Ostrava. The physical model was made of organic glass (plexiglass) at a 1:1 geometric scale for a pilot plant of warm refining ladle model. Also, two graphite baffles for suppressing excessive surface ripple and vortex formation were included in the physical modelling. Figure 1 shows a physical model assembly.

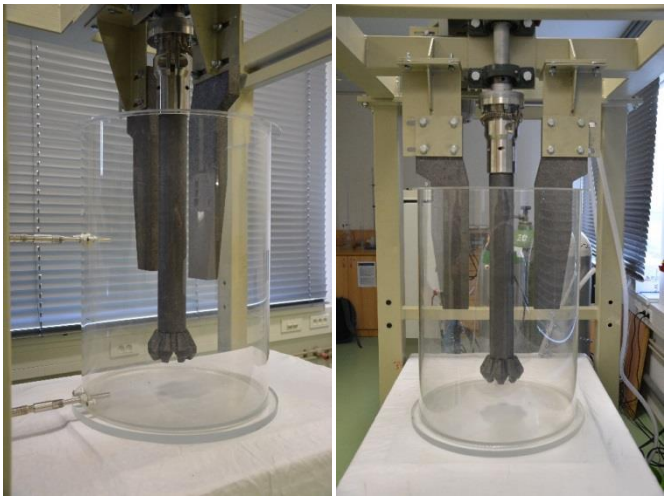

Figure 1 Physical model assembly: refining ladle, impeller, two baffles and measuring probes.

Figure 2 Detail of the impeller head used for physical modelling, variant J8.

The change of the impeller immersion was solved by a hydraulically controlled platform on which the physical model of the ladle was placed. The J8 impeller variant was used for modelling (see Figure 2). Rotary impeller speeds (revolutions per minute; rpm) were resolved by using an asynchronous motor, powered through an inverter. Mass flowmeters and needle valves were used to measure and regulate the flow of gases (oxygen – press 0.2 MPa and argon – purity 5.0) [10].

The decrease of hydrogen content in the aluminium melt during inert gas refining was simulated in the physical model by a decrease of the content of dissolved oxygen in the model liquid (water). Before each experiment, water was saturated with gaseous oxygen to the value of 23 ppm (23 mg $O_2 \cdot l^{-1}$ of water) through the rotating impeller. The actual experiment started with exact rotary impeller speeds and flow rate of argon. Two optical fluorescent probes were used for continuous measurement of oxygen content in the model bath (water), which were placed 420 mm (A1) and 30 mm (A2) above the bottom of the refining ladle. These probes were capable of recording dissolved oxygen content up to 26 ppm. Figure 3 shows the basic dimensional data of the physical model, including the location of the measuring probes.

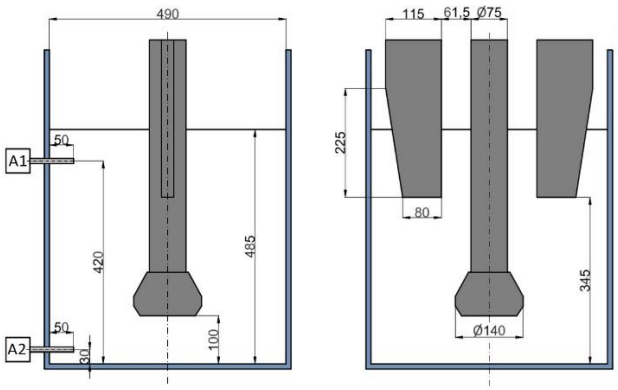

Figure 3 Basic dimensional data of physical model.

3. Experiments and their evaluation

The main aim of physical modelling was to achieve insight into the effect of relevant parameters (see Table 2) on the removal of dissolved oxygen during refining. The research concentrated on rotary impeller speeds and flow rate of inert gas.

Table 2 Overview of the experiments performed.

Variant	A	B	C	D	E	F	G	H	I
Rotary impeller speeds (rpm)	350			500			650		
Flow rate of Ar (Nl·min^{-1})	5.0	10.0	15.0	5.0	10.0	15.0	5.0	10.0	15.0

The results of individual experiments were evaluated and processed into graphs, which characterise the time dependence of the evolution of the reduction of oxygen concentration during refining by inert gas.

As already mentioned, two optical fluorescent probes were used to measure the dissolved oxygen concentration in water (A1 – upper probe, A2 – lower probe). The analysis of the results revealed that the course of change in the oxygen concentration indicated by these probes is practically identical. This behaviour was evident in all experiments, due to the high rate of turbulence, which caused an almost homogeneous concentration field across the entire refining ladle model volume. Due to this behaviour, values from the lower probe A2 were used at the next evaluation.

The most important parameters that have a significant effect on the refining process (dewatering) include the rotary impeller speeds and the flow rate of argon fed to the impeller.

The rotary impeller speeds and their influence was monitored for values 350, 500 and 650 rpm. From the graphs shown below (see Figure 4), a significant effect of increased rotary impeller speeds on the process of reduction of oxygen content can be demonstrated. The flow rate of inert gas is also a co-decision factor. At low flow rates of inert gas 5 Nl·min^{-1} (see Figure 4 a), the process of reducing dissolved oxygen is slow and the oxygen concentration is not reduced to 0 ppm. As it can be seen in the visualization photos (see Figure 6 a), the process is limited by a small number of large bubbles, which are insufficiently dispersed in the volume of the model and are sparse especially close to the impeller. This behaviour causes that the process of oxygen removal from the bath is slow and incomplete.

At higher inert gas volume flow rates of 15 Nl·min^{-1} (see Figure 4 c), even relatively low increase of rotary speeds to 350 rpm leads to an increase in the steepness of the descent curve of the oxygen concentration and thus to a significant time reduction, which is required to remove the oxygen content from the bath. A further increase in rotary speeds to 500 or 650 rpm led to another, but less significant influence. The increased rotation speed causes a greater distribution of the blown gas volume, resulting in a creation of bigger number of smaller bubbles. This ensures an increase in the surface of the inert gas bubbles, which is a critical parameter in the degassing process. At the same time, these bubbles are pushed to bigger distances from the impeller, resulting in an increased distribution of these bubbles. Both of these reasons are supported by observation and comparison of visualisation photos (see Figure 6 f and Figure 6 i). It can also be assumed that increasing rotary speeds above 650 rpm will no longer have a great positive effect and it can carry certain negatives with it. The flow rate of the melt can be so high, that under real conditions it can lead to the reduction of the flowing efficiency of the non-metallic inclusions, rupture of the oxide layer and subsequent re-gasification of the melt and also higher impeller wear.

The results shown above can also be interpreted as the effect of the flow rate of inert gas at constant rotary speeds of 5, 10 a 15 Nl·min^{-1} when the flow rate of argon is influenced at gradually increasing rotary speeds of 350, 500 and 650 rpm (see Figure 5). At first glance, it can be seen that increasing the volume flow rate of inert gas has a very similar effect to increasing the rotary impeller speeds. The reason is simple, by increasing the volume of the inert gas in the melt, the reaction surface of the inert gas bubbles also increases, resulting in the increase in efficiency of the oxygen removal process. Figure 5 b shows that at a constant rotary speeds of 500 rpm and a volume flow rate 5 Nl·min^{-1}, the oxygen concentration in the bath decreases from the initial 23 ppm to 4 ppm within 6 minutes, from this value to a target value of 0 ppm the content will drop in 10 minutes. With an increased flow rate of 10 Nl·min^{-1}, we achieve values of 4 minutes and 5 minutes to achieve 0 ppm. When comparing these values, it is clear that the removal of oxygen from the bath is faster at an increased flow rate and already at high concentrations. The biggest difference arises in the removal of oxygen

at its lower concentrations, where the effect of an increased flow is much more significant. This phenomenon is more noticeable at higher rotary impeller speeds, but it also occurs at lower rotary impeller speeds.

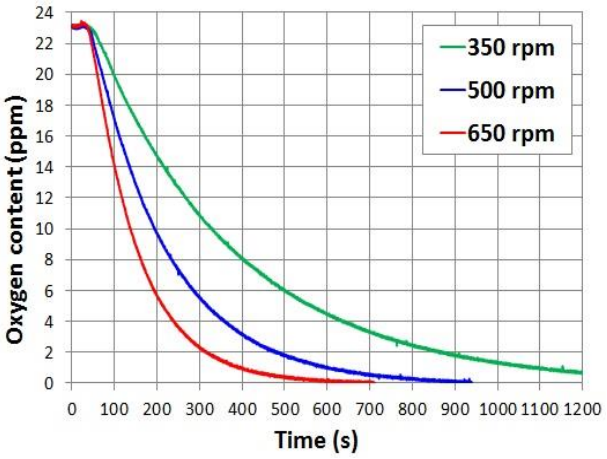

a) flow rate of Ar: 5.0 Nl·min^{-1}

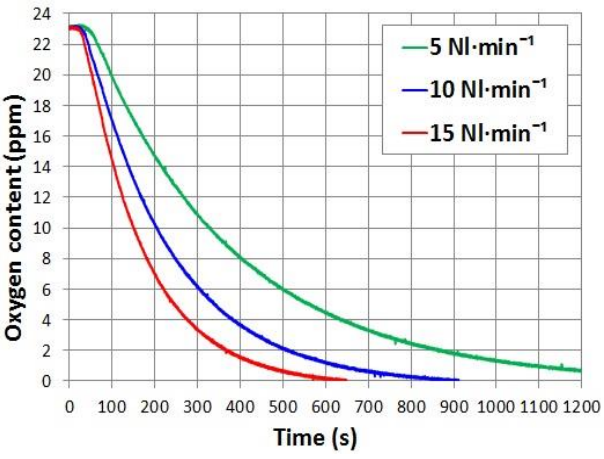

a) rotary impeller speed: 350 rpm

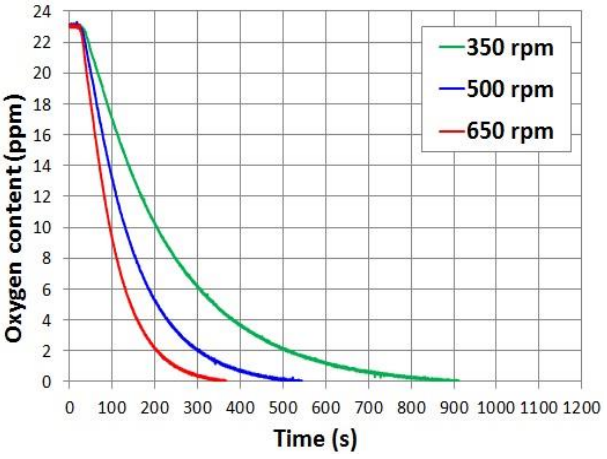

b) flow rate of Ar: 10.0 Nl·min^{-1}

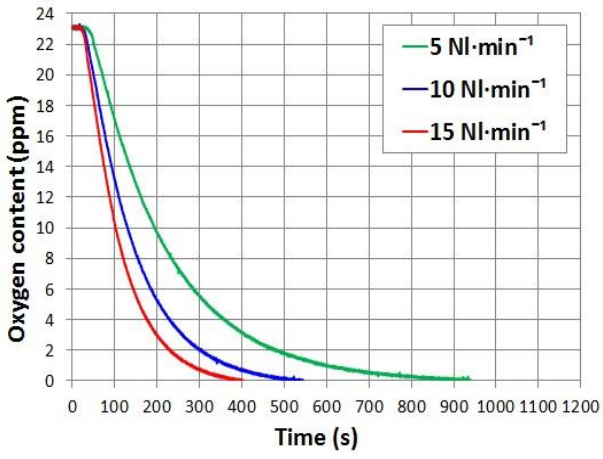

b) rotary impeller speed: 500 rpm

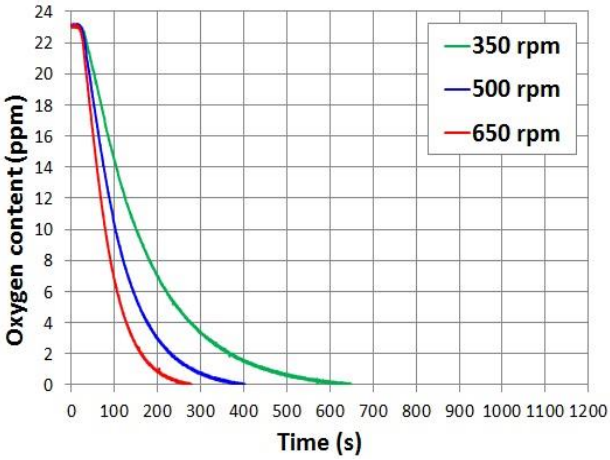

c) flow rate of Ar: 15.0 Nl·min^{-1}

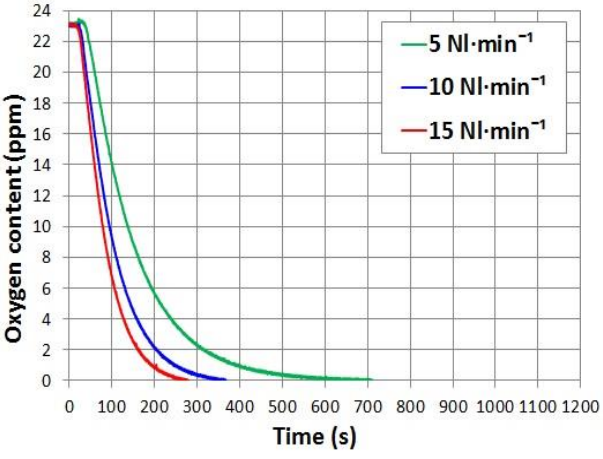

c) rotary impeller speed: 650 rpm

Figure 4 Change in the oxygen content at a different flow rate of Ar and rotary speeds in the range from 350 rpm to 650 rpm.

Figure 5 Change in the oxygen content at different rotary impeller speeds and Ar flows in the range from 5 Nl·min^{-1} to 15 Nl·min^{-1}.

During the experiments, photos of the bath behaviour inside the model were taken (see Figure 6), from which the fluid flow and the amount and distribution of inert gas bubbles could be evaluated. In these photos, the effect of increasing rotary speeds ranging from 350 to 650 rpm is evident, with the more intense distribution of bubbles throughout the refining ladle volume, as well as a higher level of bath surface ripple in the refining ladle.

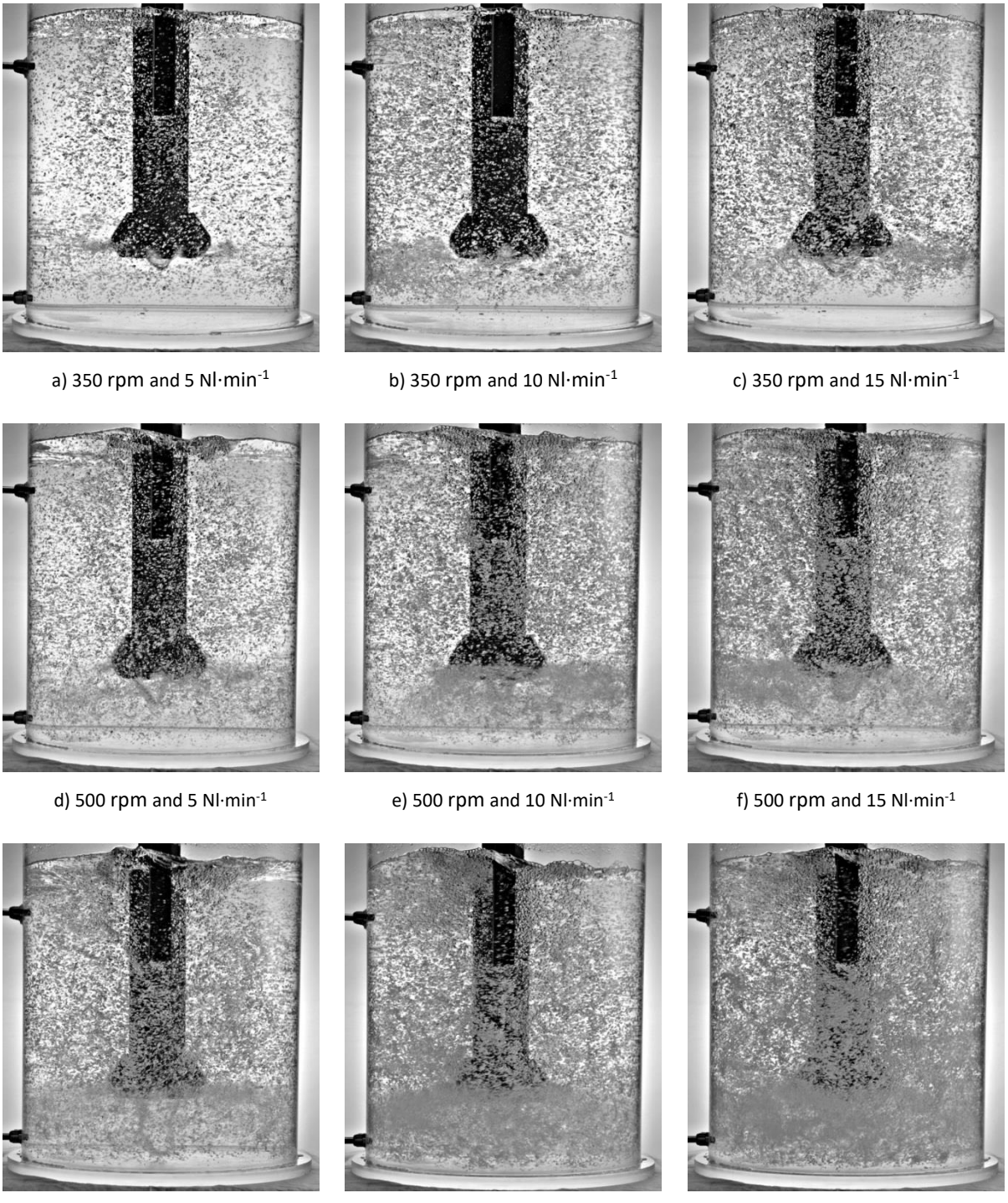

a) 350 rpm and 5 Nl·min^{-1} b) 350 rpm and 10 Nl·min^{-1} c) 350 rpm and 15 Nl·min^{-1}

d) 500 rpm and 5 Nl·min^{-1} e) 500 rpm and 10 Nl·min^{-1} f) 500 rpm and 15 Nl·min^{-1}

g) 650 rpm and 5 Nl·min^{-1} h) 650 rpm and 10 Nl·min^{-1} i) 650 rpm and 15 Nl·min^{-1}

Figure 6 Visualisation photos of the gas flow in the bath at rotary impeller speeds ranging from 350 to 650 rpm and volume flow rate of inert gas ranging from 5 to 15 Nl·min^{-1}.

The results obtained were also compared based on the time necessary to reach the dimensionless concentration of 0.5 and 0.1 (see Figure 7). The times $\tau_{0.5}$ and $\tau_{0.1}$ under which the oxygen concentration in the bath was reduced, were compared at 50 % and 90 % respectively, in which the so-called dimensionless concentrations
$C_x = 0.5$ a $C_x = 0.1$ were achieved. These parameters can therefore characterise the rate of reduction of content of oxygen dissolved in the bath. The greatest influence on the reduction of oxygen concentration has impeller speed and volume flow rate. From Figure 7 we can confirm the conclusions set out in the previous section, i.e. analyses of experiments. Increasing the rotation speeds and increasing the volume flow rate of argon result in an instant reduction of the oxygen concentration; it is the same $\tau_{0.5}$ and also at $\tau_{0.1}$.

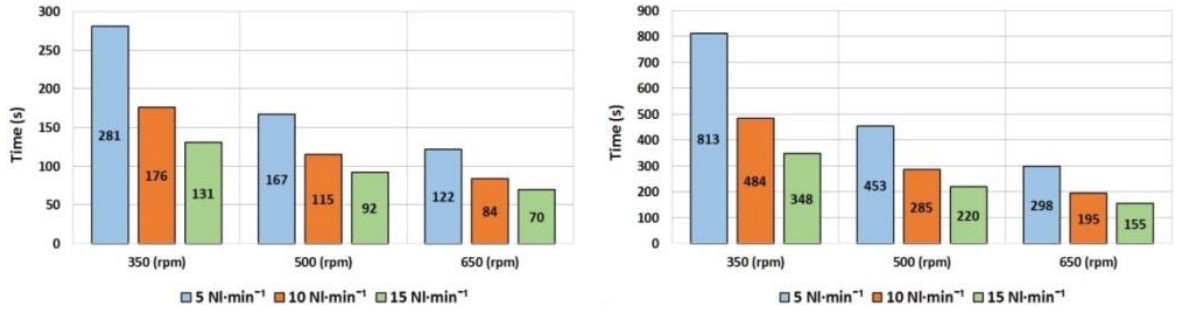

a) $\tau_{0.5}$ b) $\tau_{0.1}$

Figure 7 Comparison of the influence of the volume flow rate of argon and the impeller rotary speed.

4. Conclusions

The experiments were conducted under laboratory conditions to determine and evaluate the effect of each parameter on the efficiency of the melt refining process. The ability to influence the efficiency of the process was compared for individual parameters. The rotary impeller speeds and volume flow rate of inert gas have the greatest influence on the efficiency of the entire refining process. Other investigated parameters were the number of baffles the impeller height above the bottom of the refining ladle, the influence of the inert gas type and the effect of the bath temperature. However, these parameters have small or almost insignificant influence.

The evaluation of the experiments was carried out in three phases. In the first phase, visualisation photos were taken, where the size of bubbles and the distribution of these bubbles into the volume of the refining ladle were studied. During the experiments, the oxygen concentration in the bath was obtained and recorded and used in the graphs. In the last evaluation phase, the results were compared on the basis of the time necessary for reaching a certain concentration in the bath (in this case 0.5 and 0.1).

From the results of the physical modelling we can see that the used optical fluorescence probes allow the correct measurement of the evolution of reduction of the oxygen content in water. Based on a series of experiments, it was proven that the rotary impeller speeds and the volume flow rate of the refining gas have a significant impact on the process of decreasing the oxygen content in water.

Acknowledgements

The work was created under the support of the Czech Ministry of Industry and Trade within the frame of the programme TRIO within the solution of the project reg. No. FV10080 “Research and Development of Advanced Refining Technologies of Aluminium Melts for Increase in Product Quality.“

References

[1] Michalek, K. Využití fyzikálního a numerického modelování pro optimalizaci metalurgických procesů. (Using physical and numerical modelling to optimize metallurgical processes) 1st edition. Ostrava: VŠB-Technical University of Ostrava, 2001, p. 125, ISBN: 80-7078-861-5 (in Czech).

[2] Lichy, P., Kroupová, I., Radkovský, F., Nguyenová, I. Possibilites of the controlled gasification of aluminium alloys for eliminating the casting defects. 25th Anniversary International Conference on Metallurgy and Materials (METAL). Brno, Czech Republic, May 25-27, 2016, p. 1474-1479, ISBN: 978-80-87294-67-3.

[3] Cagala, M., Bruska, M., Lichy, P., Beno, J., Špirutová, N. Influence of aluminium-alloy remelting on the structure and

mechanical properties. Materiali in technologije / Materials and technology. 47 (2013), 2, 239-243.

[4] Bul'ko, B., Molnar, M., Demeter, P. Physical modelling of different configurations of a tundish for casting grades of steel that must satisfy stringent requirements on quality. Metallurgist. 57 (2014), 11-12, 605-609.

[5] Rega, V., Molnar, M., Jusko, M., Bul'ko, B., Kijac, J., Demeter, P. Impact of cast speed on the occurrence of the non-metallic inclusions in steel. Acta Metallurgica Slovaca. 22 (2016), 1, 4-13, DOI: 10.12776/ams.v22i1.649.

[6] Rega, V., Molnar, M., Solc, M., Bul'ko, B., Demeter, P., Jusko, M. Impact of interstitial aluminium content on occurrence of non-metallic inclusions in steel. Acta Metallurgica Slovaca. 22 (2016), 2, 88-94, DOI: 10.12776/ams.v22i2.688.

[7] Bul'ko, B., Molnar, M., Demeter, P., Baricova, D., Pribulova, A., Futas, P. Study of the influence of intermix conditions on steel cleanliness. Metals. 8 (2018), 10, DOI: 10.3390/met8100852.

[8] Bul'ko, B., Priesol, I., Demeter, P., Gasparovic, P., Baricova, D., Hrubovcakova, M. Geometric modification of the tundish impact point. Metals. 8 (2018), 11, DOI: 10.3390/met8110944.

[9] Saternus, M. Rafinacja aluminium i jego stopów przez przedmuchiwanie argonem. Gliwice: Wydawnictwo Politechniky Ślaskej, **2011**, p. 167, ISBN: 978-83-7335-892-8 (in Polish).

[10] Michalek, K., Tkadlečková, M., Socha, L., Gryc, K., Saternus, M., Pieprzyca, J., Merder, T. Physical modelling of degassing process by blowing of inert gas. Arch. Metall. Mater. 63 (2018), 2, 987-992, DOI: 10.24425/122432.

ZINC LOSSES IN THE MELTING PROCESS OF AL-ZN ALLOYS IN INDUCTION CRUCIBLE FURNACES

Węcki B.[1,2], Makieła E.[2]
[1] Faculty of Materials Engineering and Metallurgy,
[2] ZETOM Research and Certification of Prof. F. Staub in Katowice, b.wecki@zetom.eu, edwart@zetom.eu
*Correspondence: bartosz.wecki@polsl.pl

Abstract
During the melting of the metal alloy we may have to deal with the unfavourable phenomenon of evaporation of alloy elements with high vapour pressure from the bath. An example of such an alloy is Al-Zn. During the melting process in an induction vacuum furnace, the process of zinc evaporation can be intensified by a significant increase in the bath surface due to the formation of meniscus. The paper presents the results of studies on the evaporation of zinc from the alloy. Al-Zn5,5MgCu in VIM 20-50 furnace taking into account the influence of electrical parameters of furnace operation on the size of mass exchange surface in the analysed evaporation process.

Keywords: metals evaporation; induction melting; meniscus; Al-Zn zinc losses; vacuum induction furnace

1. Introduction

The new generation of induction crucible furnaces are used for melting, overheating and storage of liquid metals and for the production of metal alloys. They are used mainly for melting cast iron, cast steel, copper and aluminum as alloys of these two metals. These aggregates ensure the homogeneity of the produced alloys thanks to intensive mixing of metallic baths. During the operation of this type of devices, its power is usually smooth. However, the control of load symmetry and reactive power compensation takes place automatically. Although the melting aggregates have been used in industrial practice for many years, it should be remembered that during the melting of metal alloys containing components characterized by significant differences in vapour pressure, we may have to deal with an unfavorable phenomenon of evaporation of some alloy components. The factors that may significantly affect the intensification of this harmful phenomenon include the pressure in the system, the type of gas atmosphere, temperature and hydrodynamics of the system in which the melting process is carried out. Below, for example, the process of zinc evaporation from an aluminum alloy melted in an induction furnace is discussed, focusing mainly on the possibility of influencing this process by the size of the surface of the liquid alloy.

2. Possible evaporation of zinc from Al-Zn alloy

The value determining from the thermodynamic point of view the possibility of evaporation of the component B of a liquid metal alloy is the so-called volatility coefficient of the Oletto [1]. For the two-component alloy A-B, in case when we are dealing with pairs of metal in atomic form, this coefficient determines the relation:

$$\Phi_B = \left(\gamma_B \frac{p_B^0}{p_A^0} \right) \cdot \left(\frac{M_A}{M_B} \right)^{0,5} \quad (1)$$

where: Φ_B – volatility factor,
M_A, M_B – atomic (molar) masses of the main alloy component and component respectively evaporating,
γ_B - the activity coefficient of component B in the alloy,
$P^0_{A,B}$ – partial pressures

where: Φ_B – volatility factor,
M_A, M_B – atomic (molar) masses of the main alloy component and component respectively evaporating,

γ_B - the activity coefficient of component B in the alloy,

$P^0_{A,B}$ – partial pressures.

The evaporation process volatility factor of B is assumed to be possible when the condition is achieved:

$$\Phi > 1 \quad (2)$$

In order to determine the value of zinc volatility coefficient Φ_{Zn} from the relation (1), the equilibrium pressure values aluminium and zinc were estimated using thermodynamic data contained in the HSC Chemistry database [2]. The values of these pressures are presented in Table 1. The values of the coefficient of activity of zinc in the Al-Zn alloy were determined from the relation [3]:

$$\ln \gamma Zn = (1172/T - 0{,}413)\ 1{,}82XAl \quad (3)$$

where XAl – the molar fraction of Al in the alloy

Figure 1 shows the estimated change in the volatility coefficient of zinc ΦZn for the analyzed liquid Al-Zn alloy in the temperature range 933-1283 K. The data presented in this figure show that from the thermodynamic point of view there is a possibility of zinc evaporation from this alloy. For mentioned temperature conditions as well as for the alloy composition, the coefficient ΦZn takes values > 1.

Table 1 Vapour pressure of aluminium and zinc vapours over a clean bath.

Temperature, K	Aluminium vapour pressure, Pa	Zinc vapour pressure, Pa
933	3,284E-07	4400,842
958	9,447E-07	6540,607
983	2,575E-06	9518,651
1008	6,674E-06	13585,85
1033	1,65E-05	19044,32
1058	3,908E-05	26255,24
1083	8,885E-05	35640,1
1108	0,0001945	47685,87
1133	0,0004111	62941,55
1158	0,0008408	82045,47
1183	0,0016674	105691,8
1208	0,0032121	134666,5
1233	0,0060221	169807,4
1258	0,0110065	212032,5
1283	0,0176542	239570,7

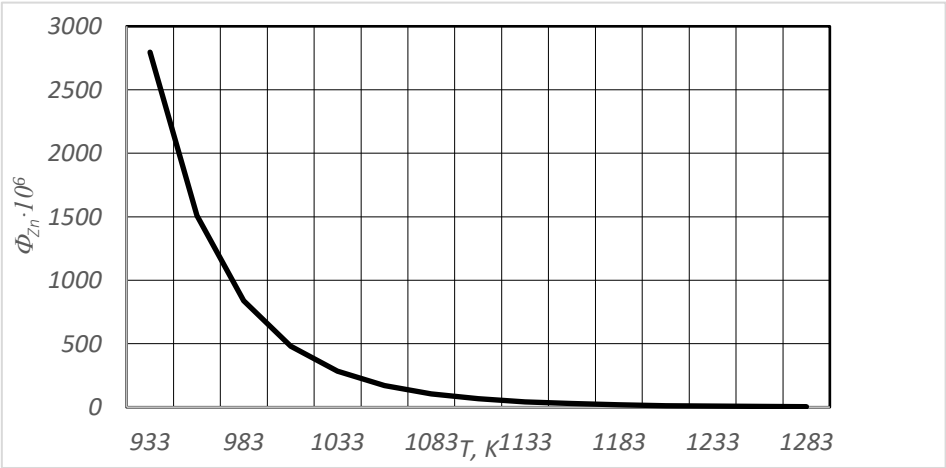

Figure 1 Change in the volatility coefficient value ΦZn for the Al-Zn alloy being tested.

3. Own research

The tests were carried out on an aluminium-zinc alloy of the composition given in Table 2. This alloy was selected in such a way that one of the components present in it was characterized by a much higher value of vapour pressure (zinc) in relation to the matrix metal (aluminium).

Table 2 Chemical compositions of the aluminium alloy used in the test.

Alloy components, % weight.											
Alloy symbol	Zn	Mg	Cu	Mn	Fe	Si	Cr	Ti	Zr	Other	Al
Al-Zn5,5MgCu	5,1-6,1	2,5	1,6	<0,3	<0,5	<0,4	0,23	<0,2	-	Zr + Ti:<0,25	balance

The test programme was carried out with the use of a SECO-WARWICK VIM 20-50 vacuum induction crucible furnace. This unit is equipped with, among others, the following equipment:

- operator panel enabling control of working parameters and control of processes taking place in the furnace,
- inductor tilt drive,
- a system for introducing alloying additives without disturbing the protective atmosphere,
- a system enabling the ingot mould to be heated,
- sampling mechanism.

Additionally, the device made it possible to measure temperature in a contact way using a thermoelectric sensor and a non-contact sensor using a pyrometer.
The experiments were carried out according to the following scheme. After a certain amount of alloy was loaded into the crucible and the Roots pump generated the assumed working pressure, the furnace power supply generator was started. After melting, the charge was kept in the crucible for 20 minutes. The temperature was measured with the use of a thermoelectric sensor type B - PtRh30-PtRh6 and an optical pyrometer. At strictly defined time intervals, liquid alloy samples were taken and subjected to chemical analysis. This analysis was performed three times for each sample taken. After the experiment, the liquid alloy was cast into a graphite ingot mould. To analyse the chemical composition, the absorption atomic spectrometry method was used, using the ASA Solar M6 device.

4. Results of the research and their discussion

Table 3 shows an example of the zinc content in the alloy for different melting times for different power values of the input. Graphical interpretation of these results is presented in Fig. 2.

Table 3 Changes in zinc content of the examined Al-Zn alloy obtained during remelting carried out in 5kW, 10kW and 15kW of power in function of the time.

Duration of remelting, min	Zinc content in the alloy, % weight		
	5 kW	10 kW	15 kW
0	5,56	5,69	5,61
5	5,00	4,87	4,44
10	4,84	4,76	4,07
15	4,74	4,31	2,73
20	4,60	4,24	2,17

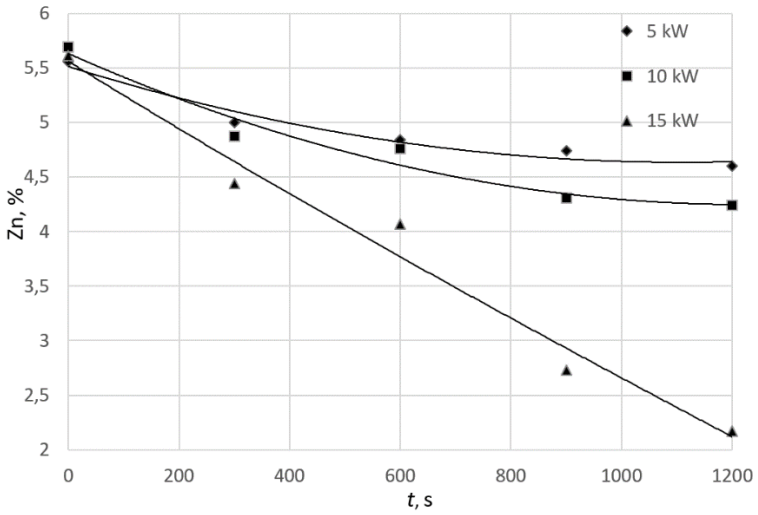

Figure 2 Changes in zinc content of the examined Al-Zn alloy obtained during remelting carried out at different intensities secreted in the deposit.

The data presented in this figure show that a significant increase in the weight loss of zinc from the alloy is observed due to an increase in the power emitted in the melt deposit in the induction furnace. For the value of 5 kW of power after 20 minutes of the melting process, the zinc content decreased to 4.6 wt. % at the output content of 5,7 wt. %. For the process carried out at the power of 10 and 15 kW this value decreased to 4,24 and 2,17 wt. % respectively.

In order to explain the above observations, let us consider the process of evaporation of zinc from the Al-Zn alloy as the penetration of mass, the exchange of mass between the core of one phase (liquid alloy) and the core of the other phase (gas being the furnace atmosphere). The stream of zinc penetrating between the cores of both phases can be described by the relation [4]:

$$G_{Zn} = k_{Zn} F \Delta\pi, \qquad g \cdot cm^{-2}s^{-1} \qquad (4)$$

where: k_{Zn}- the coefficient of penetration of zinc, also called the general coefficient of mass transport
F - mass exchange surface (liquid metal-to-gas phase interphase surface)
$\Delta\pi$ – general drive module of the process

From the form of equation (4) it follows that the value of the evaporating flux of zinc is directly proportional to the surface of liquid metal. In the case of melting of metals and their alloys in induction furnaces, this surface is significantly dependent on the electromagnetic field acting on the liquid metal and on the properties of the liquid metal [5-8].

To determine the actual mass exchange area in the analyzed process of zinc evaporation from liquid aluminium, a method consisting of four stages was proposed:

- taking pictures of molten metal with the use of a fast camera,
- marking the resulting meniscus geometry on the basis of the photographs obtained,
- determination of the function of curves describing meniscus for different furnace operating parameters,
- estimation of the surface area using Wolfram Mathematica programs.

The estimated actual surface area of the liquid aluminium alloy, using the above mentioned methodology, was 68,1 cm^2 for melting at input power of 5 kW and 77 and 95 cm^2 for 10 and 15 kW respectively. The internal surface area of the crucible was 63,6 cm^2.

Figure 3 shows an example of a photograph of a surface of a liquid Al-Zn alloy melted at 15 kW.

Figure 3 Picture of aluminium surface melted with 15kW of power emitted in the deposit.

5. Summary

During the melting of Al-Zn alloy in an induction crucible furnace, significant zinc losses from the alloy were observed in the batch at different power values. For example, for power values of 5 kW after 20 minutes of the melting process, the zinc content decreased to 5,7 wt. % at the output content of 4,6 wt. %. For the process carried out at a power of 15 kW, this value decreased to 2.17 wt. %. The results of the tests and the analysis clearly indicate that the increase in the amount of evaporating zinc together with the increase in the value of the power emitted in the batch during the melting process in the crucible induction furnace is caused by the increase in the evaporation surface - (surface of the liquid alloy). At melting of the alloy at the power of 5kW this area was 68 cm^2. The increase in the power emitted in the charge to 15 kW resulted in an increase in the evaporation area to 95 cm^2. It should be noted that these areas are larger than the internal cross-section of the crucible - 63 cm^2.

References

[1] Olette M.: Phys. Chem of Proc. Metall. 1961, vol. 8. p 1065-1087

[2] HSC Chemistry ver.6.1. Copyright© Outokumpu Research Oy, Pori Finland.

[3] Plewa J.: Przykłady obliczeniowe z teorii procesów metalurgicznych , Wydawnictwo Politechniki Śląskiej 1987.

[4] Hobler T.: Dyfuzyjny ruch masy i absorbery, WNT Warszawa 1976.

[5] Węcki B.: Analiza wpływu wielkości powierzchni kontaktu ciekła faza metaliczna-faza gazowa na efektywność procesu rafinacji metali w tyglowych piecach indukcyjnych, praca doktorska, Poliitechnika Śląska 2018.

[6] Węcki B. own results (not published)

[7] Golak S., Przyłucki R.:"A simulation of the coupled problem of magnetohydrodynamics and a free surface for liquid metals", Transactions of Engineering Science, WIT, 2009, vol. 48,

[8] Golak S.: "Application of image analysis for the measurement of liquid metal surface", Transaction on Modelling and Simulation, WIT, 2009, vol. 48

[9] Palacz M., Melka B., Wecki B., Siwiec G., Przylucki R., Bulinski P., Golak S., Blacha L., Smolka J.:" Experimental Analysis of the Aluminium Melting Process in Industrial Cold Crucible Furnaces", Metals and Materials International, 2019, p. 1-13

[10] Węcki B.:" Wpływ mocy roboczej indukcyjnego pieca próżniowego z zimnym tyglem na wielkość powierzchni międzyfazowej ciekły metal - faza gazowa", Rudy Metale 2018 R. 63 nr 12

AOM - ACADEMY OF METALLURGY o.z.

The Academy of Metallurgy o.z. mission:

The civic organisation Academy of Metallurgy o.z. was founded in 2019. The Academy of Metallurgy o.z. is not based on business, it is a non-political, voluntary, interest association of citizens, based for an indefinite period of time under Act no. 83/1990 Coll. on Association of Citizens, as amended.

The mission of this association is to create a cultural and social environment for the individual members, where people are interested in industry, science, technology and related science of metallurgy and their positive contribution to society can enhance and develop their relationship with the subject areas of society.

The objectives:

The aim of the Academy of Metallurgy ’s activity is to support the development of civil society in the field of enhancing the cultural and educational level of all strata of the population. It´s goal is also to build and develop the relationship of the widest civil society to industry, science, technology and related science of metallurgy and also, particularly but not only, to raise interest in industry, science, technology and related science unions and to increase their reputation generally.

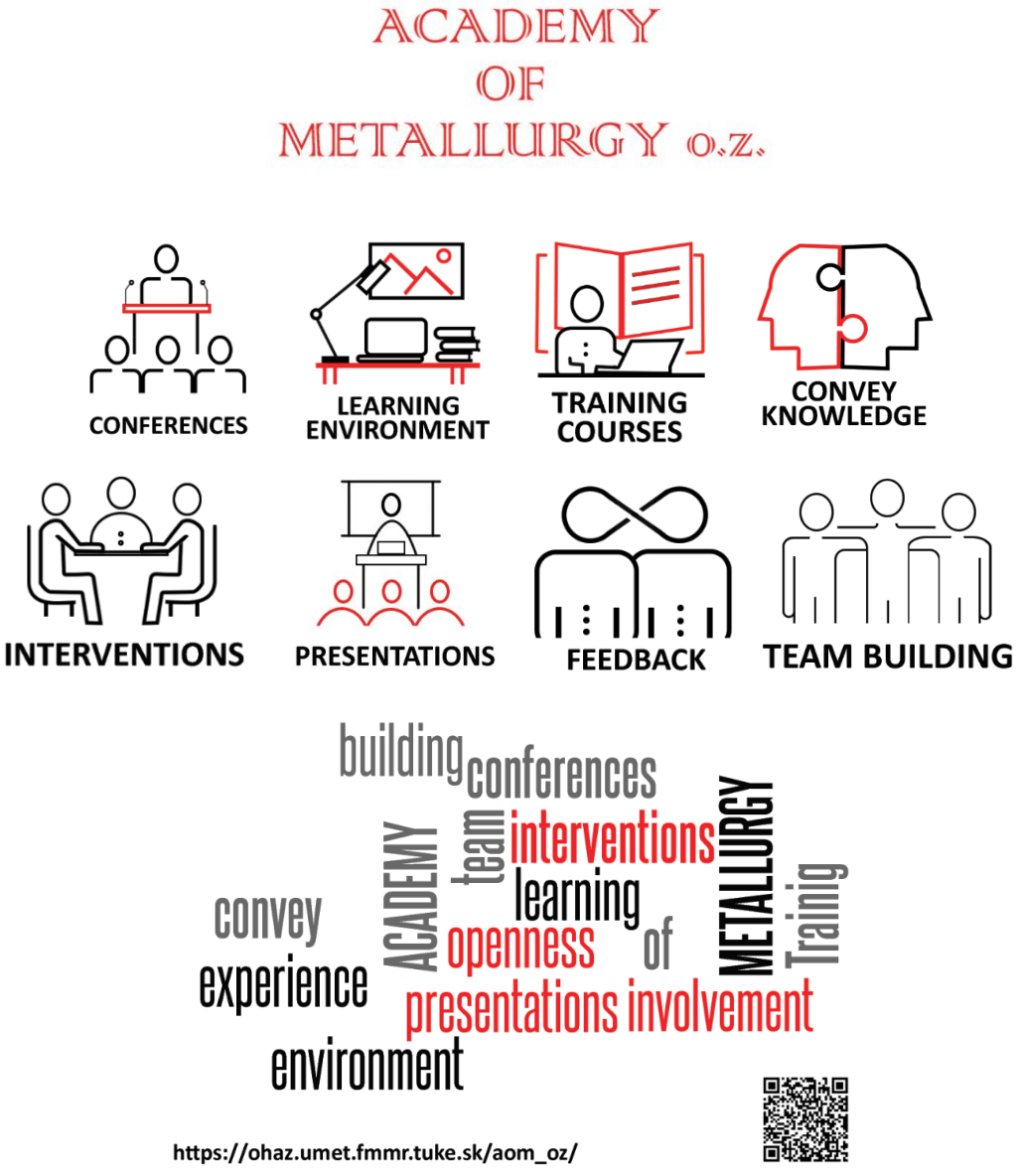

Compiler: Peter Demeter
Róbert Dzurňák
Branislav Buľko

Publisher: Technical University of Košice, Faculty of Materials, Metallurgy and Recycling (http://fmmr.tuke.sk/wps/portal), Institute of Metallurgy and Academy of metallurgy, o.z. (https://ohaz.umet.fmmr.tuke.sk/aom_oz/)